SOVIET PHYSICS

JETP

A translation of the Journal of Experimental and Theoretical Physics of the USSR.

SOVIET PHYSICS JETP VOLUME 4, NUMBER 3 APRIL, 1957

Theory of Diffuse Scattering of X-rays by Solid Solutions. I.

M. A. KRIVOGLAZ

Metal Physics Institute, Academy of Sciences, Ukrainian SSR

(Submitted to JETP editor July 19, 1955)

J. Exptl. Theoret. Phys. (U.S.S.R.) 31, 625-635 (October, 1956)

The intensity of the diffuse scattering of x-rays by mixed crystals has been determined by means of a phenomenological treatment. Thermodynamic quantities which may be found from other experiments appear in the expressions for the background intensity. Characteristic features of the scattering in the neighborhood of points of phase transitions of the second kind and of critical points on the dissociation curve have been investigated, and also the scattering by weak, by ideal and by almost completely ordered solid solutions has been examined.

X-RAYS scattered by a crystal* form sharp lines on an x-ray photograph corresponding to definite conditions of reflection, and also give rise to a diffuse background. Diffuse scattering of waves by a solid, which is not accompanied by a change in wavelength, is associated with some sort of deviations from ideal periodicity of the crystal: either thermal vibrations or static deviations from periodicity. In the present article we shall not take into account effects related to thermal and zero-point vibrations of the atom and also to Compton scattering. It is also assumed that all the atoms of the solid solution are situated exactly at the lattice points. The neglect of the geometric imperfections of the lattice introduced by these assumptions is approximately justified if the sizes of the various atoms of the solution differ little from each other, while the imperfections associated with a plastic deformation have been removed. Thus, the only cause for a deviation from periodicity of the crystal which is taken into account in this paper is the more or less random distribution of the atoms of the solution among the various lattice points. Because of the unequal scattering properties of the various kinds of atoms, this also leads to diffuse scattering.

An investigation of the scattering of x-rays presents a more complicated problem than the scattering of light, since the wavelengths of x-rays are of the same order of magnitude as the interatomic distances in the crystal. The situation is simplified considerably if the direction of the scattered wave, which corresponds to diffuse scattering, is

* In what follows we shall examine the scattering of x-rays. However, all the results apply equally well to neutron scattering (not taking into account the background which is connected with the presence of isotopes and with magnetic scattering). In such a case the atomic scattering factors should be interpreted as the neutron scattering factors averaged over the isotopes. The results given below are also applicable in the study of scattering of other types of waves, provided the Born approximation is applicable and the scattering centers are situated at the lattice points. Thus, one may study the scattering of electrons, and the scattering of elastic waves by the fluctuations in the isotopic composition in a solution of isotopes. In an analogous way one may study the scattering of sound waves in the more general case of mixed crystals when not only the masses of the atoms are different, but also the forces acting between them.

close to the direction of the coherent wave corresponding to some particular condition for interference, or which is close to the direction of the incident beam. In such a case the differences in phase of waves scattered by different atoms begin to deviate appreciably from a value which is an integral multiple of π only if the distances between the atoms are much larger than the lattice constant. Therefore, a phenomenological examination of scattering becomes possible for the investigation of background near the lines on an x-ray photograph and near the incident beam. In such an investigation the crystal is regarded as a purely periodic structure which consists of effective atoms on top of which are superimposed fluctuations in the composition and in the degree of long range order. The periodic structure guarantees the production of the coherent wave, while the fluctuations give rise to the diffuse scattering. In calculating the intensity of the background near the lines on the x-ray photograph only those fluctuations are important which are spread over a large numberof lattice constants. The probabilities of such fluctuations, and consequently the intensity of the scattered radiation, may be expressed in terms of certain thermodynamic quantities without using a specific model of the solution.

A phenomenological investigation of the scattering of x-rays by crystals was first carried out by Landau[1] who investigated the scattering in the neighborhood of superstructure lines at a temperature close to the temperature of a phase transition of the second kind. In this work it was assumed that the diffuse scattering is brought about by fluctuations in the degree of long range order. The results of Landau are applicable only to those crystals for which only fluctuations in the long range order are significant (for example, in the case of orientational ordering). In mixed crystals, and in particular in alloys, in addition to fluctuations in the long range order, there exist also fluctuations in composition. Since they are not statistically independent one should, in determining the probability of fluctuations, consider simultaneously the deviations from equilibrium values both of the composition and of the degree of long range order. Using a method analogous to thatdeveloped by Landau[1] we shall determine, by calculating such probabilities, the intensity of the background near the superstructural and the structural lines, and also for small scattering angles.

Calculations are carried out for those cases in which expressions for the thermodynamic potential Φ of the mixed crystal are known. Thus, we shall examine the scattering in the neighborhood of the points of ordering, which takes place as a phase transition of the second kind, when one may use Landau's thermodynamic theory. In a similar manner one may obtain an expression for Φ near the critical point on the dissociation curve. In addition, an investigation is made of the scattering by ideal, by weak, and by almost completely ordered solutions where the expressions for Φ are also known as functions of the composition and of the degree of ordering.

1. GENERAL EXPRESSIONS FOR THE INTENSITY OF THE BACKGROUND NEAR LINES ON AN X-RAY PHOTOGRAPH

We shall examine a binary solid solution A–B. In the disordered state it has a crystal lattice of the Bravais type; the probabilities of the various lattice points being occupied by atoms of a given kind are all the same, and are equal to the corresponding atomic concentrations $\bar{c}_A$ and $\bar{c}_B$. If the solution goes over into an ordered state, then its lattice points are subdivided into several different kinds, and the probabilities of the different types of lattice points being occupied are no longer the same. In what follows we shall restrict ourselves to the case when in the ordered state the crystal lattice is subdivided into points of only two types, with the number of points of the first and the second kinds being equal, and with the amplitudes of the radiation scattered by atoms situated at lattice points of either kind and leading to the formation of superstructure lines also being equal. In this case the probabilities of the lattice points being occupied by atoms A and B may be specified by means of a single degree of long range order $\bar{\eta}$:

$$p_A^{(1)} = \bar{c}_A + {}^1/_2\bar{\eta}; \quad p_A^{(2)} = \bar{c}_A - {}^1/_2\bar{\eta};$$

$$p_B^{(1)} = \bar{c}_B - {}^1/_2\bar{\eta}; \quad p_B^{(2)} = \bar{c}_B + {}^1/_2\bar{\eta}.$$

In spite of the limitations introduced above, this procedure will apparently include all the ordered solutions known at present that correspond to the stoichiometric composition AB, and all the disordered solutions.

As is well known, the amplitude of the monochromatic radiation scattered by a single crystal may be represented within the framework of the kinematic scattering theory in the form

$$a = \int \rho(\mathbf{r})\, e^{i(\mathbf{k}_2 - \mathbf{k}_1,\, \mathbf{r})}\, d\tau. \qquad (1)$$

Here a is expressed in electronic units, $\mathbf{k}_1$ and $\mathbf{k}_2$ are propagation vectors of the incident and the scattered waves, $\rho(\mathbf{r})$ is the density of the electronic charge in the crystal divided by the charge of the electron.

The calculation of the Fourier component of $\rho(\mathbf{r})$ which enters Eq. (1) is considerably simplified if one makes use of the assumption made above that all the atoms are situated exactly at the lattice points of an ideally periodic lattice, and if one also assumes that the distribution of the charge density of a given atom does not depend on the kind of atoms surrounding it, on the composition, or on the degree of order. The latter assumption holds with a sufficient degree of accuracy for almost all the atoms, with the exception of the lightest ones. The probability density $\rho(\mathbf{r})$ in a mixed crystal is a function of coordinates which has an extremely complicated variation in space. However, since the exponential factor (1) remains constant in the plane perpendicular to $\mathbf{k}_2 - \mathbf{k}_1$, the function $\rho(\mathbf{r})$ can be replaced for integration purposes by a function which is averaged over the different kinds of atoms in the plane referred to above. If one takes into account the simplifying assumptions made above, then this averaged function will have the following form:

$$\bar{\rho}(\mathbf{r}) = c_A \rho_A(\mathbf{r}) + c_B \rho_B(\mathbf{r}) + \eta \rho'(\mathbf{r}). \qquad (2)$$

Here c_A, c_B and η denote the atomic concentration of the atoms A and B and the degree of long range order in the plane under consideration, the functions $\rho_A(\mathbf{r})$ and $\rho_B(\mathbf{r})$ have a symmetry identical with the symmetry of the crystal lattice, while $\rho'(\mathbf{r})$ has the symmetry of the ordered crystal which is lower than the symmetry of the lattice; ρ_A, ρ_B and ρ' do not depend on c_A and η. Because of the fluctuations of composition and order present in the crystal, the values of the quantities c_A, c_B and η, corresponding to different planes, differ from the values $\bar{c}_A$, $\bar{c}_B$ and $\bar{\eta}$ averaged over the whole crystal, and are functions of the coordinate specifying the plane.

The periodic functions $\rho_A(\mathbf{r})$, $\rho_B(\mathbf{r})$ and $\rho'(\mathbf{r})$ may be expanded in Fourier series:

$$\rho_A(\mathbf{r}) = \sum_i \lambda_{Ai} e^{i\mathbf{K}_i \mathbf{r}}; \quad \rho_B(\mathbf{r}) = \sum_i \lambda_{Bi} e^{i\mathbf{K}_i \mathbf{r}}; \qquad (3)$$

$$\rho'(\mathbf{r}) = \sum_j \lambda'_j e^{i\mathbf{K}'_j \mathbf{r}}.$$

Here $\mathbf{K}_i$ and $\mathbf{K}'_j$ are 2π times the lattice vectors of lattices which are respectively reciprocal to the lattices of the disordered and the ordered crystal, while in the expansion of $\rho'(\mathbf{r})$, those terms are missing for which $\mathbf{K}'_j$ coincides with any one of the $\mathbf{K}_i$. Substituting Eqs. (2) and (3) into (1) and breaking up the quantities c_A, c_B and η into their average values plus a fluctuating part we whall obtain

$$a = 8\pi^3 \sum_i (\bar{c}_A \lambda_{Ai} + \bar{c}_B \lambda_{Bi}) \delta(\mathbf{q}_i) + 8\pi^3 \bar{\eta} \sum_j \lambda'_j \delta(\mathbf{q}'_j) \qquad (4)$$

$$+ \sum_i (\lambda_{Ai} - \lambda_{Bi}) \int \Delta c_A e^{i\mathbf{q}_i \mathbf{r}} d\tau + \sum_j \lambda'_j \int \Delta\eta e^{i\mathbf{q}'_j \mathbf{r}} d\tau;$$

$$\mathbf{q}_i = \mathbf{K}_i + \mathbf{k}_2 - \mathbf{k}_1; \quad \mathbf{q}'_j = \mathbf{K}'_j + \mathbf{k}_2 - \mathbf{k}_1.$$

Here $\delta(\mathbf{q})$ denotes the product of three δ-functions for the individual components of the vector, and it has been taken into account that $\Delta c_B = -\Delta c_A$.

The intensity of the scattered radiation is proportional to the square of the amplitude a. All the cross terms in the expression for a^2 drop out after statistical averaging. The square of the δ-function defined for a finite volume V (the crystal volume) is equal to this δ-function multiplied by $V/8\pi^3$. Below we shall calculate the intensity of scattering near the principal or the superstructure lines on an x-ray photograph. In this calculation one of the quantities q_i or q'_j is small, and in the expression for a^2 one may keep the square of only that Fourier component of Δc_A or of η, for which the corresponding q is small. As may be easily seen, the squares of all the other Fourier components are in order of magnitude smaller by a factor $q^2 a_0^2$ (where a_0 is the lattice constant) and are not taken into account in what follows. Noting further that

$$\lambda_{Ai} = (N/V) f_A;$$

$$\lambda_{Bi} = (N/V) f_B; \quad \lambda'_j = (N/2V)(f_A - f_B)$$

(N is the total number of all the lattice points, f_A and f_B are the atomic scattering factors of atoms A or B corresponding to the given angle of scattering), we shall find that the intensity of the scattered radiation, expressed in electronic units, near the principal line which corresponds to the $\mathbf{K}_i$th Fourier component of the electron density is equal to

$$I = 8\pi^3 \frac{N^2}{V}\left[|\bar{c}_A f_A + \bar{c}_B f_B|^2 \delta(\mathbf{q}_l) + \frac{|f_A - f_B|^2}{8\pi^3 V}\left|\int \Delta c_A e^{i\mathbf{q}_l \mathbf{r}}\, d\tau\right|^2\right]. \quad (5)$$

In the same units, the intensity of radiation in the neighborhood of the superstructure line which corresponds to the $\mathbf{K}_j'$-th Fourier component of the electron density $\rho(\mathbf{r})$ is determined by means of the formula:

$$I = 2\pi^3 \frac{N^2}{V}|f_A - f_B|^2\left[\bar{\eta}^2 \delta(\mathbf{q}_j') + \frac{1}{8\pi^3 V}\left|\int \Delta\eta e^{i\mathbf{q}_j'\mathbf{r}}\, d\tau\right|^2\right]. \quad (6)$$

The first terms in Eqs. (5) and (6) which contain δ-functions determine the intensities of the lines on the x-ray photograph while the second terms determine the intensity of diffuse scattering, i.e., of the background.

Thus the intensity of the background is determined by the distribution throughout the crystal of the fluctuations Δc_A and $\Delta\eta$. As is well known the probability of the occurrence of a certain distribution of fluctuations is proportional to $w \sim e^{-R/kT}$, where R is the minimum work required for the production in a reversible manner of this distribution of fluctuations, and T is the temperature of the external medium. In the case of a cubic crystal the expression for R can be written in the following form:

$$R = {}^1/_2 \int [\varphi_{\eta\eta}(\Delta\eta)^2 + 2\varphi_{\eta c}\Delta\eta\Delta c_A + \varphi_{cc}(\Delta c_A)^2 + \alpha(\nabla\eta)^2 + 2\gamma\nabla\eta\nabla c_A + \beta(\nabla c_A)^2]\, d\tau. \quad (7)$$

Here φ is the thermodynamic potential per unit volume of the crystal

$$\varphi_{\eta\eta} = \partial^2\varphi/\partial\eta^2;\ \varphi_{\eta c} = \partial^2\varphi/\partial\eta\partial c_A;\ \varphi_{cc} \equiv \partial^2\varphi/\partial c_A^2;$$

the terms which contain derivatives of c_A and η take into account the inhomogeneity of the fluctuations in space, and play a particularly important role in the neighborhood of critical points and of points of phase transition of the second kind, guaranteeing that the fluctuations at these points remain finite (see Refs. 1-3).

As may be seen from (5) and (6), in order to calculate the diffuse scattering, it is sufficient to know the Fourier components of the fluctuations Δc_A and $\Delta\eta$. Therefore, in what follows we shall determine not the distribution of the fluctuations in composition and in the degree of long range order, but directly the average values of the squares of the Fourier components of these fluctuations. In order to do this, we expand Δc_A and $\Delta\eta$ into Fourier series:

$$\Delta c_A = \sum_{\mathbf{f}} (c_{\mathbf{f}} e^{i\mathbf{f}\mathbf{r}} + c_{\mathbf{f}}^* e^{-i\mathbf{f}\mathbf{r}}), \quad (8)$$

$$\Delta\eta = \sum_{\mathbf{f}} (\eta_{\mathbf{f}} e^{i\mathbf{f}\mathbf{r}} + \eta_{\mathbf{f}}^* e^{-i\mathbf{f}\mathbf{r}}),$$

where $f_x > 0$. Substituting Eqs. (8) into Eq. (7) for the minimum work and performing the integration we shall find that the distribution of the probabilities of the Fourier components of the fluctuations Δc_A and $\Delta\eta$ has the form

$$w \sim \exp\left\{-\frac{V}{kT}\sum\left[(\varphi_{\eta\eta} + \alpha f^2)|\eta_{\mathbf{f}}|^2 + (\varphi_{cc} + \beta f^2)|c_{\mathbf{f}}|^2 + (\varphi_{\eta c} + \gamma f^2)(\eta_{\mathbf{f}} c_{\mathbf{f}}^* + \eta_{\mathbf{f}}^* c_{\mathbf{f}})\right]\right\}. \quad (9)$$

From formula (9) it may be seen that each term in the sum over $\mathbf{f}$ depends only on those $\eta_{\mathbf{f}}$ and $c_{\mathbf{f}}$ which correspond to the given $\mathbf{f}$. Consequently, the fluctuations of the Fourier components corresponding to different $\mathbf{f}$ are statistically independent (but the fluctuations of the quantities $c_{\mathbf{f}}$ and $\eta_{\mathbf{f}}$ with the same $\mathbf{f}$ are statistically dependent), and therefore it is not difficult to find the average squares of these fluctuations. For the calculation of the latter we shall assume that $\mathbf{f}$ is sufficiently small (this assumption also justifies the neglect made in (7) of the higher derivatives of c_A and η). We may then retain terms which contain the factor f^2 only close to small terms which are independent of $\mathbf{f}$ (which vanish near the point under consideration in the phase diagram), and we may neglect terms proportional to f^4. Substituting the expression obtained in this way for $|\eta_{\mathbf{f}}|^2$ with $\mathbf{f} = \mathbf{q}_{\mathbf{f}}'$ into Eq. (6), and taking into account that

$$\int \Delta\eta e^{i\mathbf{q}_j'\mathbf{r}}\, d\tau = V\eta_{\mathbf{q}_j'}^* (\text{or } V\eta_{-q_j}),$$

we shall find the following expression for the intensity of the background in the neighborhood of a superstructure line (for small q_j'):

$$I = 2\pi^3 \frac{N^2}{V} |f_A - f_B|^2 \left\{ \bar{\eta}^2 \delta(\mathbf{q}_j') + \right. \quad (10)$$

$$+ kT/8\pi^3 \left[\varphi_{\eta\eta} - \frac{\varphi_{\eta c}^2}{\varphi_{cc}} \right.$$

$$\left. \left. + \left(\alpha - 2\frac{\varphi_{\eta c}}{\varphi_{cc}} \gamma + \frac{\varphi_{\eta c}^2}{\varphi_{cc}^2} \beta \right) q_j'^2 \right]^{-1} \right\}.$$

If we then determine $|c_{\mathbf{q}_i}|^2$ and take into account Eq. (5), we shall find an analogous expression for the intensity of the background near a principal line

$$I = 8\pi^3 \frac{N^2}{V} [|\bar{c}_A f_A + \bar{c}_B f_B|^2 \delta(\mathbf{q}_i)$$

$$+ \frac{|f_A - f_B|^2 kT}{8\pi^3}$$

$$\times \frac{\varphi_{\eta\eta} + \alpha q_i^2}{\varphi_{\eta\eta}\varphi_{cc} - \varphi_{\eta c}^2 + (\alpha\varphi_{cc} + \beta\varphi_{c\eta} - 2\gamma\varphi_{\eta c}) q_i^2}] \quad (11)$$

or

$$I = 8\pi^3 \frac{N^2}{V} [|\bar{c}_A f_A + \bar{c}_B f_B|^2 \delta(\mathbf{q}_i) \quad (12)$$

$$+ \frac{kT|f_A - f_B|^2}{8\pi^3} \frac{1}{(d^2\varphi/dc_A^2) + \beta' q_i^2}].$$

In the above the derivative $\partial/\partial c_A$ (or $\partial/\partial\eta$) in (10) and (11) is evaluated for the equilibrium values of the degree of long range order $\eta = \bar{\eta}$ (or of composition). On the other hand, the derivative d/dc_A in Eq. (12) is calculated for the values of η, which correspond to the changed (due to fluctuations) composition of the alloy (and to the same temperature). The quantity β' denotes the coefficient of $(\nabla c)^2$ in the corresponding expansion of the thermodynamic potential. The equivalence of Eqs. (11) and (12) follows from the condition $\partial\varphi/\partial\eta = 0$.

The general formulas obtained above for the intensity of scattered radiation may be applied to various special cases for which expressions for thermodynamic potential as a function of c_A and η are known.

2. THE SCATTERING BY SOLID SOLUTIONS NEAR POINTS OF PHASE TRANSITION OF THE SECOND KIND

In this section we shall examine the distinctive features of diffuse scattering of x-rays by solid solutions in the order-disorder transition which takes place as a phase transition of the second kind. Phase transitions of this type occur in a number of alloys, for example, in CuZn, AgZn with an admixture of Au, Fe_3Al, etc. The distinctive features referred to above occur because at the point of a phase transition of the second kind, the derivatives $\varphi_{\eta\eta}$ and $\varphi_{\eta c}$ vanish. Because of this, anomalously large fluctuations in the degree of long range order should be observed, and also the very intense diffuse scattering in the neighborhood of the superstructure line which is connected with these fluctuations.

According to the thermodynamic theory of phase transitions of the second kind[3,4] the expression for φ in the neighborhood of the transition temperature T_0 may be represented in the form of an expansion in powers of η:

$$\varphi = \varphi_0 + {}^1/_2 A\eta^2 + {}^1/_4 B\eta^4, \quad (13)$$

$$A = a(T - T_0),\ a > 0,\ B > 0,$$

where φ_0, A and B are functions of c_A, T and P. The coefficients a and B may be determined from the experimental data on the discontinuity in the specific heat during the phase transition and on the temperature dependence of $\bar{\eta}$ by means of the formulas[3]:

$$\Delta C_p = a^2 T_0/2B;\ \bar{\eta} = \sqrt{a(T_0 - T)/B}.$$

Evaluating the second derivatives of φ with respect to η and c_A near the transition point and substituting them into (10) we shall find that the intensity of scattered radiation near a superstructure line below the temperature of ordering ($T \leq T_0$) in the special case of cubic crystals is equal to

$$I = 2\pi^3 \frac{N^2}{V} |f_A - f_B|^2 \frac{aT_0}{B} \left\{ \frac{T_0 - T}{T_0} \delta(\mathbf{q}_j') \right. \quad (14)$$

$$+ \frac{k}{16\pi^3 \Delta C_p} \left[2\frac{T_0 - T}{T_0} \left[1 - \frac{\Delta C_p}{T_0} \left(\frac{dT_0}{dc_A} \right)^2 \left(\frac{d^2\varphi_0}{dc_A^2} \right)^{-1} \right] \right.$$

$$\left. \left. + \frac{\alpha}{aT_0} q_j'^2 \right]^{-1} \right\}.$$

For $T \geq T_0$ only the diffuse part of the scattered radiation remains

$$I = \frac{1}{8} \frac{N^2}{V} |f_A - f_B|^2 \frac{aT_0}{B} \frac{k}{\Delta C_p} \quad (15)$$

$$\times \left[\frac{T - T_0}{T_0} + \frac{\alpha}{aT_0} q_j'^2 \right]^{-1}.$$

For crystals of different symmetry $\alpha q_j'^2$ should, in Eqs. (14) and (15), be replaced by

$$\sum_{k,l=1}^{3} \alpha_{kl} q'_{jk} q'_{jl}.$$

Expression (15) for the intensity of scattering from a solid solution in the disordered region agrees with the corresponding expression obtained by Landau[1] in the case when there are no fluctuations in composition. The presence of such fluctuations leads to a change in the expression for the intensity of scattering for $T < T_0$: formula (14) has acquired a square bracket in place of unity which appeared in the corresponding formula of Ref. 1. In the scattering from an ordered crystal a sharp line is formed whose shape is described by a δ-like function, and whose intensity is proportional to the temperature difference $T_0 - T$ and which vanishes at the temperature of ordering. At the same time, near the temperature T_0, both in the ordered and in the disordered region for small values of q_j', one should observe a very intense background on an x-ray photograph because of a sharp increase in the magnitude of fluctuations of long range order. The maximum of this intensity lies at $q_j' = 0$ and is inversely proportional to the temperature difference $|T - T_0|$. For a given q_j', the intensity of the background is a maximum* at $T = T_0$, and its decrease is proportional to $|T - T_0|$. For alloys whose composition corresponds to a maximum temperature of ordering, the intensity of background decreases as we go away from T_0 twice as fast in the ordered region as in the disordered region**. In other cases the ratio of the rates of decrease in the intensity of the background is less than two.

All the parameters which occur in Eqs. (14) and (15) (with the exception of the quantity α / aT_0) may be determined if we know from other experiments the form of the functions $T_0(c_A)$, ΔC_p, the dependence on the concentration of the chemical potentials of the atoms of the crystal at $T \approx T_0$ and the temperature dependence of $\overline{\eta}(T)$ near the transition point. The only unknown parameter is determined by comparing the calculated background intensity with the experimental one (it may also be calculated by means of the statistical theory of solutions), and from this one may calculate the values of the intensity of scattered radiation for various angles of scattering (near superstructure lines) and for various temperatures (close to T_0) for all the superstructure lines.

As is shown in Ref. 4, at the point O where the curve of the points of phase transition of the second kind AO goes over into the curve of phase transitions of the first kind---the dissociation curve OB (Fig. 1), the condition

$$B = \tfrac{1}{2}(\partial A / \partial c_A)^2 \varphi_{cc}^{-1}$$

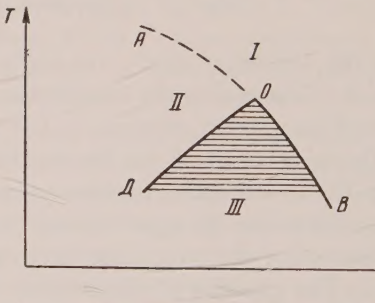

FIG. 1. *I* – Disordered crystal; *II* – Ordered crystal; *III* – Two phase region.

is fulfilled. This means that the expression which appears in the square brackets of Eq. (14) reduces to zero at the point O. Near such a point for $T < T_0$ the expression for the intensity of the radiation scattered by the ordered crystal may be represented near a superstructure line in the following form:

$$I = 2\pi^3 \frac{N^2}{V} |f_A - f_B|^2 \frac{aT_0}{B} \left\{ \frac{T_0 - T}{T_0} \delta(\mathbf{q}_j') + \frac{k}{16\pi^3 \Delta C_p} \left[2 \frac{T_0 - T}{T_0} \left(r_1 \frac{T_{cr} - T}{T_0} + r_2 \frac{T_0 - T}{T} \right) + \frac{\alpha}{aT_0} q_j'^2 \right]^{-1} \right\}, \quad (16)$$

---

* For $T = T_0$, the intensity of the background becomes infinite at the point $\mathbf{q}_j' = 0$ in accordance with Eqs. (14) and (15). This circumstance is related to the fact that for $\mathbf{q}_j' = 0$ the magnitude of the fluctuations in the long range order is not limited (as it is for $\mathbf{q}_j' \neq 0$) by the necessity of performing work related to the formation of an inhomogeneous fluctuation. However, in this case the finite dimensions of the crystal lead to a finite value of the intensity of the background and at the same time to the breakdown of Eqs. (14) and (15). This breakdown occurs only in a range of angles λ / L (where L is the size of the region of coherent scattering) and within a very narrow range of temperatures $\sim (\lambda/L)^2 T_0$.

**The quoted value for the ratio of the rates of change of the intensities of the background as we move away from T_0 in the ordered and in the disordered regions is only correct for sufficiently small values of q_j'. For large values of q_j' this ratio will become larger because of the temperature dependence of α and of the factor kT in Eq. (10).

where T_{cr} is the temperature which corresponds to the point O, while r_1 and r_2 may be considered to be constant in the neighborhood of this point. Thus for $T < T_0$ the background intensity which corresponds to a given q_j' decreases extremely slowly as the temperature is decreased in the case under consideration. If $T > T_0$, then as T_0 is approached, the background intensity increases in accordance with Eq. (15), i.e., in accordance with the same law which holds far from the critical point O.

In contrast to the neighborhood of the ordinary points of phase transition of the second kind, the magnitude of the fluctuations of the composition in an ordered crystal also increases very markedly in the neighborhood of the point O, while the intensity of scattering near a principal line in accordance with Eq. (11) becomes equal to

$$I = 8\pi^3 \frac{N^2}{V} \left\{ |\bar{c}_A f_A + \bar{c}_B f_B|^2 \delta(\mathbf{q}_j') + \frac{|f_A - f_B|^2}{8\pi^3} \frac{kT}{\varphi_{cc}} \times \frac{2(T_0 - T) + (\alpha/a) q_j'^2}{2(T_0 - T)[r_1 (T_{cr} - T)/T_0 + r_2 (T_0 - T)/T_0] + (\alpha/a) q_j'^2} \right\}. \quad (17)$$

Thus in the neighborhood of the critical point mentioned above, one should observe very intense diffuse scattering in the neighborhood of both the superstructure and the principal lines. For a disordered crystal in the neighborhood of the point at which ordering takes place $\varphi_{\eta c} = 0$, and since φ_{cc} does not vanish at the point O the diffuse scattering in the neighborhood of the principal lines is not large.

We[5] have also examined the special features of diffuse scattering by pure crystals near the point at which the curve of the points of phase transition of the second kind goes over into the curve of points of phase transition of the first kind, and also in the neighborhood of an isolated point of phase transitions of the second kind.

The formulas which have been obtained until now refer to the scattering of monochromatic x-rays by a single crystal. In order to be able to analyze a Debye photograph we must average the above expressions over all the orientations of the crystal. An averaging of this kind was carried out by Landau[1]. In the cases under consideration the result of Landau's calculation[1] for an ordered crystal in the neighborhood of superstructure lines has the form:

$$I = 4\pi^2 n \frac{N^2}{V} |f_A - f_B|^2 \frac{aT_0}{B} \frac{1}{K_j'^3} \left\{ \frac{T_0 - T}{T_0} \operatorname{tg} \frac{\psi_j}{2} \delta(\psi - \psi_j) - \frac{kK_j'}{32\pi^2 \Delta C_p (\alpha/aT_0)} \times \ln \left[\frac{\operatorname{ctg}^2(\psi_j/2)}{16} (\psi - \psi_j)^2 + \frac{P}{4(\alpha/aT_0) K_j'^2} \right] \right\}. \quad (18)$$

Here ψ is the angle of scattering, ψ_j is the angle of scattering for the superstructure line under consideration, n is the number of families of atomic planes taking part in the formation of this line, while P denotes the term next to $(\alpha/aT_0) q_j'^2$ in the denominator of the corresponding Eq. (14) or (16) for an ordered crystal, and in the denominator of Eq. (15) for a disordered crystal. It is evident that in the last case the first term in (18) is absent.

3. SCATTERING NEAR A CRITICAL POINT ON THE DISSOCIATION CURVE, AND ALSO BY WEAK, IDEAL AND ALMOST COMPLETELY ORDERED SOLUTIONS

At critical points on dissociation curves (point K in Fig. 2) the concentrations of both phases

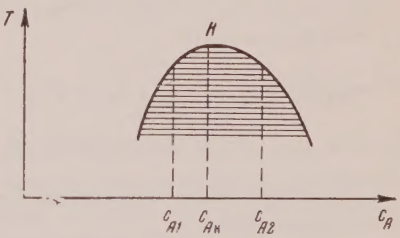

FIG. 2.

become the same. At these points, as is well known, the derivatives $d^2\varphi/dc_A^2$ and $d^3\varphi/dc_A^3$ vanish, and therefore in the neighborhood of the critical point very large fluctuations in composition must take place, and very intense scattering of waves by such fluctuations should be observed.

We expand the thermodynamic potential into a series in powers of $c_A - c_{Ak}$, where c_{Ak} is the composition which corresponds to the critical point*

* For the sake of definiteness, we shall assume that the solution has an "upper" critical temperature, i.e., the state diagram has the form shown in Fig. 2. In the case of a "lower" critical temperature, the results will be altered in an obvious way.

$$\varphi = \varphi_0 + f_1(c_A - c_{Ak}) + {}^1/_2 f_2 (c_A - c_{Ak})^2 + {}^1/_3 f_3 (c_A - c_{Ak})^3 + {}^1/_4 f_4 (c_A - c_{Ak})^4 + \ldots \quad (19)$$

In the neighborhood of the critical point one may take

$$f_2 = b(T - T_k);\ f_3 = \gamma (T - T_k);\ f_4 > 0,$$

where T_k is the critical temperature. In order to find the equation of the dissociation curve in the neighborhood of the critical point, one must substitute expression (19) into the conditions of equilibrium

$$\left.\frac{\partial \varphi}{\partial c_A}\right|_{c_A = c_{A1}} = \left.\frac{\partial \varphi}{\partial c_A}\right|_{c_A = c_{A2}};$$

$$\left.\frac{\partial \varphi}{\partial c_A}\right|_{c_A = c_{A1}} = \frac{\varphi(c_{A1}) - \varphi(c_{A2})}{c_{A1} - c_{A2}},$$

where c_{A1} and c_{A2} are the concentrations of atoms A in the first and in the second phases which are in equilibrium at a given T and P. On solving the resulting system of equations, and on neglecting in the expression for $c_A - c_{Ak}$ terms proportional to $|T - T_k|^{3/2}$, we shall find that the equation of the dissociation curve for small $|T - T_k|$ has the form:

$$T_k - T_p = Q(c_A - c_{Ak})^2 - (2\gamma/3b)(c_A - c_{Ak})(T_k - T_p) \approx Q(c_A - c_{Ak})^2;\ Q = f_4/b. \quad (20)$$

Here T_p is the dissociation temperature for a solution of given composition c_A.

Thus b and f_4 may be determined from experimental data if the curvature of the dissociation curve in the neighborhood of the critical point and the discontinuity in the specific heat at that point are both known. Using (19) and (20), and determining the amounts of both phases by means of "the rule of the lever", we shall find that the thermodynamic potential of the solution of critical composition in a two-phase region is equal to $\varphi = \varphi_0 - (b^2/4f_4)(T - T_k)^2$. Consequently, in going over into a two-phase region the specific heat at the critical point increases discontinuously by an amount $\Delta C_p = T_k b^2/2f_4$. The derivative $d^2\varphi/dc_A^2$ in the neighborhood of the critical point may also be expressed in terms of ΔC_p and Q:

$$d^2\varphi/dc_A^2 = 2\Delta C_p Q (T + 2T_k - 3T_p)/T_k.$$

Substituting this expression into (12) we shall obtain the following formula for the intensity of scattering from cubic crystals in the neighborhood of the critical point for small q_i:

$$I = 8\pi^3 \frac{N^2}{V} \left\{ |\bar{c}_A f_A + \bar{c}_B f_B|^2 \delta(\mathbf{q}_i) + \frac{kT_k |f_A - f_B|^2}{16\pi^3 Q \Delta C_p} \left[\frac{T + 2T_k - 3T_p}{T_k} + \frac{\beta'}{bT_k} q_i^2 \right]^{-1} \right\}. \quad (21)$$

The formula obtained above contains only one unknown parameter $\beta' bT_k$ and allows one to determine the intensity of scattered radiation near the principal lines and for small angles for solutions of different compositions at various temperatures near the critical point. This formula shows that in the case indicated above, as in the case of a phase transition of the second kind, the background intensity is anomalously large when ordering takes place. It attains a maximum at the critical point for $T = T_p = T_k$.

The formula takes on a particularly simple form in the case of small angle scattering when

$$q_i^2 = |\mathbf{k}_1 - \mathbf{k}_2|^2 = (4\pi/\lambda)^2 \sin^2(\psi/2).$$

In this case

$$I = \frac{1}{2} \frac{N^2}{V} |f_A - f_B|^2 \frac{kT_k}{Q\Delta C_p} \left[\frac{T + 2T_k - 3T_p}{T_k} + \frac{\beta'}{bT_k} \frac{16\pi^2}{\lambda^2} \sin^2 \frac{\psi}{2} \right]^{-1}. \quad (22)$$

The intensity of the scattered radiation near the principal lines on a Debye photograph (calculated for a portion of the ring equal to its radius) for a solution which is near the critical state is determined by a formula of type (18)

$$I = 4\pi^2 n \frac{N^2}{V} \frac{1}{K_i^3} \left\{ |\bar{c}_A f_A + \bar{c}_B f_B|^2 \operatorname{tg} \frac{\psi_i}{2} \delta(\psi - \psi_i) - \frac{kT_k K_i |f_A - f_B|^2}{32\pi^2 \Delta C_p Q(\beta'/bT_k)} \ln \left[\frac{\operatorname{ctg}^2 \frac{\psi_i}{2}}{16} (\psi - \psi_i)^2 + \frac{T + 2T_k - 3T_p}{T_k} \frac{1}{(\beta'/bT_k) K_i^2} \right] \right\}, \quad (23)$$

where the angle ψ_i corresponds to a principal line. From (23) it follows that the background intensity falls off comparatively slowly as $|\psi - \psi_i|$ increases: the distance at which the intensity of the background is reduced by a factor 2 in the close neighborhood of the critical point is proportional to $[(T + 2T_k - 3T_p)/T_k]^{1/4}$, with the coefficient of proportionality being equal to unity in order of magnitude. The background intensity in the neighborhood of the Roentgen lines also depends weakly on the temperature--logarithmically. A more pronounced dependence on the temperature and on angles of the background on a Debye photograph near a critical point should be observed at small angles. In this case the intensity of radiation scattered by an individual crystal does not depend on its orientation, and therefore the averaging over orientations will not change expression (22), and it will be applicable also for the calculation of the intensity of the background in a Debye photograph. From (22) it follows that at very small angles (or large λ), when the second term in the denominator of this formula is considerably less than the first term, I is inversely proportional to the difference $T + 2T_k - 3T_p$. The background intensity decreases with increasing ψ faster than in the neighborhood of lines on a Roentgen photograph, and the distance at which I attains half of its maximum value is proportional to

$$[(T + 2T_k - 3T_p)/T_k]^{1/2}.$$

Equation (22) is evidently applicable not only to the scattering of x-rays but also to the scattering of light by transparent dielectric solutions near the critical point. Since the wavelength of a light wave is considerably larger than the lattice constant, Eq. (22) in this case is applicable not only for small, but for arbitrary scattering angles. The effective cross sections for scattering of visible light at frequencies considerably smaller than the frequency of self-absorption are in this case inversely proportional to λ^4 and far from the critical point $I \sim \lambda^{-4}$. Near the critical point because of the last factor in (22) the intensity of the scattered radiation depends more weakly on λ (the dependence is λ^{-2} right at the critical point).

We note that the results for small angle scattering obtained above are applicable not only to solids, but also to liquids. It is true that in liquids density fluctuations play a significant role. However, in the neighborhood of the critical dissociation point the scattering by density fluctuations is considerably smaller than by composition fluctuations (which we consider to be statistically independent). Therefore, Eq. (22) may also be applied for the determination of small angle scattering of x-rays by liquid solutions in the neighborhood of the critical point, and for the scattering of light by liquid solutions through arbitrary angles.

As is well known, the general expression for the thermodynamic potential of a solution may be obtained without utilizing a specific statistical model of the solution in the case of small concentration of one of the components ($c_A \ll 1$). Neglecting terms quadratic in c_A^2 we shall write the expression for φ in the form (see, for example, Ref. 3):

$$\varphi = \varphi_B + N_0 c_A kT \ln c_A + c_A f(P, T). \quad (24)$$

Here φ_B is the thermodynamic potential per unit volume of the pure crystal B, N_0 is the number of atoms per unit volume, and $f(P, T)$ does not depend on c_A. The derivative of the thermodynamic potential (24) $d^2\varphi/dc_A^2 = N_0 kT/c_A$ for sufficiently small c_A is considerably larger than the second term in the denominator of Eq. (12), and therefore in this case the following formula is valid for the determination of the intensity of scattering at all angles

$$I = 8\pi^3 (N^2/V) \sum_i |c_A f_A + c_B f_B|^2 \delta(\mathbf{q}_i) + N |f_A - f_B|^2 c_A. \quad (25)$$

As should be expected in the case of weak solutions the background intensity does not depend on the temperature at which the crystal becomes ordered, and is proportional to c_A.

The expression for φ has a simple form also in the case of ideal solutions

$$\varphi = \varphi^0 + kTN_0 (c_A \ln c_A + c_B \ln c_B), \quad (26)$$

where φ^0 does not depend on the composition. Since the coefficient β' in the expansion of φ in powers of Δc_A is equal to zero in the ideal solution approximation, it follows from (12) and (26) that the following formula holds for the intensity of scattering by ideal solutions at arbitrary angles of scattering

$$I = 8\pi^3 (N^2/V) \sum_i |c_A f_A + c_B f_B|^2 \delta(\mathbf{q}_i) + N |f_A - f_B|^2 c_A (1 - c_A). \quad (27)$$

In this case the background intensity also does not depend on the temperature and has a simple dependence on the composition. We note that (27) agrees with the formula obtained by a different method by Laue[6] on the assumption of a completely random distribution of atoms of different kinds among the lattice points. This assumption is evidently fulfilled in the case of an ideal solution.

The thermodynamic expression for φ may also be obtained for ordered solid solutions whose composition is close to the stoichiometric, at low temperatures, when the numbers of atoms at "wrong" lattice points may be considered as small parameters. In this case for the solid solutions of the structure under examination in which the numbers of lattice points of the first and second kinds are the same, the thermodynamic potential is equal to (Ref. 7):

$$\varphi = \varphi' + \chi_1 c_A + \chi_2 \eta_1 + \frac{kTN_0}{2}[p_A^{(1)} \ln p_A^{(1)} \qquad (28)$$

$$+ p_A^{(2)} \ln p_A^{(2)} + p_B^{(1)} \ln p_B^{(1)} + p_B^{(2)} \ln p_B^{(2)}]$$

$$+ kTN_0[(p_B^{(1)})^2 e_1 + p_B^{(1)} p_A^{(2)} e_2 + (p_A^{(2)})^2 e_3].$$

Here φ', χ_1, χ_2, e_1, e_2, e_3 depend only on T and P and do not depend on c_A and η. For sufficiently low temperatures, and for compositions sufficiently close to the stoichiometric one, i.e., in the region of applicability of Eq. (28), χ may be considered to be constant, while $p_B^{(1)}$ and $p_A^{(2)}$ decrease rapidly as the temperature is decreased--faster than e_1, e_2 and e_3 increase. The coefficients of $(\Delta\eta)^2$, $\nabla\eta\,\Delta c_A$ and $(\nabla c_A)^2$ in the expansion of φ also increase more slowly as $T \to 0$ than $p_B^{(1)}$ and $p_A^{(2)}$ decrease. Therefore, at sufficiently low temperatures the background intensity for arbitrary scattering angles has the form:

$$I = 8\pi^3 (N^2/V)\Big[\sum_i |c_A f_A + c_B f_B|^2 \delta(\mathbf{q}_i) \qquad (29)$$

$$+ {}^1/_4 \eta_1^2 \sum_j |f_A - f_B|^2 \delta(\mathbf{q}_j)\Big]$$

$$+ N|f_A - f_B|^2 (c_A c_B - {}^1/_4 \eta_1^2).$$

The background intensity in a Debye photograph in the case of weak, ideal and almost completely ordered solutions is also determined by Eqs. (25), (27) and (29), respectively. Equation (29) agrees with the expression for the intensity of diffuse radiation scattered by an ordered crystal which was obtained by Lifshitz[8] on the assumption of the absence of correlation in the alloy. Thus the correlation in the alloy becomes of small importance not only at high but also at low temperatures in the neighborhood of the state of complete ordering.

It should be emphasized that all the above results have been obtained for the scattering by a system which is in a condition of equilibrium (corresponding to a certain annealing temperature).

I take this opportunity to express my gratitude to A. A. Smirnov for his interest in this work and for the discussion of the results.

[1] L. D. Landau, J. Exptl. Theoret. Phys. (U.S.S.R.) 7, 1232 (1937).

[2] L. Ornstein and F. Zernike, Proc. Amst. Akad. Sci. 17, 793 (1914); 18, 1520 (1916); 19, 1321 (1917); Physik. Z. 19, 134 (1918); 27, 761 (1926).

[3] L. D. Landau and E. M. Lifshitz, *Statistical Physics*, State Publishing House for Technical and Theoretical Literature, 1951.

[4] L. D. Landau, J. Exptl. Theoret. Phys. (U.S.S.R.) 7, 19 (1937).

[5] M. A. Krivoglaz, Ukrainian J. Phys. (in press).

[6] M. Laue, Ann. Physik 78, 167 (1925).

[7] M. A. Krivoglaz, Zh. Fiz. Khim. (in press).

[8] E. M. Lifshitz, J. Exptl. Theoret. Phys. (U.S.S.R.) 8, 959 (1938).

Translated by G. M. Volkoff
127

An Investigation of the Elastic Scattering of 590 MEV Neutrons by Neutrons

B. M. GOLOVIN AND V. P. DZHELEPOV
Institute for Nuclear Problems, Academy of Sciences, USSR

(Submitted to JETP editor April 23, 1952)
J. Exptl. Theoret. Phys. (U.S.S.R.) 31, 194-201 (August, 1956)

The differential scattering cross section for the elastic scattering of neutrons by neutrons has been determined using a neutron telescope. The effective energy of the neutrons was 590 mev. A striking anisotropy of the $(n-n)$ scattering has been established:

$$\sigma_{nn}(30^\circ)/\sigma_{nn}(90^\circ) = 2.3.$$

It has been found that the differential $(n-n)$ scattering cross section in the investigated angular region ($30^\circ \leq \vartheta \leq 90^\circ$) is equal to the proton-proton cross section at the same energy within experimental error. This fact, together with the results of our earlier work[1] (on neutron-neutron scattering at 300 mev) definitely points to the charge symmetry of nuclear forces at high energy.

1. INTRODUCTION

AT low energies information about the interaction of neutrons with neutrons is obtained, for example, in the analysis of the binding energies of mirror nuclei and in the studies of nuclear reactions which give rise to two neutrons moving with small relative velocity. A survey of this experimental material obtained at low energies leads to the conclusion that the forces acting between two neutrons are the same as those acting between two protons to an accuracy up to electromagnetic effects[2].

At high energies, data on this neutron-neutron interaction can be obtained primarily from experiments in which the angular distribution of neutrons scattered by deuterons and protons is compared under identical conditions. Such experiments were carried out by Dzhelepov, Golovin and Satarov[1], using 300 mev neutrons. These experiments showed that the neutron-neutron differential scattering cross section in the investigated angular region of $40^\circ \leq \vartheta \leq 90^\circ$ (ϑ being the center-of-mass angle) was equal to the corresponding proton-proton scattering cross sections within experimental error. This definitely pointed toward the validity of the hypothesis of the charge symmetric character of nuclear forces.

There is, however, a special interest in getting similar evidence at neutron energies where meson production processes are appreciable.

The present work, therefore, was directed at studying the elastic neutron-neutron scattering at 590 mev. The experiments were carried out at the synchrocyclotron of the Institute for Nuclear Studies of the Academy of Sciences of the USSR.

In order to establish the possibility of determining the elastic neutron-neutron scattering using experiments on neutron-deuteron scattering, we first carried out a theoretical analysis (using a nonrelativistic momentum approximation) of the processes by which high energy neutrons could interact with deuterons. This yielded formulas connecting the probability of emission of neutrons into an angle θ (θ being the laboratory scattering angle) relative to the incoming beam, with the scattering cross section of neutrons by free neutrons and protons[3].

A series of such studies have already appeared in the literature[4-7], but the majority of them have the drawback that they use a central force between the nucleons. Moreover, in several cases, there is used a radial nucleon potential even though it is well known that a unique selection of such an interaction cannot be made at the present time. This reduces the generality of the results obtained and makes desirable a similar calculation under the most general assumptions possible concerning the interactions between nucleons.

We present below calculations carried out using the same method as was used by Pomeranchuk[8] and Shmushkevich[9], but keeping the complete expressions for the nucleon-nucleon scattering amplitudes. This permits us to hope that the results obtained should be applicable over a wider angular region than was the case in previous work.

2. CALCULATION OF $(n-d)$ SCATTERING

Let $\mathbf{r}_1$, $\mathbf{r}_2$ and $\mathbf{r}_3$ be the coordinates (in the lab. system) of the incoming nucleon, of the nucleon in the deuteron with the same isotopic spin, and of the nucleon in the deuteron with the opposite isotopic spin. Let us take as a wave function (not antisymmetrized with respect to coordinates of identical particles) for the initial state the expression

$$\Psi_i = \Omega^{-1} e^{i\mathbf{k}_0\mathbf{r}_1}\Phi_0(|\mathbf{r}_2-\mathbf{r}_3|)\,\chi^i_{1,23}\,, \tag{1}$$

and for the final state

$$\Psi_f = \Omega^{-3/2}\exp\{i\mathbf{k}'\mathbf{r}_1\} \tag{2}$$
$$\times\exp\{i(\mathbf{k}_2+\mathbf{k}_3)(\mathbf{r}_2+\mathbf{r}_3)/2\}\,\Phi_f(\mathbf{r}_2-\mathbf{r}_3)\chi^f_{1,23}.$$

In these equations, Ω is the normalizing volume, Φ_0 is the wave function for the ground state of the deuteron, Φ_f is the wave function for the relative motion of particles 2 and 3 after collision, $\mathbf{k}_2$ and $\mathbf{k}_3$ are the wave vectors of these particles in the final state and $\chi^i_{1,23}$ and $\chi^f_{1,23}$ are the spin functions corresponding to the initial and final states.

We will write the pseudo-potential of the interaction between the incoming nucleon and the deuteron in the form:

$$V = (4\pi\hbar^2/m)\{A_{12}\delta(\mathbf{r}_1-\mathbf{r}_2)+A_{13}\delta(\mathbf{r}_1-\mathbf{r}_3)\}, \tag{3}$$

where A_{12} and A_{13} are the amplitudes for the scattering of the nucleon by the nucleons (in the center-of-mass system of the colliding nucleons),

$$A_{12} = \alpha_{12}+\beta\sigma_1\sigma_2+\gamma_{12}(\sigma_1+\sigma_2)\,\mathbf{n} \tag{4}$$
$$+\delta_{12}(\sigma_1\mathbf{e}_+)(\sigma_2\mathbf{e}_+)+\varepsilon_{12}(\sigma_1\mathbf{e}_-)(\sigma_2\mathbf{e}_-);$$
$$A_{13} = \alpha_{13}+\beta_{13}\sigma_1\sigma_3+\gamma_{13}(\sigma_1+\sigma_3)\,\mathbf{n}$$
$$+\lambda_{13}(\sigma_1-\sigma_3)\,\mathbf{n}+\delta_{13}(\sigma_1\mathbf{e}_+)(\sigma_3\mathbf{e}_+)$$
$$+\varepsilon_{13}(\sigma_1\mathbf{e}_-)(\sigma_3\mathbf{e}_-);$$
$$\mathbf{e}_+ = (\mathbf{k}_i+\mathbf{k}_f)/|\mathbf{k}_i+\mathbf{k}_f|;$$
$$\mathbf{e}_- = (\mathbf{k}_i-\mathbf{k}_f)/|\mathbf{k}_i-\mathbf{k}_f|;\quad \mathbf{n} = [\mathbf{k}_i\mathbf{k}_f]/|[\mathbf{k}_i\mathbf{k}_f]|.$$

The matrix element for the transition of the system from the state in which the deuteron is at rest and the incoming nucleon has the momentum $\hbar\mathbf{k}_0$, to the state where the scattered nucleon has momentum $\hbar\mathbf{k}'$, and the two nucleons move with relative momentum $\hbar\mathbf{f} = \hbar(\mathbf{k}_2-\mathbf{k}_3)/2$ can be written in the form:

$$V_{k'k_0} = (4\pi\hbar^2/m\Omega^{3/2})\{(\chi^{f*}_{1,23}A_{12}\chi^i_{1,23})\,T_1 \tag{5}$$
$$+(\chi^{f*}_{1,23}A_{13}\chi^i_{1,23})\,T_2-(\chi^f_{1,23}A_{23}\chi^i_{2,13})\,T_3\}$$
$$=(4\pi\hbar^2/m\Omega^{3/2})\{a_{12}T_1+a_{13}T_2-a_{23}T_3\},$$
$$T_1=\int\Phi^*_f(\rho)\,e^{-i\Delta\mathbf{k}\rho/2}\Phi_0(\rho)\,d\rho;$$
$$T_2=\int\Phi^*_f(\rho)\,e^{i\Delta\mathbf{k}\rho/2}\Phi_0(\rho)\,d\rho;$$
$$T_3=\int\Phi^*_f(0)\,e^{i\mathbf{k}'\rho}\Phi_0(\rho)\,d\rho;\quad \Delta\mathbf{k}=\mathbf{k}'-\mathbf{k}_0. \tag{6}$$

The cross section corresponding to this transition is equal to:

$$d\sigma(\theta) = \frac{1}{(2J_d+1)(2S+1)} \tag{7}$$
$$\times\frac{2\pi\Omega}{\hbar v}\sum_{\chi^i}\sum_{\chi^f}|V_{k'k_0}|^2\rho_E,$$
$$\rho_E = \frac{\Omega^2}{(2\pi)^3}k'^2\left(\frac{\partial k'}{\partial E}\right)do'\,\frac{d\mathbf{f}}{(2\pi)^3}$$
$$=\frac{\Omega^2}{(2\pi)^6}\,d\mathbf{f}\,\frac{m}{\hbar^2}\,\frac{k'\,do'}{1+{}^1/_2(k'-k\cos\theta)/k'};$$

where J_d is the spin of the deuteron, S is the spin of the incoming nucleon, v is the velocity of the incoming nucleon and $do' = 2\pi\sin\theta\,d\theta$.

In order to carry out further calculations it is necessary to know the actual form of the wave function $\Phi_f(\mathbf{r}_2-\mathbf{r}_3)$ of the nucleons 2 and 3 in the final state. These functions are not known at the present time and the calculations, therefore, involve some additional assumptions concerning their properties. The problem is somewhat simplified because we are primarily interested in the total intensity of neutrons scattered at a given angle; their energy spectrum, which depends on the motion and initial state of the nucleons in the deuteron before collision, has only secondary interest. For this reason, Eq. (7) must be integrated over all possible values of the relative momentum $\hbar f$ consistent with conservation laws. The integration is simplified if one keeps in mind the experimental fact that in $(p-d)$ collisions the momenta of the scattered particles in the majority of cases is little different from that which they would have in the scattering from free nucleons into the same angle[10]. For this reason we will not make a big mistake if in Eq. (7) we place $k' = k\cos\theta$, which corresponds to this situation in most cases. In this case, k', and consequently also Δk, can be considered as constant (for a given angle of scattering) independent of f.

Expanding the integral in terms with T_1 and T_2 to infinity (which makes possible the use of the completeness theorem) and evaluating the result of the integration in the region in which $|\mathbf{f}|>f_m$, where $\hbar f_m$ is the largest value of the momentum of relative motion $\hbar\mathbf{f}$ (consistent with conservation

laws), we arrive at the formula for the total cross section of $(n-d)$ scattering into an angle θ:

$$\frac{d\sigma(\theta)}{do'} = \frac{4k'}{6k_0}\{|a_{12}|^2(1-T_1') \quad (8)$$

$$+|a_{13}|^2(1-T_2') + 2\mathrm{Re}\,(a_{12}^* a_{13})(J(\theta)-J'(\theta))$$

$$+\int \frac{df}{(2\pi)^3}[|a_{23}|^2|T_3|^2 - 2\mathrm{Re}\,(a_{12}^* a_{23}^* T_1^* T_3)$$

$$-2\mathrm{Re}\,(a_{13}^* a'_{23} T_2^* T_3)]\}.$$

In this equation

$$T_1' = (2\pi)^{-3}\int\limits_{f\geqslant f_m} df\left|\int e^{-i\Delta k\rho/2}\Phi_f^*(\rho)\,\Phi_0(\rho)\,d\rho\right|^2; \quad (9)$$

$$T_2' = (2\pi)^{-3}\int\limits_{f\geqslant f_m} df\left|\int e^{i\Delta k\rho/2}\Phi_f^*(\rho)\,\Phi_0(\rho)\,d\rho\right|^2;$$

$$J(\theta) = \int e^{i\Delta k\rho}|\Phi_0(\rho)|^2\,d\rho;$$

$$J'(\theta) = (2\pi)^{-3}\int\limits_{f\geqslant f_m} df T_1^* T_2.$$

The multipliers in front of the integrals, $|a_{12}|^2$, $|a_{13}|^2$, etc., are various combinations of the coefficients α, β, γ, etc., appearing in the scattering of nucleons by free nucleons. Comparison of these multipliers with the nucleon-nucleon cross sections expressed in terms of the same parameters leads to the following relations:

$$\tfrac{1}{6}|a_{12}|^2 = [\sigma_{nn}(\vartheta)]_{\text{c.g.}}; \quad (10)$$

$$\tfrac{1}{6}|2\mathrm{Re}\,(a_{12}^* a_{13})| \leqslant [\sigma_{nn}(\vartheta) + \sigma_{np}(\vartheta)]_{\text{c.g.}};$$

$$\tfrac{1}{6}|a_{13}|^2 = [\sigma_{np}(\vartheta)]_{\text{c.g.}};$$

$$\tfrac{1}{6}|2\mathrm{Re}\,(a_{12}^* a_{23})| \leqslant 3[\sigma_{nn}(\vartheta) + \sigma_{np}(\vartheta)]_{\text{c.g.}};$$

$$\tfrac{1}{6}|a_{23}|^2 = [\sigma_{np}(\vartheta)]_{\text{c.g.}};$$

$$\tfrac{1}{6}|2\mathrm{Re}\,(a_{13}^* a_{23})| \leqslant 3[\sigma_{np}(\vartheta)]_{\text{c.g.}}.$$

The completeness theorem cannot be used for terms containing T_3; however, it is easy to see that these contribute significantly only at scattering angles close to $\pi/2$. In fact, numerical integration of the integrals $(2\pi)^3\int df|T_3|^3$ and $(2\pi)^3\int df \times T_{1(2)}^* T_3$ with the function $\Phi_f(\mathbf{r}_2-\mathbf{r}_3)$, taken either as a plane wave or as a function taking into account the interaction between nucleons 2 and 3 only in the state $l=0$ [11], shows that these integrals are sufficiently small for scattering into angles $\theta < 60°$.

A knowledge of the exact form of the function Φ_f is also necessary to evaluate the functions T_1', T_2' and $J'(\theta)$; however, in these cases the integration is carried out only in the region of large relative momenta and therefore the use of Φ_f as a plane wave appears more justified.

Thus we can write down the total $(n-d)$ scattering cross section for angles $\theta < 60°$ in the form:

$$d\sigma(\theta)/do' = 4\cos\theta\{[\sigma_{nn}(\vartheta)]_{\text{c.g.}} \quad (11)$$

$$(1-T_1') + [\sigma_{np}(\vartheta)]_{\text{c.g.}}\,(1-T_2)$$

$$+\tfrac{1}{6}[2\mathrm{Re}(a_{12}^* a_{13})]\,I(\theta)\},$$

$$I(\theta) = J(\theta) - J'(\theta).$$

The last term in the formula represents the scattering due to interference of waves scattered by the different nucleons of the deuteron. From Eq. (10), the upper limit of this scattering is given by

$$[d\sigma_{\text{int}}(\theta)/do']_{\max} = 4\cos\theta\{[\sigma_{nn}(\vartheta)]_{\text{c.g.}} \quad (12)$$

$$+[\sigma_{np}(\vartheta)]_{\text{c.g.}}\}\,I(\theta).$$

The multipliers of the terms $1-T_1'$ and $1-T_2'$ are not significantly different for angles $\theta \leq 50°$ and they decrease rapidly for larger angles. The numerical values of the functions $I(\theta)$ are given in Fig. 1 for nucleon energies of 300, 450 and 600 mev.

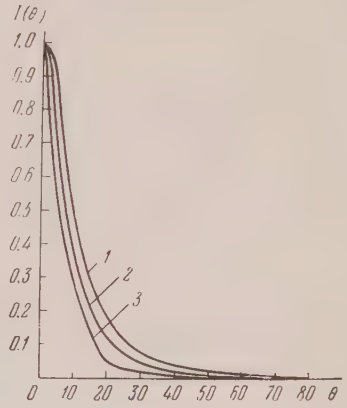

FIG. 1. Calculated values of the integral $I(\theta)$ for various neutron energies: 1 – 300, 2 – 450, 3 – 600 mev.

Even though present-day theory allows only an approximate evaluation of interference terms contributing to scattering, the result of the calculations indicates that there is a region of angles where the total $(n-d)$ scattering cross section is essentially equal to the sum of the scattering of the neutrons by free neutrons and protons. It is evident that the difference in scattering cross sections for $(n-d)$ and $(n-p)$ processes in these angle region will be equal to the scattering of neutrons by neutrons.

As already indicated, the calculation of the functions $I(\theta)$ was carried out nonrelativistically. There existed, therefore, the possibility that the inclusion of relativistic effects would contract significantly the angular region in which the calculations indicate that interference effects are important. However, since the relativistic generalization of the momentum approximation has not yet been proposed, it was decided to examine experimentally the angular region in which the scattering of nucleons by deuterons has an additive character.

3. EXPERIMENTS WITH THE PROTON BEAM

In these experiments a proton beam was scattered by D_2O, H_2O, CH_2 and C. The scattered protons were measured by a telescope consisting of three scintillation counters. In order to minimize the effect of the different energies of protons scattered by deuterons and protons, the measurements were performed with a telescope having a low energetic threshold (E_{thr} was taken close to 50 mev). Under these conditions the relative yield of protons from $(p-d)$ and $(p-p)$ scattering is practically indistinguishable from the ratio of the total cross section of $(p-d)$ scattering into the given angle to the differential $(p-p)$ cross section scattering into the same angle.

The experiments were carried out using 300 and 400 mev protons. From the measurements one obtained the ratio $[\sigma_{pd}(\theta)-\sigma_{pp}(\theta)]/\sigma_{pp}(\theta)$, which, according to the calculations, is equal to $[\sigma_{pn}(\theta)+\sigma_{int}(\theta)]/\sigma_{pp}(\theta)$. Comparison of these relations with the relative cross sections of $(n-p)$ and $(p-p)$ scatterings makes possible the determination of that angular region of scattering where $\sigma_{int}(\theta) \ll \sigma_{np}(\theta)$. The results obtained indicate that at least in the angular region

$$30^\circ \leqslant \vartheta \leqslant 90^\circ \quad \text{for} \quad E_p = 300 \text{ mev}, \qquad (13)$$
$$25^\circ < \vartheta \leqslant 90^\circ \quad \text{for} \quad E_p = 400 \text{ mev}$$

the total $(p-d)$ scattering cross section is equal to the sum of the $(p-p)$ and $(p-n)$ scatterings to within a few percent. For completeness, it would have been desirable to carry out similar experiments with protons of even higher energy. Such experiments were not carried out because of difficulties in excluding meson effects. However, the tests we did carry out indicate that the angular region of scattering where the interference processes in $(n-d)$ collisions contribute a significant part to the scattering of nucleons by nucleons decreases with increasing energy. For this reason we conclude that for neutrons having an energy of 590 mev, the region of additive scattering will be at least no narrower than for 400 mev neutrons. Therefore, the $(n-n)$ scattering can be determined for this particular region of angles ($30^\circ \leq \vartheta \leq 90^\circ$) as the difference between the scattering of neutrons by deuterons and by free protons.

4. DETERMINATION OF THE NEUTRON-NEUTRON SCATTERING CROSS SECTION

The determination of the $(n-n)$ scattering cross section was carried out by a comparison yield of high energy neutrons from $(n-d)$ and $(n-p)$ scatterings at the same angle relative to the neutron beam. For this purpose, scatterers of D_2O, H_2O, CH_2 amd C were successively interposed in the beam. The replacement of one scatterer by another was accomplished by use of a specially constructed sample changer operable from a distance, so that the accelerator did not have to be shut off during the changing process. The scattered neutrons were counted by means of a neutron telescope. This consisted of an aluminum converter, four scintillators in coincidence to register exchange protons in back of the converter, and one scintillator in front of it. The counter in front of the converter was in anti-coincidence with the others and was used to exclude charged particles arising from the scatterer. The energetic threshold of the neutron telescope was established by placing absorbers in the path of the exchange protons, and corresponded to neutrons having an energy of 470 mev. The effective energy of the incident neutrons in these experiments was 590 mev*. The monitoring of the neutron beam was carried out via a telescope T_M consisting of three scintillators placed in an auxiliary beam. The general lay-out of the experiment is given in Fig. 2.

* The energy spectrum of the neutron beam had been established earlier[12].

Establishment of the absorber thickness of the neutron telescope. In order to determine the thickness of absorber corresponding to the selected energetic threshold for the neutrons, it is necessary to know the energy spectrum of the exchange protons from the converter. The broad energy distribution of the primary neutrons and the low intensity of the beam complicate the investigation of this exchange proton spectrum and thus the comparison of it with the spectrum of the neutrons. For this reason we carried out measurements which made it possible to decide on the absorber thicknesses without a detailed knowledge of the form of the spectrum of the protons. In these experiments the telescope was placed at a certain angle relative to the neutron beam and the dependence of the counting rate of the neutrons scattered from free protons was determined as a function of the absorber thickness. The statistical accuracy of these experiments was insufficient to establish the differential spectrum of the exchange protons, but was sufficient to establish the absorber thickness needed to cut out the fastest protons, and therefore to determine their energy. On the assumption that such protons arise from the charge exchange of the highest energy neutrons we can conclude that this absorber thickness corresponds to an energetic threshold of the telescope equal to the maximum energy of neutrons scattered into this angle.

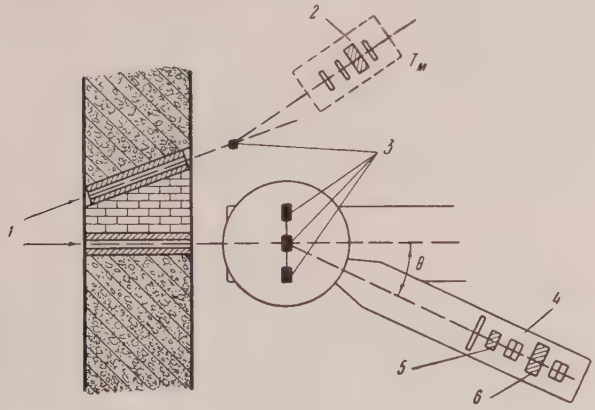

FIG. 2. Measurement of elastic $(n-n)$ scattering (plan of the experiment). *1* – neutrons, *2* – monitor, *3* – scatterers, *4* – neutron telescope, *5* – converter, *6* – absorber.

Experiments carried out at scattering angles of 30, 40 and 50° showed that under the conditions of these experiments (a polychromatic spectrum of primary neutrons, the geometrics of the converter, telescope, etc.) the magnitude of the effective relative energy loss of the neutrons upon charge exchange, Δ_{eff}, was equal to

$$(E_n(\theta)_{max} - E_p(\theta)_{max}^{eff}) / E_n(\theta)_{max} = 0.3 \pm 0.02$$

and was practically independent of the energy in the interval from 230 to 460 mev.

The value of Δ_{eff} that was found made it possible to determine, for various scattering angles, the absorber thickness corresponding to a given energy threshold for the neutrons.

Measurements. During the measurements of the differential $(n-d)$ and $(n-p)$ scattering, the neutron telescope was placed at a given angle relative to a neutron beam and for each of the scatterers the difference in counting rate with and without the converter in place was determined. The difference of the effects produced by the polyethylene and by the C is proportional to the scattering cross section of neutrons by free protons, i.e.,

$$N_{CH_2}(\theta) - N_C(\theta) = B(\theta)\,\sigma_{np}(\vartheta). \qquad (14)$$

The corresponding difference obtained by using D_2O and H_2O is proportional to the difference between the scattering cross section of neutrons by deuterons and by protons:

$$N_{D_2O}(\theta) - N_{H_2O}(\theta) = B(\theta)\,[\sigma_{nn}(\vartheta) + \sigma_{int}(\vartheta)]. \qquad (15)$$

The proportionality constants in the two cases are equal and depend on the geometry of the experiment, the efficiency of the neutron telescope and the neutron beam intensity.

In order to avoid the difficulty of determining the absolute values of these coefficients we measured merely the ratio of the values of Eqs. (14) and (15):

$$A(\theta) = [\sigma_{nn}(\vartheta) + \sigma_{int}(\vartheta)] / \sigma_{np}(\vartheta) = S(\vartheta) / \sigma_{np}(\vartheta), \qquad (16)$$

From this, using the differential cross sections for elastic $(n-p)$ scattering determined by Kazarinova and Simonova[13], at the same neutron energy, we deduce the desired quantities $S(\vartheta)$.

5. RESULTS AND DISCUSSION

The measurements were carried out for scattering angles between 30 and 90° in the center-of-mass. The results obtained are listed in the Table and presented in Fig. 3.

TABLE

$\vartheta°$	$10^{27}\sigma_{nn}(\vartheta)$, cm^2/sterad^{-1}
30	5.8±0.8
49	4.7±0.5
55	3.8±0.4
67	2.9±0.35
78	2.3±0.30
89	2.5±0.25

In view of the fact that the results of the experiments carried out in the proton beam (Sec. 3), and likewise the results of our calculations (Sec. 2) point to the additive character of the $(n-d)$ scattering at neutron energies larger than 400 mev for angles between 30 and 90°, we can conclude that the cross sections, $S(\theta)$, that we have determined at 590 mev, correspond to the elastic scattering of neutrons by free neutrons.

The most striking feature of the elastic neutron-neutron scattering which appears on going from 300 mev to 590 mev is that, like $(p-p)$ scattering, it gets to be strongly anisotropic. If the relative scattering $\sigma_{nn}(30°)/\sigma_{nn}(90°)$ is close to unity for 300 mev neutrons[1], then at 590 mev the $(n-n)$ scattering at 30° is 2.3 times higher that at 90°.

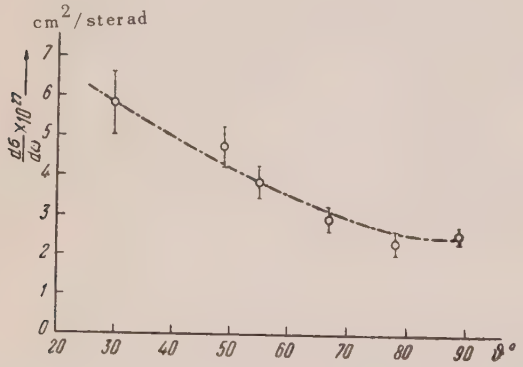

FIG. 3. Differential cross section for elastic scattering of neutrons by neutrons at 590 mev. Curve – $\sigma_{pp}(\vartheta)$ at $E_p = 590$ mev [14]; Points – $\sigma_{nn}(\vartheta)$ for $E_n = 590$ mev.

The significant anisotropy of $(n-n)$ scattering at this energy presumably reflects the increased importance of nuclear interactions in states of higher angular momentum. However, it is also possible that the anisotropy arises from the significant rise in the inelastic processes occurring when the energy is raised from 300 to 590 mev.

As is seen from Fig. 3 the differential cross section for elastic $(n-n)$ scattering at 590 mev in the angular region investigated agrees within experimental error with the corresponding $(p-p)$ scattering cross section measured by Smith *et al.* at the same energy*[14]. This fact, together with the earlier results of analogous experiments carried out with 300 mev neutrons is direct evidence for the charge symmetry of nuclear forces at high energies.

The identity of nuclear forces between two neutrons and two protons is likewise supported (within the accuracy of the experiments and electromagnetic effects) by the equality of total cross sections of $(n-d)$ and $(p-d)$ interactions at high energies[12,16]. It is obvious that, to the extent that charge symmetry of nuclear forces has been established, all known conclusions concerning the purely nuclear interactions between two protons become equally valid when applied to the interaction of neutrons with neutrons.

The comparison of the differential $(n-p)$ elastic scattering at 580 mev with the cross sections for proton-proton scattering, has been shown not to contradict the hypothesis of charge independence of nuclear forces[13]. The results of the experiments described here with neutrons make it possible to extend this conclusion to neutron-neutron scattering also.

The authors take this opportunity to express their appreciatoin to R. N. Rindin for discussion of a series of questions in the theory of $(n-d)$ scattering and to G. N. Tentiukov, I. V. Popov and L. A. Kuliukin for performing calculations.

[1] Dzhelepov, Golovin and Satarov, Dokl. Akad. Nauk SSSR 99, 943 (1954).

[2] See, e.g., J. Blatt and V. Weisskopf, *Theoretical Nuclear Physics*, 1954; R. Phillips and K. Crowe, Phys. Rev. 96, 484 (1954).

[3] B. M. Golovin, Report, Inst. Nucl. Probl. No. 259 (1955).

[4] Ta You Wu and J. Ashkin, Phys. Rev. 73, 986 (1948).

[5] R. Gluckstern and H. Bethe, Phys. Rev. 81, 761 (1951).

[6] G. Chew, Phys. Rev. 84, 710 (1951).

* Our measured σ_{nn} for $\vartheta = 30°$ and 90° agree likewise within experimental error with the corresponding $\sigma_{pp}(\vartheta)$ obtained by interpolating the curves for $\sigma_{pp}30°(E)$ and $\sigma_{pp}90°(E)$ presented in Ref. 15.

[7] Horie, Tomura and Yoshida, Progr. Theor. Phys. 8, 341 (1952).

[8] I. Ia. Pomeranchuk, J. Exptl. Theoret. Phys. (U.S.S.R.) 21, 1113 (1951).

[9] J. M. Shmushkevich, Doctoral dissertation, Leningrad Phys. Tech. Inst., 1953.

[19] Gladis, Hadley and Hess, Phys. Rev. 86, 110 (1952).

[11] R. Frank and Y. Cammel, Phys. Rev. 93, 463 (1954).

[12] Dzhelepov, Satarov and Golovin, Dokl. Akad. Nauk SSSR 104, 717 (1955).

[13] Y. M. Kazarinov and I. N. Simonov, J. Exptl. Theoret. Phys. (U.S.S.R.) 31, 177 (1956).

[14] Smith, McReynalds and Snow, Phys. Rev. 97, 1186 (1955).

[15] Meshcheriakov, Neganov, Soroko and Vzorov, Dokl. Akad. Nauk SSSR 99, 959 (1954).

[16] V. P. Dzhelepov and V. I. Moskalev, J. Exptl. Theoret. Phys. (U.S.S.R.) (in press).

Translated by A. Turkevich
39

SOVIET PHYSICS JETP VOLUME 4, NUMBER 3 APRIL, 1957

The Theory of Collisions of Electrons with Atoms

G. F. DRUKAREV
Leningrad State University

(Submitted to JETP editor May 17, 1955)
J. Exptl. Theoret. Phys. (U.S.S.R.) 31, 288-301 (August, 1956)

The collision between an electron and an arbitrary atom is considered. The wave function of the system "atom + electron" with given spin is described by the coordinate and spin functions of this system. The coordinate function of the system is constructed from the atomic and one-electron functions in such a way that it possesses in explicit form the correct symmetry properties relative to a transposition of the arguments. A system of integro-differential equations, similar to the Fock self-consistent field equations have been obtained for the one-electron coordinate functions. These equations can be transformed into integral equations. The angular variables have been separated and integral equations have been obtained for the radial one-electron functions. The integral equations can be simplified if approximate atomic functions are used. The problem is reduced to a system of Volterra integral equations which are suitable both for general investigations and for computations. An analysis of the asymptotic expressions is carried out and formulas are derived for effective cross sections.

INTRODUCTION

RECENT investigations (see, for example, Ref. 1) have revealed the unsuitability of the Born approximation (and its modification which takes exchange into account --- the method of Born-Oppenheimer) for calculation of collisions of slow electrons with atoms. Especially poor results are obtained in the calculation of the effective cross section for excitation near the threshold in those cases in which exchange effects play a role.

In a number of cases the effective excitation cross section calculated according to the Born-Oppenheimer method exceeds the theoretical limit imposed by conservation of the number of particles. For example, the effective excitation cross section of the 2S level of the hydrogen atom in the antisymmetric case (parallel spins) for 13.5 ev is twice the theoretical limit. For the excitation of the 2^3S level of helium at 22.5 ev the cross section computed according to Born-Oppenheimer is 1.1 times the theoretical limit and exceeds experimental values by a factor of 20.

In the methods of Born and Born-Oppenheimer, the interaction of the electron with the atom is considered weak, and therefore the wave function of the electron is taken in the form of a plane wave. Refinement of the methods of calculation is obtained by consideration of the perturbation of the electronic wave function by the strong field of the atom and by exchange interaction.

Representing the wave function of the system "atom + electron" in the form of a properly symmetrized sum of products of atomic and one-electron functions, and carrying out the computa-

tions based on the use of the Schrödinger equation, one can obtain a system of integro-differential equations for the one-electron functions. These equations, similar to the self-consistent field equations of V. A. Fock, describe the interaction of the electron with the atom. The simplest equations of such form for the elastic collisions of electrons with atoms of hydrogen and helium were first considered by Morse and Ellis[2] and were integrated numerically. For excitation of the $2S$ level of the hydrogen, and of the 2^1S and 2^3S levels of the helium atom, such equations were considered in the researches of Massey and Erskine[3] and Massey and Moiseiwitsch[4] which were devoted to the application of variational methods to collision problems.

In 1953 it was shown by the author[5] that the integro-differential equations of the type obtained in Refs. 2 and 3 could be transformed into a system of Volterra integral equations and a system of algebraic equations for certain constants. The integral equations to which the problem reduces are suitable both for general investigations and for computations.

In the present work we consider the general problem of the collision of an electron with an arbitrary atom or ion. An expression for the coordinate wave function of the system "electron + atom" is constructed from atomic functions and one-electron functions which possesses in explicit form the appropriate properties of symmetry relative to a transposition of arguments. In this case some results of Fock[6] are used that are concerned with the wave functions of many-electron systems. Integro-differential equations are obtained for one-electron functions. The potential energy of interaction of the electron with the atom and the exchange operator are expressed by quantities which are constructed from atomic functions according to the type of the density matrix*. Integro-differential equations are transformed into integral equations. Separation of angular quantities is carried out and integral equations for the radial functions are obtained.

In practice, the atomic wave functions are expressed approximately in the calculations in the form of a combination of products of one-electron functions. If this approximation is used, then the equations for the radial functions reduce to a system of integral equations of the Volterra type and to a system of algebraic equations.

* The general equations for the collision of electrons with an atom were also considered by Seaton[7]. However, Seaton began from a wave function system in which the spin and coordinate variables were not separated; therefore, his equations have a symbolic character.

1. THE WAVE FUNCTION OF THE SYSTEM "ATOM + ELECTRON"

Let us consider the wave function of the N-electron system $\Phi(\mathbf{r}_1\sigma_1, \ldots, \mathbf{r}_N\sigma_N)$. It must be antisymmetric relative to a permutation of any pair $(\mathbf{r}_i, \sigma_i)$ and $(\mathbf{r}_j, \sigma_j)$. Neglecting spin-orbit interaction, we can subject Φ to the condition that it be an eigenfunction of the square of the spin

$$S^2\Phi = s(s+1)\,\Phi \tag{1.1}$$

($\hbar = 1$). As Fock[6] has pointed out, the wave function Φ satisfying (1.1) can be chosen from the coordinate function $\Psi(\mathbf{r}_1 \ldots \mathbf{r}_k \,|\, \mathbf{r}_{K+1} \ldots \mathbf{r}_N)$, where

$$k = {}^1\!/_2 N - s, \tag{1.2}$$

and the spin function $\chi(\sigma_1 \ldots \sigma_k \,|\, \sigma_{k+1} \ldots \sigma_N)$ which possess definite properties of symmetry relative to permutation of the arguments. (In what follows, we shall write

$$\Psi(1\ldots k\,|\,k+1\ldots N) \text{ and } \chi(1\ldots k\,|\,k+1\ldots N)$$

in place of $\Psi(\mathbf{r}_1 \ldots \mathbf{r}_k \,|\, \mathbf{r}_{k+1} \ldots \mathbf{r}_N)$ and $\chi(\sigma_1 \ldots \sigma_k \,|\, \sigma_{k+1} \ldots \sigma_N)$, or even Ψ, χ where these would not lead to misunderstanding.)

The function Ψ is antisymmetric relative to a permutation of arguments up to or after the vertical bar; this can be described with the help of the permutation operator P_{ij} in the form

$$(1 + P_{ij})\,\Psi = 0;\ i,\ j < k \quad \text{or} \quad i,\ j > k. \tag{1.3}$$

Moreover, $\Psi(1 \ldots k \,|\, k+1 \ldots N)$ possesses the property of cyclic symmetry

$$\Big(1 - \sum_{j=k+1}^{N} P_{kj}\Big)\,\Psi = 0\,. \tag{1.4}$$

The function χ is symmetric relative to a permutation of arguments up to or after the vertical bar:

$$(1 - P_{ij})\,\chi = 0,\ i,\ j < k \quad \text{or} \quad i,\ j > k. \tag{1.5}$$

Following Fock[6], we construct the expression

$$\Phi = \left[\frac{(N-k)!k!}{N!}\right]^{1/2} \times \sum_{\lambda_1 \ldots \lambda_k} (-1)^P \Psi(\lambda_1 \ldots \lambda_k \mid \lambda_{k+1} \ldots \lambda_N) \times \chi(\lambda_1 \ldots \lambda_k \mid \lambda_{k+1} \ldots \lambda_N), \quad (1.6)$$

where $\lambda_1 \ldots \lambda_N$ is a set of N different numbers from the series $1 \ldots N$ and P is the parity of the permutation $\begin{pmatrix} 1\,2 \ldots N \\ \lambda_1 \lambda_2 \ldots \lambda_N \end{pmatrix}$.

By virtue of the properties (1.3)-(1.5) and the relations (1.2), the function (1.6) satisfies the relation (1.1) and possesses the necessary asymmetry property relative to the permutation of $(\mathbf{r}_i, \sigma_i)$ and $(\mathbf{r}_j, \sigma_j)$. The coefficient of the sum in Eq. (1.6) is introduced so that, in the normalization of Ψ and χ to unity, Φ will also be normalized to unity.

If we choose χ in the form

$$\chi = \beta_1 \ldots \beta_k \alpha_{k+1} \ldots \alpha_N, \quad (1.7)$$

where $\alpha = \delta_{\sigma,1}$, $\beta = \delta_{\sigma,-1}$ then Φ will be the eigenfunctions of the operator S_z which correspond to the eigenvalue s (i.e., the spin of the system is directed along the z axis). The function Ψ which possesses the properties (1.3) and (1.4) can be obtained by subjecting an arbitrary function of N arguments to symmetrization according to the scheme of Young pictured in the Figure (Landau and Lifshitz[8]), i.e., we first carry out symmetrization over the variables entering into a row and then alternation over the variables entering into the columns*. We shall denote such a scheme by the symbol $(k; N-K)$.

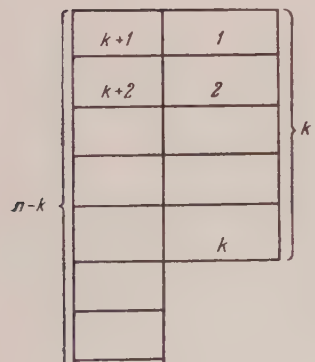

As an illustration, we consider the example of a function of three variables, symmetrized according to the scheme (1; 2). The scheme (1; 2) corresponds to the action of the operator $(1 - P_{23})(1 + P_{12})$. It is evident that by using such an operator, we obtain a function which is antisymmetric relative to the permutation of the indices 2 and 3. It is not difficult to prove further that, using the operator $(1 - P_{12} - P_{13})(1 - P_{23})(1 + P_{12})$ on an arbitrary function of three variables we obtain zero. Thus the function obtained as a result of symmetrization according to the scheme (1; 2) actually possesses the properties of symmetry which ought to be had by $\Psi(1 \mid 23)$.

We return to the problem of interest to us, namely, the construction of a coordinate function system "atom + electron" from atomic and one-electron coordinate functions. For this purpose we consider the particular case $\Psi(1 \ldots k \mid k+1 \ldots n+1)$ which is formed from the product of the functions $\psi(1 \ldots j \mid j+1 \ldots n)$ and $F(n+1)$.

We note that in the expression for Ψ there can enter only two types of function ψ:

$$\psi_1 = \psi(1 \ldots k \mid k+1 \ldots n), \quad (1.8)$$

$$\psi_2 = \psi(1 \ldots k-1 \mid k \ldots n).$$

This follows from consideration of the Young scheme. Actually, one can obtain the scheme $(k; n-k+1)$ by adding one cell either in the second column of the scheme $(k; n-k)$ or in the first column of the scheme $(k-1; n-k+1)$.

The same result follows from the rule for the addition of momenta. Actually, for a given square of the spin moment of the $(n+1)$-electron system, $s(s+1)$, there are two possible states of the n-electron system: $s_1 = s - \frac{1}{2}$ and $s_2 = s + \frac{1}{2}$. In the first case, in accord with (1.2), $j_1 = \frac{1}{2}n - (s - \frac{1}{2})$, in the second, $j_2 = \frac{1}{2}n - (s + \frac{1}{2})$. Inasmuch as $k = \frac{1}{2}(n+1) - s$, then $j_1 = k$, $j_2 = k - 1$. The expression for Ψ, which consists of the products $\psi_1 F$ and $\psi_2 F$, which satisfy the conditions (1.3) and (1.4) (for $N = n+1$), can be got by carrying out symmetrization of these products according to the Young scheme $(k; n-k+1)$ and making use of the fact that ψ_1 and ψ_2 were already symmetrized according to the schemes $(k; n-k)$ and $(k-1; n-k+1)$.

However, this leads to cumbersome calculations; therefore, we proceed otherwise: we set up the

* This circumstance was brought out as a result of discussions with Iu. N. Demkov.

expressions*

$$\Psi_1 = \sum_{j=k+1}^{n+1} a_i P_{i,n+1}\psi_1(1\ldots k\,|\,k+1\ldots n) \qquad (1.9)$$

$$\times F(n+1);$$

$$\Psi_2 = \sum_{t=1}^{k}\sum_{i=k}^{n+1} b_{t,i}P_{t,k}P_{i,n+1} \qquad (1.10)$$

$$\times\psi_2(1\ldots k-1\,|\,k\ldots n)\,F(n+1)$$

and we determine the coefficients a_i and $b_{t,i}$ so that Ψ_1 and Ψ_2 satisfy Eqs. (1.3) and (1.4).

We note that all the calculations necessary for the determination of a_i and $b_{t,i}$ can be put in compact form if we make use of the "permutation relations"

$$P_{ab}P_{bc} = P_{ac}P_{ab} = P_{bc}P_{ac}. \qquad (1.11)$$

We shall not carry out the calculations here, but shall at once write the result:

$$\Psi_1 = \Big(1 - \sum_{i=k+1}^{n} P_{i,n+1}\Big)\psi_1 F, \qquad (1.12)$$

$$\Psi_2 = \Big(1 - \sum_{t=1}^{k-1} P_{t,k}\Big)\Big(1 - \sum_{i=k+1}^{n} P_{i,n+1} + (n-2k+2)\,P_{k,n+1}\Big)\psi_2 F.$$

It is shown in Appendix I that (1.12) satisfy the conditions (1.3)- (1.4). From (1.12), in particular for $n = 1$, we get

$$\Psi(|\,12) = \psi(1)\,F(2) - \psi(2)\,F(1), \qquad (1.12a)$$

$$\Psi(1\,|\,2) = \psi(1)\,F(2) + \psi(2)\,F(1), \qquad (1.12b)$$

for $n = 2$

$$\Psi_1(1\,|\,23) = \psi(1\,|\,2)\,F(3) - \psi(1\,|\,3)\,F(2), \qquad (1.12c)$$

$$\Psi_2(1\,|\,23) = \psi(|\,1\,2)\,F(3) - \psi(|\,13)\,F(2) + 2\psi(|3\,2)\,F(1).$$

* It is understood that application of the permutation operator to the product of two functions obeys the rule $P_{ab}(fg) = (P_{ab}f)(P_{ab}g)$.

On the basis of the result (1.12) we now construct the coordinate function of the system "atom + electron." Let ψ_{A1} and ψ_{A2} be atomic coordinate functions; the indices A show the value of the energy, the orbital momentum and its projection on the z axis. (1) and (2) have the same meaning as above. We can then write

$$\Psi = \sum_A \Big(1 - \sum_{i=k+1}^{n} P_{i,n+1}\Big)\psi_{A1}F_{A1} \qquad (1.13)$$

$$+ \sum_A \Big(1 - \sum_{t=1}^{k-1} P_{t,k}\Big)\Big(1 - \sum_{i=k+1}^{n} P_{i,n+1} + (n-2k+2)\,P_{k,n+1}\Big)\psi_{A2}F_{A2}.$$

We note that in this case, if $\psi_{A\ 1,2}$ are expressed approximately by the product of one-electron functions (or are themselves one-electron functions) we can carry out the transformation

$$F_{Aa} \to F'_{Aa} + \xi_{Aa} \quad (a = 1, 2) \qquad (1.14)$$

in (1.13), which does not change Ψ essentially. Thus, for $\Psi(|\,12)$,

$$\xi_A = \sum_{A'} B_{AA'}\psi_{A'}, \qquad (1.15)$$

where $B_{AA'}$ are constants which satisfy the condition $B_{AA'} = B_{A'A}$ but are otherwise arbitrary. For $\Psi(1\,|\,2)\,\xi_A$ also has the form (1.15), but the constants $B_{AA'}$ will satisfy the condition $B_{AA'} = -B_{A'A}$.

If, in the expression for $\Psi(1\,|\,23)$ we take ψ_{A1} and ψ_{A2} in the form

$$\psi_{A1,2} = [V_A(1)\,W_A(2) \pm V_A(2)\,W_A(1)], \qquad (1.16)$$

then

$$\xi_{A1} = \sum_{A'}(C_{AA'}V_{A'} + D_{AA'}W_{A'}), \qquad (1.17)$$

$$\xi_{A2} = \frac{1}{3}\sum_{A'}(D_{A'A}W_{A'} - C_{AA'}V_{A'}),$$

where $C_{AA'}$ and $D_{AA'}$ are arbitrary constants.

2. EQUATIONS FOR THE FUNCTIONS F_{Aa}

To derive the equations determining the functions

F_{Aa}, we shall start out with the equation

$$(H - E)\Psi = 0. \tag{2.1}$$

Multiplying (2.1) by $\psi^*_{Aa} d\tau$, where $a = 1, 2$; $d\tau = d\mathbf{r}_1, \ldots d\mathbf{r}_n$, and integrating, we get

$$\int \psi^*_{Aa} (H - E)\Psi \, d\tau = 0. \tag{2.2}$$

If Ψ is expressed approximately by a finite number of atomic functions, so that the number totaled in the sum (1.13) is finite, then (2.1) is not satisfied. In this case we shall consider that Ψ no longer satisfies (2.1), but satisfies Eq. (2.2) as before.

The energy operator H has the form (in atomic units)

$$H = H_0(\mathbf{r}_1 \ldots \mathbf{r}_n) - {}^1/_2\Delta_{n+1} + U(\mathbf{r}_1 \ldots \mathbf{r}_{n+1}). \tag{2.3}$$

Here H_0 is the energy operator of the n-electron system; U is the interaction operator of the $(n+1)$-electron with the n-electron system and with the nucleus, and is defined by the expression

$$U = -\frac{z}{\mathbf{r}_{n+1}} + \sum_{i=1}^{n} \frac{1}{|\mathbf{r}_{n+1} - r_i|}. \tag{2.4}$$

We substitute (1.13), (2.3) and (2.4) in (2.2). We note that the functions ψ_{Aa} satisfy the equation

$$H_0 \psi_{Aa} = E_{Aa} \psi_{Aa} \tag{2.5}$$

and the normalization condition

$$\int \psi^*_{Aa} \psi_{A'a'} d\tau = \delta_{AA'} \delta_{aa'}. \tag{2.6}$$

Carrying out a transformation based on the use of the symmetry properties of ψ_{Aa}, we obtain the following system of equations:

$$(\Delta + k^2_{Aa}) F_{Aa}(\mathbf{r}) = 2 \sum_{A'} U_{AA'a} F_{A'a} + \sum_{A'a'} \mathcal{A}_{AA'aa'} [F_{A'a'}(\mathbf{r}')]. \tag{2.7}$$

Here $U_{AA'a} = \int \psi^*_{Aa} U \psi_{A'a} d\tau$ is the matrix of the potential energy of interaction: $k^2_{Aa} = 2(E - E_{Aa})$; $\mathcal{A}$ is the exchange operator:

$$\mathcal{A}_{AA'aa'} [F_{A'a'}(r_{n+1})] = \int \psi^*_{Aa} [p_{aa'} P_{1, n+1} + q_{aa'} P_{n, n+1}] [\Delta + k^2_{A'a'} - 2U] \psi_{A'a'} F_{A'a'} \, d\tau, \tag{2.8}$$

where $p_{aa'}$ and $q_{aa'}$ are equal to

$$p_{11} = p_{12} = p_{21} = 0; \tag{2.9}$$

$$p_{22} = (k-1)(n - 2k + 3)/(n - 2k + 2);$$

$$q_{11} = (n - k); \quad q_{12} = k(n - k)(n - 2k + 3);$$

$$q_{21} = (n - k)(n - k + 1)/(n - 2k + 2);$$

$$q_{22} = -(n - k + 1)/(n - 2k + 2).$$

Taking into account the explicit expression (2.4) for U, making use of the symmetry properties of ψ_{Aa} and the self-conjugate property of the operator Δ, we can put the potential energy matrix and the exchange operator in the form

$$U_{AA'a} = \left[-\frac{z}{r} \delta_{AA'} + \int \frac{\rho_{AA'a}(\mathbf{r}')}{|\mathbf{r} - \mathbf{r}'|} \, d\mathbf{r}' \right]; \tag{2.10}$$

$$\mathcal{A}_{AA'aa'} [F_{A'a'}(\mathbf{r}')] = \int W_{AA'aa'}(\mathbf{r}', \mathbf{r}) F_{A'a'}(\mathbf{r}') \, d\mathbf{r}', \tag{2.11}$$

$$W_{AA'aa'}(\mathbf{r}', \mathbf{r}) = \left(\Delta' + k^2_{A'a'} + \frac{2z}{r'} - \frac{2}{|\mathbf{r} - \mathbf{r}'|} \right) \rho_{AA'aa'}(\mathbf{r}', \mathbf{r}) - 2 \int \rho_{AA'aa'}(\mathbf{r}'', \mathbf{r}', \mathbf{r}) / |\mathbf{r}' - \mathbf{r}''| \, d\mathbf{r}''. \tag{2.12}$$

$\rho_{AA'a}(\mathbf{r}')$, $\rho_{AA'aa'}(\mathbf{r}', \mathbf{r})$, $\rho_{AA'aa'}(\mathbf{r}'', \mathbf{r}', \mathbf{r})$ are expressions composed according to the type of the density matrix and having a rather cumbersome form. The explicit form is derived in Appendix II. Making use of the expression (2.11) for the exchange operator, and setting

$$2U_{AA'a} = V_{AA'a}, \tag{2.13}$$

we get Eq. (2.10) in the form

$$(\Delta + k^2_{Aa}) F_{Aa} = \sum_{A'} V_{AA'a} F_{A'a} + \sum_{A'a'} \int W_{AA'aa'}(\mathbf{r}', \mathbf{r}) F_{A'a'}(\mathbf{r}') \, d\mathbf{r}'. \tag{2.14}$$

3. TRANSFORMATION TO INTEGRAL EQUATIONS. SEPARATION OF THE ANGULAR VARIABLES

We transform the set of integro-differential equations (2.14) to a set of integral equations. For this

purpose, in the case of the collision of an electron with a neutral atom we make use of the Green's function

$$G_{Aa}(\mathbf{r}, \mathbf{r}') = \frac{\exp(ik_{Aa}|\mathbf{r}-\mathbf{r}'|)}{4\pi|\mathbf{r}-\mathbf{r}'|},$$

which satisfies the equation

$$(\Delta + k_{Aa}^2) G_{Aa}(\mathbf{r}, \mathbf{r}') = -\delta(\mathbf{r}-\mathbf{r}').$$

In the case of the collision of an electron with an ion of charge z_0, we must choose a Green's function which possesses the specific asymptoticity of the wave functions of the continuous spectrum of the Coulomb field. This condition is satisfied by G_{Aa} which is defined by the equation

$$(\Delta + k_{Aa}^2 + z_0/r) G_{Aa}(\mathbf{r}, \mathbf{r}') = -\delta(\mathbf{r}-\mathbf{r}').$$

In order to consider both cases at once, we write

$$(\Delta + k_{Aa}^2 - V_0(r)) G_{Aa}(\mathbf{r}, \mathbf{r}') = -\delta(\mathbf{r}-\mathbf{r}'); \quad (3.1)$$

$V_0 = 0$ or $-z_0/r$.

We are interested in the F_{Aa} which possesses as an asymptotic expression (for large r)

$$F_{Aa} \sim \exp(i\mathbf{k}_{Aa}\mathbf{r})\,\delta_{AA_0}\delta_{aa_0} + q_{Aa} r^{-1} \exp(ik_{Aa}r) \quad (3.2)$$

or, in the case of a collision with an ion,

$$F_{Aa} \sim \exp i[\mathbf{k}_{Aa}\mathbf{r} + \gamma \ln(\mathbf{k}_{Aa}\mathbf{r} - k_{Aa}r)] + q_{Aa} r^{-1} \exp i(k_{Aa}r + \gamma \ln 2k_{Aa}r); \quad \gamma = z_0/k_{Aa}. \quad (3.3)$$

Taking (2.14) and (3.2)–(3.3) into account, we get

$$F_{Aa}(\mathbf{r}) = \varphi_{Aa}(r)\,\delta_{AA_0}\delta_{aa_0} - \sum_{A'} \int [V_{AA'a}(\mathbf{r}') - V_0(r')\,\delta_{AA'}] \times G_{Aa}(\mathbf{r}, \mathbf{r}')\, F_{A'a}(\mathbf{r}')\, d\mathbf{r}' - \sum_{A'a'} \int G_{Aa}(\mathbf{r}, \mathbf{r}')\, d\mathbf{r}' \times \int W_{AA'aa'}(\mathbf{r}'', \mathbf{r}')\, F_{A'a'}(\mathbf{r}'')\, d\mathbf{r}'', \quad (3.4)$$

where φ_{Aa} is a regular solution of the equation

$$\Delta\varphi_{Aa} + (k_{Aa}^2 - V_0(r))\,\varphi_{Aa} = 0. \quad (3.5)$$

For $V_0 = 0$,

$$\varphi_{Aa} = \exp(i\mathbf{k}_{Aa}\mathbf{r}). \quad (3.6)$$

For $V_0 = -z_0/r$, φ_{Aa} has the asymptotic form

$$\varphi_{Aa} \sim \exp[i\mathbf{k}_{Aa}\mathbf{r} + \gamma \ln(\mathbf{k}_{Aa}\mathbf{r} - k_{Aa}r)]. \quad (3.7)$$

$$+ q_{Aa}^{(0)} r^{-1} \exp i(k_{Aa}r + \gamma \ln 2k_{Aa}r),$$

$q_{Aa}^{(0)}$ is the scattering amplitude in a Coulomb field.

Changing the order of integration in the latter integral of Eq. (3.4), and assuming

$$K_{AA'aa'}(\mathbf{r}, \mathbf{r}') = -G_{Aa}(\mathbf{r}, \mathbf{r}')\,[V_{AA'a}(\mathbf{r}') - V_0(r')\,\delta_{AA'}]\,\delta_{aa'} - \int G_{Aa}(\mathbf{r}, \mathbf{r}'')\, W_{AA'aa'}(\mathbf{r}', \mathbf{r}'')\, d\mathbf{r}'', \quad (3.8)$$

we get a system of integral equations

$$F_{Aa}(\mathbf{r}) = \varphi_{Aa}(\mathbf{r})\,\delta_{AA_0}\delta_{aa_0} + \sum_{A'a'} \int K_{AA'aa'}(\mathbf{r}, \mathbf{r}')\, F_{A'a'}(\mathbf{r}')\, d\mathbf{r}'. \quad (3.9)$$

We go on to the spherical system of coordinates and carry out a separation of the angular variables. We shall assume that the center of the coordinate system lies in the nucleus, while the Z axis is directed along the electron stream, incident on the atom. We expand F_{Aa}, φ_{Aa} and G_{Aa} in the spherical harmonics $Y_{lm}(\theta, \varphi)$, normalized to unity,

$$F_{Aa} = \sum_l a_l r^{-1} f_{Aal}(r)\, Y_{lm}(\theta, \varphi), \quad a_l = [4\pi(2l+1)]^{1/2} i^l; \quad (3.10)$$

$$\varphi_{Aa}(\mathbf{r}) = \sum_l a_l r^{-1} u_{Aal}(r)\, Y_{l,0}(\theta). \quad (3.11)$$

In the expansion of (3.10), the summation is not carried out over m. By virtue of the conservation of the Z component of the momentum of the system "atom + electron", the dependence of F_{Aa} on the angle φ is determined by the dependence of ψ_{Aa} on φ implicit in the index A. The functions u_{Aal} satisfy the equation

$$\frac{d^2u_{Aal}}{dr^2}+\left(k_{Aa}^2-\frac{l(l+1)}{r^2}-V_0\right)u_{Aal}=0, \quad (3.12)$$

where $u_{Aal}(0)=0$. For $V_0=0$:

$$u_{Aal}=(\pi r/2k_{Aa})^{1/2}J_{l+1/2}(k_{Aa}r).$$

For $V_0=-z_0/r$: $r^{-1}u_{Aal}$ is a regular radial function of the Coulomb field. Further,

$$G_{Aa}(\mathbf{r},\ \mathbf{r}') \quad (3.13)$$

$$=\sum_{lm}(rr')^{-1}\Gamma_{Aal}(r,\ r')\,Y_{lm}(\theta,\ \varphi)\,Y^*_{lm}(\theta',\ \varphi'),$$

Γ_{Aal} is a one-dimensional Green's function which satisfies the equation

$$\left(\frac{d^2}{dr^2}+k_{Aa}^2-\frac{l(l+1)}{r^2}-V_0\right)\Gamma_{Aal}(r,\ r') \quad (3.14)$$

$$=-\delta(r-r').$$

As is well known, this function can be expressed by u_{Aal} and the second independent solution of Eq. (3.12), which we denote by v_{Aal}:

(3.15)

$$\Gamma_{Aal}(r,\ r')=\begin{cases}-u_{Aal}(r)\,v_{Aal}(r')/w & \text{for } r\leqslant r'\\ -u_{Aal}(r')\,v_{Aal}(r)/w & \text{for } r\geqslant r'\end{cases}$$

$w\{u_{Aal};\ v_{Aal}\}$ is the Wronski determinant.

Corresponding to the asymptotic expressions (3.2)-(3.3), v_{Aal} ought to have the form of a diverging wave for $r\to\infty$. We choose v_{Aal} so that $w=1$. For $V_0=0$, we have

$$v_{Aal}=i^{-l}\left(\frac{\pi}{2}k_{Aa}r\right)^{1/2}H^{(1)}_{l+1/2}(k_{Aa}r).$$

We introduce the notation

$$V_{\omega\omega'}(r') \quad (3.16)$$

$$=\int Y^*_{lm}(\theta',\varphi')\,V_{AA'a}(\mathbf{r}')\,Y_{l'm'}(\theta'\varphi')d\Omega'\delta_{aa'},$$

$$W_{\omega\omega'}(r',\ r'')=r'r''\int Y^*_{lm}(\theta''\varphi'')$$

$$\times W_{AA'aa'}(\mathbf{r}',\ \mathbf{r}'')\,Y_{l'm'}(\theta'\varphi')\,d\Omega'd\Omega'',$$

where $\omega=(Aal)$. Because of the presence of the term $|\mathbf{r}-\mathbf{r}'|^{-1}$ in (2.12), $W_{\omega\omega'}(r,\ r')$ will have a different form for $r\leqq r'$ and $r\geqq r'$. In order to consider this circumstance, we shall write $W^{(1)}_{\omega\omega'}(r',\ r'')$ for $r'\leqq r''$ and $W^{(2)}_{\omega\omega'}(r',\ r'')$ for $r'\geqq r''$. Further, let us set

$$S_{\omega\omega'}(r,\ r')=[v_\omega(r)\,u_\omega(r') \quad (3.17)$$

$$-v_\omega(r')\,u_\omega(r)]\,[V_{\omega\omega'}(r')-V_0(r')\,\delta_{\omega\omega'}]$$

$$+\int_{r'}^{r}[v_\omega(r)\,u_\omega(r'')-v_\omega(r'')\,u_\omega(r)]$$

$$\times[W^{(1)}_{\omega\omega'}(r',\ r'')-W^{(2)}_{\omega\omega'}(r',\ r'')]\,dr'';$$

(3.18)

$$T_{\omega\omega'}(r,\ r')$$

$$=\int_0^r[v_\omega(r)\,u_\omega(r'')-v_\omega(r'')\,u_\omega(r)]\,W^{(2)}_{\omega\omega'}(r',\ r'')\,dr'',$$

$$c_\omega=\delta_{AA_0}\delta_{aa_0}+\sum_{\omega'}\int_0^\infty N_{\omega\omega'}(r')\,f_{\omega'}(r')\,dr', \quad (3.19)$$

$$N_{\omega\omega'}(r')=v_\omega(r')\,[V_{\omega\omega'}(r')-V_0(r')\,\delta_{\omega\omega'}]$$

$$+\int_0^\infty W_{\omega\omega'}(r',\ r'')\,v_\omega(r'')\,dr''.$$

(We note that $S_{\omega\omega'}$ and $T_{\omega\omega'}$ do not change under the transformation

$$v_\omega\to\lambda v_\omega+\mu u_\omega;\ \ u_\omega\to\lambda^{-1}u_\omega,$$

where λ and μ are constants.)

With the help of (3.17)–(3.19) we obtain*

$$f_\omega(r)=c_\omega u_\omega(r) \quad (3.20)$$

$$+\sum_{\omega'}\int_0^r S_{\omega\omega'}(r,\ r')\,f_{\omega'}(r')\,dr'$$

$$+\sum_{\omega'}\int_0^\infty T_{\omega\omega'}(r,\ r')\,f_{\omega'}(r')\,dr'.$$

* The integrals entering into (3.17)-(3.19) converge. The convergence is guaranteed by the behavior of V_0, $V_{\omega\omega'}$ and $W_{\omega\omega'}$ for large values of their arguments, and also by the fact the expressions of the type $V_{\omega\omega'}(r)\,v_\omega(r)\,f\omega(r)$ and $W_{\omega\omega'}(r',\ r)\,v_\omega(r)$ are finite for $r\to 0$.

Equation (3.20) can be simplified in this case if the wave functions of the atom, ψ_{Aa}, are approximated by one-electron wave functions. Then $W_{\omega\omega'}$ will be expressed in the form of the sum of products of functions of r' and functions of r''. Consequently, $T_{\omega\omega'}$ will have the form

$$T_{\omega\omega'}(r,\ r') = \sum_i R_{\omega\omega' i}(r)\, Q_{\omega\omega' i}(r'). \qquad (3.21)$$

For simplification of the calculation, we consider the case in which only one term enters into the sum over i in (3.21). Generalization to the case of several terms is trivial.

Substituting Eq. (3.21) in Eq. (3.20), and assuming

$$c_{\omega\omega'} = \int_0^\infty Q_{\omega\omega'}(r')\, f_{\omega'}(r')\, dr', \qquad (3.22)$$

we put Eq. (3.20) in the form

$$f_\omega(r) = c_\omega u_\omega(r) + \sum_{\omega'} c_{\omega\omega'} R_{\omega\omega'}(r) \qquad (3.23)$$

$$+ \sum_{\omega'} \int_0^r S_{\omega\omega'}(r,\ r')\, f_{\omega'}(r')\, dr'.$$

We now pass over from unknown f to the new unknown x by means of a linear transformation

$$f_\omega = \sum_{\omega'} c_{\omega'} x_{\omega\omega'}(r) + \sum_{\omega'\omega''} c_{\omega'\omega''} x_{\omega\omega'\omega''}(r). \qquad (3.24)$$

Substituting (3.23) into (3.24), we get a system of Volterra integral equations

$$x_{\omega\omega'\omega''} = R_{\omega'\omega''}\delta_{\omega\omega'} \qquad (3.25)$$

$$+ \sum_{\omega'''} \int_0^r S_{\omega\omega'''}(r,\ r')\, x_{\omega'''\omega'\omega''}(r')\, dr',$$

$$x_{\omega\omega'} = u_\omega \delta_{\omega\omega'} + \sum_{\omega''} \int_0^r S_{\omega\omega''}(r,\ r')\, x_{\omega''\omega'}(r')\, dr'.$$

As is seen from (3.25), the system of equations for $x_{\omega\omega'}$ and $x_{\omega\omega'\omega''}$ is developed in a series of independent subsystems.

If the system of equations (3.25) is solved, then we can determine the unknown constants c_ω and $c_{\omega\omega'}$. For this purpose, we must substitute the values of $x_{\omega\omega'}$ and $x_{\omega\omega'\omega''}$ which have been found, in Eq. (3.24), and substitute the resultant expression in (3.19) and (3.22). A system of algebraic equations in c_ω and $c_{\omega\omega'}$ is obtained:

$$\sum_{\omega''} c_{\omega''} L_{\omega\omega'\omega''} \qquad (3.26)$$

$$+ \sum_{\omega''\omega'''} c_{\omega''\omega'''}\left(L_{\omega\omega'\omega''\omega'''} - \delta_{\omega''\omega}\delta_{\omega'''\omega'}\right) = 0;$$

$$\sum_{\omega''} c_{\omega''}\left[M_{\omega\omega''} - \delta_{\omega''\omega}\right]$$

$$+ \sum_{\omega''\omega'''} c_{\omega''\omega'''} M_{\omega\omega''\omega'''} + \delta_{AA_0}\delta_{aa_0} = 0;$$

where

$$L_{\omega\omega'\omega''} = \int_0^\infty Q_{\omega\omega'} x_{\omega'\omega''} dr; \qquad (3.27)$$

$$L_{\omega\omega'\omega''\omega'''} = \int_0^\infty Q_{\omega\omega'} x_{\omega'\omega''\omega'''} dr;$$

$$M_{\omega\omega''} = \sum_{\omega'} \int_0^\infty N_{\omega\omega'} x_{\omega'\omega''} dr;$$

$$M_{\omega\omega''\omega'''} = \sum_{\omega'} \int_0^\infty N_{\omega\omega'} x_{\omega'\omega''\omega'''} dr.$$

We note that some of the quantities c_ω and $c_{\omega\omega'}$ can be equated to zero in certain cases. Actually, at the end of Sec. 1, it was pointed out that in the use of approximate expressions of ψ_{Aa} in terms of one-electron functions, we can change F_{Aa}, leaving unchanged the wave function of the entire system. This possibility can be used to impose on f_ω the additional condition of orthogonality to some of the $N_{\omega\omega'}$ or the $Q_{\omega\omega'}$. The number of these additional conditions depends on the spin of the system and also on the number of different one-electron functions used in the calculation.

4. ASYMPTOTIC EXPRESSIONS. EFFECTIVE CROSS SECTIONS.

Let us consider the asymptotic expressions for F_{Aa} [(3.2) and (3.3)]. We represent q_{Aa} in the form

$$q_{Aa} = \sum_l i^{-l} a_l q_{Aal} Y_{lm}(\theta, \varphi). \qquad (4.1)$$

The quantities q_{Aal} can be expressed by integrals containing the functions $x_{\omega\omega'}$ and $x_{\omega\omega' w''}$.

For this purpose we consider the integral equations (3.20). Taking into account (3.17)-(319.) and (3.23), we can write, for large r:

$$f_\omega(r) \sim u_\omega(r)\,\delta_{AA_0}\delta_{aa_0} + B_\omega v_\omega(r); \quad (4.2)$$

where

$$B_\omega = \sum_{\omega''} c_{\omega''} \int_0^\infty \sum_{\omega'} \mathcal{E}_{\omega\omega'} x_{\omega'\omega''}\, dr' \quad (4.3)$$

$$+ \sum_{\omega''\omega'''} c_{\omega''\omega'''} \int_0^\infty \sum_{\omega'} \mathcal{E}_{\omega\omega'} x_{\omega'\omega''\omega'''}\, dr';$$

$$\mathcal{E}_{\omega\omega'}(r') = u_\omega(r')\,(V_{\omega\omega'} - V_0\delta_{\omega\omega'}) + \int_0^\infty u_\omega(r'')\, W_{\omega\omega'}(r', r'')\, dr''.$$

For $V_0 = 0$, the asymptotic expressions for u_ω and v_ω have the form:

$$u_\omega \sim k_{Aa}^{-1} \sin(k_{Aa}r - l\pi/2), \qquad v_\omega \sim -\exp i(k_{Aa}r - l\pi/2). \quad (4.4)$$

Consequently,

$$q_\omega = -B_\omega. \quad (4.5)$$

For $V_0 = -z_0/r$, the asymptotic expressions for u_ω and v_ω will be

$$u_\omega \sim k_{Aa}^{-1} e^{i\eta_\omega} \sin\left(k_{Aa}r - \frac{l\pi}{2} + \eta_\omega + \gamma \ln 2k_{Aa}r\right), \quad (4.6)$$

$$v_\omega \sim -\exp i\left(k_{Aa}r - \frac{l\pi}{2} + \gamma \ln 2k_{Aa}r\right),$$

where $\eta_\omega = \arg\Gamma(l + 1 - i\gamma)$. Then we get for q_ω

$$q_\omega = q_\omega^{(0)}\delta_{AA_0}\delta_{aa_0} - B_\omega. \quad (4.7)$$

We now return to the asymptotic behavior of the wave function of the system "electron + atom", when any of the large r are large, for example, r_{n+1}.

We substitute (1.13) in (1.6) and make use of Eq. (1.7) for χ. (Consequently, we consider the spin of the system directed along z.) In view of the presence of transformation operators, there enter into the expression for Φ [in addition to terms $\psi_{Aa}F_{Aa}(\mathbf{r}_{n+1})$] terms in which the argument r_{n+1} enters into ψ_{Aa}. If we now let $r_{n+1} \to \infty$, then the terms, in which the ψ_{Aa} belonging to the discrete spectrum contain r_{n+1}, disappear. Similar terms, in which ψ_{Aa} belong to a continuous spectrum, remain finite but will play no role whatever in the following. Therefore, considering Φ for large r_{n+1}, we take into consideration only those terms in which r_{n+1} enters into F_{Aa}.

Carrying out some transformations and neglecting the factor in front of Φ, which is not essential in what follows, we get

$$\Phi \sim \sum_A \Phi_{A1} F_{A1}(\mathbf{r}_{n+1})\,\alpha_{n+1} + k^{1/2} \sum_A \Phi'_{A_2} F_{A_2}(\mathbf{r}_{n+1})\,\alpha_{n+1} - (n - 2k + 2)\,k^{1/2}(n - k + 1)^{-1/2} \times \sum_A \Phi_{A2} F_{A2}(\mathbf{r}_{n+1})\,\beta_{n+1}. \quad (4.9)$$

Here Φ_{A1} is the atomic wave function with spin $s - 1/2$, composed, according to (1.6), of ψ_{A1} and $\chi = \beta_1 \ldots \beta_k \alpha_{k+1} \ldots \alpha_n$, Φ_{A2} is the atomic wave function with spin $s + 1/2$, composed, by (1.6), of ψ_{A2} and $\chi = \beta_1 \ldots \beta_{k-1}\alpha_k \ldots \alpha_n$, Φ'_{A2} is composed also of ψ_{A2}, but χ in this case has the form

$$\chi = (n - k + 1)^{-1/2} \times \left(1 + \sum_{j=k+1}^{n} P_{k,j}\right)\beta_1 \ldots \beta_k \alpha_{k+1} \ldots \alpha_n. \quad (4.10)$$

Φ'_{A2} corresponds to the spin $s + 1/2$, but the value of the projection of the spin on the Z axis for this function is equal not to $s + 1/2$ but to $s - 1/2$. Substituting the asymptotic expressions (3.2) or (3.3) for F_{Aa} in (4.9), calculating the vector current and summing over the spins, we can obtain, in the usual way, the expressions for the effective cross sections.

We now consider, as an example, the case of the collision of an electron with an atom which has spin 0 before collision.

Taking (1.2) into consideration, and omitting the index $n + 1$, we get from (4.9):

$$\Phi \sim \Phi_{A_0 1}\exp(i\mathbf{k}_{A_0 1}\mathbf{r})\,\alpha + \sum_A \Phi_{A1} q_{A1} r^{-1}\exp(ik_{A1}r)\,\alpha + \left(\frac{n}{2}\right)^{1/2}\sum_A \Phi'_{A2} q_{A2} r^{-1}\exp(ik_{A2}r)\,\alpha - 2\left(\frac{n}{n+2}\right)^{1/2} \times \sum_A \Phi_{A2} q_{A2} r^{-1}\exp(ik_{A2}r)\,\beta. \tag{4.11}$$

Hence, the differential effective cross section of collision with no change in the spin of the atom is

$$d\sigma_{A1,A_0 1} = (k_{A1}/k_{A_0 1})\,|q_{A1}|^2\,d\Omega, \tag{4.12}$$

but with a change in the value of the spin of the atom,

$$d\sigma_{A2,A_0 1} = (k_{A2}/k_{A_0 1})\,[n/2 + 4n/(n+2)]\,|q_{A2}|^2\,d\Omega.$$

If the atom had spin differing from zero before the collision, say, s_0, then there would be two possible values of the spin of the system: $s = s_0 + \frac{1}{2}$ and $s = s_0 - \frac{1}{2}$. Therefore, there are two different problems. In the first of these the initial state of the atom is described by the functions $\Phi_{A_0 1}$, in the other, by the functions $\Phi_{A_0 2}$.

In order to obtain the observed cross section, we must carry out an averaging over the spins.

I express my gratitude for discussions to V. A. Fock and Iu. N. Demkov.

APPENDIX I

We show that the expressions Ψ_1 and Ψ_2 satisfy the conditions (1.3)-(1.4). Let us first consider Ψ_1.

1. *Condition of antisymmetry up to the vertical bar* is evidently satisfied, inasmuch as the arguments in Ψ_1 and ψ_1 are identical up to the bar.

2. *Antisymmetry after the bar.* We apply the operator $(1 + P_{i,j})$. Making use of Eq. (1.11), we get

$$(1+P_{i,j})\Psi_1 = \begin{cases} \left(1 - \sum_{l=k+1}^{n} P_{l,n+1}\right)(1+P_{i,j})\,\psi_1 F & \text{for } i,j \neq n+1, \\ -\sum_{i\neq l} P_{i,n+1}(1+P_{i,l})\,\psi_1 F & \text{for } j = n+1, \end{cases} \tag{1}$$

which vanishes since $(1 + P_{i,l})\,\psi_1 = 0$.

3. *Condition of cyclic symmetry.* Making use of (1.11), we can show that

$$\left(1 - \sum_{j=k+1}^{n+1} P_{k,j}\right)\left(1 - \sum_{i=k+1}^{n} P_{i,n+1}\right) = \left(1 - \sum_{j=k}^{n} P_{k,j}\right)\left(1 - \sum_{i=k-1}^{n} P_{k,i}\right), \tag{2}$$

inasmuch as

$$\left(1 - \sum_{i=k+1}^{n} l_{k,i}\right)\psi_1 = 0,$$

consequently,

$$\left(1 - \sum_{j=k+1}^{n+1} P_{k,j}\right)\Psi_1 = 0.$$

Let us now consider Ψ_2.

1. *Antisymmetry after the vertical bar.*

$$(1+P_{i,j})\Psi_2 = \begin{cases} \left(1 - \sum_{t=1}^{k-1} P_{t,k}\right)\left(1 - \sum_{j=k+1}^{n} P_{j,n+1} + (n-2k+2)\,P_{k,n+1}\right)(1+P_{i,j})\,\psi_2 F & \text{for } i,j \neq n+1, \\ \left(1 - \sum_{t=1}^{k-1} P_{t,k}\right)\left[(n-2k+2)\,P_{k,n+1}(1+P_{i,k}) - \sum_{t\neq l} P_{l,n+1}(1+P_{i,l})\right]\psi_2 F & \text{for } j = n+1, \end{cases} \tag{3}$$

which vanishes, since

$$(1 + P_{i,j})\,\psi_2 = (1 + P_{i,k})\,\psi_2 = 0.$$

2. *Antisymmetry up to the bar.* For $i, j \neq k$, the condition is evidently satisfied. For $j = k$,

$$(1 + P_{i,k})\,\Psi_2 = -\sum_{t\neq i} P_{t,k}\left(1 - \sum_i P_{i,n+1} + (n-2k+2)\,P_{k,n+1}\right)(1+P_{t,i})\,\psi_2 F, \tag{4}$$

which vanishes, since $(1 + P_{t,i})\,\psi_2 = 0$.

3. *Condition of cyclic symmetry.* Making use of

the properties of ψ_2, we get, after some transformations,

$$\left(1-\sum_{j=k+1}^{n+1} P_{k,j}\right)\Psi_2 \qquad (5)$$
$$=\left(1+\sum_{j=k}^{n} P_{j,n+1}\right)\left[\left(1-\sum_{j=k+1}^{n} P_{k,j}\right)\right.$$
$$\left.-\sum_{t=1}^{k-1} P_{t,k}\left(1-\sum_{j=k+1}^{n} P_{t,i}\right)-(n-2k+2)\right]\psi_2 F.$$

Furthermore, we can show that by virtue of the properties of ψ_2, the equality

$$\left[\left(1-\sum_{j=k+1}^{n} P_{k,j}\right)\right. \qquad (6)$$
$$\left.-\sum_{t=1}^{k-1} P_{t,k}\left(1-\sum_{j=k+1}^{n} P_{t,j}\right)\right]\psi_2=(n-2k+2)\psi_2$$

exists. Consequently,

$$\left(1-\sum_{j=k+1}^{n+1} P_{k,j}\right)\Psi_2=0.$$

APPENDIX II

We derive expressions for the quantities $\rho_{AA'a}(\mathbf{r}')$, $\rho_{AA'aa'}(\mathbf{r}', \mathbf{r})$ and $\rho_{AA'aa'}(\mathbf{r}'', \mathbf{r}', \mathbf{r})$.

In order to write down these expressions in the most compact form, we introduce the notation for the integral of the product $\psi^*_{Aa}\psi_{A'a'}$ over all variables except certain exclusions. For example, the integral of the product $\psi^*_{Aa}\psi_{A'a'}$ over all variables except $\mathbf{r}_i$, entering into ψ^*_{Aa}, and $\mathbf{r}_j$ entering into $\psi_{A'a'}$, we denote by the symbol

$$(r_i)_{Aa}(r_j)_{A'a'}$$
$$=\int \psi^*_{Aa}\psi_{A'a'}\,d\mathbf{r}_1\ldots d\mathbf{r}_{i-1}d\mathbf{r}_{i+1}\ldots d\mathbf{r}_{j-1}d\mathbf{r}_{j+1}\ldots d\mathbf{r}_n.$$

If, after integration, $\mathbf{r}_i$ is replaced by $\mathbf{r}$, and $\mathbf{r}_j$ by $\mathbf{r}'$, then we can describe this case by

$$\begin{pmatrix} r \\ r_i \end{pmatrix}_{Aa}\begin{pmatrix} r' \\ r_j \end{pmatrix}_{A'a'}.$$

The expressions of interest to us have the form:

$$\rho_{AA'1}(\mathbf{r}')=k\begin{pmatrix} r' \\ r_1 \end{pmatrix}_{A1}\begin{pmatrix} r' \\ r_1 \end{pmatrix}_{A'1}+(n-k)\begin{pmatrix} r' \\ r_n \end{pmatrix}_{A1}\begin{pmatrix} r' \\ r_n \end{pmatrix}_{A'1};$$

$$\rho_{AA'2}(\mathbf{r}')=(k-1)\begin{pmatrix} r' \\ r_1 \end{pmatrix}_{A2}\begin{pmatrix} r' \\ r_1 \end{pmatrix}_{A'2}+(n-k+1)\begin{pmatrix} r' \\ r_n \end{pmatrix}_{A2}\begin{pmatrix} r' \\ r_n \end{pmatrix}_{A'2};$$

$$\rho_{AA'11}(\mathbf{r}', \mathbf{r})=q_{11}\begin{pmatrix} r' \\ r_n \end{pmatrix}_{A1}\begin{pmatrix} r \\ r_n \end{pmatrix}_{A'1};\quad \rho_{AA'12}(\mathbf{r}'\mathbf{r})=q_{12}\begin{pmatrix} r' \\ r_n \end{pmatrix}_{A1}\begin{pmatrix} r \\ r_n \end{pmatrix}_{A'2};$$

$$\rho_{AA'21}(\mathbf{r}', \mathbf{r})=q_{21}\begin{pmatrix} r' \\ r_n \end{pmatrix}_{A2}\begin{pmatrix} r \\ r_n \end{pmatrix}_{A'1};$$

$$\rho_{AA'22}(\mathbf{r}', \mathbf{r})=q_{22}\begin{pmatrix} r' \\ r_n \end{pmatrix}_{A2}\begin{pmatrix} r \\ r_n \end{pmatrix}_{A'2}+p_{22}\begin{pmatrix} r' \\ r_1 \end{pmatrix}_{A2}\begin{pmatrix} r \\ r_1 \end{pmatrix}_{A'2};$$

$$\rho_{AA'11}(\mathbf{r}'', \mathbf{r}', \mathbf{r})=q_{11}\left[k\begin{pmatrix} r'' & r' \\ r_1 & r_n \end{pmatrix}_{A1}\begin{pmatrix} r'' & r \\ r_1 & r_n \end{pmatrix}_{A'1}+(n-k-1)\right.$$
$$\left.\times\begin{pmatrix} r'' & r' \\ r_{n-1} & r_n \end{pmatrix}_{A1}\begin{pmatrix} r'' & r \\ r_{n-1} & r_n \end{pmatrix}_{A'1}\right];$$

$$\rho_{AA'12}(\mathbf{r}'', \mathbf{r}', \mathbf{r})=q_{12}\left[(k-1)\begin{pmatrix} r'' & r' \\ r_1 & r_n \end{pmatrix}_{A1}\begin{pmatrix} r'' & r \\ r_1 & r_n \end{pmatrix}_{A'2}+\begin{pmatrix} r'' & r' \\ r_k & r_n \end{pmatrix}_{A1}\begin{pmatrix} r'' & r \\ r_k & r_n \end{pmatrix}_{A'2}\right.$$
$$\left.+(n-k-1)\begin{pmatrix} r'' & r' \\ r_{n-1} & r_n \end{pmatrix}_{A1}\begin{pmatrix} r'' & r \\ r_{n-1} & r_n \end{pmatrix}_{A'2}\right];$$

$$\rho_{AA'21}(\mathbf{r}'', \mathbf{r}', \mathbf{r})=q_{21}\left[(k-1)\begin{pmatrix} r'' & r' \\ r_1 & r_n \end{pmatrix}_{A2}\begin{pmatrix} r'' & r \\ r_1 & r_n \end{pmatrix}_{A'1}\right.$$
$$\left.+\begin{pmatrix} r'' & r' \\ r_k & r_n \end{pmatrix}_{A2}\begin{pmatrix} r'' & r \\ r_k & r_n \end{pmatrix}_{A'}+(n-k-1)\begin{pmatrix} r'' & r' \\ r_{n-1} & r_n \end{pmatrix}_{A2}\begin{pmatrix} r'' & r \\ r_{n-1} & r_n \end{pmatrix}_{A'1}\right];$$

$$\rho_{AA'22}(\mathbf{r}''\mathbf{r}'\mathbf{r})=q_{22}\left[(k-1)\begin{pmatrix} r'' & r' \\ r_1 & r_n \end{pmatrix}_{A1}\begin{pmatrix} r'' & r \\ r_1 & r_n \end{pmatrix}_{A'2}\right.$$
$$\left.+(n-k)\begin{pmatrix} r'' & r' \\ r_{n-1} & r_n \end{pmatrix}_{A2}\begin{pmatrix} r'' & r \\ r_{n-1} & r_n \end{pmatrix}_{A'2}\right]$$
$$+p_{22}\left[(k-2)\begin{pmatrix} r' & r'' \\ r_1 & r_2 \end{pmatrix}_{A2}\begin{pmatrix} r & r'' \\ r_1 & r_2 \end{pmatrix}_{A'2}+(n-k+1)\begin{pmatrix} r' & r'' \\ r_1 & r_n \end{pmatrix}_{A2}\begin{pmatrix} r & r'' \\ r_1 & r_n \end{pmatrix}_{A'2}\right].$$

[1] D. R. Bates et *al.*, Phil. Trans. Soc. (London) **A243**, 93 (1950).

[2] P. M. Morse and W. P. Allis, Phys. Rev. **44**, 269 (1933).

[3] G. A. Erskine and H.S.W. Massey, Proc. Roy. Soc. (London) **A212**, 521 (1952).

[4] H.S.W. Massey and B. L. Moiseiwitsch, Proc. Roy. Soc. (London) **A227**, 38 (1954).

[5] G. F. Drukarev, J. Exptl. Theoret. Phys. (U.S.S.R.) **25**, 139 (1953).

[6] V. A. Fock, J. Exptl. Theoret. Phys. (U.S.S.R.) **10**, 961 (1940).

[7] M. J. Seaton, Phil. Trans. Roy. Soc. (London) **A245**, 469 (1953).

[8] L. D. Landau and E. M. Lifshitz, *Quantum mechanics*, Moscow-Leningrad, 1948, Ch. IX, Sec. 61.

Translated by R. T. Beyer
51

SOVIET PHYSICS JETP VOLUME 4, NUMBER 3 APRIL, 1957

Inelastic Scattering of Photons by Indium-115 Nuclei

O. V. Bogdankevich, L. E. Lazareva and F. A. Nikolaev
P. N. Lebedev Physical Institute, Academy of Sciences, USSR

(Submitted to JETP editor April 4, 1956)
J. Exptl. Theoret. Phys. (U.S.S.R.) 31, 405-412 (September, 1956)

The yields of the reactions $In^{115}(\gamma, \gamma')In^{115m}$ and $In^{115}(\gamma, 2n)In^{113m}$ and the yield of neutrons accompanying the photodisintegration of indium were measured at various maximum energies of x-rays from 5 to 27 mev. Cross sections were calculated by the photon difference method.

THE yield of the reaction $In^{115}(\gamma, \gamma')In^{115m}$ at various maximum x-ray energies E_{max} from 5 to 27 mev was measured on the 30 mev synchrotron. The number of isomeric states of In^{115m}, formed after the irradiation, was measured by a scintillation counter which registers the γ-radiation emitted during the transition from the metastable level to the ground level ($h\nu = 335$ kev, $T = 4.5$ hours).

If the conversion coefficient is not very large, this method of registration of metastable states seems to be more effective than the measurement of the induced activity by means of soft conversion electrons, since it makes possible a considerable increase in the number of counts at the expense of increasing the effective thickness of the sample, and simplifies the corrections for absorption and scattering of the radiation which is being registered. The photo-excitation cross sections of the metastable state of In^{115m} so obtained give a lower bound for the cross section of the reaction $In^{115}(\gamma, \gamma')$.

In reducing the γ-decay curves of the activity induced in the indium sample, the yield curve of the reaction $In^{115}(\gamma, 2n)In^{113m}$ was also obtained.

For simultaneous comparison of radiative and neutron width at various energies of x-rays, neutron fields during photodisintegration of indium were measured.

1. YIELD CURVE OF THE REACTION $In^{115}(\gamma,\gamma')In^{115m}$

The sample of indium (95.8% In^{115}; 4.2% In^{113}), 2.55 gm/cm^2 thick, was irradiated at a distance of 60 cm from the target of the synchrotron. In order to decrease the γ-activity arising as a result of capture of slow neutrons [$In^{115}(n, \gamma)In^{116m}$, $T = 54$ min], the sample of indium was placed during irradiation in a cadmium case (wall thickness 0.5 mm) wrapped in rhodium foil 0.4 mm thick.

The flux of γ-quanta falling on the sample was measured with an ionization chamber with thick aluminum walls (7.5 cm). The ionization in the air spaces of such a chamber for bremsstrahlung was calculated in Ref. 1. The measurement of the x-ray flux was made by placing the chamber at the position of the sample each time before and after irradiation. In order to avoid having to make a correction for the distribution of the γ-quanta flux over the

surface of the sample, the cross section of the air space in the aluminum block had the shape and dimensions of the irradiated surface of the sample (40×40 mm).

After irradiation, the duration of which at different energies varied from 20 min to 4 hrs, the disintegration curve of the γ-decay induced in the sample was taken over a period of 12/24 hrs.

The γ-activity was measured with the aid of a set-up consisting of two multipliers (FEU-19) working on coincidences from the same NaI crystal. The NaI crystal (diameter 32 mm, thickness 20 mm) was located in a cylindrical box filled with vaseline jelly. The bottom and top of the box, which were in contact with the photocathodes of the multipliers, were of quartz glass 1 mm thick, the side walls of aluminum 1 mm thick. Indium samples in the form of two strips 19 mm wide were wrapped around the lateral surface of the box with the crystal.

The photomultipliers were operated at 900 volts. Before arriving at the coincidence scheme, the impulses from the multipliers were amplified by a saturated amplifier with amplification factor of 4×10^4. The low supply voltage of the multipliers completely eliminated the optical coupling observed at high voltages and markedly lowered the number of noise impulses, which made it possible to use the Rossi type coincidence scheme $\tau = 10^{-6}$ sec with good selection coefficient. High amplification and amplitude form of the impulses guaranteed a high effectiveness and stability of functioning of the apparatus.

The effectiveness of the apparatus in registering the γ-rays of 335 kev, emitted in the transition of In^{115} from the isomeric state to the ground state, was measured with the aid of a standard source Cr^{51} ($h\nu = 330$ kev), prepared in the Isotope Laboratory of the Academy of Sciences. Cr^{51}, in the form of chromium sulfate, was deposited in a thin layer on a strip of aluminum foil 19 mm wide. The activity of the source was determined with accuracy of ±5%. in measuring the effectiveness of the apparatus the foil with the radioactive layer deposited on it was wrapped around the NaI crystal instead of the indium sample. In order to make a correction for absorption of γ-rays in the indium sample (1.20 ± 0.2), the absorption curve in indium of γ-rays from Cr^{51} source was determined with the same geometry.

In the decay of In^{115m} 94.5% of the nuclei pass into the ground state of In^{115} and 5.5% undergo β-decay ($E_{max} = 0.84$ mev). Electrons were not registered by the apparatus since they were practically totally absorbed in the walls of the box containing the NaI crystal.

The coefficient of internal conversion of γ-rays emitted in the isomeric transition of In^{115m} was measured in Refs. 2-5. Experimental values obtained in these papers coincide to within 15%; the mean value of the conversion coefficient $\alpha = 0.98$.

Figure 1*a* gives the yield curve obtained for the reaction $In^{115}(\gamma, \gamma')In^{115m}$ after introducing the correction for internal conversion and 5.5% β-transitions. The x axis gives maximum energy of x-rays, E_{max}, the y axis, the number of isomeric nuclei In^{115m} formed per second during irradiation of a mol of In^{115} by a flux of x-rays which produces in the air space of the thick-walled aluminum chamber a current of 1 A. Each point represents an average of 4 to 6 separate measurements. Mean square errors are also given.

The absolute yield of the reaction $In^{115}(\gamma,\gamma')^{115m}$ at maximum energy $E_{max} = 15.75$ mev, as a control, was measured using electrons of internal conversion. For this, indium samples with diameter of 40 mm and thickness 100-250 mg/cm^2 were irradiated in the cadmium case, wrapped in rhodium foil, and the curves of β-decay were measured with a column counter (window diameter 40 mm; thickness of mica covering the window, 4.5 mg/cm^2). The value of yield obtained is given in Fig. 1*a*. The absolute yields obtained by the two different methods agree to within 14%. The ratio of yields at $E_{max} = 16.7$ and 26.5 mev, measured by means of conversion electrons, also agrees, within experimental error, with the ratio obtained by the method of registering γ-radiation.

Metastable states of In^{115m} could be partially excited as a result of inelastic scattering of background neutrons and photoneutrons formed in the sample [$In^{115}(n, n')In^{115m}$]. Since the neutron background around the synchrotron is approximately isotropic, in order to estimate the effect caused by background neutrons, at energies $E_{max} = 16.7$ and 26.5 mev, controlled irradiations of indium samples were made outside of the x-ray beam. In these indium samples, while activity with period $T = 54$ min was present, no noticeable activity with period of half-life of 4.5 hours was observed. From the ratio of number of background neutrons to the number of photoneutrons formed in the sample, as measured in the present investigation (see Sec. 2), it follows that the fraction of isomeric states

of In^{115m} connected with the inelastic scattering of neutrons, did not exceed 2-3%.

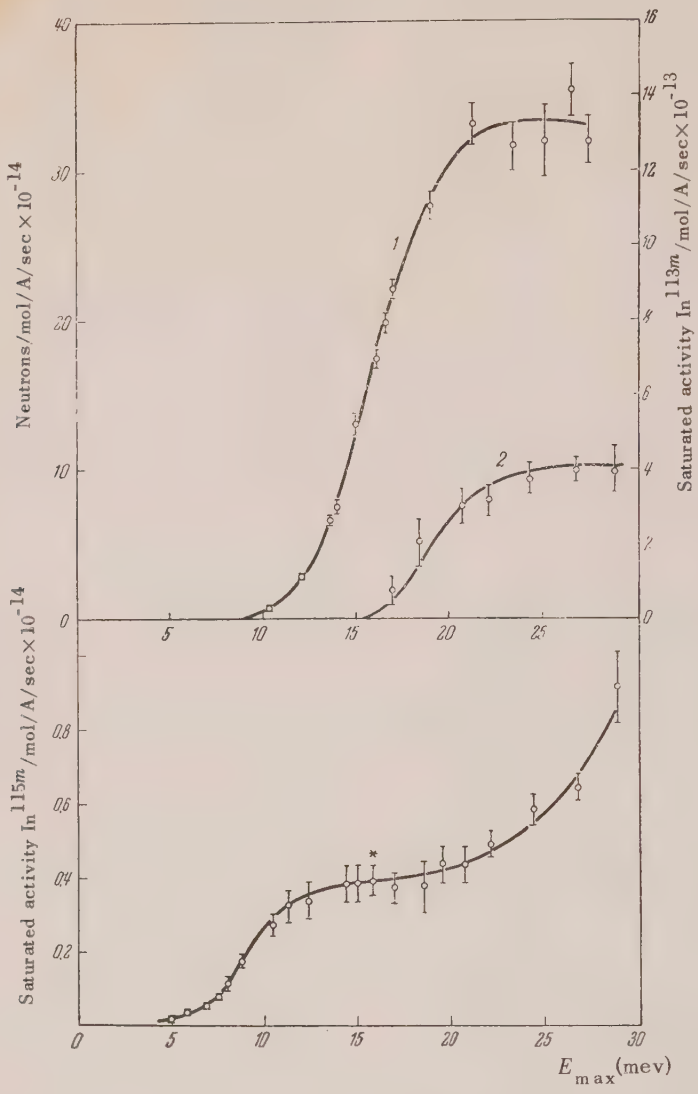

FIG. 1. *a* – yield curve of reaction $In^{115}(\gamma,\gamma')In^{115m}$. Star indicates yield of reaction measured by menas of internal conversion electrons; *b*: *1* – photoneutron yield curve; *2* – yield curve of reaction $In^{115}(\gamma, 2n)In^{113m}$ (scale on the right).

2. PHOTONEUTRON YIELD CURVE

In measuring the neutron yield, the indium sample was placed at the center of a paraffin block (80 × 80 × 70 cm) in a transparent canal of 5 cm diameter, along the axis of the x-ray beam. Neutrons, emitted in the photodisintegration of indium, after slowing down in the paraffin, were registered by a KH-14 ionization chamber filled with BF_3. The indium sample was a disc of 4 cm diameter and 4.97 gm/cm^2 thick.

In order to maintain the same conditions of neutron absorption in measuring the neutron yield from the sample and in measuring the background, the sample was placed in an aluminum box with double walls between which boron carbide powder was poured (0.5 gm/cm^2). In measuring the background, instead of the sample, an empty box with boron carbide was placed in the paraffin block. At various maximum enegies of x-rays the background was from 10 to 40%.

The absolute yield of neutrons was determined

from the ratio of neutrons registered with the irradiated sample to the neutrons from the standard source (Ra_{α} + Be) placed, instead of the sample, in the box with boron walls. The intensity of the source was measured with accuracy of ±6%. During the standardization process, curves were taken of the space distribution of neutrons for the sample and for the standard source.

In order to introduce a correction for absorption of x-rays in the indium sample, curves were taken of the dependence of neutron yield on thickness of the irradiated sample, for three different energies E_{max}. The method of neutron registration is described in detail in Refs. 6 and 7.

The flux of γ-quanta was measured with an ionization chamber with thick aluminum walls, as in the measurements of yield of the reaction $In^{115}(\gamma, \gamma')In^{115m}$ (Sec. 1). The irradiated surface of the sample and the cross section of the air space of the chamber were the same.

Figure 1*b* gives the yield curve for photoneutrons from indium, measured from the threshold of the reaction (γ, n) to $E_{max} = 27$ mev (curve *1*). Since the indium sample contains 95.8% of the isotope Indium-115, and for nuclei with $Z \sim 50$ neutron yields for photodisintegration of different isotopes of the same element differ little[8-10], the curve in question is practically the one for In^{115}.

The same figure gives the yield curve for the reaction $In^{115}(\gamma, 2n)In^{113m}$ (curve *2*). The yield of this reaction was obtained from the decay curve of induced γ-activity in the measurement of the yield of the reaction $In^{115}(\gamma, \gamma')In^{115m}$ (Sec. 1).

The metastable state In^{113m} ($h\nu = 392$ kev, $T = 105$ min) is also excited during the reaction $In^{113}(\gamma, \gamma')In^{113m}$. Because of the relatively small proportion of the isotope In^{113}, the formation of In^{113m} must be attributed to the process $(\gamma,2n)$. The yields of the reaction $In^{115}(\gamma, 2n)In^{113m}$ were measured with low accuracy, since the separation of the γ-activity of In^{113m} (with half-life $T = 105$ min) after separating out the activity of In^{115m} (against the background of a marked activity with period of $T = 54$ min resulting from the reaction $In^{115}(n, \gamma)In^{116m}$) involves large errors, especially near the threshold of the reaction $(\gamma, 2n) - E_{n,n} = 15.5$ mev.

The effectiveness of the apparatus and the correction for absorption in the indium sample for the γ-rays of In^{113m} were obtained by recomputing the corresponding quantities determined for the γ-rays of the standard source Cr^{51}. The coefficient of internal conversion $\alpha = 0.39 \pm 0.04$ was taken from Ref. 4.

3. CROSS SECTION CURVES

From the yield curves given in Fig. 1, differential cross sections were computed. For the bremsstrahlung spectrum, the Schiff spectrum was used, corrected for absorption of γ-rays in the walls of the accelerator chamber. The calculation was made by the method of photon difference over the interval of 1 mev.

Figrue 2 gives the cross-section curve obtained for the reaction $In^{115}(\gamma, \gamma')In^{115m}$.

Curves for cross section for photoexcitation of the metastable state In^{115m} were also obtained in the paper of Goldemberg and Katz[11] (up to 18 mev) and by Burkhardt, Winhold and Dupree[12] (up to 14 mev). In these investigations the reaction yield was measured by means of the conversion electrons.

Table I gives the basic characteristics of the cross-section curve of the reaction $In^{115}(\gamma,\gamma')In^{115m}$ obtained in the present paper and in Refs. 11 and 12. The maximum of the cross section, within limits of error, coincides with the maximum cross section obtained in Ref. 11. The shape of the curve, given in Fig. 2, agrees rather well, in the region of the maximum, with the value obtained in Ref. 12.

The sharp drop in the cross section at the threshold of the reaction $(\gamma, n) - (9.05 \pm 0.2)$ mev is connected with the exponential increase in neutron width. Completely unexpected was the sharp increase of the cross section starting at the energy ~ 16 mev.

The samples of indium used in this investigation were of high purity ($\geq$ 99.5%), and possible impurities could not produce the sharp increase in yield observed at energies $E_{max} > 20$ mev.

In the photodisintegration of indium, of all reactions energetically possible at these energies, a decay period near to the period $T = 4.5$ hours, is produced only with the reaction $In^{115}(\gamma, 2p)Ag^{113}$ (binding energy $E_{p,p} = 17.3$ mev). The silver isotope 113 decays with period $T = 5.3$ hours; the limiting energy of the β-spectrum $E_{max} = 2.1$ mev; no γ-radiation accompanying the decay was observed. In order to check whether the rise in the yield curve is not due to the reaction $(\gamma, 2p)$,

β-activity of the samples irradiated at energies E_{max} = 16.7 and 26.5 mev was measured with a column β-counter without a filter and with an aluminum filter 130 mg/cm^2 thick which absorbs electrons of energy below 400 kev. At both energies (16.7 mev and 26.5 mev), the aluminum filter completely absorbed the β-activity attributed to the decay of In^{115m}.

The increase of the observed γ-activity could be due to the formation of a heretofore unknown isomer with a not too different decay period. In order to exclude this possibility, the spectrum of γ-radiation from indium samples irradiated with x-rays with E_{max} = 16.1 and 25.1 mev was measured with a scintillation spectrometer. In both cases a sharp peak was observed at the energy 335 kev, whose amplitude decreased by one-half in 4.5 hrs. In the case E_{max} = 25.1 mev, the amplitude of the peak was $\sim$1.9 times greater than with E_{max} = 16.1 mev.

Control experiments were made which showed that the increase of the yield of the reaction at energies $E_{max} > 20$ mev, observed both with γ-ray and with conversion electron registration, is obviously due to the increase in the cross section for photoexcitation of In^{115m}.

The emission of photons by excited nuclei of In^{115} does not lead to the isomeric state In^{115m} in all cases. If the ratio of transitions to the ground and the metastable states is known, it is possible to obtain the cross section for the reaction $In^{115}(\gamma, \gamma')$.

The analysis of the ratios of the cross sections of (γ, n) reactions leading to the ground and the isomeric states, carried out in the paper of Katz, Becker and Montalbetti[11,13], shows that these ratios are practically unchanged when the excitation energy varies from 10 to 20 mev, and that transitions between levels with not too different values of spin are more probable than transitions between levels with large spin differences. The spins of the ground and the metastable levels of indium-115 nuclei are, respectively, 9/2 and 1/2. With dipole absorption of γ-quanta the spins of the excited nuclei may be 11/2 (0.400);9/2 (0.336) and 7/2 (0.267); the numbers in parentheses give the statistical weight of the state with the spin in question. Transitions to the ground state must be much more probable than the transitions to the metastable state.

In each individual case the transition probability must depend on the properties of low-lying levels[13]. A rough statistical consideration shows that the ratio of the number of states passing in cascade into the ground state through a metastable state, to the total number of transitions to the ground state, is $(2I_m + 1)/(2I_m + 1) + (2I_g + 1)]$, where I_m and I_g are the spins of the metastable and the ground state[14]. In the case of In^{115m} this ratio is 1/6.

A coefficient equal to 6 is also obtained from the following estimate. Near the threshold of the reaction (γ, n), the competing reactions are (γ, n) and (γ, γ'). Below the threshold of the reaction (γ, n) the cross section for absorption of γ-quanta is $\sigma_\gamma = \sigma(\gamma, \gamma')$, while above the binding energy of the neutron, $\sigma_\gamma = \sigma(\gamma, \gamma') + \sigma(\gamma, n)$, and even at energies 11 to 12 mev $\sigma_\gamma \approx \sigma(\gamma, n)$. Since the cross section for absorption of γ-quanta must change continouusly with energy, it is possible to obtain an estimate of the upper bound of the (γ, γ') cross section by extrapolating the curve for $\sigma(\gamma, n)$ from 11-12 mev into the region below 9 mev.

Figure 3 gives the curve, obtained in this investigation, of the photoneutron cross section $\sigma_n = \sigma(\gamma, n) + 2\sigma(\gamma, 2n) + \sigma(\gamma, pn)$. The extrapolated value of the cross section σ_γ at energy of 8.6 mev, equal to 10.5-12 mbn, is six times greater than the cross section for the reaction $In^{115}(\gamma, \gamma')In^{115m}$, obtained in this investigation. Thus the cross section for the reaction $In^{115}(\gamma,\gamma')$ equals the measured cross section of the process $In^{115}(\gamma, \gamma')In^{115m}$ multiplied by the coefficient 6.

Comparison of the cross section of the reaction (γ, γ') with the photoneutron cross section σ_n makes it possible to compare the radiative and neutron width at various energies of excitation of In^{115} nuclei.

The yield curve for photoneutrons from indium was also obtained by a method similar to the one described in Sec. 2.up to energy E_{max} = 24 mev by Montalbetti, Katz and Goldemberg[8]. The curve for σ_n obtained by these authors is given in Fig. 3 (dotted line). Table II gives the main characteristics of the cross section σ_n, obtained in this investigation and in Ref. 8. Integral cross sections and maximum cross sections, obtained in both investigations, agree to within 15%. The 1.5

times greater value of the cross section of the reaction $In^{115}(\gamma, n)$ obtained in Ref. 11 by the induced β-activity method, is apparently due to the large errors incurred in separating out the long-lived activity of In^{114m} ($T = 49$ days).

The ratio of the cross sections $\sigma(\gamma,\gamma')/\sigma_n$,

TABLE I. Photoexcitation cross section of the Isomeric state of In^{115m}.

Authors	Position of maximum of cross section, mev	Cross section at max, mbn	Half-width of peak, mev	Integral cross section to 18 mev mev-bn
Goldemberg, Katz	9	2.2*	9	0.0167*
Burkhardt, Winhold, Dupree	8±1	1.18∓0.35	2∓1	—
Bogdankevich, Lazareva, Nikolaev	8.6∓0,5	1.92∓0.29	2.6	0.0112∓0.017

* Cross sections were recomputed for conversion coefficient $\alpha = 0.98$ instead of $\alpha = 0.33$, used in Ref. 11.

equal to ~1 at energy 9.5 mev, at first sharply decreases with increase of energy. At 11 mev it equals ~ 1/10. In the region of the dipole maximum, the cross section for the reaction (γ, γ') is about 2% of the cross section for the reaction (γ, n).

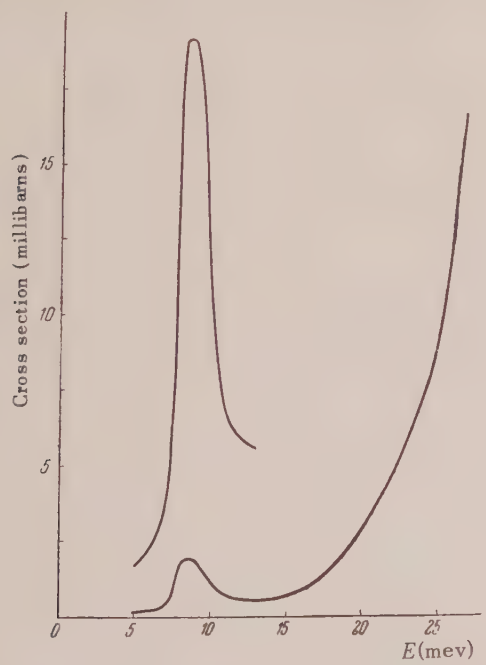

FIG. 2. Cross section of the reaction $In^{115}(\gamma,8)In^{115m}$. The upper curve is on a ten-fold scale.

Since on the average the photon carries off an energy much smaller than the total energy of excitation of the nuclei, the emission of a photon has a large probability of being accompanied by the emission of a neutron [reaction $(\gamma, \gamma' n)$]. This decreases the cross section $\sigma(\gamma, \gamma')$ and increases the cross section of the reaction (γ, n). According to estimates made in Ref. 11, at energies 14-15 mev the ratio of the cross sections $\sigma(\gamma,\gamma')/\sigma(\gamma,n)$

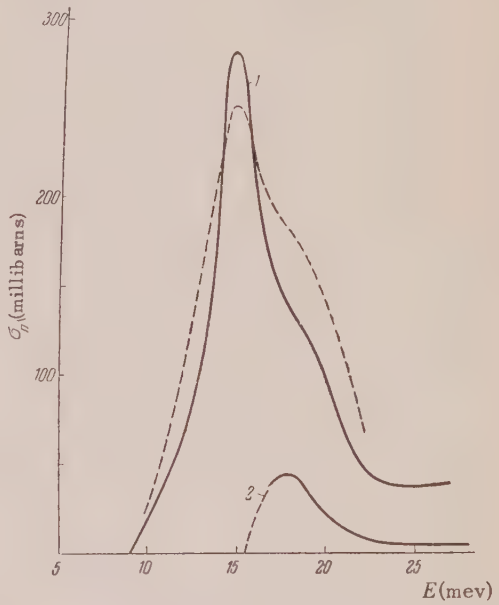

FIG. 3. *1* – cross section $\sigma_n = \sigma(\gamma, n) + 2\sigma(\gamma, 2n) + \sigma(\gamma, pn)$ calculated for the yield curve for neutrons accompanying the photodisintegration of indium; dotted line gives $\sigma_n(E)$ obtained in Ref. 8; *2* – cross section of reaction $In^{115}(\gamma, 2n)In^{113m}$, times coefficient 6.

is 1.5 to 2 times less than the ratio of the corresponding widths Γ_γ/Γ_n. Therefore, at energies about 15 mev the radiative width is 3 to 4% of the

neutron width. Starting at the energy ~16 mev, the cross section for the reaction $In^{115}(\gamma,\gamma')$ increases sharply, reaching, at 27 mev, a value ~100 mbn. To some extent the increase in the cross section for the reaction $In^{115}(\gamma, \gamma')In^{115m}$ may be due to increase in probability of transition of excited nuclei to the metastable level. In this case the cross section of the reaction $((\gamma, \gamma')$ would be less. However, the observed increase in the cross section for photoexcitation of the metastable state In^{115m} cannot be explained without assuming a strong increase in radiative width.

TABLE II. Principal characteristics of the photoneutron cross section σ_n.

Authors	Position of maximum of cross section, mev	Cross section at maximum, mbn	Half width of curve, mev	Integral cross section mev-bn
Montalbetti, Katz, Goldemberg	15.2	250	8.0	~2,0 (up to 22 mev)
Bogdankevich, Lazareva, Nikolaev	15.1∓0.5	280∓29	~5.0	1.8∓0.2 (up to 27 mev)

The marked increase in probability of radiation at energies above 20 mev is supported by a comparison of the photoneutron cross section σ_n and the cross section for the reaction $In^{115m}(\gamma,2n)In^{113m}$.

As in the case of the reaction (γ, γ'), upon emission of two neutrons, the 113 isotope of indium is formed in the ground and the isomeric states. In the ground state In^{113} has spin 9/2, in the isomeric state, 1/2. According to a statistical estimate, the probability of decay of the excited nucleus through a metastable state is also 1/6. Figure 3 gives the curve of the cross section $\sigma(\gamma, 2n) = 6 \cdot \sigma[In^{115}(\gamma, 2n)In^{113m}]$, (curve 2).

Knowing the cross section of the reaction $(\gamma, 2n)$, from the curve $\sigma_n = \sigma(\gamma, n) + 2\sigma(\gamma,2n) + \sigma(\gamma, pn)$ it is possible to find the ratio $\sigma(\gamma, 2n)/[\sigma(\gamma, n) + \sigma(\gamma, pn)]$. The proton-neutron binding energy $E_{n,p}$ = 16 mev, the height of the Coulomb barrier is ~10 mev. The yield of photoprotons from indium at E_{max} = 24 mev forms only 1.2% of the photo-neutron yield[15]. At excitation energy E = 17.5 mev the ratio $\sigma(\gamma, p)/\sigma(\gamma, n)$ for indium does not exceed 1-2%[16]. Hence, up to energy ~23 mev the cross section of the reaction (γ, pn) must be relatively small and the ratio

$$\sigma(\gamma, 2n)/[\sigma_n - 2\sigma(\gamma, 2n)] \approx \sigma(\gamma, 2n)/\sigma(\gamma, n).$$

The ratio $\sigma(\gamma, 2n)/\sigma(\gamma, n)$ calculated from the data given in Fig. 3, at first increases to 0.9 at energy of 18 mev, in agreement with estimates made according to the statistical theory. Instead of further increase of the relative probability of the reaction $(\gamma, 2n)$ the ratio $\sigma(\gamma, 2n)/\sigma(\gamma, n)$ decreases to ~0.2 at 23 mev. If the cross section for nonelastic scattering of photons on In^{113} nuclei increases as in the case of In^{115}, then, at energies higher than 20 mev, In^{113m} is formed in a fraction of the cases due to photoexcitation of the isomeric state of indium 113 and the cross section of the reaction $(\gamma, 2n)$ is still smaller.

The decrease of the relative probability of the reaction $(\gamma, 2n)$ with increase of nuclear excitation energy can take place only when there is a decay process competing with neutron emission, whose probability increases sharply from 18 to 23 mev. This is in agreement with the observed sharp increase of photon emission probability at energies of 16-27 mev.

In conclusion, the authors express their gratitude to Prof. V. I. Veksler for discussion of the results.

[1] Flowers, Lawson and Fossey, Proc. Phys. Soc. (London) 65B, 286 (1952).

[2] Langer, Moffat and Graves, Phys. Rev. 86, 632 (1952).

[3] J. L. Lawson and J. M. Cork, Phys. Rev. 57, 982 (1940).

[4] I. V. Estulin and E. M. Moiseeva, J. Exptl. Theoret. Phys. (U.S.S.R.) 28, 541 (1955); Soviet Phys. JETP 1, 463 (1955).

[5] Jagdish Varma and C. E. Mandeville, Phys. Rev. 97, 977 (1955).

[6] Valuev, Gavrilov, Zatsepina and Lazareva, J. Exptl. Theoret. Phys. (U.S.S.R.) 29, 280 (1955) Soviet Phys. JETP 2, 106 (1956).

[7] Lazareva, Ratner and Shtranikh, J. Exptl. Theoret. Phys. (U.S.S.R.) **29**, 274 (1955); Soviet Phys. JETP **2**, 301 (1956).

[8] Montalbetti, Katz and Goldemberg, Phys. Rev. **91**, 659 (1953).

[9] R. Nathans and J. Halpern, Phys. Rev. **93**, 437 (1954).

[10] B. I. Gavrilov and L. E. Lazareva, J. Exptl. Theoret. Phys. (U.S.S.R.) **30**, 855 (1956); Soviet Phys. JETP **3**, 871 (1956).

[11] J. Goldemberg and L. Katz, Phys. Rev. **90**, 308 (1953).

[12] Burkhardt, Winhold and Dupree, Phys. Rev. **100**, 199 (1955).

[13] Katz, Baker and Montalbetti, Canad. J. Phys. **31**, 250 (1953).

[14] Martin, Diven and Taschek, Phys. Rev. **93**, 199 (1954).

[15] M. E. Thoms and W. E. Stephens, Phys. Rev. **92**, 362 (1953).

[16] O. Hirzel and H. Waffler, Helv. Phys. Acta **20**, 373 (1947).

Translated by A. V. Bushkovitch
82

The Self-Consistent Field Equations in an Atom

A. S. KOMPANEETS AND E. S. PAVLOVSKII
Institute of Chemical Physics, Academy of Sciences, USSR

(Submitted to JETP editor May 31, 1955)
J. Exptl. Theoret. Phys. (U.S.S.R.) 31, 427-438 (September, 1956)

The Thomas-Fermi equations for the potential in an atom are obtained from the Fock self-consistent field method, together with all corrections of order $Z^{-2/3}$, where Z is the atomic number of the element. It is shown that the correction put forward earlier by Weizsäcker was too large by a factor of 9. The exchange correction found by Dirac is in principle correct only if it is small in comparison with the main term in the potential.

1. THE EQUATION FOR THE DENSITY MATRIX

As is well known, the best method for finding the terms of the many-electron atom is that due to V. A. Fock. Fock's method is based on the fact that the integral $\int \Psi^* H \Psi dq$ is stationary for all eigenvalues of the Hamiltonian H of the atom. In particular, this integral has an absolute minimum for the ground state of the atom (q denotes the set of all space and spin coordinates of the atom). The wave function is subject to the condition

$$\int |\Psi|^2 dq = 1. \tag{1}$$

In the Fock method the wave equation is chosen in the form of a symmetrized product of the wave functions of the individual electrons $\psi_i(q)$:

$$\Psi = (Z!)^{-1/2} \sum_P (-)^P \cdot \prod_i \psi_i(Pq) \tag{2}$$

(P denotes a permutation of the variables of the individual electrons).

The wave functions $\psi_i(q_i)$ can always be regarded as mutually orthogonal and normalized, since they can be orthogonalized by a method of linear substitution. If the function ψ is chosen in the form (2), then it is possible, without further limitation of generality, to introduce, as an additional condition on the wave function,

$$\int \psi_i^*(q)\, \psi_k(q)\, dq = \delta_{ik} \tag{3}$$

in place of the earlier requirement (1).

Before varying the energy integral, we put it in a special form, making use of the fact that the Hamiltonian contains only terms that refer to the individual electrons and to their pairwise interaction,

$$H = \sum_i U(q_i) + \frac{1}{2} \sum_{i,\, k \neq i} V(q_i, q_k), \tag{4}$$

where the function V is symmetric relative to both variables entering into it. In the atom, U is the sum of the kinetic and potential energies of the electron in the field of the nucleus, V is the energy of electrostatic interaction of the electrons. Substituting (2) and (4) in the expression $\int \Psi^* H \Psi\, dq$, and making use of Eq. (3), we get

$$\int \Psi^* H \Psi dq = \sum_i \int \psi_i^* U \psi_i\, dq + \sum_{i,\, k<i} \iint \psi_i^*(q')\, \psi_k^*(q)\, V(q, q')\, [\psi_i(q')\, \psi_k(q) - \psi_i(q)\, \psi_k(q')]\, dq dq'. \tag{5}$$

Here q on the left refers to the entire atom, while on the right it refers to the individual electron. The variation of Eq. (5) is given by

$$\begin{aligned} \int \delta\Psi^* H \Psi\, dq = \sum_i \int \delta\psi_i^*(q)\, dq \Big\{ & U\psi_i(q) + \sum_{k<i} \int \psi_k^*(q')\, V(q, q')\, [\psi_i(q)\, \psi_k(q') - \psi_i(q')\, \psi_k(q)]\, dq' \Big\} \\ \equiv \sum_i \int \delta\psi_i^*(q)\, dq \Big[& U\psi_i(q) + B(q)\, \psi_i(q) - \sum_k B_{ik}(q)\, \psi_k(q) \Big], \end{aligned} \tag{6}$$

where the following abbreviating notation is used:

$$B_{ik}(q) \equiv \int \psi_k^*(q')\, V(q, q')\, \psi_i(q')\, dq', \qquad B(q) \equiv \sum_k B_{kk}(q). \tag{7}$$

Multiplying the additional condition (3) by the variation parameter a_{ik} and adding the variation of Eq. (3) to the variation of the energy integral, we get a system of equations for the desired wave functions ψ_i:

$$U(q)\psi_i(q) + B(q)\psi_i(q) - \sum_k B_{ik}(q)\psi_k(q) + \sum_k a_{ik}\psi_k(q) = 0. \quad (8)$$

It is essential that the term in which $i = k$ is not excluded.

It is easy to express the parameters a_{ik} in terms of integrals of U, B and B_{ik}, making use of the condition (3). That is,

$$a_{ik} = \int \psi_k^* U \psi_i dq + \int \psi_k^* B \psi_i dq - \sum_l \int \psi_k^* B_{il} \psi_l dq. \quad (9)$$

Making use of the definitions, it can be shown that the matrix a_{ik} is Hermitian: $a_{ik} = a_{ki}^*$.

Equations (8) can be rewritten in very compact form if we introduce the density matrix $\rho(q, q')$, which is defined in the following form[1]:

$$\rho(q, q') = \sum_i \psi_i(q)\psi_i^*(q'). \quad (10)$$

Here the wave functions $\psi_i(q)$ are excluded from the equations.

In order to arrive at the density matrix $\rho(q, q')$, we write down, along with Eq. (8), the equation for the complex conjugate function $\psi_i^*(q')$:

$$U^*(q')\psi_i^*(q') + B^*(q')\psi_k^*(q') - \sum_k B_{ik}^*(q')\psi_k^*(q') + \sum_k a_{ik}^*\psi_k^*(q') = 0. \quad (8^*)$$

We now multiply Eq. (8) by $\psi_i^*(q')$ and Eq. (10) by $\psi_i(q)$, sum over i and subtract (8*) from (8). Terms containing a_{ik} and a_{ik}^* vanish in this case since

$$\sum_k a_{ik}\psi_k(q)\psi_i^*(q') - \sum_k a_{ik}^*\psi_k^*(q')\psi_i(q) = \sum_k a_{ik}\psi_k(q)\psi_i^*(q') - \sum_k a_{ki}^*\psi_i^*(q')\psi_k(q) = 0$$

by virtue of the Hermitian character of the matrix a_{ik}.

The terms in U and B involve the matrix $\rho(q, q')$. The expression containing B_{ik} can also be described with the aid of ρ. Actually, we get in Eq. (8)

$$\sum_k B_{ik}(q)\psi_k(q)\psi_i^*(q') = \sum_{ik}\int \psi_k^*(q'')V(q, q'')\psi_i(q'')dq''\psi_k(q)\psi_i^*(q') = \int V(q, q')\rho(q, q'')dq''\rho(q'', q') \quad (11)$$

and in the analogous transformation of (8*),

$$\sum_{i,k}\psi_i(q)\psi_k^*(q')\int \psi_k(q'')V(q', q'')\psi_i^*(q'')dq'' = \int \rho(q, q'')dq''\rho(q'', q')V(q'', q'). \quad (11^*)$$

If we introduce the operator

$$A_{qq''} \equiv \rho(q, q'')V(q, q''), \quad (12)$$

then Eq. (11) is rewritten as

$$\sum_{i,k} B_{ik}(q)\psi_k(q)\psi_i^*(q') = \int A_{qq''}dq''\rho(q'', q'), \quad (13)$$

while (11*) has the form

$$\sum_{i,k} B_{ik}^*(q')\psi_i(q)\psi_k^*(q') = \int \rho(q, q'')dq''A_{q''q'}, \quad (13^*)$$

where use is made of the obvious symmetry of the interaction operator V:

$$V(q', q'') = V(q'', q').$$

Terms which derive from B can also be expressed in terms of the density matrix:

$$B\sum_i \psi_i(q)\psi_i^*(q') = \left(\int \rho(q'', q'')V(q, q'')dq''\right)\rho(q, q').$$

Introducing the operators

$$B_{qq''} = \delta(q - q'')\int \rho(q''', q''')V(q, q''')dq'''; \quad (14)$$

$$U_{qq''} = \delta(q - q'')U,$$

we get an equation for the density matrix in the form

$$\int dq''[(U_{qq''} + B_{qq''} - A_{qq''})\rho(q'', q') - \rho(q, q'')(U_{q''q'} + B_{q''q'} - A_{q''q'})] = 0. \quad (15)$$

This latter equation represents the Poisson bracket between the operators

$$H_{qq''} \equiv U_{qq''} + B_{qq''} - A_{qq''} \tag{16}$$

and the density matrix:

$$H\rho - \rho H = 0. \tag{17}$$

In other words, H is the effective Hamiltonian operator. In this operator, the term B corresponds to the self-consistent field which is associated with the electron density distribution , while the term A is the so-called exchange energy operator.

It is evident in these equations, therefore, that the antisymmetrized wave function Ψ [see Eq. (2)] was taken, from the very beginning, in accordance with the Pauli principle for the electron system. Equation (17) differs somewhat from the usual equations of quantum mechanics by the fact that the Hamiltonian operator H itself depends on the density ρ.

We now eliminate the spin variable, making use of the fact that the initial Hamiltonian (4) did not depend on the spins. The density matrix is diagonal relative to the spin variable since, in the sum over i, one can substitute the entire system of spin functions. Therefore, the exchange operator is also diagonalized in the spin variables. The operator $B_{qq''}$ contains, in comparison with $A_{qq''}$, an additional integration over q''', which also includes summation over the spins. This gives an additional factor of 2 in $B_{qq''}$ in comparison with $A_{qq''}$ (Dirac[2] first wrote the A with the extra factor of 2, which was latter corrected by Jensen[3]).

Thus we need no longer describe all the quantities by the total set of variables q but only by the space variable r, because all the expressions are diagonal relative to the spin variable:

$$A_{\mathbf{r}\mathbf{r}''} = \frac{e^2}{|\mathbf{r} - \mathbf{r}''|}\rho(\mathbf{r} - \mathbf{r}''), \tag{18}$$

$$B_{\mathbf{r}\mathbf{r}''} = 2\delta(\mathbf{r} - \mathbf{r}'')e^2\int \frac{\rho(\mathbf{r}''', \mathbf{r}''')}{|\mathbf{r} - \mathbf{r}'''|}\,d\mathbf{r}'''. \tag{19}$$

2. TRANSITION TO THE QUASICLASSICAL APPROXIMATION

Dirac[2] has pointed out that, by way of a transition to the quasiclassical approximation one can obtain the well-known Thomas-Fermi potential distribution in the atom from Eq. (17). In this case the Dirac exchange operator gave a term in the equation for the potential which was less than the other terms in the ratio $Z^{-2/3}$, where Z is the atomic number of the element. This exchange term is treated by many authors[3-5] not as a small correction relative to the equation itself, but on a level with all the other terms of the equation. We shall show that it is not possible to treat it in this fashion.

The limiting transition to the quasiclassical approximation in the work of Dirac consisted of the fact that the quantum Poisson bracket for the density matrix $\rho(r, r')$ was simply the substitution of the classical Poisson bracket for the Fourier coefficient of the density matrix. Meanwhile it appears that if we do not restrict ourselves to this approximation, but find the term of next order of smallness, a correction appears that is proportional to $Z^{-2/3}$, and also an "exchange term", omitted by Dirac in the equation. As will be shown below, this additional term, proportional to $Z^{-2/3}$, enters with a numerical coefficient that is small in comparison with the exchange term. But in each case it is appropriate to solve the equation with the "exchange term" accurately. Each term proportional to $Z^{-2/3}$ must be considered only as a correction of the corresponding order to the usual Thomas-Fermi equation.

It should be pointed out that Weizsäcker[6] attempted to improve the Thomas-Fermi equation by introducing other correction terms in it of order $Z^{-2/3}$ in addition to the exchange terms. But the method used by Weizsäcker is not convincing. In fact, it is shown that the correct expression, corresponding to corrections following from Eqs. (17), is less than Weizsäcker's by a factor of 9. From this it follows that the exchange correction is predominant in comparison with the other terms of order $Z^{-2/3}$, so that in the numerical expression, the corrections, thus far produced, of the usual Thomas-Fermi equation must be considered valid. But this conclusion is correct only so long as the exchange correction term is small in comparison with the fundamental. The latter condition is not always fulfilled: for example, at great distances from the nucleus the correction already surpasses the fundamental term.

We now perform the transition to the quasiclassical approximation. For this purpose we first represent the matrix elements $\rho(x, x')$ and $H(x, x')$ in the form of expansions in Fourier integrals in the difference of the arguments $x - x'$:

$$\rho(x, x') = \int \rho\left(p, \frac{x+x'}{2}\right) e^{ip(x-x')} dp, \quad (20)$$

$$H(x, x') = \int H\left(p, \frac{x+x'}{2}\right) e^{ip(x-x')} dp, \quad (21)$$

where all the arguments are vectors, so that x stands for r, etc. We substitute these expansions in the Poisson bracket:

$$H\rho - \rho H = \int dx'' [H(x, x'')\rho(x'', x') - \rho(x, x'')H(x'', x')] \quad (22)$$

$$= \iiint dx'' dp dp_1 \left[H\left(p_1, \frac{x+x''}{2}\right)\rho\left(p, \frac{x''+x'}{2}\right) - \rho\left(p_1, \frac{x+x''}{2}\right)H\left(p, \frac{x''+x'}{2}\right)\right] \times \exp\{ip_1(x-x'') + ip(x''-x')\}.$$

In the first component of this integral we make the following change in variables: $x'' = x + \zeta + \Delta$, $x' = x - \Delta$, $p_1 = p - q$. In the second component we exchange the designations p and p_1 and set $x'' = x + \zeta$, $x' = x - \Delta$, $p_1 = p + q$. After these changes, the Poisson bracket takes on the form

$$\int dp e^{ip\Delta} \iint dq d\zeta e^{iq(\zeta+\Delta)} \rho\left(p, x + \frac{\zeta}{2}\right) \times \left[H\left(p-q, x + \frac{\zeta}{2} + \frac{\Delta}{2}\right) - H\left(p+q, x + \frac{\zeta}{2} - \frac{\Delta}{2}\right)\right] = 0. \quad (23)$$

In the transition to the quasiclassical approximation we must consider the region of motion and the momentum in the integral (23) to be large. In other words, we have a large momentum p and coordinate ζ because ζ enters only in the combination $x + \zeta/2$ (we set $\hbar = 1$, and we also employ $e = 1$ and $m = 1$ in what follows, i.e., we shall use atomic units). But if the coordinate ζ is large, then the momentun difference q is correspondingly small, since the product $q\zeta$ appears in the exponent. The difference in coordinates Δ must also be regarded as small because it enters into the exponent multiplied by a large momentum p. Consequently, the difference of Hamiltonians under the integral sign can be expanded in a power series in q and Δ. We limit ourselves to the third term of the expansion. It is evident that the zeroth and second terms vanish, leaving only the first and the third. We shall first write the formulas without tensor notation, which is easily inserted in the final result. The expansion is as follows [7]:

$$H\left(p-q, x + \frac{\zeta}{2} + \frac{\Delta}{2}\right) - H\left(p+q, x + \frac{\zeta}{2} - \frac{\Delta}{2}\right) = -2q\frac{\partial H}{\partial p} + \Delta\frac{\partial H}{\partial x} + \frac{1}{3}\left[-q^3\frac{\partial^3 H}{\partial p^3} + 3q^2\frac{\Delta}{2}\frac{\partial^3 H}{\partial p^2 \partial x} - 3q\left(\frac{\Delta}{2}\right)^2\frac{\partial^3 H}{\partial p \partial x^2} + \left(\frac{\Delta}{2}\right)^3\frac{\partial^3 H}{\partial q^3}\right]. \quad (24)$$

It is easy to get rid of the factors q and Δ by integration by parts, replacing $qe^{i\zeta q}$ and $\Delta e^{ip\Delta}$ by $-i(\partial/\partial\zeta)e^{iq\zeta}$ and $-i(\partial/\partial p)e^{ip\Delta}$. Equating the Fourier coefficient to zero, we obtain (upon integration by parts) the following expression, written in tensor form:

$$\frac{\partial H}{\partial p_i}\frac{\partial \rho}{\partial x_i} - \frac{\partial H}{\partial x_i}\frac{\partial \rho}{\partial p_i} + \frac{1}{24}\left(\frac{\partial^3 H}{\partial x_i \partial x_k \partial x_l}\frac{\partial^3 \rho}{\partial p_i \partial p_k \partial p_l} - 3\frac{\partial^3 H}{\partial x_i \partial x_k \partial p_l}\frac{\partial^3 \rho}{\partial p_i \partial p_k \partial x_l} + 3\frac{\partial^3 H}{\partial x_i \partial p_k \partial p_l}\frac{\partial^3 \rho}{\partial p_i \partial x_k \partial x_l} - \frac{\partial^3 H}{\partial p_i \partial p_k \partial p_l}\frac{\partial^3 \rho}{\partial x_i \partial x_k \partial x_l}\right) = 0. \quad (25)$$

The first two terms in this equation represent the classical Poisson bracket of the Fourier coefficient of the density ρ, while the remaining terms give the quantum correction to the Poisson bracket. The study of this correction is a fundamental purpose of the present research.

3. INVESTIGATION OF THE SELF-CONSISTENT FIELD IN THE QUASICLASSICAL APPROXIMATION

In the simplest approximation, the Fourier coefficient of the density matrix has the form

$$\rho_0 = \rho_0(p - p_0(r)) = \begin{cases} 1, & p \leqslant p_0(r), \\ 0, & p > p_0(r) \end{cases} \quad (26)$$

In other words, all states in which the momentum is less than a certain limiting momentum $p_0(r)$ are occupied, while the states for which $p > p_0(r)$ are unoccupied. With the help of ρ_0 one can determine the Fourier coefficients of the various terms of the Hamiltonian (we are dealing here with the Fourier coefficients relative to the difference in arguments $x - x'$, so that the coordinate dependence enters into them through half sums of the arguments).

The self-consistent potential B [see Eq. (19)] gives the following expression for the Fourier coefficient:

$$B = \frac{2}{(2\pi)^3}\int \frac{d\mathbf{r}''}{\mathbf{r}-\mathbf{r}''}\int \rho_0(p-p_0)\,d\mathbf{p} \qquad (27)$$
$$= \frac{1}{3\pi^2}\int \frac{d\mathbf{r}''}{\mathbf{r}-\mathbf{r}''}\,p_0^3(r').$$

Here $(2\pi)^{-3}$ is the Fourier coefficient of the δ-function $\delta(r-r')$, and the inner integral is equal to $4\pi p_0^3/3$ according to the definition of the function ρ_0. The spin states lack the factor 2 entering into B.

The exchange operator is transformed as follows:

$$A_p = \int \frac{e^{i\mathbf{p}(\mathbf{r}-\mathbf{r}')}}{|\mathbf{r}-\mathbf{r}'|}\frac{d\mathbf{r}'}{(2\pi)^3}\int d\mathbf{p}'\rho_0(p'-p_0)\,e^{-i\mathbf{p}'(\mathbf{r}-\mathbf{r}')} \qquad (28)$$
$$= \frac{1}{(2\pi)^3}\int d\mathbf{p}'\rho_0(p'-p_0)\int \frac{d\mathbf{r}'}{|\mathbf{r}-\mathbf{r}'|}\,e^{i(\mathbf{p}-\mathbf{p}',\,\mathbf{r}-\mathbf{r}')}.$$

As is known, the inner integral is equal to $4\pi|\mathbf{p}-\mathbf{p}'|^{-2}$. Subsequent integration over $d\mathbf{p}'$ is elementary and yields

$$A_p = \frac{1}{2\pi}\left(\frac{p_0^2-p^2}{p}\ln\frac{p_0+p}{p_0-p}+2p_0\right). \qquad (29)$$

In comparison with B, A_p has the smaller order of magnitude, which will be shown later after transition to Thomas-Fermi units. Therefore, in this approximation, the Hamiltonian is

$$H_0 = \frac{p^2}{2}-\frac{Z}{r}+B \qquad (30)$$
$$= \frac{p^2}{2}-\frac{Z}{r}+\frac{1}{3\pi^2}\int \frac{d\mathbf{r}''}{|\mathbf{r}-\mathbf{r}''|}\,p_0^3(r'').$$

In accordance with Eq. (25), the function ρ_0 in this approximation should cause the vanishing of the classical Poisson bracket:

$$\frac{\partial H_0}{\partial p_i}\frac{\partial \rho_0}{\partial x_i}-\frac{\partial H_0}{\partial x_i}\frac{\partial \rho_0}{\partial p_i}=0.$$

From the expressions for H_0 and ρ_0 we get

$$\frac{\partial H_0}{\partial p_i} = p_i; \quad \frac{\partial H_0}{\partial x_i} = \frac{x_i}{r}\frac{d}{dr}\left(\frac{1}{3\pi^2}\int \frac{d\mathbf{r}''}{|\mathbf{r}-\mathbf{r}''|}\,p_0^3(r'')-\frac{Z}{r}\right);$$
$$\frac{\partial \rho_0}{\partial p_i} = \frac{p_i}{p}\rho_0'; \quad \frac{\partial \rho_0}{\partial x_i} = -\frac{x_i}{r}\frac{dp_0}{dr}\rho_0',$$

so that the Poisson bracket has the following form:

$$\frac{(\mathbf{p},\mathbf{r})}{pr}\rho_0'\left[p\frac{dp_0}{dr}+\frac{d}{dr}\left(\frac{1}{3\pi^2}\int \frac{d\mathbf{r}''}{|\mathbf{r}-\mathbf{r}''|}\,p_0^3(r'')-\frac{Z}{r}\right)\right]=0. \qquad (31)$$

The function ρ_0' differs from zero only for $p=p_0$. Consequently, for this value of p, the expression in the square brackets vanishes:

$$p_0\frac{dp_0}{dr}+\frac{d}{dr}\left(\frac{1}{3\pi^2}\int \frac{p_0^3(r'')}{|\mathbf{r}-\mathbf{r}''|}\,d\mathbf{r}''-\frac{Z}{r}\right)=0. \qquad (32)$$

This equation is directly integrated; from the condition at inifnity, the integration constant must be set equal to zero:

$$\frac{p_0^2}{2}+\frac{1}{3\pi^2}\int \frac{p_0^3}{|\mathbf{r}-\mathbf{r}'|}\,d\mathbf{r}'-\frac{Z}{r}=0. \qquad (33)$$

The expression on the left side of this equation is the energy computed for the limiting value of the momentum p_0. As we see, it is equal to zero. Therefore, the function ρ_0 can be written in the following form, which is very useful for further calculations:

$$\rho_0=\rho_0(E_0)=\begin{cases}1, & E_0\leqslant 0,\\ 0, & E_0>0.\end{cases} \qquad (34)$$

It is easy to transform Eq. (33) to its usual form. Actually, setting

$$\varphi_0 = -\frac{1}{3\pi^2}\int \frac{p_0^3(r'')}{|\mathbf{r}-\mathbf{r}''|}\,d\mathbf{r}''+\frac{Z}{r}, \qquad (35)$$

we see that

$$\Delta\varphi_0 = 4\pi p_0^3/3\pi^2. \qquad (36)$$

But, according to Eq. (33), $p_0^2=2\varphi_0$, so that the potential satisfies the Thomas-Fermi equation:

$$\Delta\varphi_0 = (2^{7/2}/3\pi)\,\varphi_0^{3/2}. \qquad (37)$$

We now proceed to the equations of first approximation. For this case we write the density matrix and the potential in the form of expansions

$$\rho=\rho_0+\rho_1=\rho_0(E_0)+\rho_1, \qquad \varphi=\varphi_0+\varphi_1. \qquad (38)$$

Here φ_0 is by definition the sum of the potential of the nucleus and the self-consistent field of

zeroth approximation. The function $\rho_0(E_0)$ is determined by Eq. (34). We shall substitute the correction terms φ_1 and ρ_1 only in the Poisson bracket of zero approximation; in all the remaining terms of Eq. (25) and in the exchange operator, we shall use the zeroth approximation.

If we substitute the Hamiltonian H_0 according to Eq. (30) in the part of Eq. (25) which contains third derivatives, then it is easy to become convinced that there remains only the first term in the square brackets. Actually, all the mixed derivatives of H_0 with respect to x_i and p_i are equal to zero; moreover, H_0 has only a derivative with respect to p_i no higher than second order. Calculating the derivatives, we have

$$\frac{\partial^3 H_0}{\partial x_i \partial x_k \partial x_l} = -x_i x_k x_l \frac{d}{dr}\frac{1}{r}\frac{d}{dr}\frac{1}{r}\frac{d\varphi_0}{dr} - (\delta_{ik}x_l + \delta_{il}x_k + \delta_{kl}x_i)\frac{d}{dr}\frac{1}{r}\frac{d\varphi_0}{dr}, \tag{39}$$

$$\frac{\partial^3 \rho_0}{\partial p_i \partial p_k \partial p_l} = (\delta_{ik}p_l + \delta_{kl}p_i + \delta_{il}p_k)\frac{d^2\rho_0}{dE_0^2} + p_i p_k p_l \frac{d^3\rho_0}{dE_0^3}.$$

It is useful to split off the factor $(\mathbf{p}, \mathbf{r})$ and, in the remaining part, to change the independent variables entering into the problem: instead of p, r and $(\mathbf{p}\ \mathbf{r})$ we introduce the variables

$$E_0 = {}^1/_2 p^2 - \varphi_0, \qquad M^2 = [\mathbf{r}, \mathbf{p}]^2 = p^2 r^2 - (\mathbf{p}\ \mathbf{r})^2 \tag{40}$$

and r. In the new variables, the third derivatives take the form

$$\frac{\partial^3 H_0}{\partial x_i \partial x_k \partial x_l}\frac{\partial^3 \rho_0}{\partial p_i \partial p_k \partial p_l} = -\frac{(\mathrm{pr})}{r}\frac{\partial}{\partial r}\left\{\frac{d^3\rho_0}{dE_0^3}\left[2E_0\frac{d^2\varphi_0}{dr^2} + 2\left(\varphi_0\frac{d^2\varphi_0}{dr^2} - \frac{1}{2}\left(\frac{d\varphi_0}{dr}\right)^2\right) - M^2\frac{1}{r}\frac{d}{dr}\frac{1}{r}\frac{d\varphi_0}{dr}\right] + 3\frac{d^2\rho_0}{dE_0^2}\left(\frac{d^2\varphi_0}{dr^2} + \frac{2}{r}\frac{d\varphi_0}{dr}\right)\right\} \equiv -\frac{(\mathrm{pr})}{r}\frac{\partial I}{\partial r}, \tag{41}$$

where the meaning of I is obvious.

It follows that the exchange energy A [see Eq. (29)] is substituted only in the Poisson bracket of zeroth approximation:

$$\frac{\partial A}{\partial p_i}\frac{\partial \rho_0}{\partial x_i} - \frac{\partial A}{\partial x_i}\frac{\partial \rho_0}{\partial p_i} = -\frac{(\mathrm{pr})}{pr}\frac{dp_0}{dr}\left(\frac{\partial A}{\partial p} + \frac{\partial A}{\partial p_0}\right)_{p=p_0}\frac{\partial \rho_0}{\partial p} = -\frac{(\mathrm{pr})}{r}\frac{1}{\pi}\frac{dp_0}{dr}\frac{d\rho_0}{dE_0} = -\frac{(\mathrm{pr})}{r}\frac{1}{\pi}\frac{d}{dr}\sqrt{2\varphi_0}\frac{d\rho_0}{dE_0}. \tag{42}$$

We shall assume that the correction to the density is given in terms of E_0, M^2 and r. As is well known, the classical Poisson bracket of any integral of motion or of any function of integrals of motion reduces to zero. Therefore, upon substitution of ρ_1 into the Poisson bracket of zeroth approximation, only that term fails to vanish which has a derivative with respect to r. This term is equal to

$$\frac{\partial H_0}{\partial p_i}\frac{\partial \rho_1}{\partial x_i} = \frac{(\mathrm{pr})}{r}\frac{\partial \rho_1}{\partial r}. \tag{43}$$

The correction to the potential φ_1 depends, by definition, only on r. Therefore, it yields the term

$$\frac{(\mathrm{rp})}{r}\frac{d\varphi_1}{dr}\frac{\partial \rho_0}{\partial E_0}. \tag{44}$$

All the expressions entering into Eq. (25), after contraction to $\mathbf{p}\ \mathbf{r}/r$, have the form of derivatives with respect to r of the different expressions:

$$\frac{\partial \rho_1}{\partial r} + \frac{d\varphi_1}{dr}\frac{d\rho_0}{dE_0} = -\frac{1}{\pi}\frac{d}{dr}\left(\sqrt{2\varphi_0}\right)\frac{d\rho_0}{dE_0} + \frac{1}{24}\frac{\partial I}{\partial r}. \tag{45}$$

Since ρ_0 does not depend on r, this equation can be integrated immediately, setting the arbitrary additive function of E_0 and M^2 equal to zero because of the condition at infinity. This integration with respect to r is possible because of the choice of the independent variables E_0, M^2 and r. Thus,

$$\rho_1 + \varphi_1\frac{d\rho_0}{dE_0} = -\frac{\sqrt{2\varphi_0}}{\pi}\frac{d\rho_0}{dE_0} + \frac{1}{24}\frac{d^3\rho_0}{dE_0^3}\left[2E_0\frac{d^2\varphi_0}{dr^2} + 2\varphi_0\frac{d^2\varphi_0}{dr^2} - \left(\frac{d\varphi_0}{dr}\right)^2 - M^2\frac{1}{r}\frac{d}{dr}\frac{1}{r}\frac{d\varphi_0}{dr}\right] + \frac{1}{8}\frac{d^2\rho_0}{dE_0^2}\left(\frac{d^2\varphi_0}{dr^2} + \frac{2}{r}\frac{d\varphi_0}{dr}\right). \tag{46}$$

The other equation, which connects φ_1 and ρ_1, is the Poisson equation for the potential:

$$\Delta\varphi_1 = \frac{1}{\pi^2}\int \rho_1 d\mathbf{p}. \tag{47}$$

Although the corrections to ρ_0 are large for $E_0=0$, they enter integrally into the potential, and therefore, the resultant addition to the potential is small.

It is useful to carry out integration by parts in Eq. (47). In this case the terms which do not depend on angle acquire a factor of 4π, while the terms proportional to M^2 gain the factor $4\pi(2/3)\times r^2p^2$ because M^2 is proportional to the square of the sine of the angle between r and p. With the help of Eq. (40), the expression in the square brackets in Eq. (46), after integration over the angular variables, has the form

$$\frac{8\pi}{3}(E_0+\varphi_0)\left(\frac{d^2\varphi_0}{dr^2}+\frac{2}{r}\frac{d\varphi_0}{dr}\right)-4\pi\left(\frac{d\varphi_0}{dr}\right)^2.$$

It is easy to carry out integration over p if we make use of the definition of ρ_0 in Eq. (34).

Actually, we write $\sqrt{2(E_0+\varphi_0)}\,dE_0$ in place of p^2dp and make use of the fact that $d\rho_0/dE_0=-\delta(E_0)$. The integrals of the second and third derivatives of ρ_0 are obtained with the aid of the well-known formula

$$\int f(E_0)\frac{d^{n+1}}{dE_0^{n+1}}\rho_0(E_0)\,dE_0 = (-1)^n\left(\frac{d^n}{dE_0^n}f(E_0)\right)_{E_0=0}. \tag{48}$$

Substituting ρ_1 from (46) in Eq. (47), we get

$$\Delta\varphi_1-\frac{4}{\pi}\sqrt{2\varphi_0}\,\varphi_1=\frac{8}{\pi^2}\varphi_0 + \frac{1}{12\pi\sqrt{2\varphi_0}}\left[4\Delta\varphi_0-\frac{1}{\varphi_0}\left(\frac{d\varphi_0}{dr}\right)^2\right]. \tag{49}$$

This is also the equation for the correction to the potential. Here the first component on the right takes exchange into account, and the second follows from the addition to the classical Poisson bracket. If we substitute the expression $\Delta\varphi_0$ in the right side of Eq. (49), then we get the value $(8/9\pi^2)\varphi_0$, which is nine times smaller than the exchange term. In numerical integration it is shown that the ratio of both corrections to the potential is of the same order. We now transform to the dimensionless Thomas-Fermi variables, which are based on m, e and h:

$$r=\frac{(3\pi)^{2/3}}{2^{7/3}}\frac{x}{Z^{1/3}}\frac{\hbar^2}{me^2}; \tag{50}$$

$$\varphi_0=\frac{Ze^2}{r}\chi;\quad \varphi_1=\frac{Z^{5/3}}{(6\pi)^{4/3}}\frac{y}{x}\frac{me^4}{h^2}.$$

Then the dimensionless potential in zero approximation satisfies the well-known equation

$$d^2\chi/dx^2=\chi^{3/2}x^{-1/2}, \tag{51}$$

and the dimensionless correction y is found from the linear inhomogeneous equation

$$\frac{d^2y}{dx^2}-\frac{3}{2}\sqrt{\frac{\chi}{x}}\,y=\left[40\chi-\sqrt{\frac{x^5}{\chi}}\left(\frac{d}{dx}\frac{\chi}{x}\right)^2\right]. \tag{52}$$

We note that the potential in zeroth approximation is proportional to $Z^{4/3}$, and in first approximation, it is proportional to $Z^{2/3}$. Consequently, the relative order of the correction is $Z^{-2/3}$ (the numerical coefficient $40/(6\pi)^{4/3}$ differs but slightly from unity).

4. INTEGRATION OF THE EQUATION FOR THE CORRECTION TO THE POTENTIAL

The boundary conditions for Eq. (51) are $\chi(0)=1$, $\chi(\infty)=0$, because the potential is purely Coulombic in the immediate vicinity of the nucleus, but at large distances from the nucleus, the potential falls more rapidly than Coulombic (due to electron screening). The condition at infinity for y is evidently $y(\infty)=0$, and at zero, $y(0)=0$, inasmuch as the value of the potential in the neighborhood of $x=0$ is described by the function $\chi(x)$.

On the other hand, Eq. (52) is invalid both in the immediate neighborhood of the nucleus and also at large distances from the nucleus. One can raise the question: is it valid to integrate Eq. (52) with the boundary conditions $y(0)=y(\infty)=0$ if these conditions are applied outside the region of applicability of the equation*?

Let us first consider the solution for small values of x, of the order of the radius of the K-shell. In the region of the K-shell, the quasiclassical approximation assumed in the work is known to be inapplicable. But the charge included in this shell is of the order of unity, so that its effect on the potential of the self-consistent field in the atom is of order $1/Z$ relative to the total potential.

Further, the accuracy assumed by us is $Z^{-2/3}$ so that a correction of the order of $1/Z$ ought to be neglected. Also, it is evident that $Z^{-2/3}$ is the highest approximation compatible with the classical approach to the problem.

* This question was raised and answered for us by L. D. Landau.

Therefore, one does not integrate the "exact" equation, in which terms proportional to $Z^{-2/3}$ are considered on a par with the main term (as, for example, Jensen does [3]). It suffices to integrate the equation for the first approximation (52) only *once*, as also the main equation (51), and for different atoms, to consider the dependence of the potential on Z only according to Eq. (50).

We can estimate [directly, by Eq. (52)] the order of magnitude of those distances from the nucleus (on the side of small x), where the correction is comparable with the zeroth approximation. A more suitable estimate can be obtained if we compare not the potentials but the fields which are produced from the given density distribution of electronic charge. We shall also make this comparison. The function near the origin of the coordinates has the form $\chi = 1 - 1.589x + 4/3\,x^{3/2}$, as is well known. The number one appearing in the first part corresponds to the potential of the nucleus, and is not of interest to us in the computation of the field. The field due to the electrons, in zeroth approximation, is

$$\mathcal{E}_0 = -Z^{1/3}\frac{d}{dx}\frac{\chi - 1}{x} = -\frac{2}{3}Z^{1/3}x^{-1/2}.$$

The expression y for very small x is easily obtained by setting $\chi = 1$ on the right-hand side of Eq. (52), which gives $y = 4\sqrt{x}$ or, in accord with Eq. (50),

$$\mathcal{E}_1 = \frac{4}{(6\pi)^{4/3}}Z^{2/3}\frac{d}{dx}\frac{1}{\sqrt{x}} = 0.04Z^{2/3}x^{-3/2}.$$

Comparing $\mathcal{E}_0$ and $\mathcal{E}_1$, we see that $\mathcal{E}_1$ is of order of $\mathcal{E}_0$ when $x_{min} \sim 0.06\,Z^{-2/3}$, $r_{min} \sim 0.07h^2/Zme^2$, i.e., ~ 0.07 of the radius of the K-shell.

In this way, extrapolating the boundary condition for y to the point $x = 0$, we commit an error whose relative order is $1/Z$, with a small numerical coefficient.

Now let us consider the applicability of the boundary condition $y = 0$ for large x. As is well known, the asymptotic form of the solution of $\chi(x)$ for large x is $144/x^3$. In practice, however, this form of the solution is not obtained. It is therefore appropriate to assume that the function $\chi(x)$ (for large x) is $A^2(x)x^{-3}$, where $A(x)$ is a slowly changing function of x. Correspondingly, we determine the asymptotic solution of the homogeneous equation

$$y_0'' - {}^3/_2\, y_0\sqrt{\chi/x} = 0.$$

We shall seek y_0 in the form $y_0 = x^{\lambda(x)}$, neglecting the derivatives $d\lambda/dx$. Then,

$$\lambda_{1,2} = -{}^1/_2 \pm \sqrt{(3A/2) + {}^1/_4}.$$

One solution, y_{01}, vanishes at infinity as x^{λ_1}, and the other solution, y_{02}, goes to infinity as x^{λ_2}.

One can choose an arbitrary solution of the inhomogeneous equation (52) in the form of the quadrature of the right-hand side, with the help of the solutions y_{01} and y_{02}. But the right side is known to us, not for arbitrary values of x, but only for such x in which the correction is still small in comparison with the main solution. Let us assume that, beginning with each $x = x_0$ and larger, the function on the right side of Eq. (52) is some unknown $F(x)$. We shall show that the solution $y(x)$ for $x < x_1$ does not depend on this function $F(x)$ if $y(x_1)$ is sufficiently large that the solution vanishing at infinity is already small. This means that we can set $y(\infty) = 0$ without making any error.

We denote the known right side of Eq. (52) by $f(x)$. Then the solution for $x < x_1$ can be written in the following form:

$$y(x) = C_1 y_{01}(x) + C_2 y_{02}(x) + \int_0^x f(x')\,(y_{01}(x')\,y_{02}(x) - y_{01}(x)\,y_{02}(x'))\,dx', \tag{53}$$

if the solution y_{02} is connected with y_{01} by the well-known relation $y_{02} = y_{01}\int y_{01}^{-2}\,dx$. There exists a relation between the coefficients C_1 and C_2 that is determined from the boundary condition at zero. This dependence has the form $C_2 = \beta C_1$, where the coefficient β is independent of the values $x = x_1$ chosen, and is not connected with the function $F(x)$.

For large x the solution runs as

$$y(x) = C_3 y_{01}(x) + C_4 y_{02}(x) + \int_{x_1}^x F(x')\,(y_{01}(x')\,y_{02}(x) - y_{01}(x)\,y_{02}(x'))\,dx'. \tag{54}$$

In order that the solution remain finite at infinity, it is necessary to impose on C_3 the condition

$$C_3 = \int_{x_1}^{\infty} F(x)\, y_{02}(x)\, dx. \qquad (55)$$

The solutions of Eqs. (53) and (54) must join smoothly for $x = x_1$, i.e., the functions and their derivatives must be equal. This yields

$$C_1 = \int_0^{x_1} f(x')\, y_{02}(x')\, dx' + \int_{x_1}^{\infty} F(x')\, y_{02}(x')\, dx' \qquad (56)$$

But this also means that for large x_1 it is possible to set $x_1 = \infty$, if only to provide that the function $F(x)$ does not increase to infinity, which is quite natural. But then the solution of Eq. (52) for $x \leq x_1$ generally ceases to depend on the value of x_1 and on the unknown function $F(x)$. Consequently, we can assume that the condition $y(\infty) = 0$ applies in the region of applicability of Eq. (52).

Equation (52) has been integrated numerically by the method of Numerov[8]. In this method a new unknown function $y(x) - (a^2/12)y''$ is chosen in place of the unknown function $y(x)$. Here a is the interval in the numerical integration. The second derivative of the new unknown differs from the second difference by a quantity of sixth order relative to a. Thanks to this method of Numerov, it was possible to integrate equations numerically, solved relative to the second derivative, by choosing a large interval.

In order to satisfy the condition at infinity, we must proceed in the following fashion. We first determine by the method of numerical integration the solution of the homogeneous equation, which is equal to zero for $x = 0$; then, also by numerical integration, we find the similar solution of the inhomogeneous equation (52). The ratio of the two solutions tends toward a constant value for $x = 0$. Then, if we subtract from the solution of the inhomogeneous equation the solution of the homogeneous equation, multiplied by this constant ratio, we obtain a solution which satisfies both the boundary conditions.

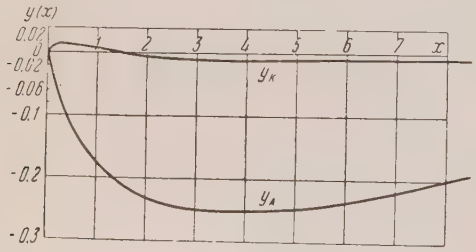

For comparison with the calculations carried out by other authors, we have divided the right-hand side into two components: the purely "exchange" correction, equal to 36χ, and the remainder, the "quantum" part, which is found in the present work. The corresponding components are labeled y_A and y_K. The curves y_A and y_K are plotted separately on the graph. As a consequence of the large numerical coefficient, y_A dominates for all x; therefore, the results of Jensen are practically valid, but only so long as the exchange correction in them is small in comparison with the main term. The final condition of Jensen was not observed for large x.

As far as the quantum correction is concerned, it is shown to be 9 times smaller than predicted by Weizsäcker. We can therefore consider it as finally established that only the exchange correction is appreciable in the Thomas-Fermi potential.

[1] P.A.M. Dirac, *Principles of Quantum Mechanics*, GTTI, 1932, pp. 243-256 (Russian translation).

[2] P.A.M. Dirac, Proc. Cambr. Phil. Soc. **26**, 376 (1930).

[3] H. Jensen, Z. Physik **111**, 373 (1930).

[4] Feynman, Metropolis and Teller, Phys. Rev. **75**, 1561 (1947).

[5] P. Gombas, *Statistical theory of the atom*, IIL, Moscow, 1951.

[6] C. F. Weizsäcker, Z. Physik **96**, 431 (1935).

[7] A. S. Kompaneets, J. Exptl. Theoret. Phys. (U.S.S.R.) **26**, 153 (1954).

[8] B. Numerov, Monthly Not. Roy. Astron. Soc. **84**, 592 (1924); G. Pratt, Jr., Phys. Rev. **88**, 1217 (1952).

Translated by R. T. Beyer
86

Polarization of 660 mev Protons Scattered by Nuclei

M. G. MESHCHERIAKOV, S. B. NURUSHEV AND G. D. STOLETOV
Institute for Nuclear Problems, Academy of Sciences, USSR

(Submitted to JETP editor June 1, 1956)
J. Exptl. Theoret. Phys. (U.S.S.R.) 31, 361-370 (September, 1956)

Results of experiments on double scattering of 660 mev protons are described. The angular dependence of the asymmetry was measured in scattering of polarized 565 and 635 mev protons from beryllium. The polarization in quasi-elastic $p-p$ scattering at 635 mev was measured by the method of coupled telescopes. The results of the measurements are given for the asymmetry in scattering of protons at 9° from carbon, aluminum, lead and bismuth and a detection limit of 230 and 620 mev.

1. INTRODUCTION

UNTIL now the effects of polarization of protons in scattering by nuclei were detected up to 439 mev in experiments involving double scattering of the primary unpolarized beam.[1-6] It was found that the polarization of protons reaches a maximum at energies and angles corresponding to the diffraction scattering of protons by nuclei. The magnitude and directions of the polarization of the spin may be qualitatively explained by assuming the same spin orbit interaction between the fast protons and the nucleus which is assumed in the nuclear shell model.[7-10]

The present work is concerned with the polarization effects in scattering of 660 mev protons by nuclei.

2. PRODUCTION OF THE BEAM OF POLARIZED PROTONS

The first scattering of protons was carried out inside of a 6 m synchrocyclotron chamber from a 4cm beryllium target (polarizer), placed in the path of the circulating beam of 660 mev protons. It is evident that only diffraction scattering of protons, single quasi-elastic $p-p$ scattering, and $p-n$ scattering without exchange at small angles do not lead to losses of energy for the protons. In the first case the scattered protons are concentrated in a narrow cone directed forward with an apex angle of the order of λ/R (λ is the wavelength of the incident proton, R is the radius of the scattering nucleus). Their energy is slightly smaller than the initial energy only if such collisions are not accompanied by transitions of the nuclei into excited states. In the second case there is no unique correlation between the scattering angle and the energy of the particle because of the zero-point vibrations of the nucleons in the nucleus. As a result the scattered nucleons have a rather broad energy distribution whose maximum is at about the same energy as for free collisions. The general character of the angular distribution of quasi-elastically scattered nucleons should be the same as for elastic scattering of nucleons. Nuclear cascades and nucleon collisions connected with generation of π-mesons are accompanied by emission of protons whose energies are considerably smaller than the energies of quasi-elastically scattered protons.

The direct measurement of the energy distribution of the first scattered protons was made in our laboratory using an analyzing magnet to obtain the momentum spectrum of protons issuing from the beryllium target.[11] One of the first results of these measurements was a discovery at angles 7.3° and 12.2° (relative to the primary beam) of a maximum corresponding to diffraction scattered protons superimposed in the upper energy region on a dome-shaped distribution of the quasi-elastically scattered protons. At the angles of 18°, 24° and 30° in the high energy region of the spectrum, only quasi-elastically scattered protons were found.

In the present experiments two polarized beams were used. Their trajectories are shown in Fig. 1. One of them (beam A) was composed only of protons experiencing quasi-elastic scattering to the left at an angle of 18°. Inelastically scattered protons and protons emitted in a nuclear cascade process were removed from the beam by the analyzing action of the fringing magnetic field of the synchrocyclotron The beam passed through a 3.6 m long steel collimator K_1, located in 4m reinforced concrete shielding wall, and then fell on the second target (analyzer). The flux density of protons was approximately 10^4 protons/cm^2 at the location of the analyzer. The solid curve of Fig. 2 gives the results of the measurements of absorption of protons in copper for beam A. From these results it follows that the average energy of the protons is 565 mev and the maximum energy deviation ±60 mev. Taking into account the slowing down of the protons in the analyzer the average energy is the same as for $p-p$ scattering

of free nucleons at an 18° angle.

The beam B, composed of protons scattered to the left at an angle of 9°, was formed inside of the vacuum chamber of the synchrocyclotron using a steel collimator K_2 which was also a magnetic channel. The beam was deflected 9° to the right by a steering magnet after its exit out of the vacuum chamber. All these operations increased the monochromaticity of the beam and excluded the possibility of particles falling into the shielded

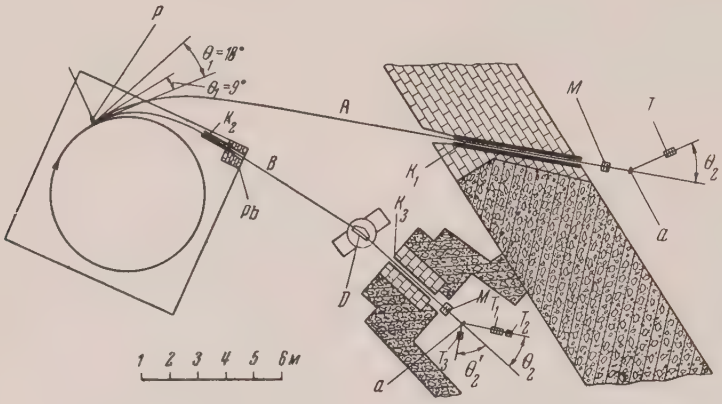

FIG. 1. Plane view of the experimental arrangement. P is the polarizer; a the analyzer; D the steering magnet; K_1, K_2, K_3 the collimators; T, T_1, T_2, T_3 telescopes.

cave directly from the synchrocyclotron chamber through the collimator K_3. The proton density behind the collimator K_3 at the location of the analyzer was approximately 10^5 protons/ cm^2 sec. Here the proton energy, determined by the range of protons in copper, was found to be 242 gm/cm^2 (Fig. 2) which corresponds to 635 mev with a maximum deviation ±15 mev. Under the given experimental conditions, diffraction-scattered

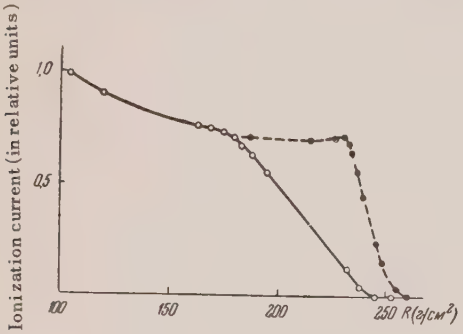

FIG. 2. Absorption curves of protons in copper. The solid curve shows the data for beam A, the dotted line for beam B.

protons of the same energy should be emitted at an angle of 9°. Assuming that the shape of the spectrum of the quasi-elastically scattered protons is similar at the angle of 24° to that at small angles, it was possible to separate for the spectra at 7.3° and 12.2° the diffraction peak from the continuous distribution. From the ratio of the areas under the appropriate curves it was also possible to evaluate the admixture of the quasi-elastically scattered protons in an energy interval 30 mev wide whose center coincides with the maximum of the diffraction peak. For the above angles, the admixture turned out to be 9% and 28% from which, by interpolation, the admixture of quasi-elastically scattered protons in beam B was calculated to be about 16%. Figure 3 gives the spectrum of the first scattered protons separated in this manner for the angles 7.3° and 12.2°.

The trajectories of beams A and B inside the synchrocyclotron chamber and in the fringing magnetic field were traced by means of a thin, stretched current carrying wire. A small mirror was attached to this wire at the point where the wire was fixed to the polarizer. As the wire was moved from the trajectory of the circulating beam to the direction of the trajectory of the scattered proton beam, the rotation angle of the mirror was measured. Collimators were thus located on the axes of the beams with an accuracy of about ± 2′. The beam diameter near the analyzer was usually about 3 cm. The uniformity of the current density in the cross section of the beam was verified with photoemulsions.

3. METHODS OF MEASUREMENTS

The second scattered protons were detected by telescopes consisting of two and three scintillation counters set for coincidence counts. The

toluene crystals, 3 mm thick, were surrounded by aluminum foil shields so that the scintillation light was reflected onto the cathode of the photomultiplier. The photo-multiplier was very carefully shielded from stray magnetic fields by soft iron and Permalloy. The resolution time of the coincidence channels of the telescopes was about 3×10^{8} sec. The efficiency of the proton detection was close to 100%. The detection limit of the proton energy was determined by the thickness of a copper absorber in the telescope.

The apparatus for the second scattering was composed of a round bevel protractor disc 800 mm in diameter, with the target-analyzer placed at the center. With remote control equipment the target could be removed from the beam and be replaced by another target. The telescopes were placed on supports which could be rotated in the plane of scattering about an axis passing through the analyzer and fixed at a given angle relative to the proton beam. The alignment of the telescopes with the trajectory of the beam was within $\pm 3'$ and was regularly checked photographically while the measurements were being carried out. In the same manner the position of the counters in the scattering plane was checked. The intensity of the beams was recorded by an ionization chamber filled with argon and an integrating amplifier of the resulting d. c. current.

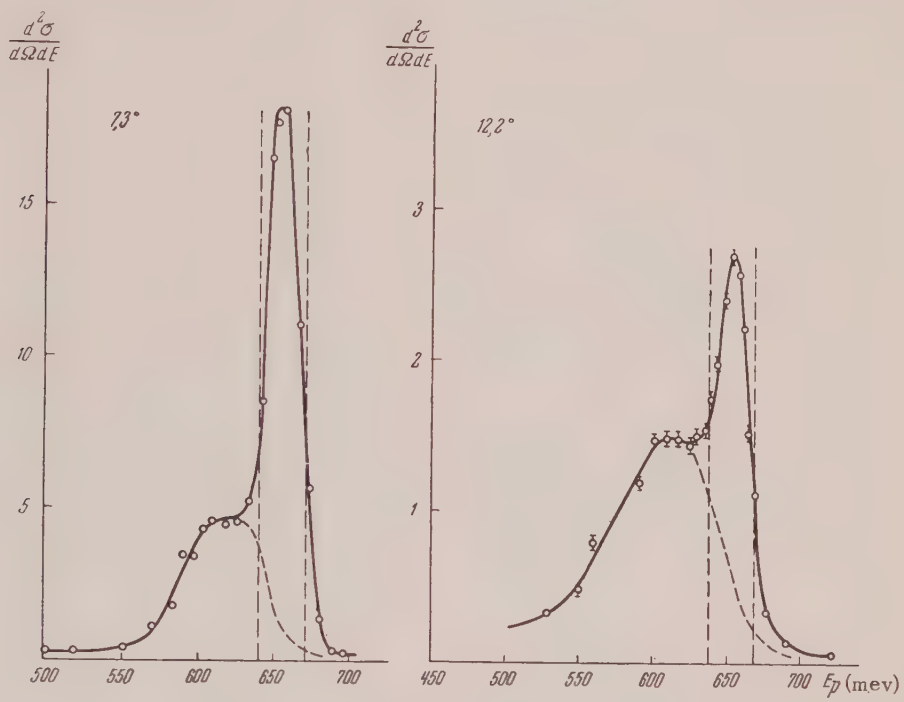

FIG. 3. Energy spectrum of 660 mev protons scattered by Be target; $d^2\sigma/d\Omega dE$ in arbitrary units.

The execution of the experiments fundamentally reduced to the measurement of the angular asymmetry $\epsilon = (L-R)/(L+R)$ where L and R are the normalized counting rates of the protons second scattered to the left and to the right at the same angle relative to the direction of the beam of the first scattered protons. The two scattering planes coincided. At large angles the counting rate of triple coincidences with the analyzer removed from the beam did not exceed 1% of the effect of the analyzer. The background increased as a rule with a decrease in the angle because of the scattering of protons in the walls of the collimator.

4. POLARIZATION OF 565 MEV PROTONS*

To determine the angular dependence of the asymmetry of the second scattered protons, scattered at an angle of 18° from a beryllium target bombarded by 660 mev protons, measurements were made with beam A at angles θ_2 from 6° to 30° in the laboratory system of coordinates. A beryllium disc 30 mm thick and 6 5 mm in diameter was used as an analyzer. In the majority of measurements the second scattered protons were detected in a solid angle 2×10^{-3} steradian by a single

*The experiments described in this section were carried out in 1954.[12]

telescope with three counters. The angular resolution of the telescope was $\pm 1.5°$. The detection limit of the protons was chosen to be $0.85\ E_A \cos^2 \theta_2$ where E_A is the average energy of the protons in the beam A. With this energy choice charged particles from three processes were observed: diffraction scattering, quasi-elastic p–p scattering and p–n scattering without exchange and also production of mesons whose energies were close to the maximum.

The results averaged from three independent series of measurements are given in Fig. 4. There, as in the remaining figures and tables, the given standard deviations are determined only by the statistics of the experiment. It is evident that the asymmetry of the angular distribution may be described by a smooth curve with a maximum at $\theta_2 = 9°$.

TABLE I

Values of the asymmetry $\epsilon\,(18°)$ for various energy detection limits*

Thickness of copper absorber in cm	0	15	20
Energy detection limit in mev	30	435	530
$\epsilon\,(18°)$	0.09 ± 0.01	0.11 ± 0.01	0.14 ± 0.02

At the angle $\theta_2 = 18°$ the dependence of the asymmetry was measured as a function of the detection limit. The resulting data are shown in Table 1.

It was found that the asymmetry increases noticeably with the thickness of the absorber after 20 cm of Cu. With 23.5 cm thick Cu absorber the counting rate became vanishingly small. From the data of

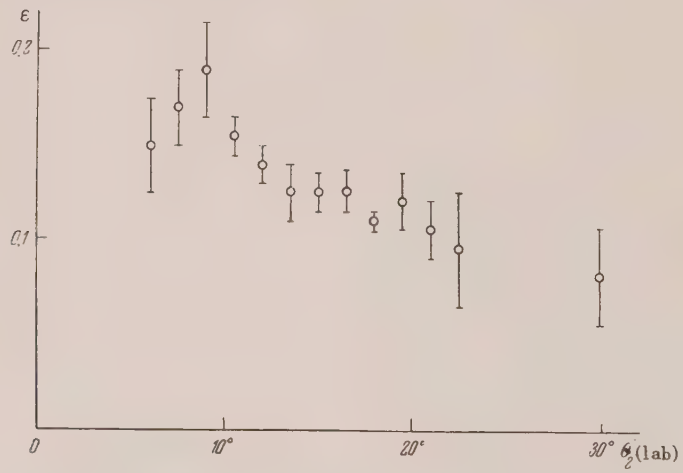

FIG. 4. Angular dependence of the asymmetry in scattering 565 mev protons from beryllium.

measurements on the spectra of charged π-mesons emitted in scattering of 660 mev protons from Be^{14} it is calculated that for energy of 565 mev and the total current of charged particles scattered at an angle of 18° and passed through the copper absorbers 20 cm thick, the contribution of the charged π-mesons did not exceed 2%. It did not exceed

*Observation of nuclear fission in photo-emulsions G5 placed in the beam A in the plane of the first scattering showed that there was an asymmetry in the forward scattering of charged particles equal to 0.11 ± 0.03. The density of its tracks corresponded to proton energy of 200 mev. The asymmetry was not found exposing the plates in a plane perpendicular to the plane of the first scattering.

5% with a 15 cm thick absorber. On the basis of these calculations the asymmetry observed with copper absorbers 15 – 20 cm thick was interpreted as the asymmetry in the scattering of protons.

The increase in the asymmetry with an increase in the thickness of the absorber may be explained: a) by a small admixture of diffraction-scattered protons in the beam of the charged particles; b) by a smaller asymmetry in the nuclear cascade and processes generating π-mesons than for quasi-elastic $p-p$ scattering and $p-n$ scattering without exchange; c) by a variation in the behavior of the polarization in the spectrum of the quasi-elastically scattered protons. Since in a broad range of angles the polarization for the quasi-elastic scattering increases with a decrease in angle (cf. Sec. 7), it may be expected that in quasi-elastic scattering, protons scattered at given angles at energies greater than average energy will be somewhat more strongly polarized.

Neglecting the effect of the energy losses of protons and assuming that both in the first and in the second scattering of protons at an angle of 18° the major role is played by quasi-elastic $p-p$ scattering and by $p-n$ scattering without exchange, it is possible to obtain the polarization of the beam from the relationship $\epsilon = P_1(\theta)_1 P_2(\theta_2)$, where $P_1(\theta_1)$ and $P_2(\theta_2)$ are the polarizations for the first and second scattering, respectively. For $\theta_1 = \theta_2$ and for the experimental data with 15 cm thick copper absorber, the polarization of the beam is $P_1(18^\circ) = \sqrt{\epsilon(18^\circ)} = 33 \pm 2\%$. From this value of $P_1(18^\circ)$ it follows that the magnitude of the asymmetry $\epsilon = 0.19 + 0.03$ at the maximum of the angular distribution; i.e., at $\theta_2 = 9^\circ$, it corresponds to the polarization of $60 \pm 10\%$. It is quite clear that an increase in the relative importance of the diffraction scattering among the observed processes is one of the major causes in the increase in the asymmetry with a decrease in the scattering angle.

5. POLARIZATION OF 635 MEV PROTONS

Two aligned telescopes adjusted for coincidence counts were used to determine the angular dependence of the asymmetry of the second scattered protons in beam B. The telescope closest to the beryllium analyzer was composed of three scintillation counters, and the one farther from the beryllium analyzer of two scintillation counters. The coincidence count in the first telescope and the coincidence count between the two telescopes were recorded simultaneously. A copper absorber was placed between the two counters so that the detection limit of the first telescope was 230 mev while the detection limit of the system of the two telescopes varied with the scattering angle as $E_B \cos^2 \theta_2$ where $E_B = 635$ mev is the average proton energy in the beam B. Under these conditions, the quintuple coincidences were caused almost entirely by diffraction scattered protons and the effects caused by a variation in the proton energy in the profile of the beam were still negligible. By introducing delays into the electronic circuits, it was found that in the entire range of angles at which second scattered protons were observed, the number of accidental coincidences between the two telescopes did not exceed 1% of the total number of coincidences recorded with the analyzer in the beam. In the range of angles from 9° – 50°, measurements were carried out with angular resolution of ±2°. In the range of angles from 3–9°, where the effect of multiple scattering was still negligible, the measurements were made with angular resolution of ±1°. The scattered protons were observed in solid angles of 2×10^{-3} and 6×10^{-4} steradian, respectively.

The results of the measurements of the angular dependence of the asymmetry are shown in Fig. 5. The white circles represent the values of asymmetry obtained from the quintuple coincidence counts; the black circles show the values of asymmetry calculated from the data obtained with the telescope closest to the analyzer. One observes that the asymmetry for the particles with a long path increases sharply with an increase in the scattering angle, reaches the maximum value of $.36 \pm .04$ at $\theta_2 = 7^\circ$ and then smoothly decreases up to 30°. The asymmetry of the total flux of fast charged particles is observed up to 42°, and is almost constant in the region of angles from 7° to 20°.

The data on the dependence of the asymmetry on the detection limit were obtained from measurements carried out with absorbers of various thicknesses placed between the two telescopes. The results of these measurements are given in Table II. The fact that for small scattering angles, the asymmetry turned out to be very much larger for particles with the maximum path, seems to be a definite proof of a greater polarization of diffraction scattered protons compared with particles emitted as a result of collisions with individual nucleons in the nucleus.

At the angle $\theta_2 = \theta_1 = 9^\circ$ the asymmetry is found to be 0.33 ± 0.03 from the data on quintuple coincidences. Therefore the polarization of

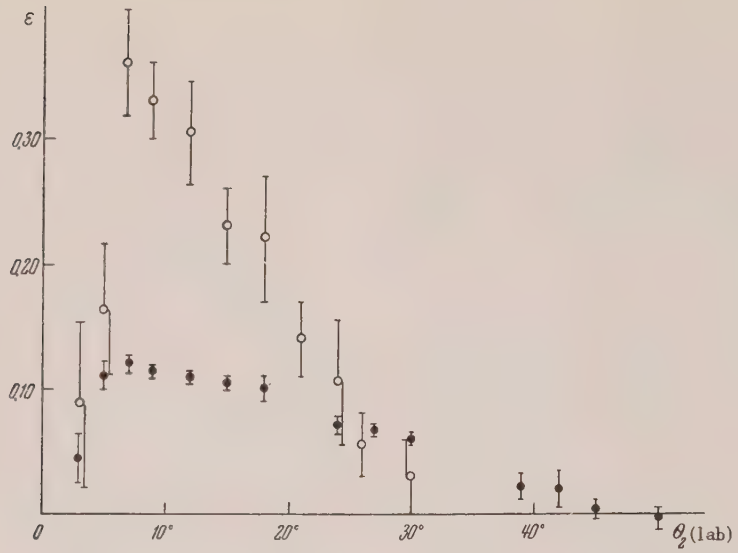

FIG. 5. Angular dependence of the asymmetry in scattering of 635 mev protons from beryllium: O—detection limit $E_{lim} = E_D \cos^2 \theta_2$, ● detection limit 230 mev.

protons in the beam B is 58 ±3%. To the maximum value of $\epsilon = 0.36 \pm 0.04$, observed at the angle of 7°, corresponds polarization of 62 ±10%. Indeed, the polarization of protons diffraction

TABLE II

The dependence of the asymmetry on the detection limit at 9°, 12° and 18°

Detection limit in mev	ε (9°)	ε (12°)	(ε 18°)
160			0.06±0.03
190			0.08±0.03
230	0.11±0.01	0.11±0.01	0.10±0.01
480			0.12±0.02
565		0.17±0.05	
580			0.23±0.03
600	0.11±0.04	0.16±0.07	
610		0.31±0.03	
620	0.33±0.03		

scattered from beryllium is apparently even greater, since it was not possible to achieve a complete separation of the quasi-elastically scattered protons in these experiments. It should be noted that at the angle $\theta_2 = 9°$, the contribution of the charged π-mesons to the number of quintuple coincidences did not exceed 1%.

Similar experiments on double scattering of protons from beryllium at lower energy are described in Refs. 4–6 and 15. The values of polarization of diffraction scattered protons corresponding to the maximum values of the observed asymmetry given in these references are shown in Fig. 6 together with the results of the present experiments as a function of the energy of the first scattered protons. It is noteworthy to observe that the polarization of the diffraction scattered protons from beryllium does not change noticeably with an increase in the proton energy from 300 to 635 mev.

6. SCATTERING OF POLARIZED PROTONS FROM NUCLEI C, Al, Pb AND Bi

The measurements of asymmetry at $\theta_2 = 9°$ for the above listed nuclei were carried out under the experimental conditions described in the previous section. The beryllium analyzer was replaced by a target made of carbon, aluminum, lead or bismuth equivalent in its stopping power to the beryllium target. The results of these measurements are given in Table III.

The values of asymmetry obtained at the detection limit of 620 mev were very similar for all of the investigated nuclei. At the 620 mev detection limit, the diffraction-scattering of protons was dominant while multiple scattering of protons from the analyzer did not play an important role as yet. The asymmetry in the scattering of charged particles of energy greater than 230 mev decreases imperceptibly with an increase in the dimension of the scattering nucleus. A discussion of the reasons why aluminum does not fit into this rule is better left until the time when additional data

on the angular dependence of the asymmetry of scattering of protons from this nucleus are available.

7. ASYMMETRY IN THE QUASI-ELASTIC $p-p$ SCATTERING AT 635 MEV*

The observation of the elementary processes in the quasi-elastic $p-p$ collisions was carried out by the technique of coupled telescopes described in Ref. 16. The scattered protons were detected in a solid angle of 1.7×10^{-3} steradian subtended by the surface of the first crystal nearest to the analyzer. The cross section of this crystal was 35×35 mm. The second and third crystals in this first telescope had cross sections of 45×45 mm and 50×50 mm. The detection limit of this telescope was 150 mev. The coupled telescope, consisting of crystals 52×52 mm and 60×60 mm in cross section, subtended a solid angle of 4.7×10^{-2} steradian . The coincidences between the telescopes were counted by circuits with a resolution time of 5×10^{-8} sec. The angular resolution of the entire detection apparatus was about $\pm 2^0$. A beryllium disc 30 mm thick and 65 mm in diameter was used as an analyzer. The diameter of the beam at the location of the analyzer was 40 mm. In measurements of the asymmetry, the telescopes were located in the plane of the first scattering on both sides of the beam at angles θ_2 and θ_2', related by the expression $\cot\theta_2 \cot\theta_2' = 1 + E/2Mc^2$, where E is the kinetic energy of the incident proton, Mc^2 is the proton rest energy. Experimental evidence was obtained to show that the contribution of the inelastic $p-p$ and $p-n$ collisions to the counting rate of the quasi-elastic $p-p$ scattering was negligible. The experiments carried out consisted of counting the coincidences between the two telescopes in the entire range of angles with the telescopes located relative to each other at angles not satisfying the above expression.

The values of asymmetry ϵ, obtained as a function of the scattering angle θ_2 in the laboratory system of coordinates, are given in Fig. 7. Taking the polarization of the first scattered beam to be $58 \pm 3\%$, one can find the polarization $P_{<pp>}$ in quasi-elastic $p-p$ scattering from Be from the expression $\epsilon = 0.58\ P_{<pp>}$. At 40° in the center-of-mass system ($\theta_2 = 21^\circ$), the polarization $P_{<pp>} = 35 \pm 4\%$,

In the present work, the asymmetry of free $p-p$ scattering was also measured at $\theta_2 = 21^\circ$.

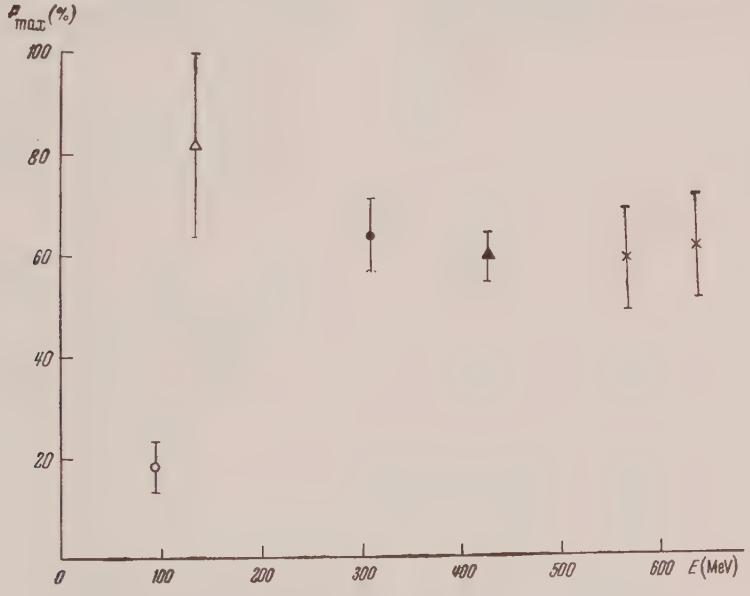

FIG. 6. Maximum value of the polarization of protons diffraction scattered from beryllium as a function of energy. The points are taken from the following references: O–Ref. 15; Δ–Ref. 6; ●–Ref. 4; ▲–Ref. 5; × –this work.

*L. B. Parfenov has participated in the experiments described in this section.

Polyethylene and graphite scatterers, equivalent in the number of carbon nuclei, were used as analyzers. The effect in hydrogen was determined by a differential method. It was found that the asyymetry is equal to 0.25 ± 0.07 with corresponding polarization $P = 43 \pm 4\%$. It is evident that for 635 mev protons, the polarization in quasi-elastic p–p scattering is only slightly smaller than the polarization in the free p–p scattering.

TABLE III. The values of asymmetry for second scattered protons of 635 mev from Be, C, Al, Pb and Bi.

	Be	C	Al	Pb	Bi
ε (E>620 mev)	0.33±0.03	0.32±0.04	0.25±0.05	0.34±0,07	0.30±0.08
ε (E>230 mev)	0.11±0.01	0.13±0.02	0.03±0.01	0.08±0,02	0.07±0,02

Similar measurements of the asymmetry in quasi-elastic p–p scattering from Be were carried out for 285 mev protons by Donaldson and Bradner.[17] From their data, the polarization at 40° in the center-of-mass system for quasi-elastic p–p scattering is $P_{<pp>} = 15 \pm 4\%$, while the polarization for free p–p scattering under the same conditions is ~ 42%.[2]

A comparison of the experimental data given above shows that with an increase in the proton energy from 285 to 635 mev: 1. the difference in the degree of polarization between quasi-elastic and free elastic p–p scattering disappears, 2. polarization in the free p–p scattering does not change noticeably.

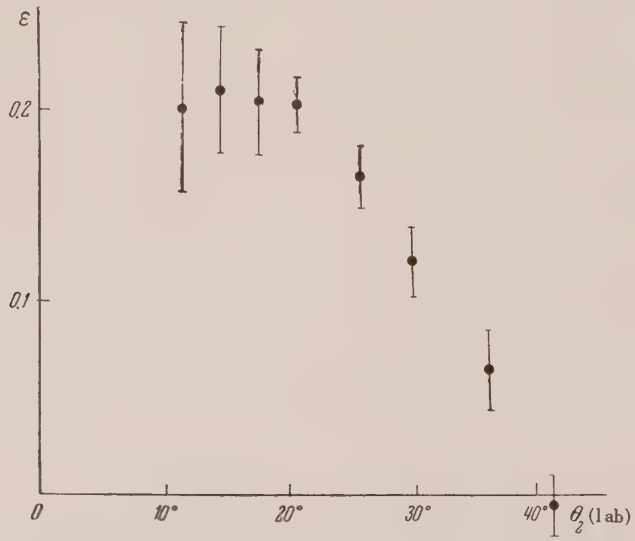

FIG. 7. Angular dependence of the asymmetry in quasi-elastic p–p scattering in beryllium at 635 mev.

8. CONCLUSIONS

From the experimental results described above, one can form the following conclusions:

1. At 660 mev the polarization of protons is due to both diffraction-scattering and quasi-elastic scattering. In both polarization processes, the spin has the same orientation as in the free p–p scattering.

2. The values of the asymmetry, obtained at the angle 9° in scattering of polarized protons with energy greater than 620 mev from Be, C, Al, Pb and Bi nuclei, were the same within the experimental error.

3. A comparison of the data currently available for double scattering of protons from beryllium

shows that:

a. The maximum value of the polarization of the diffraction-scattered protons does not change noticeably with an increase in energy from 300 to 635 mev and is not less than 60% at 635 mev.

b. The polarization of protons in quasi-elastic p–p scattering increases by more than a factor of two with an increase in the proton energy from 285 to 635 mev. It reaches values only slightly smaller than the polarization for free p–p scattering.

4. One may suspect that the polarization of protons in free p–p scattering has the same value at 300 mev as at 635 mev. However, the data obtained in this work are very sparse.

The authors express their gratitude to R. M. Ryndin for his participation in the evaluation of the experimental results and to Iu. K. Akimov and A. S. Kuznetsov for their help in the construction of the electronic apparatus.

[1] Oxley, Cartwright and Rouvina, Phys. Rev. 93, 806 (1954).

[2] Chamberlain, Segre, Tripp Wiegand and Ypsilantis, Phys. Rev. 93, 1430 (1954).

[3] Marshall, Marshall and de Carvalho, Phys. Rev. 93, 1431 (1954).

[4] de Carvalho, Marshall and Marshall, Phys. Rev. 96, 1081 (1954).

[5] Heiberg, Kruse, Marshall, Marshall and Solmitz, Phys. Rev. 97, 250 (1955).

[6] Dickson, Rose and Salter, Proc. Phys. Soc. (London) A68, 361 (1955).

[7] E. Fermi, Nuovo Cim. 11, 407 (1954).

[8] Snow, Sternheimer and Yang, Phys. Rev. 94, 1073 (1954).

[9] B. Malenka, Phys. Rev. 95, 522 (1954).

[10] W. Heckrotte and J. V. Lepore, Phys. Rev. 95, 1109 (1954).

[11] Meshcheriakov, Shabudin, Zrelov, Neganov, Vzorov, Azhgirei, Proc. Inst. Nucl. Probl. (1956).

[12] L. D. Stoletov and S. B. Nurushev, Proc. Inst. Nucl. Probl. (1954).

[13] E. L. Grigorev, J. Exptl. Theoret. Phys. (U.S.S.R.) 28, 761 (1955); Soviet Phys. JETP 1, 608 (1955).

[14] Meshcheriakov, Vzorov, Zrelov, Neganov, and Shabudin, J. Exptl. Theoret. Phys. (U.S.S.R.) 31, 55 (1956).

[15] K. Strauch, Phys. Rev. 99, 150 (1955).

[16] Meshcheriakov, Bogachev, Neganov and Piskarev, Dokl. Akad. Nauk SSSR 99, 955 (1954).

[17] R. Donaldson, and H. Bradner, Phys. Rev. 99, 892 (1955).

Translated by M. J. Stevenson
77

Investigation of the Angular and Energy Distributions of Secondary Electrons from Cuprous Oxide

N. B. GORNYI

(Submitted to JETP editor June 24, 1955)
J. Exptl. Theoret. Phys. (U.S.S.R.) 31, 386-92 (September, 1956)

The angular distribution of secondary electrons was investigated using a vacuum system containing a spherical collector whose surface was divided into several conducting belts. The observed angular distributions of the secondary electrons exhibit pronounced maxima at large angles ($\sim 60°$). It is shown that the observed distributions are distorted from the true distributions by secondary emission from the collector (tertiary electrons). A method to correct for this effect is introduced. The corrected angular distributions obey a cosine law. The energy distributions for the different angles of emission of the secondary electrons are investigated by the method of electrical differentiation.

INTRODUCTION

THE investigation of the angular and energy distributions of secondary electrons is not only interesting from the point of view of applications but it also is important in explaining the mechanism of secondary electron emission. The different theories of secondary emission[1,2] give different angular distributions. According to Viatskin's theory[2] the electrons come out mainly at large angles ($\varphi \sim 65°$) with respect to the incoming electron direction in the case of normal incidence of the primaries. On the other hand, in the theory of Kadyshevich[1] the number of secondaries increases with decreasing angle φ. It has been shown in several investigations[3] that the yield of secondary electrons j (number of secondary electrons per steradian) decreases with increasing angle between the normal and the direction of emission. Kushnir and Frumin[4] have found for Mo and Ag that in normal incidence of the primary electrons, the secondary emission j first decreases with increasing angle φ; from a certain angle on, j begins to increase and reaches a maximum at an angle $\varphi \approx 60°$ to $70°$. An investigation of the secondaries from nickel[5] and soot[6], also for normal incidence of the primary electrons, showed that j changes approximately according to $\cos \varphi$. This is in disagreement with the results of Ref. 4. The main shortcoming of the above investigations seems to be the absence of compensation of the magnetic field of the earth which may greatly influence the trajectories of slow electrons (the radius of curvature of 3 ev electrons at $H \approx 0.5$ Oe is roughly 10 cm).

EXPERIMENTAL ARRANGEMENT

The measurement of the angular distribution of secondary electrons was performed with the following apparatus. The vacuum system had a spherical part with a diameter of 110 mm, the inside of which was painted with aquadag. This served as the collector for the secondary electrons. The collector was separated into five mutually insulated belts. The secondary electrons could reach only the upper four belts, the fifth was the lower half sphere. The areas and the median values of the angle φ for the different belts are: 1. 2 cm^2 and 12.5°; 2. 3.2 cm^2 and 24.3°; 3. 5.8 cm^2 and 55.3°; 4. 6.6 cm^2 and 79.5°. The emitter E, consisting of polycrystalline cuprous oxide, was placed in the center of the sphere. The emitter was attached to a cylindrical electrode with a diameter of 20 mm and a length of 17 mm. Inside of it was placed a thermocouple for temperature measurements and a bifilar filament W which served as a heater. The preparation and baking of the system was performed in the way as described in Ref. 7. The pressure in the system as measured by an ionization gauge before sealing off of the system was 10^{-6} cm Hg. After sealing off, a getter was flashed at 450° C. When connecting only one belt to the current measuring setup, the potentials on all belts remained equal. Two coils of 1m diameter were used to compensate the earth's magnetic field.

RESULTS

Figure 1 shows the resultant curves obtained from each belt separately and from the entire collector. The primary electron energy was $V_p = 400$ v; the temperature of the emitter was 400°. Figure 2 shows the energy distribution of the electrons. This was obtained under the same conditions by the method of electrical differentiation.[7,8] The form of the curves of the current at positive V_k (Fig. 1) and also of the energy distribution (Fig. 2) is quite different for the different belts. The slope of the current collected at belt 1 shows a sharp break at $V_k \approx 0$. For positive, increasing V_k, the value I_2 / I_1 keeps increasing until it saturates at $V_k \approx 20$ V. The curve showing the current to belt 2 also has a

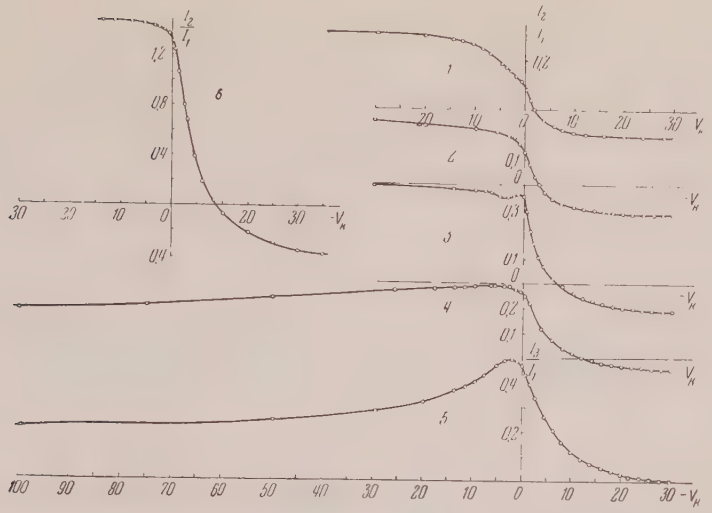

FIG. 1. Currents collected at $V_p = 400$ v and $t = 400°$; curves *1* to *5* for the belts 1 to 5 separately, curve *6* — total current.

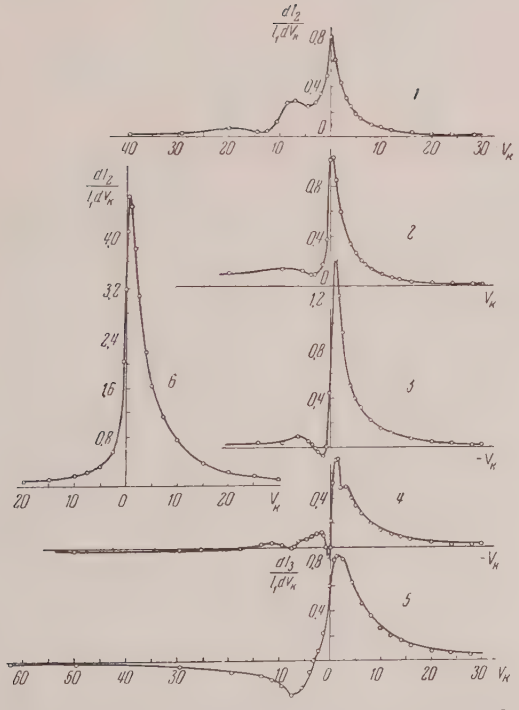

FIG. 2. Energy distributions for $V_p = 400$ v and $t = 400°$; curves *1* to *5* for the belts 1 to 5 separately, curve *6* for the whole collector.

break; it occurs at $V_k \approx 3$ v. At roughly the same voltage the curves of the currents to belts 3 and 4 even have an extremum. The currents to belts 2 and 3 increase monotonically while the currents to belts 4 and 5 decrease for increasing V_k. These collected currents, particularly for belt 5, still show rather marked variation around 30 v and reach saturation only around $V \approx 80$ v

As already mentioned, secondary electrons can not reach region 5 of the collector. Therefore the curve 5, Fig. 1, shows the current of tertiary electrons emitted from the other belts of the collector due to secondary electron impact at different collector potentials. The slight decrease of the values of this current for increasing positive V_k is due to a bending of the trajectories of the tertiary electrons by the electric field which deflects some of the electrons away from region 5 to the other belts. But even at very large positive V_k (100 – 150 v), the number of tertiaries reaching 5 is still roughly one half the value reaching it at $V_k = 0$.

The tertiary electrons emitted by any of the belts arrive not only at 5 but also at the belts 1 to 4. Therefore, the measured currents consist of the arriving secondaries, plus the tertiaries arriving from the other 3 belts, minus the tertiaries emitted by the belt under consideration and collected by the other belts and the emitter electrode. One must then reckon with the fact that the collected secondary currents to the different belts will be distorted for all values of V_k (even for large positive ones) by tertiary currents. The amount of distortion will be different for the different belts.

There was another source of errors in our setup. The secondary electrons striking the unpainted strips of glass (width 1mm) between the belts could charge up this surface, thus creating local electric fields. However it was possible to check on the existence of such fields by sudden changes in

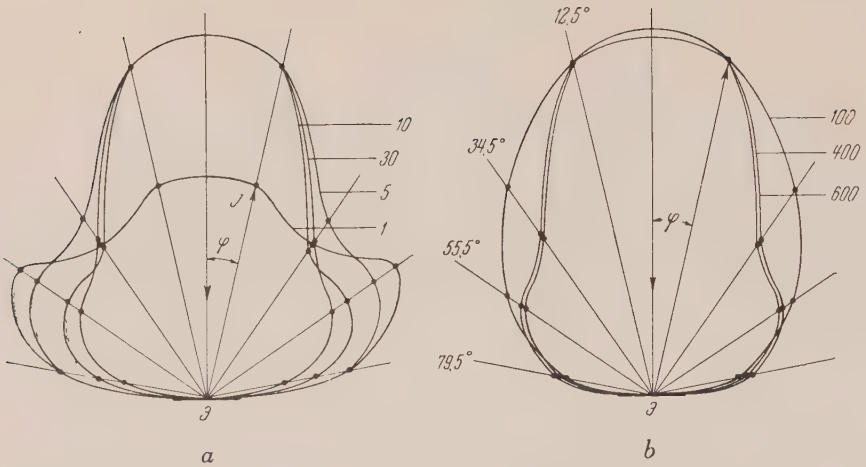

FIG. 3. Angular distributions at the following conditions: *a*. V_p = 400 v, V_k = 1, 5, 10 and 30 v; *b*. V_p = 100, 400, and 600 v, V_k = 30 v.

V_k. It turned out that the glass surfaces were essentially uncharged for positive, zero, and even for slightly negative V_k. This clearly can be explained in the following way. There are both fast electrons striking the collector for which the coefficient of secondary emission on glass, δ_1, is larger than 1, and slow electrons with a coefficient δ_2 smaller than 1. The fast ones would charge the glass positively, the slow ones negatively. Thus, under favorable ratios of fast to slow electrons as well as of δ_1 to δ_2, the glass surface will not become charged.

Figures 3 and 4 show the angular distributions as obtained in this experiment. (j is the current per steradian, φ—the angle to the normal). Except for curve *a*, Fig. 3, the different curves are normalized to coincide at $\varphi = 12.5°$. Curve *a*, Fig. 3, shows a pronounced maximum at $\varphi \approx 55°$ in addition to the high value of j at small angles This results in agreement with results of Ref. 4. However, with increasing positive values of V_k, the angular distributions become smoother by an increase of j at small angles ($\varphi = 12.5°$ and $35.5°$) and a decrease at $\varphi = 79.5°$ (see Fig. 1). At larger values of V_k, the distortions due to secondaries are somewhat smaller, due to the fact that more of them return to the belt from which they were emitted. Therefore, the angular distributions obtained for large positive V_k are closer to the actual values. The large values of j at large φ (55.3° and 79.5°) obtained here for small V_k (as well as in Ref. 4) are due to the larger distortions introduced by the tertiaries. For smaller primary electron energies (V_p = 100 v.), there should be emitted fewer tertiaries and therefore the distortions due to them should be smaller. Indeed as can be seen in Fig. 3b, the curves for V_p = 400 v and 600 v have a pronounced bump at 55° due to tertiaries which is absent from the curve for V_p = 100 v.

CORRECTION OF THE DISTORTIONS INTRODUCED BY TERTIARY ELECTRONS

In order to obtain the true angular distributions, one has to correct the experimental results for the influence of the tertiaries. It is advantageous to correct the results obtained at $V_k = 0$ since then the trajectories of the secondaries as well as the tertiaries will be straight lines and the electrons will keep the direction of their emission.

The procedure to obtain the corrections is as follows. The current of the tertiaries from the belts 1 to 4 reaching the region 5 is known. From the knowledge of the geometry of the apparatus— the areas of the belts and the solid angles with which the different belts see each other and the emitter electrode— it is possible to obtain the values of the tertiaries arriving from each of the belts at the region 5 and at the other belts and at the electrode containing the emitter. The corrected value of the secondary current reaching each belt can now be obtained by adding to the measured current the tertiary currents leaving the belt under consideration and subtracting the tertiary currents arriving from the other belts.

In order to obtain the different tertiary currents one needs to know the angular distribution of the emitted tertiaries. As pointed out earlier, the high values of j at large φ are due to tertiary electrons. One therefore can assume that the secondary emission increases monotonically with decreasing

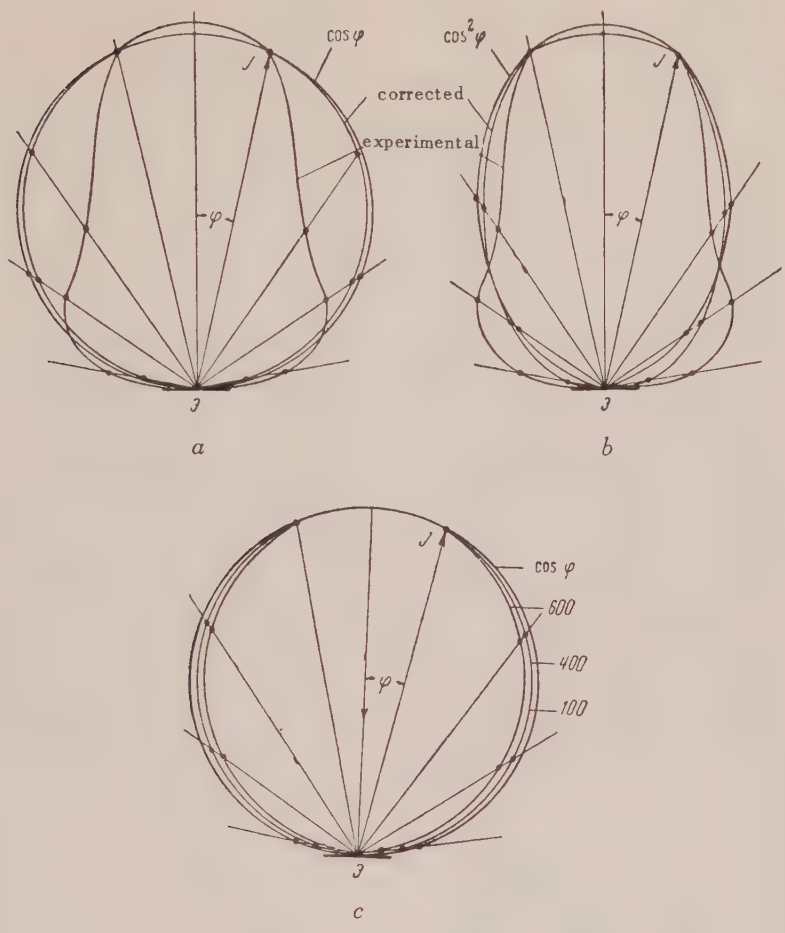

FIG. 4. Corrected angular distributions: *a*. assumed distribution ~ cos φ; *b*. assumed distribution ~ $\cos^2 \varphi$ (V_p = 400 v, V_k = 30 v for both *a* and *b*); *c*. assumed distribution ~ cos φ, V_p = 100, 400, and 600 v.

angle φ(see Fig. 3, b). A natural choice for the angular distribution seems tobe a dependence according to a power of cos φ. After applying the corrections, the distortions introduced bythe tertiaries should disappear andthe obtained angular distribution of the secondary emission should then coincide withthe assumed distribution.

DISCUSSION OF THE OBTAINED RESULTS

1. In Fig. 4a there is shown the corrected angular distribution with corrections according to a cos φdependence, while in Fig. 4b, a dependence according to $\cos^2 \varphi$ was chosen. It turned out that these powers of cos φresulted in corrected curves closest to the assumed dependence (viz. cos φor $\cos^2 \varphi$ respectively). As already mentioned the distortions introduced by the tertiaries decrease with increasing V_k. Therefore, the character of the curves of Fig. 1 indicates the sign ofthe corrections forthe different belts. Thusthe correction for belt 4 should decrease the measured value of j, since I_2 / I_1 decreases with increasing V_k (Fig. 1, curve 4). This is the case both for the cos φand the $\cos^2 \varphi$distribution (Fig. 4a and b). Similarly, the correction for belt 3 should increase the measured value of j in accordancewith curve 3, Fig. 1. However this is the case only for the distribution cos φ(Fig. 4a) and not for $\cos^2 \varphi$ (Fig. 4b). Therefore one hasto conclude that the angular distribution of secondary electrons emitted from cuprous oxide has the form cos φ.

Fig. 4c shows the angular distributions obtained with primary electron energies of 100, 400, and 600 v. The angular distributions for 100 and 400 v are almost identical while the one for 600 v is slightly narrower, indicating a decrease of emission at large angles.

2. We now shall discuss the results obtained on the energy distribution of secondary electrons for the different directions of emission. In the region of positive V_k the curves for the energy distributions (see Fig. 2) are distorted for the following reasons: as V_k decreases, (*i*) the number of tertiary electrons surmounting the retarding field and reaching the electrode with the emitter increases; (*ii*) the number of tertiary electrons arriving from the other belts increases. The first effect decreases, and the second increases, the values of the measured currents. The relative number of tertiaries leaving the first belt is considerably larger than the number of tertiaries arriving. Therefore, the distortions for this belt are larger, as is borne out by our results (Fig. 2).

The value of the total current from the collector (Fig. 1, curve *6*) is not constant for different positive V_k but decreases markedly with decreasing V_k, beginning at approximately 10 v. Accordingly, the curve showing the energy distribution of the electrons reaching the collector (Fig. 2, curve *6*) in this same region shows a large value. This decrease of the collected current can be explained by the increased number of tertiaries reaching the emitter electrode due to the decrease of the retarding field associated with the decrease of the positive value of V_k.

In the region of negative V_k there also exist distortions. As V_k becomes more negative, (*i*) the number of tertiaries reaching the electrode *E* decreases because the number of (low energy) secondaries reaching the collector decreases, and (*ii*) more tertiary electrons which were emitted in such directions as to miss the emitter electrode are deflected towards it by the electric field and reach it nevertheless.

The ratios I_2 / I_1 attain negative values starting with a certain small negative V_k (see Fig. 1). This comes about when the number of tertiaries leaving the belt is larger than the number of secondaries arriving at the belt. In our numbering of the belts the ratio of the number of tertiary electrons leaving a belt to that arriving at the belt increases with decrease of the belt number. Therefore the value of V_k at which the ratio I_2 / I_1 becomes negative decreases as one goes from belt 4 to belt 1. (Fig. 1). Negative I_2 / I_1 in the region of negative V_k have been obtained also by other authors (see for example Refs. 9,10), who obtained results corresponding to our curve *6*, Fig. 1.

Curve 5, Fig. 2, shows the "speed" of the decrease of the number of tertiaries reaching belt 5 with increasing negative V_k. To a certain degree, it shows the distortions introduced by tertiary emission in the energy distributions of the secondaries obtained for the four other belts. For a given belt, the number of arriving tertiaries increases and the number of arriving secondaries decreases with increasing φ. For belt 4, the number of arriving tertiaries is greater than the number of arriving secondaries. One therefore should expect rather large distortions here. Indeed, curve 4, Fig. 2 shows a kink at $V_k \sim 3$ v, due to the considered distortions.

The position of the maximum in the curves of the energy distribution is being displaced insignificantly towards higher electron energy with increase of the emission angle of the secondaries. This displacement amounts to roughly 1 v for a change of φ from 12.5° to 79.5.° This is considerably smaller than as observed in Ref. 4, where this displacement was 20 v and larger. It is possible that our small value for the displacement is due to distortions from tertiary electrons which may have a different influence on the energy distributions of the different belts.

I am grateful to L. M. Rakhovich, A. Iu. Reitsakas, V. A. Bolotin and R. S. Breslav, who participated in performing the measurements.

[1] A. E. Kadyshevich, J. Exptl. Theoret. Phys. (U.S.S.R.) 9, 930 (1939).

[2] A. Ia. Viatskin, J. Exptl. Theoret. Phys. (U.S.S.R.) 12, 22 (1942).

[3] K. G. McKay, *Secondary Electron Emission*, in *Advances in Electronics*, L. Marton Editor, (Acad. Press Inc., 1948) Vol. 1, p. 65.

[4] Iu. M. Kushnir and M. I. Frumin, J. Techn. Phys. (U.S.S.R.) 11, 317 (1941).

[5] J. H. L. Jonker, Philips Res. Rep. 6, 372 (1951).

[6] J. L. H. Jonker, Philips Res. Rep. 8, 434 (1953).

[7] N. B. Gornyi, J. Exptl. Theoret. Phys. (U.S.S.R.) 27, 171 (1954).

[8] N. B. Gornyi and I. M. Rakhovich, J. Exptl. Theoret. Phys. (U.S.S.R.) 26, 454 (1954).

[9] A. I. Piatnitskii, J. Techn. Phys. (U.S.S.R.) 8, 1014 (1938).

[10] J. B. Johnson and K. G. McKay, Phys. Rev. 91, 582 (1953).

Translated by M. Danos
79

Interaction of π^-–Mesons with Lead, Copper, Oxygen and Beryllium Nuclei

A. E. IGNATENKO, A. I. MUKHIN, E. B. OZEROV AND B. M. PONTECORVO
Institute for Nuclear Problems , Academy of Sciences, USSR
(Submitted to JETP editor June 15, 1956)
J. Exptl. Theoret. Phys. (U.S.S.R.) 31, 546–549 (October, 1956)

Measurements were made of the total cross sections σ_t for interaction of π^-–mesons with Be, C and O nuclei and of cross sections σ_{in} for inelastic collisions of π^-–mesons with Be, C, Cu and Pb in the energy range from 140 to 400 mev. Cross sections were determined by measuring the attenuation of a meson beam which passed through the scatterer, using scintillation counters. The energy dependence of the cross sections σ_t and σ_{in} for nuclei in general shape resemble the energy dependence of the total scattering cross sections of pions on hydrogen and deuterium. Results of the cross section measurements were analyzed on the basis of the optical model. It can be concluded, as a result of this analysis, that the optical model with parameters computed on the basis of the single Coulomb interaction of the mesons with the nuclei, satisfactorily describes the energy dependence of the cross sections in the energy range of 140 to 400 mev.

N order to study interaction processes between π^-–mesons and nuclei, measurements were made of total cross sections σ_t of π^-–meson interactions with Be, C and O nuclei and of cross sections σ_{in} for inelastic collisions of π^-–mesons with Be, C, Cu and Pb nuclei in the energy range from 140 to 400 mev. Results of total cross section σ_t measurements were reported earlier. In this communication we shall first describe results of σ_{in} measurements and then discuss the results of these measurements as well as the total cross sections.

Cross sections σ_{in} were determined by measuring the attenuation of a meson beam passed through the scatterer, by the method of scintillation counters. A description of experimental conditions and equipment for meson recording is contained in Refs. 1 and 2.

Measurements of Be and C cross sections for all values of energy were carried out at a distance of 6 cm between the center of the scatterer and the last scintillator, which corresponded to an average registration angle θ for the last detector of about 40°. Experiments with Cu and Pb were carried out at $\theta = 25°$. Results of measurements are shown in Table I. In the first column are given the π-meson energies in the center of the scatterer. In columns 2 to 5 are given the "measured" cross sections. The values of these cross sections include a number of introduced corrections. These corrections account for: 1) admixture of μ-mesons, 2) chance coincidences, 3) excess counts in the recording equipment. The above-mentioned corrections were discussed previously.[1,2] The errors shown in columns 2 to 5 include statistical errors as well as the uncertainty in the corrections.

The σ_{in} for inelastic collisions were obtained from the "measured cross sections" shown in columns 2 to 5. Corrections were introduced to account for the inelastically scattered mesons within the limits of angle θ and for the secondary charged particles capable of being registered in the last detector. It should be noted that the introduction of these corrections presents great difficulties. The difficulties arise because the investigations of the processes of scattering and absorption of mesons in nuclei have been carried out basically only for elements entering into photoemulsions. Results of Refs. 3 to 5 were used in making corrections. Corrections related to inelastic scattering of mesons were different for different energies and varied from (3 ± 1.5) to (8 ± 4)% for Be and C and from (2 ± 1) to (5 ± 2)% in the case of Cu and Pb. The corrections were higher for higher energy π–mesons.

Corrections for secondary charged particles capable of being registered in the last detector were taken to be the same in all cases and equal to (3 ± 1.5)% as evaluated from the data in Ref. 4, the only available source. Besides the above corrections, corrections were also introduced connected with mesons elastically scattered at angles greater than θ. This correction was introduced only for mesons of 140 mev, where it was substantial; in all other cases this correction was too small and was neglected. The correction was evaluated on the basis of diffraction scattering theory for a "non-transparent" nucleus.

The cross sections σ_{in} obtained for inelastic collisions of π^-–mesons with Pb, Cu, C and Be nuclei are given in columns 6 to 9 of the Table. In making the above-mentioned corrections account was also taken of the uncertainties in their values.

TABLE

Energy of π^--mesons mev	"Measured" cross sections (10^{-27} cm^2)				Cross sections for inelastic collisions σ_{in} (10^{-27} cm^2)			
	Pb $\left(8{,}4\ \frac{z}{cM^2}\right)^*$	Cu $\left(5{,}3\ \frac{z}{cM^2}\right)^*$	C $\left(6{,}5\ \frac{z}{cM^2}\right)^*$	Be $\left(7{,}2\ \frac{z}{cM^2}\right)^*$	Pb	Cu	C	Be
140±7	2244±95	999±42	327±13	300±17	2356±152	1048±67	350±24	273±20
216±7	2250±93	976±44	297±15	257±11	2430±183	1054±84	326±31	275±21
256±7	2142±90	850±41	245±13		2313±175	918±76	269±26	
290±7			150±12	137±9			166±21	150±16
350±7								

*The thickness of the used scatterer is shown in parenthesis.

The energy dependence of the cross sections σ_{in} was shown in Fig. 1. The same Figure contains values of cross sections σ_{in} for energies less than 140 mev measured by means of scintillation counters.[6,10] The given values of σ_{in} include corrections for the Coulomb interaction.

As can be seen from Fig. 1, the energy dependence of cross sections σ_t and σ_{in} for all nuclei resembles in general the energy dependence of the total cross section for scattering of π^--mesons by hydrogen and deuterium. In the energy region of 100 to 250 mev, the cross section depends only slightly on energy, while at energies greater than 250 mev, the cross section decreases comparatively rapidly. The cross section also changes at a fast rate at energies less than 100 mev. The cross sections σ_t and σ_{in} go through a maximum in the energy interval ($\sim$ 190 mev) where the total scattering cross sections of π-mesons in hydrogen and deuterium reach their maximum values. When studying phenomena associated with the entrance of mesons into nuclei, it is of interest to know the average path length λ of the mesons in the nuclear matter. In order to obtain information on the energy dependence of the path, $\lambda = f(E)$, on the basis of the optical model, an analysis was made of the results obtained in cross section measurements. With the nuclear radius taken as $R = 1.42 \times 10^{-13} \times A^{1/3}$ cm, values of λ were then found such that the magnitudes σ_{in} for Be and C satisfy the expression

$$\sigma_{in} = \pi R^2 \left\{1 - \frac{1}{2}\left[1 - (1 + 2R/\lambda) \exp\{-2R/\lambda\}\right](\lambda/R)^2\right\}$$

for all energies. The obtained values of λ are shown in Fig. 2. In the same Fig. are also shown values of λ for energies less than 140 mev as obtained by a number of workers cited in Ref. 11.

If we assume that the π-mesons interact with separate nucleons in the nucleus, then the free path can be computed from the data on cross sections of π-meson interaction with free nucleons and the expression

$$\lambda' = [\rho_p \alpha \sigma_t(\pi^-, p) + \rho_n \beta \sigma_t(\pi^-, n)]^{-1},$$

where ρ_p and ρ_n denote the density of protons and neutrons, respectively, in the nucleus, $\sigma_t(\pi^-, p)$ and $\sigma_t(\pi^-, n)$ = total interaction cross sections of π^--mesons with free protons and neutrons, α and β = coefficients smaller than unity introduced to account for the Pauli principle. In computing the values of λ' for hydrogen in the energy region from 30 to 350 mev the value $\alpha = \beta = 1$ was used. On the basis of charge symmetry values of $\sigma_t(\pi^+, p)$ were used in place of $\sigma_t(\pi^-, n)$. The

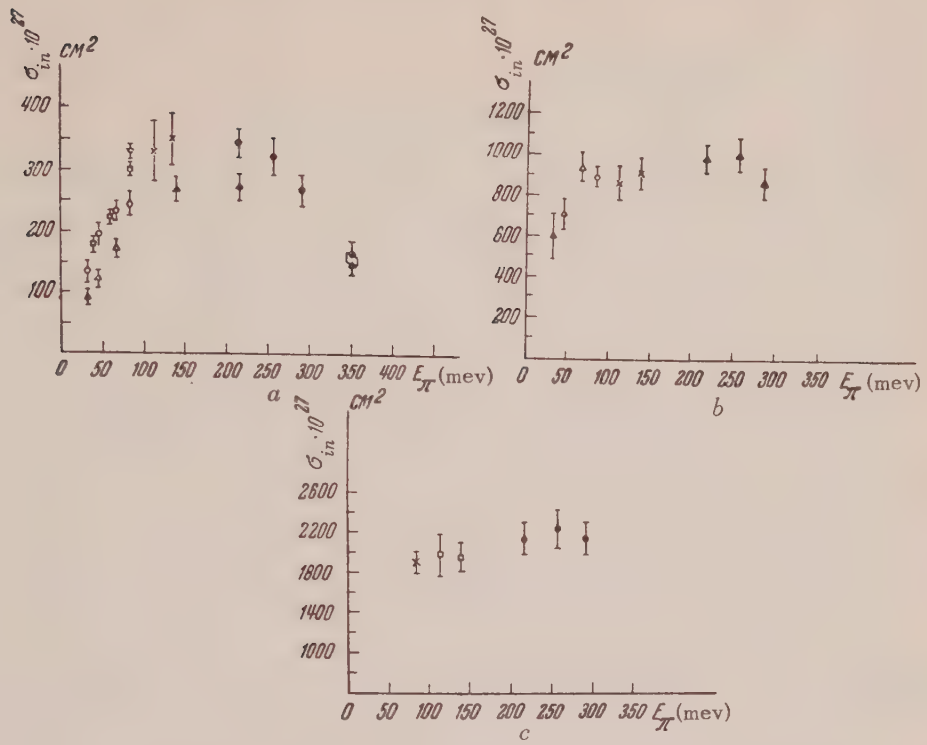

FIG. 1. Energy dependence of cross sections for inelastic collisions of π–mesons with nuclei.
a – beryllium and carbon: ●–(π^-, C), this work; ▲–(π^-, Be), this work; ○–(π^-, C), Ref. 7; Δ–(π^+, Be), Ref. 10; O–(π^+, C), Ref. 10; ◇–(π^-, Be), Ref. 8; ×–(π^-, C), Ref. 9; ▽–(π^-, C), Ref. 8.
b – Copper: ▲–(π^-, Cu), this work; ×–(π^-, Cu), Ref. 9; O–(π^-, Cu), Ref. 8; Δ–(π^+, Cu), Ref. 10.
c – lead: ●–(π^-, Pb), this work; □–(π^-, Pb), Ref. 9; ×–(π^-, Pb), Ref. 8.

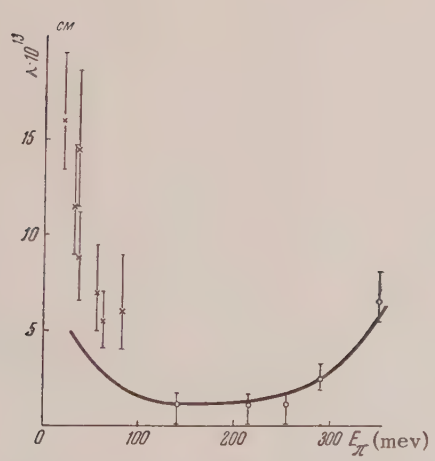

FIG. 2. Dependence on energy of the meson path λ in the nuclear matter. [O–experimental points obtained by the optical model in the present work; ×– works cited in reference 11; solid curve computed without allowance for the Pauli principle from cross section data for scattering of π-mesons by nucleons.

values of $\sigma_t(\pi^-, p)$ and $\sigma_t(\pi^+, p)$ were taken from a series of published works. Results of λ′ computations are shown in Fig. 2 in the form of a solid line.

As can be seen from Fig. 2, there is an agreement between the values of λ and λ′ in the energy region greater than 200 mev where it is more justifiable to neglect the effect of the Pauli principle. This fact indicates directly that the initial assumption was correct, i.e., that the interaction of π-mesons in the nucleus takes place basically with its separate nucleons. This conclusion can be supplemented by making a comparison between the experimentally obtained relationships $\sigma_t = f(E)$ and $\sigma_{in} = f(E)$ and the similar relationships computed by Sternheimer on the basis of the optical model in the energy region of 100 mev to 2.5 bev.[12] This comparison is especially interesting because in computing the energy dependence of the elastic scattering $\sigma_e = f(E)$, values of the real parts of

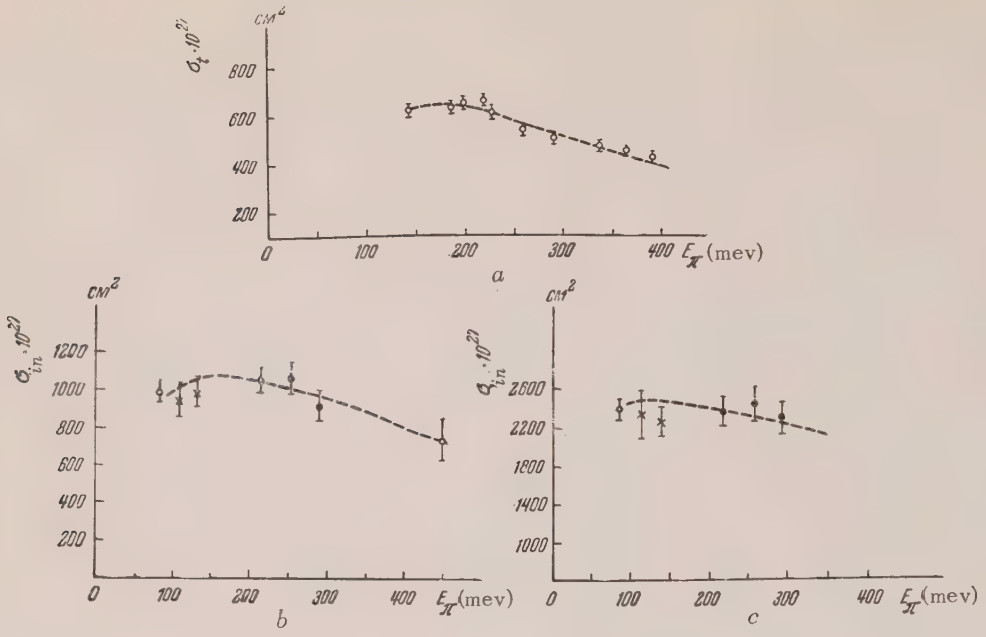

FIG. 3. Comparison of experimentally obtained energy dependence of cross sections for different nuclei computed on the basis of the causality condition.[12]

a – Total cross section for carbon [O–(π^-, C)], measured in Ref. 1.

b – Cross section of nonelastic collisions for copper: ●–(π^-, Cu), this work; ×–(π^-, Cu), Ref. 9; O–(π^-, Cu), Ref. 8; □–(π^-, Cu), Ref. 13.

c – Cross section of nonelastic collisions for lead: ●–(π^-, Pb), this work; ×–(π^-, Pb), Ref. 9; O–(π, Pb), Ref. 8.

Computed curves are shown dotted.

the forward scattering amplitudes were used, obtained in the basis of the causality condition from one data on total cross sections of meson scattering by protons. The dotted line in Fig. 3*a* represents the energy dependence of the total cross section for carbon obtained by the summation of the computed $\sigma_{in} = f(E)$ and $\sigma_e = f(E)$. Good agreement can be seen to exist between the computed and measured dependence of the total cross section on energy $\sigma_t = f(E)$. In Figs. 3*b* and 3*c*, where a comparison is made between the measured and computed cross sections for inelastic collisions in copper and lead, agreement between measured and computed cross sections can also be observed within limits of experimental errors.

Thus, the analysis of the results permits us to conclude that the optical model, with parameters computed on the basis of the single nucleon interaction mechanism between mesons and nuclei, satisfactorily describes the energy dependence of the total and inelastic cross sections for beryllium, carbon, copper and lead in the energy range of 140 to 400 mev.

From the cross sections σ_t and σ_{in} in the range of energies close to 190 mev (where the real part of the interaction potential between π^-–mesons and the nucleus passes through zero[12]) it is possible to derive information on the sizes of nuclei. Indeed, values of the total cross sections σ_t for beryllium, carbon, oxygen and of inelastic collision cross sections for beryllium, carbon, copper and lead in this energy region are equal to values of $2\pi R^2$ and πR^2, respectively, if the nuclear radius is taken equal to $R = 1.42 \times 10^{-13} \times A^{1/3}$cm.

In conclusion we consider it our pleasant duty to thank I. V. Popov and G. N. Tentiukov for the assistance given by them in carrying out certain computations.

[1]Ignatenko, Mukhin, Ozerov and Pontecorvo, Dokl. Akad. Nauk SSSR 103, 395 (1957).

[2]Ignatenko, Mukhin, Ozerov and Pontecorvo, Dokl. Akad. Nauk SSSR 103, 45 (1955).

[3]N. A. Mitin and E. L. Grigoriev, Dokl. Akad. Nauk SSSR 103, 219 (1955).

[4]Dzhelepov, Ivanov, Kozodaev, Osipenkov, Petrov and Rusakov, Reports (Otchet) Inst. Nucl. Prob. Acad. Sci. USSR (1955).

[5]A. H. Morrish, Phys. Rev. 90, 674 (1953).

[6]A. Shapiro, Phys. Rev. 84, 1063 (1951).

[7]Isaacs, Sachs and Steinberger, Phys. Rev. 85, 803 (1952)

[8]Chadester, Isaacs, Sachs and Steinberger, Phys. Rev. 82, 958 (1951).

[9]R. L. Martin, Phys. Rev. 87, 1052 (1952).

[10]D. H. Stork, Phys. Rev. 93, 868 (1954).

[11]F.H. Tenney and J. Tinlot, Phss. Rev. 92, 974 (1953).

[12]R. M. Sternheimer, Phys. Rev. 101, 384 (1956).

[13]L.C.L. Yuan and S. J. Lindenbaum, Phys. Rev. 92, 1578 (1953).

Translated by J. L. Herson
117

SOVIET PHYSICS JETP VOLUME 4, NUMBER 3 APRIL, 1957

A Calorimetric Determination of the Mean Energy of the β-Spectra of P^{32}, S^{35}, Cu^{64}, W^{185} and Au^{198}

N. S. SHIMANSKAIA
Radium Institute, Academy of Sciences, USSR

(Submitted to JETP editor March 3, 1956)
J. Exptl. Theoret. Phys. (U.S.S.R.) 31, 393-396 (September, 1956)

The mean energy $\bar{E}_\beta$ of the β-spectra of P^{32}, S^{35}, Cu^{64}, W^{185} and Au^{198} were determined by the calorimetric method. The following values of $\bar{E}_\beta$ were obtained for the above isotopes, respectively: 693 ± 22; 52 ± 2; 213 ± 12; 144 ± 7 and 317 ± 15 kev.

1. THE electrons and positrons emitted during β-decay have a continuous energy spectrum. The mean energy of the β-particles

$$\bar{E}_\beta = \int_0^{E_{max}} En(E)\,dn \Big/ \int_0^{E_{max}} n(E)\,dn \qquad (1)$$

is always less than the maximum value E_{max} and for most β-active isotopes equals 0.3–0.4 E_{max}. The exact values of $\bar{E}_\beta$ are usually found from the spectral distribution of β-electrons, measured with the help of a magnetic or any other β-spectrograph. It should be borne in mind, however, that the experimental investigation of the shape of the whole β-spectrum is difficult, and the spectral distribution obtained can be quite incorrect. The finite thickness of the source and of the counter window, the scattering of electrons from the source mount and from the walls and baffles of the spectrograph, the diffusion of radioactive atoms into the source mount, the electrical charging of the latter, and other causes can markedly alter the shape of the β-spectrum, especially in the low-energy region. The errors of the values of $\bar{E}_\beta$ obtained by this method are in most cases not less than 3–5%

The methods of determination of $\bar{E}_\beta$ with the help of an extrapolation chamber[1] and absorption measurements[2] are as yet unsufficiently developed.

The idea of the calorimetric determination of the mean energy of the β-spectrum lies in the simultaneous measurement of the calorimetric effect Q of the β-radiation and of the number of disintegrations A of the sample. The mean energy $\bar{E}_\beta$ follows from the self-evident relation

$$\bar{E}_\beta = Q/A. \qquad (2)$$

The calorimetric method, notwithstanding its numerous advantages and relative simplicity, has almost not been used. Since the well-known experiments of Ellis and Wooster[3] who measured the mean energy of the β-electrons of RaE*, the mean energy $\bar{E}_\beta$ has been determined by the calorimetric method in the last 25 years for two cases of β-emitters only, namely, for H^3 [6] and P^{32} [7].

We determined the mean energy of the β-spectra of five β-active isotopes: P^{32}, S^{35}, Cu^{64}, W^{185} and Au^{198} using double static calorimeters having a sensitivity of 5×10^{-6} W/mm.[8] The method used is described below in short and the results are

*These classical experiments which played an important role in the formation of the modern theory of the β-decay and the neutrino hypothesis were repeated by Meitner and Ortmann[4], and also by Zlotowski.[5]

Results of the calorimetric determination of the mean energy of the β-spectra of P^{32}, S^{35}, Cu^{64}, W^{185} and Au^{198}

Radio-isotope	Decay scheme	E_{max}, kev	Half-life	Original compound	Weight P, grams	Spec. activity $\rho \times 10^{-8}$ $\frac{\beta\text{-particles}}{sec \cdot g}$	Cal. effect $Q \times 10^{-6}$ W	Mean energy $\bar{E}\beta$, kev		
								Calori-metric	spectro-metric	calc.
1	2	3	4	5	6	7	8	9	10	11
P^{32}	Fig. 3*a*	1700	14.30 days	Na_2HPO_4	3.09008	17.0	581	693±22	675 [9] 698 [10]	695
S^{35}	Fig. 3*b*	167	87.1 days	Na_2SO_4	1.03831	191	165	52±3	49,1 [11]	49.4
Cu^{64}	Fig. 3*c*	571 (β^-) 657 (β^+)	12.8 hours	$CuSO_4$	2,94220	33.2	376	213±12	187 (β^-) } [12] 272 (β^+) } 215	172 (β^-) } 273 (β^+) } 206
W^{185}	Fig. 3*d*	428	73.2 days	W	2.64281	21.0	128	144±7	152 [13]	126
Au^{198}	Fig. 3*e*	960 (99%) 290 (~1%)	2.69 days	Au	0.08588	993	504 (β-calorimeter) 1010 (γ-calorimeter)	317±15; $\bar{E}_\beta + \bar{E}_\gamma = 740 \pm 40$	309 [14]	—

given for the above-mentioned isotopes.

2. A known mass of a chemical compound or element, containing radioactive atoms of the isotope in question, was placed in a thin-walled glass or brass container, and its calorimetric effect measured in a calorimeter. The absorption of the β-radiation in the source itself and in the walls of the calorimetric vessel surrounding it was accounted for, as well as the energy of the bremsstrahlung radiation not absorbed in the calorimeter in the case of hard β-rays emitters. In the case of the relatively short-lived isotopes Cu^{64} and Au^{198}, a correction was made for the heat inertia of the calorimeter used.[8] A small mass (10–30 mg) of the radioactive material was weighted carefully and dissolved in a known volume of distilled water or appropriate acid. Sources for absolute and relative β-measurements were then prepared from this solution which contained a known mass of the radioisotope per unit volume. Measurements carried out using a conventional set-up and a T–4 end window counter helped to determine the so-called mean coefficient, which was needed later for the absolute β-activities of certain sources. As a check of the radioactive purity of the sample, the half-life and the β-absorption curve in aluminum were measured using the same set-up.

The absolute β-measurements of the specific activity ρ of the sources (the number of disintegrations per mass unit of the mother radioactive material) were carried out in a special set-up with a predetermined solid angle. The value of the specific activity ρ and of the calorimetric effect Q of a given weight p being known, $\bar{E}_\beta$ could be computed with the help of the following formula:

$$\bar{E}_\beta = qQ/p\rho, \qquad (3)$$

where q is a factor equal to 6.24×10^{12} where p is in grams, ρ in disintegrations per gram second, Q in watts and where $\bar{E}_\beta$ is obtained in mev. The accuracy of the measurement of $\bar{E}_\beta$ by such a calorimetric method was limited mainly by the errors of the absolute β-measurements and in our case amounted to 3–6% for different isotopes.

3. The results of the calorimetric determinations of β-spectra mean energy of the radioisotopes P^{32}, S^{35}, Cu^{64}, W^{185} and Au^{198} obtained by us are given in column 9 of the Table. The measured values of p, ρ and Q are found in respective columns.

Since the calorimetric measurements and the absolute β-activity determinations were carried out within relatively long time intervals (usually not shorter than 1–2 half-life periods), mean values of ρ and Q were used in the computations. For this purpose, linear semi-logarithmic plots, based on experimental points, were used (see Figs. 1 and 2 for the cases of P^{32} and S^{35}), the slopes of which were equal to the half-life of the respective isotope. The values of the absolute activities and of the calorimetric effects, needed for the computation of $\bar{E}_\beta$, were taken from these plots, a procedure which tended to reduce fluctuations of single measurements and somewhat enhanced the accuracy of results. The mean values of ρ and Q for a given time are listed in respective columns of the Table. For the case

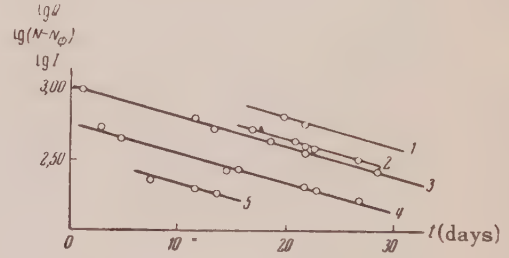

FIG. 1. Measurements of P^{32} samples: *1,2*– measurements of the absolute β-activity of the sources P^{32} II and P^{32} III used for the determination of the specific activity of the original P^{32} preparation; *3*–measurement of the half-life of the sample; *4*-calorimetric measurements; *5*–measurements of the bremsstrahlung radiation intensity with an ion chamber: $N-N_\phi$ is the number of pulses per minute (curves *1*, *2* and *3*), Q is the calorimetric effect (curve *4*), I is the ionization (curve *5*).

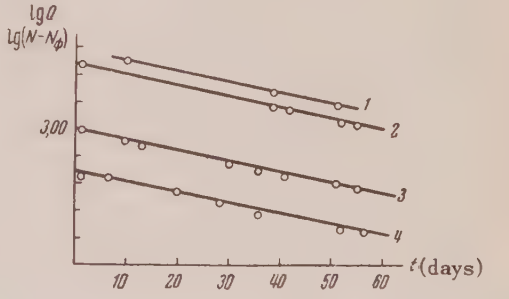

FIG. 2. Measurements of S^{35}: *1,2*–measurements of the absolute β-activity of the sources S^{35} I and S^{35} II used for the determination of the specific activity of the original S^{35} sample; *3* – measurements of the half-life of the S^{35} sample; *4* – calorimetric measurements.

of Au^{198}, the measurements were carried out not only in the thin-walled β-calorimeter, but also in a γ-calorimeter[8], in which the thickness of the walls of the inner cylinders ensured the total absorption of γ-rays up to energies of 700 kev. These

measurements made it possible not only to determine the mean energy of the β-spectrum of Au^{198}, but also the total "heat energy" of the decay, equal to $\overline{E}_\beta + \Sigma n\gamma E\gamma$. This value is also given in the table. The calorimetric measurements in the β-calorimeter as well as the absolute β-measurements of Au^{198} sources with the help of a β-counter were corrected for the 410 kev γ-conversion line, and in the case of Cu^{64} samples K-capture x-rays were accounted for. For comparison, values of mean energies computed by us from the best spectrometric values are given in column 10, and values obtained from the Fermi formula under the assumption of resolved β-spectrum in column 11.

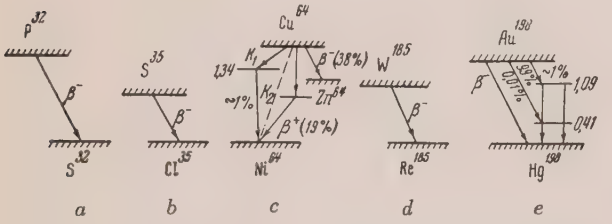

FIG. 3. Decay schemes: a—P^{32}, b—S^{35}, c—Cu^{64}, d—W^{185} and e—Au^{198}

The comparison of these values with our results of the calorimetric determination of $\overline{E}_\beta$ is generally satisfactory. It should be noted that the isotopes worked with were mainly those, the spectrum of which is well known and which corresponded to the case of the resolved β-spectrum.

[1] R. Caswell, Phys. Rev. 86, 82 (1952).

[2] H. Schopper, Ark. Fys 3, 441 (1952).

[3] C. Ellis and W. Wooster, Proc. Roy. Soc. (London) A117, 109 (1929).

[4] L. Meitner and W. Ortmann, Z. Physik 60, 143 (1930).

[5] I. Zlotowski, Phys. Rev. 60, 483 (1941).

[6] Jenks, Ghormley and Sweeton, Phys. Rev. 80, 990 (1950).

[7] I. Bayly, Canad. J. Res. 28, 520 (1950).

[8] N. S. Shimanskaia, Trudy Radium Inst., Acad. Sci., USSR 7, 198, 216 (1956).

[9] K. Siegbahn, Phys. Rev. 70, 127 (1946).

[10] H. Agnew, Phys. Rev. 77, 655 (1950).

[11] Cook, Langer and Price, Phys. Rev. 74, 548 (1948).

[12] C. Cook and L. Langer, Phys. Rev. 73, 601 (1948).

[13] F. Schull, Phys. Rev. 74, 917 (1948).

[14] A. A. Bashilov and B. S. Dzhelepov, Izv. Akad. Nauk SSSR, Ser. Fiz. 14, 299 (1950).

Translated by H. Kasha
80

Investigation of Two-Electron Capture in Collisions between Positive Carbon or Oxygen Ions and Gas Molecules

IA. M. FOGEL', R. V. MITIN AND A. G. KOVAL'
Physico-Technical Institute, Academy of Sciences, Ukrainian SSR
(Submitted to JETP editor March 10, 1956)
J. Exptl. Theoret. Phys. (U.S.S.R.) 31, 397-404 (September, 1956)

The investigation of the processes of two-electron capture by singly-charged positive carbon and oxygen ions in collisions with He, Ne, A, Kr and Xe atoms and H_2, N_2 and O_2 molecules was carried out with the help of a double mass-spectrometer set-up. The effective cross sections for these processes were measured for the C_1^+ and O_1^+ ions in the energy range 10.7-54.5 kev.

INTRODUCTION

THE effect of the double change of the charge, i.e., the capture of two electrons in single collisions between positive ions and gas molecules has not been studied sufficiently. The first order-of-magnitude measurement of the cross section for this process was reported in Ref. 1. Two-electron capture by protons in different gases was studied in Ref. 2, and that by singly charged positive oxygen ions in hydrogen, nitrogen and oxygen in Ref. 3. The effective cross sections of the two-electron capture by triply-charged argon ions in collisions with N, Ne and A atoms were measured in Ref. 4. The main result of the above investigations was the discovery that the effective cross section of the two-electron capture is not neglibly small as compared with the one-electron capture cross section, and in some cases can attain gas-kinetic values. Further study of the two-electron capture processes, its laws and connection with other inelastic processes in collisions between fast ions and gas molecules is therefore of considerable interest.

The effective cross sections of two-electron capture in the passage of C_1^+ and O_1^+ ion beams through Ne, He, A, Kr, Xe, H_2 and O_2 were measured in the course of the present work.

APPARATUS AND EXPERIMENTAL METHODS

The investigation of two-electron capture processes in the collisions between C_1^+ and O_1^+ ions and gas molecules was carried out with the help of a double-mass-spectrometer set-up, described in detail in Ref. 3. CO_2 was passed through a bimetal valve into the high-frequency ion source in order to obtain beams of the C_1^+ and O_1^+ ions. A mass-spectrometer analysis of the ion beam revealed, besides the C_1^+ and O_1^+ ions, considerable quantities of CO^+ and CO_2^+ ions and small quantities of H_1^+, H_2^+, H_3^+ and N_1^+ ions, as well as C_1^+ and O_1^+ ions resulting from the dissociation of CO^+ ions in the drift space in front of the mass-monochromator. The dispersion of the mass-monochromator was sufficient to resolve the C_1^+ peak from the adjoining N_1^+ peak, and the peak of C_1^+ ions from dissociated CO^+, and to resolve the O_1^+ peak from the adjoining N_1^+ peak as well.

The determination of the effective cross sections of the two-electron capture by C_1^+ and O_1^+ ions was effected by the mass-spectrometric method, described in detail in Refs. 1 and 3. In order to calculate the cross section, it is necessary to determine the slope of the linear part of the curve $I^-/I^+ = f(p)$ (where I^-/I^+ is the ratio of the currents of the negative and positive components of the beam which have traversed the collision chamber, filled with a gas at pressure p). It should be taken into account that a part of the negative ions in the beam that leaves the chamber is formed by the residual impurity gases in the chamber. We have accounted for this by determining the two-electron capture cross sections from the slope of the linear part of the curve

$$(I^-/I^+) - (I^-/I^+)_\phi = f(p - p_\phi),$$

where $(I^-/I^+)_\Phi$ is the ratio I^-/I^+ in the beam after traversing the residual gas in the collision chamber and p_Φ is the pressure of the residual gas. The value of $(I^-/I^+)_\Phi$ depends on the composition of the residual gas. It was shown in Ref. 2 that the value of $(I^-/I^+)_\Phi$ can be reduced by an order of

magnitude by inserting a liquid air trap into the collision chamber. Such a suppression of the background is connected with the lowering of the organic vapor pressure of the various organic substances (the diffusion pump oil and its decomposition products, the vacuum grease, etc.) always present in the residual gas, and which then condense on the cool surface of the trap. Since this freezing out of organic vapors causes a considerable rise in the value of $[I^-/I^+) - (I^-/I^+)_\Phi]/(p - p_\Phi)$ and, consequently, in the accuracy of the measurements of the two-electron capture cross section, we have used this method in the present work. For this purpose the collision chamber of Ref. 3 was replaced by a new one, fitted with a trap. Besides, it was now possible to measure the beam current directly at the outlets of the input and the output channels of the collision chamber with the help of two Faraday cylinders which could be placed into, and removed from, the beam by means of magnetic control.

The gas pressure in the region of the linear part of the plot $(I^-/I^+) = f(p)$, i.e., up to the pressure of $1 - 2 \times 10^{-4}$ mm Hg was measured with a Knudsen gauge, higher pressures were remeasured with a McLeod gauge. Changes of the I^- and I^+ currents incident on the Faraday cylinders were measured simultaneously with a mirror galvanometer and a string electrometer, which served to remove errors due to fluctuations of the primary beam intensity.

As a check of the reproducibility of the results, we measured the cross sections of the processes $H_1^+ \to H_1^-$ in argon and in helium, and $O_1^+ \to O_1^-$ in hydrogen and in oxygen, and compared the results with those obtained in Refs. 2 and 3. It was found that for the process $H_1^+ \to H_1^-$ in argon and helium the results are reproducible within the limits of the experimental error. The values obtained for the cross sections of the process $O_1^+ \to O_1^-$ in hydrogen and oxygen were 5-10 times smaller than in Ref. 3. Since the method used was different, we repeated the measurement of the cross sections of the process $O_1^+ \to O_1^-$ in hydrogen and oxygen not using the liquid air trap and obtained results consistent with those of Ref. 3 within the experimental error.

These experiments showed that the presence of condensable vapors in the residual gas of the collision chamber has a marked influence on the value of the measured cross section, which cannot be removed by determining the cross section from the plot $(I^-/I^+) - (I^-/I^+)_\Phi = f(p - p_\Phi)$. The cause is the following: a simple calculation shows that, for small gas pressures in the collision chamber, the value $(I^-/I^+) - (I^-/I^+)_\Phi$ can be represented as follows:

$$\frac{I^-}{I^+} - \left(\frac{I^-}{I^+}\right)_\Phi = \left\{\sigma_{1-1} + \frac{1}{2}\left[\sigma_{1-1}\sum_{i=1}^{N}(\sigma_{10}^i + \sigma_{1-1}^i)\,p_i\,\frac{L}{kT} + (\sigma_{10} + \sigma_{1-1})\sum_{i=1}^{N}\sigma_{1-1}^i p_i\,\frac{L}{kT}\right]\right\}(p - p_\Phi)\,\frac{L}{kT}, \quad (1)$$

where p, σ_{10} and σ_{1-1} are the pressure and the cross sections for one- and two-electron capture, respectively, for the investigated gas, and p_i, σ_{10}^i and σ_{1-1}^i the corresponding values for one of the gases present in the residual gas in the collision chamber.

The presence of the terms in the square brackets in (1) shows that the value of the cross section σ_{1-1} determined from the linear part of the relation $(I^-/I^+) - (I^-/I^+)_\Phi = f(p - p_\Phi)$ is larger than the real value because of the presence of the residual gas. The lower the pressure of residual gases in the collision chamber, the closer will be the measured value of σ_{1-1} to the real value. Using the liquid air trap in the collision chamber for the purpose of condensing the organic vapors present, we greatly reduced the pressure of the residual gas, and therefore, the systematic error.

It was shown experimentally for all ion-molecule pairs studied that further lowering of the ratio $(I^-/I^+)_\Phi$ as compared with the value reached using the liquid-air trap*, does not lead to a diminishing of the measured cross section σ_{1-1}. This means that, by using the liquid air trap, the systematic error connected with the presence in the collision chamber of gases (that are not condensing at liquid air temperature) lies within the limits of statistical errors which, in the present experiment, attained ±15%.

DISCUSSION OF EXPERIMENTAL RESULTS

The energy dependence of the two-electron capture cross section was measured for the C_1^+ and O_1^+

* This is effected by placing liquid air traps in the space before and behind the collision chamber.

ions in collisions with Ne, He, A, Kr, Xe, H_2, N_2 and O_2 molecules, in the energy interval 10.7-54.5 kev. Spectrally pure He, Ne, Kr and Xe, hydrogen filtered through palladium, 99.1% pure oxygen, 99.7% argon and nitrogen obtained from evaporation of liquid nitrogen and purified from oxygen by passage through copper filings at 600° C were used. The results obtained are shown in Figs. 1 and 2.

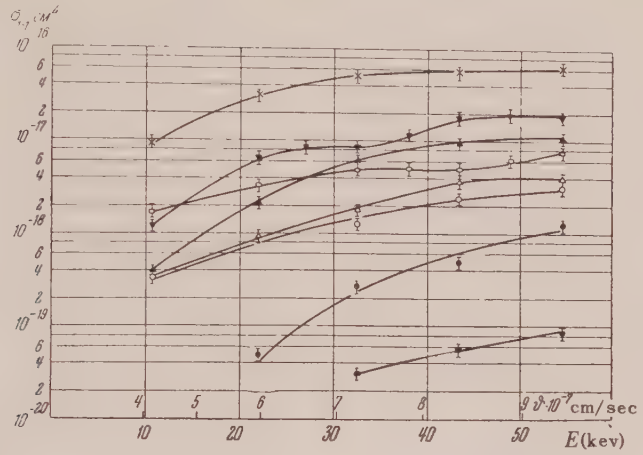

FIG. 1. $C_1^+ \rightarrow C_1^-$; ■ — He, ● — Ne, ○ — H_2, △ — N_2, □ — O_2, ▲ — Ar, ▼ — Kr, * — Xe

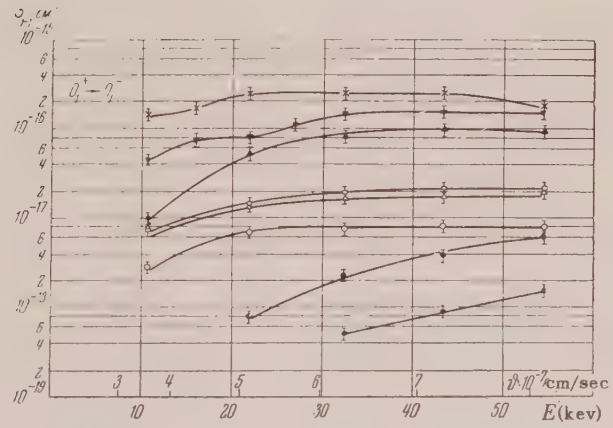

FIG. 2. $O_1^+ \rightarrow O_1^-$; ■ — He, ● — Ne, ○ — H_2, △ — N_2, □ — O_2, ▲ — A, ▼ — Kr, * — Xe

The figures show that, in the energy region under discussion, a monotonic increase in the effective cross section with the ion energy is observed for the C_1^+ ions in He, Ne, A, Xe, H_2 and N_2 and for the O_1^+ ions in He, Ne and N_2. The rate of the rise of the cross section σ_{1-1} for these ion-molecule pairs slows down with increasing ion energy, which indicates that a maximum is being approached. The cross section σ_{1-1} is constant for O_1^+ ions in A, Kr, H_2 and O_2 from about 30 kev to the upper limit of the measured inverval. Such a region of constant cross section σ_{1-1} was observed in two more cases: for C_1^+ in Kr from 27 to 32 kev and for C_1^+ in O_2 from 32 to 43 kev. In these two cases, however, the cross section increases again with the energy after the plateau. In one case only, namely, for O_1^+ in Xe, a flat maximum is observed in the measured energy interval, at about 30 kev.

The value of the cross section σ_{1-1} for a given ion changes within very wide limits: for the C_1^+ ions from 3.2×10^{-20}cm^2 (in H, at 32.4 kev) to 6.4×10^{-17}cm^2 (in Xe, at 54.5 kev) and for the O_1^+ ions from 5.1×10^{-19}cm^2 (in He, at 32.4 kev) to 2.4×10^{-16}cm^2 (in Xe, at 32.4 kev). A strong dependence of the cross section σ_{1-1} on the gas molecule from which the ions capture the electrons is observed. The cross section σ_{1-1} for the C_1^+ and O_1^+ ions of the same energy increases in the various gases in the following order: He, Ne, H_2, N_2, O_2, A, Kr, Xe. Exceptional are the $C_1^+ \rightarrow C_1^-$ processes in A and O_2 in the 10.7-28 kev region, in which the cross section σ_{1-1} is smaller for argon than for oxygen. For the same gas the same ion velocity, the cross section σ_{1-1} is as a rule larger for the O_1^+ ion than for the C_1^+.

Lack of literature on the two-electron capture by C_1^+ and O_1^+ ions makes it impossible to compare our results with other investigations.

It is impossible to calculate the effective cross sections of inelastic processes in collisions between particles with shells containing many electrons on the basis of the present theory of atomic collisions. Therefore, the discussion of our results can be made only on the basis of general theoretical considerations connected with Massey's "adiabatic hypothesis"[5]. According to this hypothesis, slow collisions between particles take place under the condition $a|\Delta E|/hv \gg 1$ (where ΔE is the resonance defect, i.e., the change of the internal energy in the given inelastic process, a is the distance at which the interaction forces between the colliding particles act, h is the Planck constant and v is the ion velocity). In the slow-collision region a sharp rise of the effective inelastic cross section with the ion velocity should be observed. The maximum value of the cross section is attained for the following condition:

$$a|\Delta E|/hv \approx 1. \qquad (2)$$

The value of the parameter $a|\Delta E|/hv$ can be estimated when a and $|\Delta E|$ are known. The value of the resonance defect for the two-electron capture processes can be easily calculated under the assumption that the colliding particles are in the ground state both before and after the collision*.

* In Refs. 2 and 3 examples of the calculation of the resonance defect are given for several ion-molecule pairs.

The resonance defect changes from 20.6 ev (in Xe) to 66 ev (in He) for the $C_1^+ \rightarrow C_1^-$ processes, and from 17.5 ev (in Xe) to 62.9 ev (in He) for the $O_1^+ \rightarrow O_1^-$ process. It should be noted that for one-electron capture processes the resonance defects are much smaller. For instance, for the $C_1^+ \rightarrow C_1^0$ process, the values vary from 0.84 ev (in Xe) to 12.4 ev (in He), and for the $O_1^+ \rightarrow O_1^0$ process, from 0.4 ev (in Kr) to 10.9 ev (in He). The value of a can be calculated from the condition (2) in the case when a maximum is attained for the cross section in the investigated energy region. In the present work, a maximum was observed only for the $O_1^+ \rightarrow O_1^-$ process in Xe at 33 kev. Calculation gives the corresponding value of a to be equal to ~1.45 A. In Ref. 2 it was found that a equals 1 and 2 A for the $H_1^+ \rightarrow H_1^-$ process in He and H_2, respectively. Hasted has shown[6,7] that in one-electron capture collision processes the value of a does not vary greatly for different ion-molecule pairs and is equal on the average to 8 A.

Under the assumption that the impact parameter varies only slightly for two-electron capture processes*, it is possible to compute the value of $a|\Delta E|/hv$, taking a to be equal to 1.45 A. For the $C_1^+ \rightarrow C_1^-$ process this value varies in the beginning of the investigated velocity interval from 1.7 (in Xe) to 3.6 (in He), and for the $O_1^+ \rightarrow O_1^-$ process from 1.8 (in Xe) to 3.3 (in He). It is therefore impossible to treat the studied velocity interval as the slow-collision region, since even for the lowest ion velocity, the criterion $a|\Delta E|/hv \gg 1$ is not fulfilled. It is possible to note, however, from Figs. 1 and 2, that the effective cross section increases with the energy more sharply for those ion-molecule pairs (C_1^+ and O_1^+ in He and Ne) for which the ratio $a|\Delta E|/hv$ is largest in the velocity interval studied. It is interesting to compare the dependence of the cross sections σ_{1-1} and σ_{10} on the

* The fact that no maximum is observed in the curves $\sigma_{1-1} = f(E)$, apart from the curve for $O_1^+ \rightarrow O_1^-$ in Xe, is a partial confirmation of the above assumption. Since the value of $|\Delta E|$ is the smallest for the $O_1^+ \rightarrow O_1^-$ process in Xe, it should be expected that for other processes the maximum cross section should be shifted in the direction of higher velocities, of only a remains constant for the processes in question.

value of $a|\Delta E|/hv$. Such a comparison is possible for the pairs $C_1^+ - Xe$, $O_1^+ - Kr$ and $O_1^+ - A$, since both the σ_{1-1} cross sections measured by us and the σ_{10} cross sections measured by Hasted[6,7] correspond to such a velocity interval that the values of $a|\Delta E|/hv$ overlap, if we take a to be equal to 1.45 A for $ion^+ - ion^-$ processes, and to 8 A for $ion^+ - atom$ processes. The dependence of σ_{10} and σ_{1-1} on $a|\Delta E|/hv$ for the $C_1^+ - Xe$, $O_1^+ - A$ and $O_1^+ - Kr$ pairs is shown in Fig. 3. The corresponding curve of the σ_{10} cross section for the $H_1^+ - A$ pair is included for comparison.

Attention is drawn to the fact that fall of the cross section σ_{10} with the rise of $a|\Delta E|/hv$ is much slower for $C_1^+ - Xe$, $O_1^+ - A$ and $O_1^+ - Kr$ pairs than for $H_1^+ - A$. An analogous phenomenon is found in comparing the curves for the σ_{10} and σ_{1-1} cross sections. The cross section σ_{10} decreases much more slowly with increasing $a|\Delta E|/hv$ than does the cross section σ_{1-1}.

From the point of view of the adiabatic hypothesis, the slow decrease of the value of the σ_{10} cross section with increasing $a|<E|/hv$ for the $C_1^+ - Xe$, $O_1^+ - A$ and $O_1^+ - Kr$ pairs represents an anomaly. Hasted proposes to explain the large σ_{10} cross sections at low velocities by the fact that the ion beam contains some excited metastable ions. In the case of the $O_1^+ + A \rightarrow O_1^0 + A^+$ process, for instance, the resonance defect for the electron exchange between ground-state particles is equal to -2.2 ev if the O_1^+ ion is in the ^2P state, the collision process can be either $O_1^+(^2P) + A \rightarrow O_1^0(^1D) + A^+$ with $\Delta E = -0.84$ ev, or $O_1^+(^2P) + A \rightarrow O_1^0 + A^+$ with $\Delta E = 1.12$ ev. The observed dependence of σ_{10} on the ion velocity is the result of superposition of a series of curves for collision processes with different values of resonance defect and, consequently, with displaced maxima. The presence of excited ions in the beam is evidently excluded in the case of the pair $H_1^+ - A$, and, correspondingly, a sharp fall of the cross section with decreasing ion velocity can be observed.

The sharper decline of the σ_{1-1} cross section as compared with the σ_{10} cross section can be explained, on the basis of Hasted's assumption, by insignificantly small quantities of excited ions in the beam used in our experiments. This assumption is confirmed by the fact that the σ_{1-1} cross section for the $H_1^+ + H_2 \rightarrow H_1^- + H_1^+ + H_1^+$ process[2], where all particles involved can be in the ground state only, also falls sharply with diminishing velocity.

It should be noted that in two-electron capture collisions the presence of excited ions in the primary beam or the formation of excited fast or slow particles after the collision will have a lesser influence on the dependence of the cross section on velocity than in the case of one-electron capture collisions. Consequently, the relative change of the resonance defect of the two-electron capture due to the presence of excited particles in the primary beam or their creation after collision will be small. The experimental curve $\sigma_{1-1} = f(v)$ will be the result of superposition of two curves with closely-spaced maxima, which will, as a final result, distort the curve relatively slightly for small velocities.

The curves shown in Fig. 3 permit also the comparison of the numerical values of the σ_{1-1} and the σ_{10} cross sections for identical values of the adiabatic parameter $a|\Delta E|/hv$. It follows from this comparison that, although the cross section σ_{1-1} is much smaller than the cross section σ_{10}, yet it cannot be regarded as negligible for the studied ion-molecule pairs.

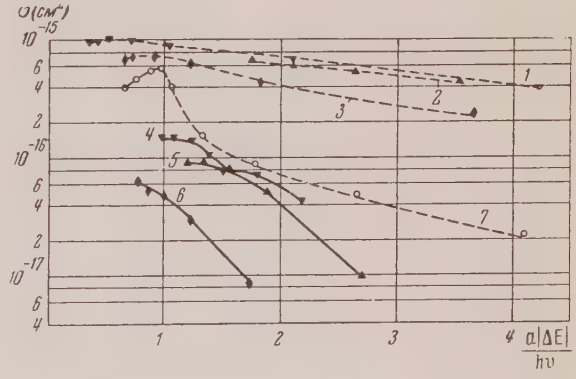

FIG. 3. *1* — $O_1^+ \rightarrow O_1^0$, Kr; *2* — $O_1^+ \rightarrow O_1^0$, A; *3* — $C_1^+ \rightarrow C_1^0$, Xe; *4* — $O_1^+ \rightarrow O_1^-$, Kr; *5* — $O_1^+ \rightarrow O_1^-$, A; *6* — $C_1^+ \rightarrow C_1^-$, Xe; *7* — $H_1^+ \rightarrow H_1^0$, A

It was mentioned above that there exists a strong dependence of the effective cross section σ_{1-1}

on the nature of both the ion and the molecule which collide. It is of considerable interest to find which physical values characterize the connection between the value of the cross section σ_{1-1} with the nature of the ion and of the molecule. It is natural to assume that a certain role should be played by the binding energy of electrons both in the negative ion formed in the collision process and in the molecule from which they are captured. The resonance defect in the investigated two-electron capture processes $A^+ + B \to A^- + B^{++}$ (B is assumed to be an atomic particle) can be written in the form:

$$\Delta E = (V_A^{\mathrm{I}} + S_A) - (V_B^{\mathrm{I}} + V_B^{\mathrm{II}}), \qquad (3)$$

where V_A^{I} and S_A are the first ionization potential and the electron affinity of the particle A, and V_B^{I} and V_B^{II} are the first and the second ionization potentials of the particle B. As it can be seen from (3) the binding energy of the exchanged electrons in the capturing and in the losing particle enter into the value of ΔE. Therefore, it is logical to find the connection between ΔE and σ_{1-1}.

The dependence of the cross section σ_{1-1} on $|\Delta E|$ for the processes $O_1^+ \to O_1^-$ and $C_1^+ \to C_1^-$ for one and the same velocity of the O_1^+ and C_1^+ ions, equal to 7.55×10^7 cm/sec, is shown in Fig. 4. The points for the different processes lie on different smooth curves (only the points for the $C_1^+ - O_2$ and $O_1^+ - H_2$ pairs fail to coincide), corresponding to the monotonic decrease of the cross section σ_{1-1} with increasing absolute value of the resonance defect. Since the value of $V_A^{\mathrm{I}} + S_A$ for each of these curves is constant (equal to 12.74 and 15.77 ev for the $C_1^+ - C_1^-$ and the $O_1^+ - O_1^-$ processes, respectively), they represent the dependence of the cross section σ_{1-1} on the electron binding energy in the particle losing them. The following can be deduced from these curves: 1) The cross section σ_{1-1} decreases with increasing binding energy of electrons in the losing particle; 2) The cross section σ_{1-1} increases with increasing electron binding energy in the negative ion, formed in the collision; 3) The resonance defect is not a universal parameter, determining the two-electron capture cross section for a ion-molecule pair. Further study of this process for a large number of ion-molecule pairs will show whether these conclusions are generally valid.

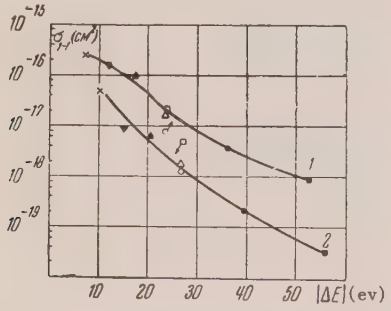

FIG. 4. *1* — $O_1^+ \to O_1^-$, *2* — $C_1^+ \to C_1^-$; ■ — He, ● — Ne, ○ — H_2, △ — N_2, □ — O_2, ▲ — A, ▼ — Kr, * — Xe

The authors wish to express their gratitude to Prof. A. K. Val'ter for his interest and attention shown for the present work.

[1] Fogel', Krupnik and Safronov, J. Exptl. Theoret. Phys. (U.S.S.R.) **28**, 589 (1955); Soviet Phys. JETP **1**, 415 (1955).

[2] Ia. M. Fogel' and R. V. Mitin, J. Exptl. Theoret. Phys. (U.S.S.R.) **30**, 450 (1956); Soviet Phys. JETP **3**, 334 (1956).

[3] Ia. M. Fogel' and L. I. Krupnik, J. Exptl. Theoret. Phys. (U.S.S.R.) **29**, 209 (195); Soviet Phys. JETP **2**, 252 (1955).

[4] N. V. Fedorenko, J. Techn. Phys. (U.S.S.R.) **24**, 769 (1954).

[5] H.S.W. Massey, Rep. Progr. Phys. **12**, 248 (1948).

[6] J. B. Hasted, Proc. Roy. Soc. (London) **A205**, 421 (1951).

[7] J. B. Hasted, Proc. Roy. Soc. (London) **A212**, 235 (1952).

Translated by H. Kasha
81

The Cross Section for the Fission of Uranium by High-Energy Protons (140 to 660 MEV)

N. S. IVANOVA
Radium Institute, Academy of Sciences, USSR
(Submitted to JETP editor April 27, 1956)
J. Exptl. Theoret. Phys. (U.S.S.R.) 31, 413-415 (September, 1956)

The thick film method was used to measure the fission cross section of U^{238} by protons of energies 140, 350, 460 and 660 mev. The probability that uranium will fission when irradiated by protons of a given energy is also obtained.

THE cross section for uranium fission induced by fast protons has been investigated by several authors[1-6]. Various experimental techniques were used: the ionization chamber[1], radio-chemistry[2,3] and the thick film method[4-6].

The isolated points in the Figure summarize the data available in the literature on the fission cross section by protons of various energies. There are no data on fission by protons at low energies: 22 to 220 mev. In the energy interval 340-380 mev the results obtained by various authors differ widely among one another. Thus, according to Ref. 1, the cross section for uranium fission by protons of energy $E = 340$ mev is 0.6 barns, while according to Ref. 3, the cross section at 380 mev is 2 barns. For energies around 460 mev the fission cross sections obtained in Refs. 4-6 agree within experimental error.

No conclusions about the dependence of the cross section on proton energy can be drawn from the above data.

In the present work thick photographic emulsions were used to obtain the fission cross section over a wide energy interval (140, 350, 460 and 660 mev). Protons of these energies were obtained by using copper and paraffin filters to slow down 660 mev protons from the synchrocyclotron of the Institute

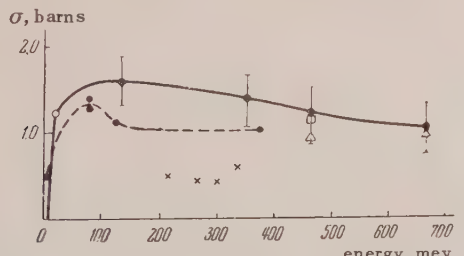

Energy dependence of proton-induced uranium fission. Solid curve—protons; Dotted curve—neutrons, according to Refs. 8 and 9; ×—Ref. 1; o—Ref. 2; ▲—(high) Ref. 3; □—Ref. 4; ●—our results.

for Nuclear Problems of the Academy of Sciences, USSR. Uranium was introduced into the photosensitive layer by washing[7] in an aqueous solution of the salt $NaUO_2(C_2H_3O_2)_3$.

The cross section was measured using two types of emulsion: first, relativistic emulsions (NIKFI-R and Ilford G-5), and second, the insensitive, fine-grained emulsion * P-9, having a proton threshold of 25-30 mev. With this emulsion, the incident proton current can be increased by a factor 20-25 over the usable current with the relativistic emulsion which allows a larger number of fissions to be observed.

The current incident on the relativistic emulsions was measured by counting the number of primary proton tracks in the same plate on which the fission events were observed. The current incident on the insensitive P-9 emulsions was measured by counting the protons in a relativistic emulsion exposed (after irradiation of the P-9 emulsion) in the same place as the P-9 was, but for an appropriately shorter time. Exposure times were controlled by an ionization chamber which was placed in the beam directly in front of the emulsions. Having measured the current incident on the sensitive emulsion and knowing how much the current was increased for the insensitive emulsion, the current on the latter could easily be calculated.

In order to calculate the fission cross section it is necessary to know not only the number of fissions per unit volume of emulsion, but also the number of uranium nuclei introduced into the same volume. The latter quantity was measured by a previously described method[7], which was based on the number of α-particles emitted per minute by the uranium in the emulsion. For each bombarding energy, the number of fissions per unit volume of emulsion was measured by scanning the plate under a microscope.

Results of the measurements are shown in the Table.

The solid line in the Figure gives the average

* The emulsion was prepared in the laboratory of Prof. N. A. Perfilov.

Energy, mev	Emulsion type	Cross section, barns	Probability of fission
140	G-5	1.56±0.4	
	П-9	1.69±0.2	0.77
350	П-9	1.4±0.3	0.86
460*	G-5	1.2±0.3	0.74
660	НИКФИ-R	1.11±0.3	
	НИКФИ-R	0.97±0.25	0.65
	НИКФИ-R	1.01±0.3	

* The fission cross section for 460 mev protons is taken from our previous work (Ref. 5).

cross section so obtained as a function of energy. We see that the uranium fission cross section increases with increasing proton energy, goes through a wide maximum at 50-150 mev and then decreases, going (within the limits of our experiment) to a constant value in the energy range 460-660 mev. In contradiction with the data of Jungerman[1], there seems to be no minimum at 200-350 mev*.

Our curve can be compared with the analogous one for the energy dependence of the cross section for fission by fast neutrons. This curve is also shown in the Figure, the data being taken from Refs. 8 and 9, and lies somewhat below the proton curve. The difference may be due to experimental errors**, but if it really exists, then for fairly low energies, such that the incident nucleon amalgamates with the nucleus, it may be explained by the two different values of Z^2/A obtained for the fissioning nucleus depending on whether a neutron or proton is absorbed by the nucleus.

The probability that fission occurs when a proton of given energy interacts with a uranium nucleus can be obtained from the fission cross section if we assume that the reaction cross section is half the total cross section* . The total cross section has been measured by several authors[10-16] for high-energy neutrons (several values up to 600 mev and one[16] at an energy 1.4 bev). Assuming that the total cross section for fast protons differs little from the corresponding value for neutrons, we obtain the probabilities for fission by protons at our energies as indicated in the last column of the Table.

According to our data, the probability that protons of energy 140-660 mev induce fission is about constant and oscillates around 70-80% of the proton reaction cross section.

In conclusion, the author wishes to thank B. S. Neganov for helping to carry out the work and Prof. N. A. Perfilov for his constant interest.

* This assumption is justified for a black nucleus. For a semitransparent nucleus the reaction cross section is not quite equal to the elastic cross section, but is close to it.

* *Note added in proof*: As the present paper was being submitted for publication, there appeared in a new paper (e.g., see Ref. 17) describing measurements on the cross section for U^{238} fission by protons of energies 100-340 mev. The fission cross section obtained agrees well with our data. The authors consider their previous results to have been erroneous.

** The errors for the neutron curve are not known.

[1] J. Jungerman, Phys. Rev. **79**, 632 (1950).

[2] G. H. McCormick and B. L. Cohen, Phys. Rev. **96**, 722 (1954).

[3] Folger, Stevenson and Seaborg, Phys. Rev. **98**, 107 (1955).

[4] V. I. Ostroumov, Report (Otchet), Radium Institute, Academy of Sciences, USSR (1953).

[5] Ivanova, Perfilov and Shamov, Dokl. Akad. Nauk SSSR **103**, 573 (1955).

[6] V. P. Shamov, Dokl. Akad. Nauk SSSR **103**, 593 (1955).

[7] N. A. Perfilov and N. S. Ivanova, J. Exptl. Theoret. Phys. (U.S.S.R.) **29**, 551 (1955); Soviet Phys. JETP **2**, 433 (1956).

[8] Gol'danskii, Penkina and Tarumov, Dokl. Akad. Nauk SSSR **101**, 1027 (1955).

[9] E. L. Kelly and C. Wiegand, Phys. Rev. **73**, 1135 (1948).

[10] W. I. Linlor and B. Ragent, Phys. Rev. **91**, 440A (1953).

[11] V. A. Nedzel, Phys. Rev. **94**, 174 (1954).

[12] Cook, McMillan, Petersen and Sewell, Phys. Rev. **72**, 1264 (1947).

[13] Dzhelepov, Satarov and Golovin, J. Exptl. Theoret. Phys. (U.S.S.R.) **29**, 369 (1955); Soviet Phys. JETP 2, 349 (1956).

[14] Dzhelepov, Satarov and Golovin, Dokl. Akad. Nauk SSSR **104**, 717 (1955).

[15] J. Dejuren and N. Knable, Phys. Rev. **77**, 606 (1950).

[16] T. Coor, D. A. Hill *et al.*, Phys. Rev. **98**, 1369 (1955).

[17] H. M. Steiner and J. A. Jungerman, Phys. Rev. **101**, 807 (1956).

Translated by A. R. Krotkov
83

SOVIET PHYSICS JETP VOLUME 4, NUMBER 3 APRIL, 1957

Uranium Fission Induced by High-Energy Protons

N. S. Ivanova and I. I. P'ianov
Radium Institute, Academy of Sciences, USSR

(Submitted to JETP editor April 27, 1956)
J. Exptl. Theoret. Phys. (U.S.S.R.) **31**, 416-423 (September, 1956)

Uranium fission induced by high-energy protons can be accompanied by the emission of charged particles. The latter can arise from a nuclear cascade process or by evaporation from the excited nucleus. We used photographic emulsions to analyze the light charged particles accompanying uranium fission induced by protons of various energies (140 to 660 mev). For incident protons of energies 460 and 660 mev, experimental data on the knock-on particles emitted from the nucleus during a cascade process were compared with the results of a Monte Carlo calculation. Satsifactory agreement was obtained. The average excitation energies of nuclei about to fission upon being bombarded by protons of energy 140, 350, 460 and 660 mev, were also obtained.

THE interaction of high-energy protons with uranium nuclei can be conveniently divided into two stages. In the first stage, the primary proton collides with the nucleons in the nucleus and starts a nuclear cascade process lasting 10^{-21} to 10^{-22} sec. Most of the knock-on nucleons emitted from the nucleus as a result of this process are fast and leave the nucleus in an excited state. In the second stage the residual nucleus de-excites itself by evaporating nucleons. Since Z^2/A is large for uranium, fission can occur in either stage. Fission can compete with nucleon evaporation. During the second stage fission and emission of relatively low-energy nucleons are observed.

Thick, high-sensitivity photographic emulsions can be used to study the emission of charged particles when high-energy protons interact with uranium nuclei. To get the whole picture, the emulsion should be able to detect particles of all energies and masses from those of the fission fragments to those of the primary protons. It is to be noted, however, that if the uranium is introduced into the emulsion as an aqueous solution of uranium salt, then proton-uranium interactions which are unaccompanied by fission cannot be detected (they are hard to separate from reactions with AgBr). However, as is evident from the measured cross sections,[1] such events are relatively rare ($\sim 20\%$). Hence a study of those proton interactions which involve fission gives information not only about fission at high energies, but also about the interaction of protons of a definite energy with the heavy nucleus—uranium.

In particular, upon considering all the charged particles accompanying uranium fission, it is interesting to separate out the knock-on particles and to compare experimental data on them with Monte Carlo calculations on the nuclear cascade process initiated by the incident protons of some definite energy.

Our experiments were for protons of energies 140 to 660 mev.

EXPERIMENTAL ARRANGEMENTS

Thick emulsions impregnated with uranium were irradiated by protons of energies 660, 460, 350 and 140 mev, from the synchrocyclotron of the Institute for Nuclear Problems of the Academy of Sciences of the USSR. Protons with energies 350 and 140 mev were obtained by slowing down 660

mev protons in paraffin and copper filters. Uranium was introduced into the photosensitive layer by washing the plates in a 4% aqueous solution of $NaUO_2(C_2H_3O_2)_3$. Several emulsions of different sensitivities were used: a) the relativistic emulsions NIKFI and Ilford G–5 and b) the fine grained emulsion P–9*, with an upper limit on proton sensitivity of 25–30 mev.

Emulsions of the first type allow one to observe all the charged particles accompanying fission. However, since all the primary protons leave tracks one is restricted to low currents, so that one can observe only a few fission events. Thus, when using the relativistic emulsions, the whole photosensitive area yields only about 50 fission events at each energy. This was enough, however, to get a general picture of the proton–uranium interaction at a given energy—in particular, the average number of charged particles per fission, the angular distribution of the fast and slow charged particles relative to the incident protons, etc.

The particle current incident on emulsions of the second type, P–9, could be nade 20–25 times greater than that incident on the relativistic emulsions. A larger number of fission events could then be observed, and such matters as the characteristics of the soft component of the charged particles emitted upon fission, the ranges of fission fragments and the angle between the fragments could be best studied in the insensitive emulsion.

At all energies except 350 mev, our experiments were carried out on both types of emulsion. For 350 mev protons only the P–9 emulsion was used.

ANALYSIS OF THE LIGHT-CHARGED PARTICLES ACCOMPANYING URANIUM FISSION INDUCED BY HIGH-ENERGY PROTONS

We found that uranium fission, as observed on relativistic emulsions, was almost always accompanied by the emission of light-charged particles. From among all the charged particles, we tried to separate out those due to nuclear cascade processes, and to estimate the number due to evaporation. Such a separation can be effected by analyzing the angular and energy distributions of the charged particles emitted upon fission. In particular, we want the average number of low-energy particles (< 25 mev) per fission. This datum can be obtained from the experiments with the fine-grained emulsion P–9.

TABLE I

Energy of incident protons, mev	Relativistic Emulsions: number of fissions	Relativistic Emulsions: Average number of charged particles per fission	Relativistic Emulsions: Ration of number of particles emitted forward to those emitted backward	P-9 Emulsions: number of fissions	P-9 Emulsions: Average number of charged particles (< 25 mev) per fission	P-9 Emulsions: Ratio of number of particles emitted forward to those emitted backward	P-9 Emulsions: Average number of charged particles (< 20-25 mev) per fission with isotropic distribution
140	60	0,4	4	376	0,25	2,6	0,14
350				359	0,56	1,6	0,43
460	47	1,65	3,3	260	0,86	1,3	0,66
660	56	3,06	3,1	150	1,05	1,3	0,81

Table I summarizes the data we obtained for protons of various energies incident on both relativistic and P–9 emulsions. At each energy the Table shows the average number of particles per fission and the direction of emission relative to the incident proton. The second, third and fourth columns refer to relativistic emulsions, and hence include particles of all energies. The remaining columns refer to events observed in P–9 emulsions and hence include only charged particles of relatively low energies (< 25–30 mev).

The average number of all charged particles per fission increases as the incident proton energy increases. This is evident both from the third column of Table I and the curves in Fig. 1. In the latter, number of fission events is plotted against number of accompanying charged particles, as observed in relativistic emulsions. The curves show that as the proton energy increases, the relative number of those fission events which do not produce charged particles decreases, and the proba-

*The P–9 emulsions were prepared in the laboratory of N. A. Perfilov.

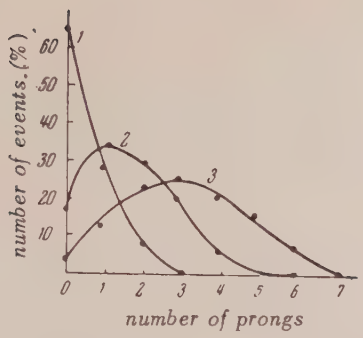

FIG. 1. Distribution functions for number of charged particles accompanying fission. Curve *1*—energy of incident protons 140 mev, Curve *2*—460 mev, Curve *3*—660 mev (relativistic emulsion).

bility of the event being accompanied by an ever-increasing number of charged particles increases.

Most of the charged particles observed in relativistic emulsions are emitted in the forward direction (with reference to the initial proton). This is evident either from the fourth column of Table I, which gives the ratio of the number of charged particles emitted into the forward hemisphere (relative to the incident proton) to the number emitted into the backward hemisphere, and also from the angular distributions shown in Fig. 2 [in these, most of the particles (~ 75%) are emitted with angles smaller than 90°].

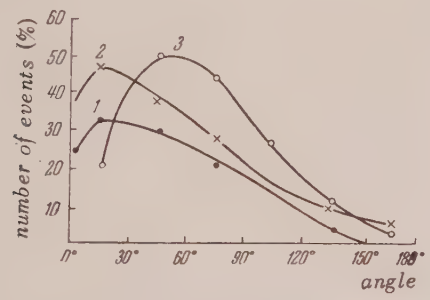

FIG. 2. Angular distribution of light charged particles accompanying fission. Curve *1*—energy of incident protons 140 mev, Curve *2*—460 mev, Curve *3*—660 mev (relativistic emulsions).

It is noteworthy that even particles with energy < 25 mev tend to be emitted forward (seventh column of Table I). This is especially noticeable for incident energy 140 mev, where a large fraction of the low-energy charged particles are apparently knock-on particles. This is to be expected, because when the uranium nucleus is, on the average, little excited, few nucleons evaporate off and most of the charged particles accompanying fission are directly knocked out of the nucleus by the incident protons.

As the energy of the incident protons increases, the directional effect in the emission of charged particles (E < 25 mev) decreases (seventh column). This is due to an increase in the number of charged particles emitted isotropically; more particles evaporate as the mean excitation energy decreases.

Viewed in this way, the data in Table I clearly demonstrate the presence of a nuclear cascade process in the interaction of a uranium nucleus with protons of energy more than 140 mev. The data also show how the knock-on particles fit in with all the low-energy particles (E < 25 mev).

In order to separate out completely the knock-on particles from among all the charged particles, we must estimate the number of evaporation particles per fission at various proton energies.

The average number of low-energy (E < 20–25 mev) particles per fission which are emitted isotropically (these are given by the last column in Table I) can be considered to be an upper limit on the mean number of evaporation particles per fission.* A comparison of the average number of charged particles emitted per fission, regardless of energy, with the corresponding number emitted isotropically (E < 25 mev, Fig. 3, curves *1* and *2*) then gives the fraction of particles due to a nuclear

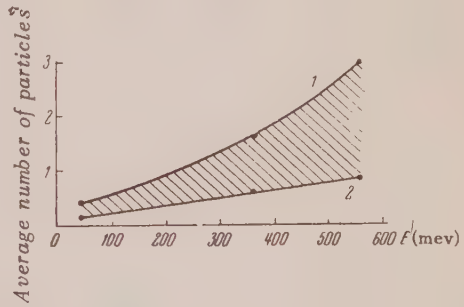

FIG. 3. Dependence of the average number of charged particles per fission on the energy of the incident protons. *1*—charged particles of all energies, *2*—charged particles with E < 20–25 mev and having an isotropic distribution.

cascade process. The shaded area in Fig. 3 gives the average number of knock-on particles at various proton energies. Clearly, at the energies considered, a large part (~ 70%) of the particles emitted upon fission are knock-on particles.

It is interesting to compare our experimental data on the number of knock-on particles with Monte Carlo type calculations on a nuclear cascade process. We carried out such calculation for the

*This is only an upper limit because it includes knock-on particles scattered through large angles.

interaction of 460 and 660 mev protons with uranium nuclei. The heavy nucleus is considered to be a "Fermi gas"[2] in which the incident proton undergoes successive collisions with the nucleus in the nucleus. The Pauli principle was taken into account—i.e., collisions in which the final state of one of the colliding nucleons had an energy less than the maximum Fermi energy for the type of nucleon in question were forbidden. Calculations were performed by the method described in Ref. 3, with certain simplifications.

In order to carry out the computations, it was necessary to know the probabilities of the various elementary processes which can occur when high energy nucleons (660 mev and less) collide with nucleons in the nucleus. We used the latest experimental data on the total cross section[4] and the differential cross section for elastic scattering of nucleons.[5] However, in calculations on the interaction of 660 mev protons with uranium nuclei we did not take meson formation into account, although in this case it can be important. This is because the experimental data available are insufficient.

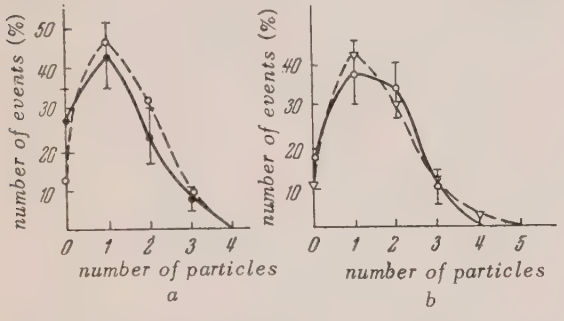

FIG. 4. Distribution functions for the number of charged knock-on particles ($E > 20$ mev). Solid curves—experimental, dotted—calculated. Curve *a*—incident proton energy 460 mev, curve *b*—incident proton energy 660 mev.

At each energy of the primary proton, 50 proton–nucleus interactions were computed. This should be enough to show the fundamental character of the process. The results could in some measure be compared with the experimental data.

Of particular interest in a nuclear cascade process is the distribution function for the number of emitted particles. Experimentally, we can obtain this from our experiments with sensitive emulsions, which register particles of all energies. Number of events was plotted as a function of the number of emitted particles with energy > 20 mev and compared with the corresponding distribution obtained by calculation. In Fig. 4, the solid curve is the experimental distribution, while the dotted curve was calculated [*a*) corresponds to 460 mev and *b*) to 660 mev]. The two curves agree well at both energies.

The angular distributions of fast charged particles ($E > 20$ mev), as obtained experimentally (relativistic emulsions), and by calculation, could also be compared. This is done in Fig. 5 [*a*) and *b*)].

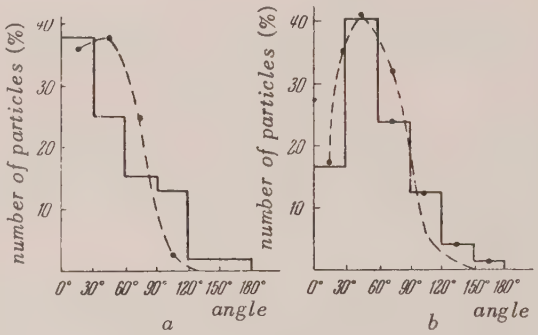

FIG. 5. Histograms for the angular distribution of charged knock-on particles ($E > 20$ mev). Dotted curves are calculated. Angles are measured from the direction of the incident proton. Curve *a*—incident proton energy 460 mev, curve *b*—660 mev.

The histograms show the experimental angular distributions for the fast ($E > 20$ mev) charged particles relative to the incident current at 460 and 660 mev. The general shapes of the experimental and calculated curves are the same. Unfortunately, few particles (52) were available in constructing the histogram at $E = 460$ mev, so the statistical errors are large. The histogram for 660 mev protons was constructed from 100 particles, and agrees well with the calculated curve. The fact that slightly more particles were observed at large angles than indicated by the calculations might be due to meson formation, which we did not take into account.

At $E = 460$ mev, there is satisfactory agreement (within experimental error) between the experimental and calculated values for the average number of knock-on particles (with $E > 20$ mev) per fission (Table II). For 660 mev protons the experimental value is somewhat larger than the theoretical. This effect can presumably be accounted for by the meson production our calculations neglected.

TABLE II.

Energy of incident proton (mev)	Averzge number of charged knock-on particles ($E > 20$ mev)	
	Experimental	Calculated
460	1.0±0.2	1.3
660	2.2±0.3	1.6

We consider that the agreement between the experimental data and the results calculated under the stated assumptions is satisfactory.

We present now some further results obtained in the course of the calculations. Figure 6 shows the energy distribution of the knock-on particles, as calculated by us for $E = 660$ mev. There are many particles with energy 20–30 mev. These will be superimposed on the spectrum of the evaporation particles.

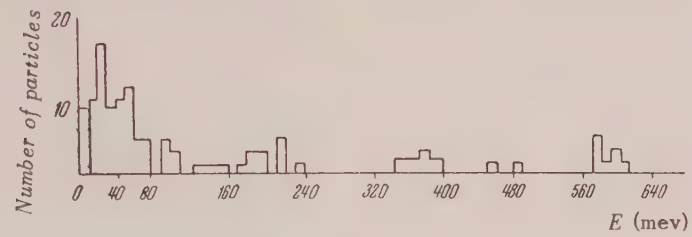

FIG. 6. Energy distribution of charged knock-on particles for incident proton energy 660 mev. Obtained from calculations on a nuclear cascade process in uranium.

AVERAGE EXCITATION ENERGY IN A FISSIONING URANIUM NUCLEUS AND EVAPORATION PARTICLES

Collisions bewween the primary protons and the nucleons in the nucleus knock out particles from the nucleus and leave the residual nucleus in an excited state. The work described in Ref. 6 shows that the mean excitation energy of the fissioning nucleus can be estimated from the angle between the fission fragments. As the nucleus fissions under the influence of a fast particle, the fragments do not go off in opposite directions, but make a certain small angle with this line, the angle depending on the speed of the fissioning nucleus. According to Ref. 6, the average energy of excitation of a nucleus about to fission under the action of protons of various energies is given by the formula

$$E_{exc} = E_p + m_0c^2 - c\sqrt{m_0^2c^2 + (p_p - m_n v_n)^2} - E_b.$$

Here E_p , p_p and m_0 are the energy (mev) , momentum and mass of the primary proton, c is the velocity of light, m_n and v_n are the mass and velocity of the fissioning nucleus (the velocity being obtained from the angle between the fragments) and E_b is the average binding energy per fission going into the knock-on particles. The latter quantity can be estimated from the average number of protons knocked out, assuming that the relative numbers of knock-on protons and neutrons is the same as in the original nucleus, uranium.

Table III shows the average excitation energies so obtained for various proton energies.

TABLE III.

Energy of incident proton (mev)	140	350	460	660
Average excitation energy (mev)	80±20	140±40	165±45	185±60

The values in Table III for proton energies 460 nnd 660 mev are somewhat larger than those in Ref. 7, but the difference lies within experimental error.

Another quantity of interest in fission is the range distribution of the fragments. As is well known, this changes radically as the energy of the primary, fission-inducing particles increases from thermal energies to 50–60 mev. The change is from the twin-peaked curve characteristic of asymmetric fission to a single-peak curve (symmetric fission). Fig. 7 shows our measurements on the range dis-

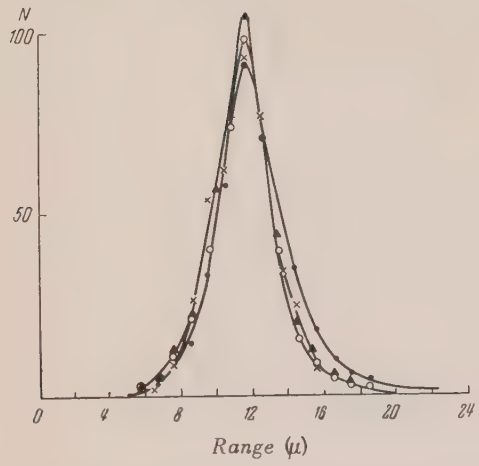

FIG. 7. Range distribution of isolated fission fragments. O–incident proton energy 140 mev, ×–350 mev, Δ–660 mev.

tribution of isolated fragments at the excitation energies presented above. The range distribution is clearly insensitive to changes in the excitation energy from 80 to 180 mev.

The excited nucleus can lose energy by evaporating nucleons (mostly neutrons); since the uranium nucleus has a large Z^2/A (which becomes even larger as neutrons escape), fission competes with evaporation. Inasmuch as up to now there has been no data indicating that fission takes a considerably longer time than neutron evaporation, fission can in general occur in any excited state. Only if neutron evaporation went much faster than fission could the nucleus completely de-excite itself by evaporation before undergoing fission.

The average number of charge particles evaporating from nuclei excited to the energies shown in Table III is given in the eighth column of Table I. It would be natural to compare these data with calculations based on existing theories of evaporation. However, it should be pointed out that even if experimental and calculated values for the average number of charged particles evaporating were to agree, we could not yet conclude, as was done in Ref. 7, that the nucleus de-excites itself completely by evaporation before undergoing fission. Calculations for uranium based on evaporation theory[8] indicate that the average number of charged evaporation particles depends but little on whether the nucleus fissions at about half it original excitation energy or whether it fissions after having completely de-excited itself by evaporation. In the former case, the excited fission fragments have an excess of neutrons and hence emit mostly neutrons, so that the difference in the numbers of charged particles emitted in the two cases will be the number of protons and α-particles which would have evaporated from the nucleus had it gone from half its excitation energy to zero. This number is quite small since, as is well known, most of the charged particles evaporate at the beginning, at the higher excitation energies. For example, according to calculations,[8] a nucleus excited to 150 mev and losing all its excitation energy by evaporation will emit 0.7 charged particles, while if it fissions at half this energy (75 mev) with the excited fission fragments then evaporating off particles, 0.6 charged particles are emitted. The average number of charged particles will be much smaller than in two cases above if the nucleus fissions immediately, before losing any excitation energy at all. This is because the excited fission fragments emit mostly neutrons. Hence, it would be of interest to compare experimental and calculated data on the number of charged evaporation particles for the case of uranium. However, calculations carried out by two different methods—Le Couteur[8] and Hagedorn[9]—give, at the relatively low nuclear temperatures of interest here, quite different values for the average number of charged evaporation particles. It is difficult to know which of the two methods is preferable. On the one hand, for nuclei with mass number 100 and temperatures 2–3 mev the method of Ref. 8 gives too low a value* for the average number of charged particles, so that the same may be expected for uranium. On the other hand, although calculations with the method of Ref. 9 give results in agreement with experiment for AgBr (in the indicated temperature range), the ratio of the probabilities for neutron and proton emission in this method does not depend on excitation energy. This is clearly not realistic, and should lead to too many charged evaporation particles in our temperature range. It is therefore our opinion that in view of the inadequacy of evaporation theory, a comparison of the experimental with the calculated data on the average number of charged evaporation particles would not give a reliable answer to the question of interest.

In conclusion the authors would like to express their gratitude to Prof. N. A. Perfilov for his constant interest in their work.

*According to references[10,11] the average number of charged particles evaporating from AgBr excited by 50 mev is about 2.0. The calculated value from Ref. 8 is 0.4 for the same excitation energy.

[1] N. S. Ivanova, J. Exptl. Theoret. Phys. (U.S.S.R.) 31, 413 (1956); Soviet Phys. JETP 3, 300 (1956).

[2] R. Serber, Phys. Rev. 72, 1114 (1947).

[3] V. V. Chavchanidze, Izv. Akad. Nauk SSSR, Ser. Fiz. 19, 629 (1955).

[4] V. P. Dzelepov *et al.*, Dokl. Akad. Nauk SSSR 104, 717 (1955).

[5] J. Hadley *et al.*, Phys. Rev. 75, 351 (1949); E. Kelly *et al.*, Phys. Rev. 79, 96 (1950); R. W. Birge *et al.*, Phys. Rev. 83, 274 (1951); O. A. Towler, Phys. Rev. 84, 1262 (L) (1951); O. Chamberlain and C. Wiegand, Phys. Rev. 79, 81 (1950); V. P. Dzhelepov and Iu. M. Kazarinov, Dokl. Akad. Nauk SSSR 99, 939 (1954); Ia. M. Selektor *et al.*, Dokl. Akad. Nauk SSSR 99, 967 (1954); M. G. Meshcheriakov, Session of the Academy of Sciences SSSR on the peaceful uses of atomic energy, plenary session, page 39 (1955).

[6] V. I. Ostroumov, Dokl. Akad. Nauk SSSR 103, 409 (1955).

[7] V. P. Shamov, Dokl. Akad. Nauk SSSR 103, 593 (1955).

[8] K. J. Le Couteur, Proc. Phys. Soc. (London) 63A, 259 (1950).

[9] R. Hagedorn and W. Macke, *Kosmische Strahlung*, 201 (1953).

[10] A. D. Sprague, D. M. Haskin *et al.*, Phys. Rev. 94, 994 (1954).

[11] G. Bernardini *et al.*, Phys. Rev. 85, 826 (1951).

Translated by R. Krotkov
84

SOVIET PHYSICS JETP VOLUME 4, NUMBER 3 APRIL, 1957

Scattering of π^+-Mesons by Hydrogen. II. Discussion and Interpretation of the Results

A. I. MUKHIN AND B. M. PONTECORVO
Institute for Nuclear Problems, Academy of Sciences, USSR

(Submitted to JETP editor June 7, 1956)
J. Exptl. Theoret. Phys. (U.S.S.R.) 31, 550-559 (October, 1956)

A phase analysis is made of the data obtained on scattering by hydrogen of π^+-mesons of different energies up to 307 mev. The analysis was carried out, using a high-speed electronic computer, on the assumption that the scattering process can be sufficiently accurately described by S- and P-waves [(S-P)-analysis], as well as on the assumption that the scattering process must be described by five parameters [(S-P-D)-analysis]. The energy dependence of the various phase shifts obtained for the (S-P)- and (S-P-D)-analyses are shown in the Figures. It follows from the measurements that the radius of meson-nucleon interaction is about 7×10^{-14} cm.

As is known, Fermi and others[1] analyzed the aggregation of data on scattering of π^+-mesons up to 200 mev on the assumption that only S- and P-waves are involved in the scattering and therefore the scattering processes are described by six phase shifts. In the case of positive pions and in the absence of D-waves the scattering is described by only three phase shifts α_3, α_{31} and α_{33} which determine the corresponding interaction in the S-, $P_{1/2}$- and $P_{3/2}$-states with isotopic spin 3/2.

In the present work, which is a continuation of the work described in Ref. 2, the data on scattering of positive pions are analyzed on the assumption that the contribution of D-states to the scattering process is negligibly small, i.e., the interaction takes place only in the S- and P-states [(S-P)-analysis] as well as on the assumption that the contribution of the D-states cannot be neglected [(S-P-D)-analysis]. The latter assumption is quite reasonable for such high energies as 300 mev. Besides, the data of Ref. 2 presented in Table 10 confirm this assumption to a certain extent.

In the case when S-, P- and D-waves contribute to the scattering of π^+-mesons, beside the above-mentioned three phase shifts α_3, α_{31} and α_{33}, the phase shifts corresponding to the D-states with total angular momenta 3/2 and 5/2 are different from zero and will be subsequently designated by δ_{33} and δ_{35}.

1. (*S-P*)-ANALYSIS

A. Phase Shifts

In the case when the interaction between the pions and hydrogen takes place only in the *S*- and *P*-states, the analysis of scattering is sufficiently simple, and the phase shifts can be determined, in the first approximation, by the graphical method[3].

Expressions for the coefficients of angular distribution in terms of the scattering phases have, as known, the following form

$$A = \sin^2\alpha_3 + \sin^2(\alpha_{33} - \alpha_{31}), \tag{1}$$

$$B = 2\sin\alpha_3\,[2\sin\alpha_{33}\cos(\alpha_{33} - \alpha_3) + \sin\alpha_{31}\cos(\alpha_{31} - \alpha_3)], \tag{2}$$

$$C = 3[\sin^2\alpha_{33} + 2\sin\alpha_{31}\sin\alpha_{33}\cos(\alpha_{33} - \alpha_{31})]. \tag{3}$$

Results of graphical analysis are given in Table I. In the same Table are given the "optimized" phase shifts[4] obtainedwith a high-speed electronic computer. In the latter case total cross sections were also used in this analysis as independent measurements.

In Table I, M denotes the quantity

$$\sum_i \left\{ \frac{f_i(\alpha_3,\ \alpha_{31},\ \alpha_{33}) - \sigma_i}{\Delta\sigma_i} \right\}^2 .$$

Only the "resonant" solution was examined, i.e., the Fermi type solution, in which α_{33} passes through 90° in the energy region 170 to 200 mev. The basis for this procedure was discussed in the paper by Anderson *et al.*[5]. Data for 307 mev agree well with the results of Ref. 6.

TABLE I.

Phases of π^+-meson scattering by protons (in degrees)

Meson Energy, mev	Graphical Method			High-Speed Electronic Computer				
	α_3	α_{31}	α_{33}	α_3	α_{31}	α_{33}	M	Number of independent measurements
176	—11	—16	67	—10.6	—19.5	69.0	3.1	10
200	— 9	4	96	— 9.1	10.0	102.0	7.0	7
240	—14	— 8	113	—18.1	— 2.6	114.7	4.2	8
270	—21	— 6	128	—20.2	— 6.7	129.3	5.8	7
307	—24	— 8	134	—23.2	— 8.4	133.2	12.0	9

B. Behavior of S-Phase α_3 on the Assumption that Scattering is Determined only by Three Phase Shifts

It should be emphasized that in the "resonance" region the values of all three phases cannot be determined with good accuracy. As seen from Eqs. (1)-(3), in the region where the phase α_{33} approaches 90°, it is very sensitive to small changes in the coefficients A, B and C. The difficulty in determining the S-phase α_3 is due to the fact that the interference coefficient B, which primarily determines this phase, is close to zero and is not accurately known in the "resonance" region. region. At energies which considerably exceed the "resonance" value there is a possibility of determining α_{33} as well as α_3 with comparatively high accuracy; therefore, the large values of α_3 phase for 240, 270 and 307 mev deserve special study. The magnitudes of this phase shift exceed considerably those which could be expected if the linear dependence of the α_3 phase on the meson momentum as proposed by Orear[7], and which well describes experimental data for small energies, were applicable up to the energies under consideration. As known, Orear proposed the following phase equations:

$$\alpha_3 = -0.11\eta; \tag{4}$$

$$(\eta^3/\omega)\,\mathrm{ctg}\,\alpha_{33} = 8.05 - 3.8\omega; \tag{5}$$

$$\alpha_{31} = 0, \tag{6}$$

where η denotes the meson momentum in the center-of-mass system, in units μc and ω---the total energy, exclusive of the proton rest energy. It is true that not all the values of the "optimized" phase shifts satisfy Eqs. (4)-(6), but this can possibly be connected with the inaccuracies in the determination of "optimized" phases, especially phase α_3 at energies near "resonance". In particular, Orear showed that all known differential cross sections up to 220 mev are not contrary to these equations.

In view of the considerable theoretical interest in the behavior of the S-phase, it is desirable to investigate the reasons for the observed deviation, at energies 240, 270 and 307 mev, of α_3 from the linear relationship observed in investigations of a whole series of processes in the region of small meson energies. It is reasonable to ask the question, whether or not this deviation can be explained only by the inaccuracies in the obtained values of phase shifts α_3. To answer this question, the magnitudes of the differential cross sections (experimental values) given in Tables 2-6 (Ref. 2) were compared with the cross sections computed on the basis of Eqs. (4)-(6). Results of the comparison are presented in Table II.

TABLE II.

Meson Energy, mev	Number of experimental points	$M_{(4)-(6)}$
176	9	4.6
200	7	8.5
240	7	31
270	6	260
307	8	240

In the last column are given the values:

$$M_{(4)-(6)} = \sum_i \left\{ \frac{f(\alpha_3, \alpha_{33}, \theta_i) - \sigma(\theta_i)}{\Delta\sigma(\theta i)} \right\}^2,$$

which give the degree of deviation of the curve $f(\alpha_3, \alpha_{33}, \theta_i)$, computed according to Eqs. (4)-(6), from the experimentally measured values of differential cross sections $\sigma(\theta_i)$. It can be seen from the Table that at energies 176 and 200 mev the experimental data do not contradict Eqs. (4) and (6), which is also confirmed by analyzing other data in this energy range, obtained by Orear. At higher energies, however, it is completely impossible to reconcile the experimental results with the values of phase shifts predicted by Eqs. (4) and (6).

If it is assumed that up to energies of the order of 300 mev scattering is sufficiently well described by S- and P-waves only; it must then be definitely concluded from the above that the linear dependence of the phase α_3 on the meson momentum does not hold for energies higher than 200-240 mev. On the other hand, in view of the attractiveness of such a simple dependence, it is necessary to investigate carefully whether the linear dependence of the S-phase on the meson momentum is preserved with the introduction of higher angular moments ($l = 2$), especially since our experimental data for 307 mev mesons point to the difficulty of approximating the observed angular distribution by a function of the type $a + b\cos\theta + c\cos^2\theta$ (see Table 7 of Ref. 2).

2. (S-P-D)-ANALYSIS

In the case when S-, P- and D-waves contribute to the scattering, the angular distribution can be represented in the form

$$\lambda^{-2}\frac{d\sigma}{d\Omega} = \mathcal{A} + \mathcal{B}\cos\theta + C\cos^2\theta + \mathcal{D}\cos^3\theta + \mathcal{E}\cos^4\theta.$$

The phase shifts and the above-indicated coefficients of angular distribution are connected by the relationships:

$$\mathcal{A} = |S|^2 + |P_+ - P_-|^2 + |{}^3/_2 D_+ + D_-|^2 - 2I\left(S/{}^3/_2 D_+ + D_-\right); \quad (7)$$

$$\mathcal{B} = 2I(S/2P_+ + P_-) - 2I\left({}^3/_2 D_+ + D_-/2P_+ + P_-\right) + 6I(P_+ - P_-/D_+ - D_-); \quad (8)$$

$$C = |2P_+ + P_-|^2 - |P_+ - P_-|^2 + 9|D_+ - D_-|^2 - 6\left|{}^3/_2 D_+ + D_-\right|^2 + 6I\left(S/{}^3/_2 D_+ + D_-\right); \quad (9)$$

$$\mathcal{D} = 6I\left(2P_+ + P_-/{}^3/_2 D_+ + D_-\right) - 6I(P_+ - P_-/D_+ - D_-); \quad (10)$$

$$\mathcal{E} = 9\left|{}^3/_2 D_+ + D_-\right|^2 - 9|D^+ - D_-|^2. \quad (11)$$

Here we use the symbols:

$$S = e^{i\alpha_3}\cdot\sin\alpha_3;$$

$$P_- = e^{i\alpha_{31}}\cdot\sin\alpha_{31}; \quad P_+ = e^{i\alpha_{33}}\cdot\sin\alpha_{33}.$$

$$D_- = e^{i\delta_{33}}\cdot\sin\delta_{33}; \quad D_+ = e^{i\delta_{35}}\cdot\sin\delta_{35};$$

$$I(a/b) = \frac{1}{2}(ab^* + a^*b).$$

The total cross section is expressed in terms of phase shifts as follows:

$$\lambda^{-2}\frac{\sigma_t(\pi^+, p)}{4\pi} = \sin^2\alpha_3 + \sin^2\alpha_{31} + 2(\sin^2\alpha_{33} + \sin^2\delta_{33}) + 3\sin^2\delta_{35}. \quad (12)$$

From an examination of the coefficients (Table 9, Ref. 2) obtained for 307 mev, computations were made to evaluate the phases of scattering for the D-waves. For simplicity, an approximate solution of the system of Eqs. (10) and (11) was sought by assuming that $\alpha_{31} = 0$ and $\alpha_{33} = 134°$, i.e., the magnitude of the phase shift α_{33} was used as obtained graphically in the (S-P)-analysis. Such an assumption is quite natural since the perturbation introduced by the D-waves has a relatively weak influence on the phase α_{33}. The result was that the obtained values for δ_{33} and δ_{33} can satisfy the equations for all coefficients, the phase shift α_3 obtained thereby being considerably less than 24°, i.e., much less than the value obtained if only the S- and P-waves are considered*. In view of this, the experimental data of Ref. 2 and of Refs. 2-5, 7 cited in Ref. 2, were again analyzed with the aid of the high-speed electronic computer BESM of the Academy of Sciences, USSR*. Computations were made of the optimal phase shifts α_3, α, α_{33}, δ_{33} and δ_{35}, thereby only such solutions were sought in which α_3 is negative and α_{33} lies between the limits $\pm 10°$ from the values given in Table I.

In the computations, the differential and total cross sections were expressed by the five phase shifts according to Eqs. (7)-(12). A minimum was sought for the quantity

$$M = \sum_i \left\{\frac{f_i(\alpha_3, \alpha_{31}, \alpha_{33}, \delta_{33}, \delta_{35}) - \sigma_i}{\Delta\sigma_i}\right\}^2,$$

where $f_i(\alpha_3, \alpha_{31}, \alpha_{33}, \delta_{33}, \delta_{35})$ denotes a function expressing the cross section in terms of phase shifts, and σ_i is the cross section as measured experimentally with an error $\Delta\sigma_i$. The values of phase shifts obtained by (S-P)-analysis with the aid of Ashkin diagrams served as the initial data. As a first approximation the phases were changed in turn, beginning with α_3, within given limits for each degree. This cycle was repeated several times, as long as the value of M has not ceased to diminish, after which the measurements were made every half degree, etc.

The "optimized" scattering phases for 270 and 307 mev obtained in this manner are presented in Table III.

As seen from this Table, the experimental values for 307 mev, which are not well satisfied by three parameters (see Table 7, Ref. 2 and Table I of this work), are well satisfied by the five phase shifts. At this energy, δ_{33} and δ_{35} are approximately equal in absolute value and have different signs. This property, as follows from Eq. (10) may explain the fact that the coefficient $\mathbb{D}$ determined by the interference of P- and D-waves is not observable in practice. As far as coefficient $\mathbb{B}$ is concerned, it is determined by the interference of (S-P)-as well as by interference of (P-D)-waves, whence it follows that for all energies up to 300 mev it is extremely difficult to determine the separate contributions of S- and D-waves.

* It should be noted that Orear already attempted some time ago to account for the effect of D-waves[8] by interpreting the experimental data on π-meson scattering in hydrogen in the energy range up to 220 mev. However, he took into consideration only the effect of the D-wave with a total angular momentum 5/2. As seen from the equations, phase δ_{35} produces a small "perturbation" in the phase shift α_3 if the value of δ_{35} is taken to be of the order of several degrees at 160-200 mev. The value $\delta_{35} = -0.013\eta^5$ proposed by Orear (which agrees with experimental data in the energy range of 100-200 mev) is definitely excluded by the results of the present work. Besides, as shown in a later work of Orear[7], all experimental data in the energy range up to 220 mev satisfy Eqs. (4)-(6) sufficiently well, a fact also confirmed by our measurements (see Table II).

* The authors are thankful to the director of the Computation Center, of the Academy of Sciences, USSR, Academician A. A. Dorodnitsyn for the opportunity to make computations on the BESM and also to the collaborators of the Computation Center, Academy of Sciences, USSR and of the Institute of Exact mechanics & Computation Techniques, Academy of Sciences, USSR, who rendered assistance in this work.

TABLE III.

"Optimum" phase shifts (in degrees)

Meson energy, mev	α_3	α_{31}	α_{33}	δ_{33}	δ_{35}	M	Number of experimental points
270	—13.6	—4.3	128.8	4.3	— 6.9	4.03	7
307	—13.0	—4.0	133.7	9.5	—10.0	3.78	9

A. D-Phases δ_{33} *and* δ_{35}

It is difficult, on the basis of only the "optimum" solution presented in Table III, to assert anything with certainty concerning the size of *D*-waves contribution at energies of the order 300 mev. Nevertheless, it is of definite interest to examine the results of such a procedure. This will be carried out in the following section, chiefly in the discussion of the *S*-phase behavior.

It is known that for small values of phase shifts their dependence on the meson momentum η, in the center-of-mass system, can be written in the form const $\times \eta^{2l+1}$. As a working hypothesis, therefore, the values of phase shifts for the *D*-waves were taken as equal (in degrees) to $\delta_{33} = 0.20\eta^5$ and $\delta_{35} = -0.21\eta^5$, where the coefficients are determined from the "optimum" values of phases δ_{33} and δ_{35} for 307 mev. Of course, such a choice is entirely arbitrary, especially in the case of phase δ_{33}, the "optimum" values of which are not regular. The dependence of phase shift δ_{35} as written above is shown in Fig. 1. In the same Figure, for comparison, are shown the optimum phase shifts δ_{33} and δ_{35} obtained with the aid of the electronic computer. The tendency of the *D*-phase, particularly phase δ_{35}, to increase with the meson energy is seen from the graph. Considering the accuracy of the initial data and the nature of the mathematical problem, it can be only stated that there is no contradiction between $\delta \sim \eta^5$ dependence and the obtained data.

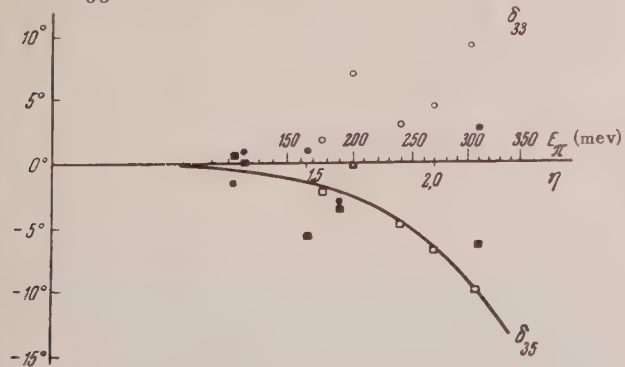

FIG. 1. "Optimized" *D*-wave phase shifts, obtained by (*S-P-D*)-analysis. δ_{33} o—data analysis, the present work; ●—data analysis, other papers. δ_{35}: □—data analysis, present work; ■—data analysis, other papers. Solid curve $-\delta_{35} = \eta - 21 \times \eta^5$.

B. S-Phase α_3

Figure 2 shows the values of phase shifts α_3

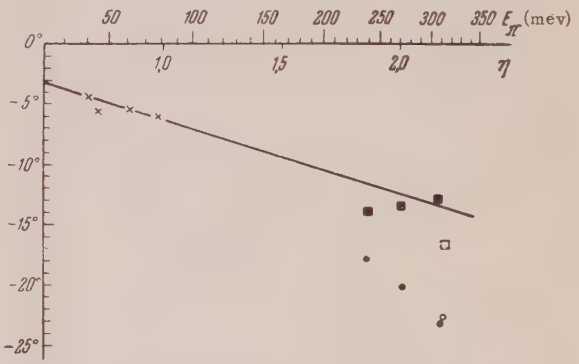

FIG. 2. Phase shift α_3 for low- and high-energy mesons. ×—data cited in Ref. 7; ■—(*S-P-D*) data analysis, present work; □—(*S-P-D*) data analysis, Ref. 6; ●—(*S-P*)-analysis of data, present work; o—(*S-P*)-analysis of data in Ref. 6. Solid curve—dependence $\alpha_3 = 6.3^\circ\eta$.

as a function of the meson momentum η in the energy range less than 100 and greater than 240 mev, i.e., in those energy regions where this phase can be determined relatively accurately. The straight line represents the relationship $\alpha_3 = -6.3^\circ\eta$, which best satisfies the experimental data at low energies. The values of α_3 at low energies are indicated by crosses. At energies of

240 mev and higher, the "optimized" values of α_3, obtained on the assumption that only S- and P-waves figure in the scattering, are shown as small circles.

It is seen from the Figure that, as already pointed out above, the linear dependence of α_3 is incompatible with the values obtained in the region of high energies using the (S-P)-analysis. This indicates that at energies ~200-240 mev the meson wavelength, in the center-of-mass system, becomes comparable to the interaction radius r_0 ($r_0 \approx \lambda\!\!\!^{-} \sim 8 \times 10^{-14}$ cm). In the same Figure, small squares indicate "optimized" values of α_3 for energies 240, 270, 307 and 310 mev when the D-wave is also considered in the analysis of the data. As can be seen, the values of phase α_3 are in complete agreement with the dependence obtained at low energies. This behavior of the S-phase shows indirectly, but, of course, does not prove, that even at energies of the order of 300 mev the contribution of the D-waves cannot be neglected in the evaluation of the S-phase.

It should be emphasized that if the assumed relationship $\delta_{33} = 0.20\eta^5$ is indeed correct, then the influence of the D-wave on the α_3-phase determining coefficient B becomes noticeable even at energies 100-150 mev. To illustrate this, the solid curve in Fig. 3 represents the energy dependence

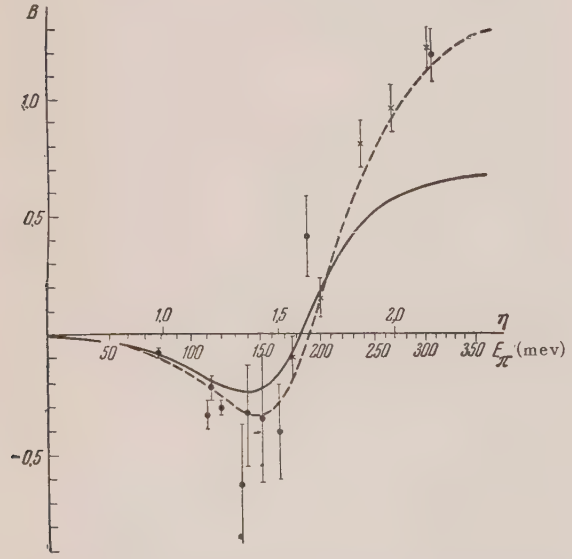

FIG. 3. Dependence on meson energy of coefficient B. Experimental points — values of coefficient B obtained by the method of least squares using as an approximation of the angular distribution the function $\lambda\!\!\!^{-2}\, d\sigma/d\Omega = A + B\cos\theta + C\cos^2\theta$. × — data, present work; ● — data, works of other authors.

of the coefficient B computed by considering the S- and P-waves only (α_3 taken as equal to 6.3η), while the dotted curve represents the energy dependence of the coefficient B computed by considering the S-, P- and D-waves ($\alpha_3 = -6.3\ M$ and $\alpha_{33} = -\alpha_{35} = +0.20\eta^5$) (all values of phase shifts are given in degrees). In the same Figure are given the values of the coefficient B for different energies obtained by the method of least squares, if the angular distribution is approximated by the function:

$$\lambda\!\!\!^{-2}\ \frac{d\sigma}{d\Omega} = A + B\cos\theta + C\cos^2\theta.$$

It is seen from this that the linear dependence in the form proposed by Orear, even at relatively low energies, agrees better with experimental data when the D-wave contribution is taken into consideration.

The linear dependence of α_3 which manifests itself when (S-P-D)-analysis is used, deserves consideration. It is known that phase shifts will be proportional to η^{2l+1} under the condition that the radius of the meson-nucleon interaction r_0 is smaller than the wavelength $\lambda\!\!\!^{-}$ of the meson in the system of the center-of-mass; therefore, linear or almost linear dependence of α_3 up to 307 mev indicates that r_0 cannot appreciably exceed $\lambda\!\!\!^{-}$ (307 mev) $= 6.5 \times 10^{-14}$ cm. Thus, independently of whether or not S- and P-waves alone are sufficient to describe scattering, it follows from our measurements, that the radius of meson-nucleon interaction is $\sim 7 \times 10^{-14}$ cm. Strictly speaking, r_0 is here the radius of interaction between the meson and the nucleon in the S-state with an isotopic spin 3/2. However, it is natural to correlate this value with "dimensions" of the proton, if we consider the experimental results on scattering of electrons and protons by protons[9].

C. Phase Shift α_{31}

"Optimized" phase shifts α_{31}, previously obtained by a series of authors, and also those obtained in the present work, are extremely irregular at energies up to 220 mev so that even the sign of this phase cannot be uniquely determined. However, in the region of higher energies phase, α_{31} behaves regularly. It can be definitely concluded, from data obtained in this work, that phase α_{31} is negative and apparently less than 10° up to 310 mev. This is shown in Fig. 4, where the "optimum" values of phase α_{31}, obtained from analysis

of data with consideration of S- and P-waves only, are shown as little squares, and the results which include the D-waves as well are shown as little circles. It is seen from the Figure that α_{31} is systematically decreasing when the data are expressed through the five phase shifts.

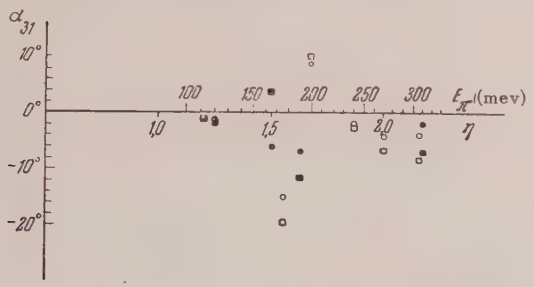

FIG. 4. Phase shift α_{31} at different meson energies. □ – (S-P)-analysis of data, present work; o – (S-P-D)-analysis of data, present work; ■ – (S-P-D)-analysis, other papers; ● – (S-P-D)-analysis of data, other papers.

D. Phase Shift α_{33}

In Fig. 5 are shown "optimized" values of phase α_{33} obtained by a series of authors (see, for example, summary 5 in Ref. 2). The "optimized" values of α_{33} obtained in this work by data analysis which includes D-waves is indicated by small circles. It should be noted that, if only S- and P-waves are considered, the phase shifts α_{33} are very little different from those shown in the Figure. Data for higher than 240 mev cannot be represented in the form of a straight line on the Chew and Low diagram[10]. The theoretical significance of this fact is not clear.

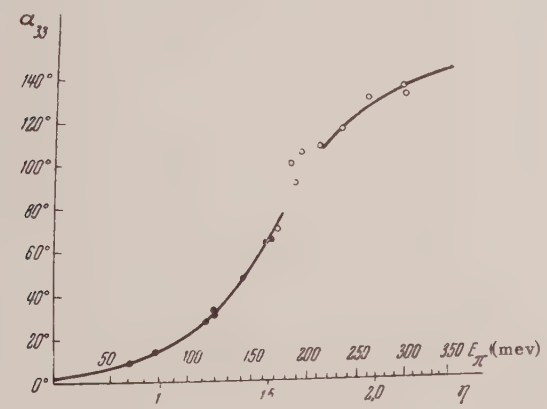

FIG. 5. Dependence of the phase shift α_{33} on π-meson energy. o – data, present work; ● – data, other papers. Solid curve – relation $\eta^3 \times \arctan \alpha_{33} = 4.3 + 0.6\eta^2 - 0.8\eta^4$.

As should be expected, at high energies the values of α_{33} given in Fig. 5 definitely exceed those obtainable from total cross section data (see Fig. 17, Ref. 2, and also the work of Lindenbaum and Yuan[11]) if it is considered that the interaction is completely determined by the state $P_{3/2}$.

Since the values of α_{33} near "resonance" cannot be determined with good accuracy, we have made an attempt to obtain an analytical dependence of this phase in a form that preserves for small energies the dependence $\alpha_{33} = 0.235\eta^3$ (Ref. 7) and conforms to the data obtained in this work for high energies. We have selected the relation[12] of the form $\eta^3 \arctan \alpha_{33} = 4.3 + 0.6\eta^2 - 0.8\eta^4$, which is shown in Fig. 5 as a solid curve. Naturally, the relation obtained in this manner may not reflect the behavior of α_{33} in the resonance region. The behavior of α_{33} in this region of energy is discussed below.

According to the data of Lindenbaum and Yuan[11], the maximum $\sigma_t(\pi^+, p)$ is found at ~175 mev, while from our data (see Fig. 17 of Ref. 2) this maximum is found approximately at 185 mev. Considering the experimental errors in our measurements and those in Ref. 11, it can be stated that there is no significant disagreement between the experimental results. However, the statement by Lindenbaum and Yuan that α_{33} can pass through 90° at as low an energy as 175 mev, can, in our opinion, be refuted on the basis of the behavior of the coefficient B. As it is known, considering S- and P-waves only,

$$B = 2\sin\alpha_3 [2\sin\alpha_{33} \cdot \cos(\alpha_{33} - \alpha_3) + \sin\alpha_{31}\cos(\alpha_{31} - \alpha_3)].$$

Considering that in the energy region near "resonance", α_3 is approximately $-10°$, and α_{31} close to zero and negative, it can be stated that the value of α_{33} does not exceed 80° when $B = 0$. It is seen in Fig. 3 that B cannot be equal to zero at energy less than 176 mev, from which follows that the "resonance" energy can hardly be less than 190 mev. This conclusion is confirmed by the analysis of Bethe and others[13].

3. CAUSALITY

Based on the work of Goldberger, Myazowa and Oehme[14] on the application of the causality principle to the meson-nucleon scattering, Anderson

and others[5] and also Sternheimer[15] obtained the energy dependence of the real part of the scattering amplitude below 0° from the combined data on total scattering cross sections of mesons by protons. The real part of the scattering amplitude below 0° obtained in this manner was compared by Anderson, Davidon and Kruse with its expression in terms of phase shifts up to 220 mev. New data obtained in this work permitted the extension of this comparison to 310 mev; here the phase shift values obtained by (*S-P*)-analysis were used as well as those obtained by (*S-P-D*)-analysis.

If we denote by $D_+(\eta)$ the real part of the forward scattering amplitude and by $\lambda\!\!\!^{-}$ and $\lambda\!\!\!^{-}_{cm}$ the meson wavelengths in the laboratory system and in the center-of-mass system, respectively, then

$$\frac{2\lambda\!\!\!^{-}}{\lambda\!\!\!^{-2}_{cm}} D_+(\eta) = \sin 2\alpha_3 + \sin 2\alpha_{31} + 2(\sin 2\alpha_{33} + \sin 2\delta_{33}) + 3\sin 2\delta_{35}.$$

In Fig. 6 are shown results of data analysis of this work and also analysis of certain π^+-p scattering data of other authors (Refs. 2-5, 7 in Ref. 2).

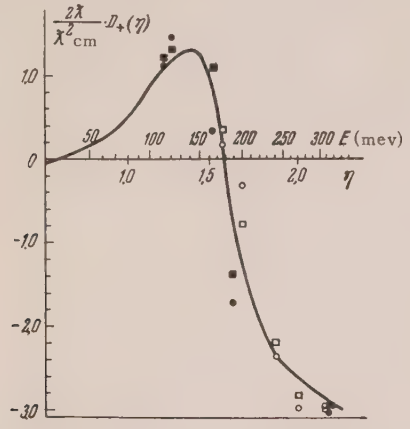

FIG. 6. Comparison of the value $(2\lambda\!\!\!^{-}/\lambda\!\!\!^{-2}_{cm})D_+(\eta)$, computed on the basis of causality conditions with the values: $\sin 2\alpha_3 + \sin 2\alpha_{31} + 2(\sin 2\alpha_{33} + \sin 2\delta_{33}) + 3\sin 2\delta_{35}$ { o — present work; ● — result of data analysis, other papers } $2\sin 2\alpha_3 + \sin 2\alpha_{31} + 2\sin 2\alpha_{33}$ { □ — present work; ■ — other papers }.

It is noted from the Figure that agreement between the real parts of the forward scattering amplitudes computed on the basis of the causality principle with the corresponding data obtained from the angular distribution in π^+-p scattering continues to be good up to meson energies of 310 mev. The question whether better agreement is obtained by using (*S-P*)-or (*S-P-D*)-analysis for the computed curve cannot be answered. This was to be expected since the basic characteristics of the solid curve shown in the Figure, even at energies ~300 mev, is determined in the final count by the phase shift α_{33} which is practically equal for both (*S-P*)- and (*S-P-D*)-data analysis.

CONCLUSION

Below is a summary of the contents of the preceding[2] and present papers.

1. Angular distribution of π^+-meson scattering by hydrogen at 176, 200, 240, 270 and 307 mev, as measured by the scintillation counting method, are presented in Figs. 12-16 of Ref. 2.

2. Energy dependence of the total cross section $\sigma_t(\pi^+, p)$ is shown in Fig. 17, Ref. 2.

3. With the aid of a high-speed electronic computer, a phase analysis was made of the data on the assumption that the scattering process is described by *S*- and *P*-waves only [(*S-P*)-analysis, Table I], as well as on the assumption that *S*-, *P*- and *D*-waves contribute to the scattering [(*S-P-D*)-analysis, Table III; Figs. 1-5]. Among the possible solutions only the phase group in which α_3 is negative and α_{33} passes through 90° in the energy region 170-200 mev, was examined.

4. Phase shifts α_{33} are shown in Fig. 5. They are practically the same for (*S-P*)- and (*S-P-D*)-analysis. Some evidence is presented indicating that α_{33} passes through 90° at an energy > 176 mev.

5. It is impossible to reconcile the obtained values of α_3 for 240, 270 and 307 mev with Orear's equation $\alpha_3 = -0.11\eta$, which approximates well the data for low energies, if the data is described only by the three phase shifts of *S*- and *P*-waves, α_3, α_{31} and α_{33}.

6. There is no direct indication of the need for using (*S-P-D*)-analysis for the data presentation if we discount the measurements made at 307 mev, which are approximated only with difficulty by a function of the type $a + b\cos\theta + c\cos^2\theta$.

7. The "optimized" values of phase α_{31}, which are, as known, highly irregular up to ~200 mev, become regular at higher meson energies (see Fig. 4). It can be stated that α_{31} is negative and is apparently less than 10° up to 310 mev. Phase α_{31} is definitely decreasing when the data are expressed by five phase shifts.

8. "Optimized" *D*-wave phase shifts δ_{33} and

δ_{35} are positive and negative, respectively. The phases are represented in Fig. 1 where their tendency to grow with energy can be seen.

9. With (S-P-D)-analysis the values of S-phase α_3 are considerably smaller compared with those obtained by (S-P)-analysis (see Fig. 2). If we consider the possible D-wave contribution, α_3 depends linearly or almost linearly on the meson momentum up to 310 mev, according to the equation determined for low energies $\alpha_3 = -0.11\eta$.

10. At any rate, independent of whether or not S- and P-waves only are sufficient to describe scattering, it follows from 5 and 9 that the radius of meson-nucleon interaction is $r_0 \sim 7 \times 10^{-14}$ cm.

11. The real part of the forward scattering amplitude, obtained from the causality condition, agrees well with its representation by phase shifts up to 310 mev.

The authors deem it a pleasure to thank I. E. Tamm and L. D. Landau for valuable advice, L. I. Lapidus for numerous discussions, and also I. B. Popov and G. N. Tentiukov for their considerable assistance in making the computations.

---

[1] Anderson, Fermi, Martin and Nagle, Phys. Rev. **91**, 155 (1953).

[2] Mukhin, Ozerov and Pontecorvo, J. Exptl. Theoret. Phys. (U.S.S.R.) **31**, 371 (1956); Soviet Phys. JETP **3**, 237 (1957).

[3] J. Askin and S. H. Vosko, Phys. Rev. **91**, 1248 (1953).

[4] Mukhin, Pontecorvo, Popova and Tentiukova, Presentation before the all-union conference on the physics of high-energy particles, May 14-22, 1956.

[5] Anderson, Davidon and Kruse, Phys. Rev. **100**, 339 (1955).

[6] E. L. Grigoriev and N. A. Mitin, Report (Otchet) Inst. Nucl. Phys. USSR, 1955; Presentation at the all-union conference on the physics of high-energy particles, May 14-22, 1956.

[7] J. Orear, Phys. Rev. **96**, 176 (1954); **100**, 288 (1955).

[8] J. Orear, Phys. Rev. **98**, 1155A,(1955).

[9] See, for example, Ia. Smorodinskii, Usp. Fiz. Nauk **56**, 425 (1955).

[10] G. F. Chew and F. E. Low, Proceedings of the Fifth Rochester Conference on High-Energy Nuclear Physics (Interscience Publishers, Inc., New York, 1955).

[11] S. J. Lindenbaum and L.C.L. Yuan, Phys. Rev. **100**, 306 (1955).

[12] K. Brueckner, Phys. Rev. **87**, 1026 (1952).

[13] de Hoffmann, Metropolis, Alei and Bethe, Phys. Rev. **95**, 1586 (1954).

[14] Goldberger, Miyazawa and Oehme, Phys. Rev. **99**, 986 (1955).

[15] R. M. Sternheimer, Phys. Rev. **101**, 384 (1956).

Translated by J. L. Herson
118

Nuclear Magnetic Relaxation in Ionic Crystals

G. R. KHUTSISHVILI
Institute of Physics, Academy of Sciences, Georgian SSR
(Submitted to JETP editor May 30, 1955)
J. Exptl. Theoret. Phys. (U.S.S.R.) 31, 424-426 (September, 1956)

We present results of a calculation of the nuclear magnetic relaxation time in ionic crystals. Two mechanisms of relaxation are considered: relaxation due to quadrupole effects, and relaxation produced by paramagnetic impurities. The results obtained are in qualitative agreement with the experimental data.

1. Experimental and theoretical investigation of nuclear magnetic resonance and relaxation phenomena are of considerable interest. A theoretical treatment of nuclear magnetic relaxation in ionic crystals was first given by Waller[1], who calculated the relaxation time resulting from modulation of the spin-spin interaction of the nuclear magnetic moments by the thermal vibrations of the lattice. However, this mechanism gives nuclear magnetic relaxation times far exceeding the experimental values. Another possible mechanism of nuclear magnetic relaxation in ionic crystals was considered in a paper of the author[2], but this mechanism also gives large values for the relaxation time.

The present paper gives results of calculations of the nuclear magnetic relaxation time in ionic crystals for two other mechanisms (for a more detailed presentation, cf. Refs. 3 and 4).

2. Pound[5] showed experimentally that, in sufficiently pure ionic crystals, the relaxation of nuclei with spin greater than ½ is often produced by quadrupole effects. The most convincing experiments were done with single crystals of $NaNO_3$ at room temperature (where the relaxation of Na nuclei was studied).

A nucleus with spin greater than ½ possesses a quadrupole moment. Because of the thermal vibrations of the lattice, the quadrupole energy of the nucleus in the crystalline field will be a function of the time. This varying energy is the perturbation which causes spin transitions of the nuclei. Both pure quadrupole transitions and transitions due to interference of the nuclear quadrupole energy (V_q) with the elastic energy (V_e) are possible. We expand the quadrupole and elastic energy of the nucleus in powers of the deformation tensor w. (The expansion is justified because of the smallness of the thermal vibrations of the lattice.) It is well known that the components of the deformation tensor have nonzero matrix elements for the emission or absorption of one phonon.

Next we calculate the probability of a spin transition for processes involving various numbers of phonons. The calculation is done by the standard scheme of perturbation theory, where we limit ourselves to determining orders of magnitude (i.e., we disregard numerical coefficients of order unity).

The results of the calculation show that for $T < \Theta$ (the Debye temperature), the most important process is the pure quadrupole, two-phonon process, which is caused by the term quadratic in w, in V_q, in the first approximation of perturbation theory; for $T > \Theta$, the most important process is the four-phonon interference process (which is caused by the interference of the first order term in w in V_q with the third order term in w in V_e, i.e., with the anharmonic term. Such a process occurs in the second approximation of perturbation theory). The calculations of nuclear magnetic relaxation time due to quadrupole effects give

$$T_1 = (C_1/\omega_m)\,(Mv^2/b)^2\,(\Theta/T)^4 \quad \text{for} \quad T > \Theta, \tag{1}$$

$$T_1 = (C_2/\omega_m)\,(Mv^2/b)^2\,(\Theta/T)^7 \quad \text{for} \quad T \ll \Theta, \tag{2}$$

where ω_m is the maximum frequency of the acoustic vibrations, M is the nuclear mass, v is the velocity of propagation of elastic waves, C_1 and C_2 are numerical coefficients which are not determined by our crude calculations, and b is given by

$$b \approx e^2 Q/a^3, \tag{3}$$

where e is the elementary charge, a is the distance to nearest neighbor ions, and Q is the nuclear quadrupole moment. A more detailed treatment shows that b is actually somewhat greater than the value given by formula (3), because of the so-called antishielding effect[6,7].

There is no point in making a more exact calculation of T_1 at present, since almost nothing is

known about the coefficients in the expansions of V_q and V_e, except their order of magnitude.

We note that Ref. 7 is also concerned with the theoretical treatment of nuclear magnetic relaxation caused by quadrupole effects. In that paper, the pure quadrupole two-phonon effect was calculated; however, we see from our calculations that, for $T > \Theta$, the four-phonon interference process is more important.

Since there are at present no experimental data concerning the temperature dependence of T_1 (for nuclei with spins greater than ½), we shall make a qualitative comparison with experiment in the following way: we calculate the constant b, using formula (1) and the experimental data on the relaxation time of Na in $NaNO_3$ at room temperature[5]. This gives $b \sim 3 \times 10^{-20}$ ergs.

This value of b corresponds to e^2Q/a^3 with a approximately equal to one Angstrom. (We take the value[8] $Q = 10^{-25}$ cm^2 for the quadrupole moment of Na^{23}.) Our calculations are quite crude, but still the value obtained for b is reasonable.

3. Bloembergen[9] has shown experimentally that in many nonconducting solids nuclear magnetic relaxation is due to paramagnetic impurities. In this paper the following mechanism for relaxation was proposed: the spin of a paramagnetic ion (for example, Cr^{+++} or Fe^{+++}), because of its interaction with the lattice, changes its direction periodically, with a period of the order of ρ, where ρ is the paramagnetic relaxation time. Therefore, a time-varying local magnetic field acts on the nuclear spins in the neighborhood of the paramagnetic ion and tends to reorient them. Because of this, the nuclear spins which are close to the paramagnetic ions rapidly approach thermal equilibrium with the lattice vibrations. A gradient of spin temperature is thus produced, which gives rise to spin diffusion, as a result of which equilibrium of the nuclear spins and lattice is finally established throughout the body.

In Ref. 9, a calculation was made of the time for direct nuclear magnetic relaxation at a distance r from a paramagnetic ion. In treating the spin diffusion, several doubtful assumptions were made in Ref. 9. In addition, the solution of the differential equation was carried out by numerical methods, so that it is of interest to consider once again the process of spin diffusion.

We have solved the differential equation for M (the nuclear magnetization) subject to the appropriate boundary conditions. The calculation was made for a nuclear spin ½, and the spatial dependence $M(r)$ was obtained. From the asymptotic form of this function, it is easy to obtain the flux of nuclear magnetic moment and then find the nuclear magnetic relaxation time. We obtain

$$T_1 = 1/4\pi DcN, \tag{4}$$

where N is the number of paramagnetic ions per unit volume, D is the diffusion coefficient for the nuclear spin, and c is given by

$$c = 2^{-5/4}\pi\Gamma^{-2}(5/4)\,\beta^{1/4} = 0.68\,\beta^{1/4}, \tag{5}$$

where

$$\beta = (\gamma\gamma'\hbar)^2 S(S+1)/5\pi\rho\nu^2, \tag{6}$$

γ, γ' are the gyromagnetic ratios of nucleus and paramagnetic ion, respectively, S is the spin of the paramagnetic ion, ν is the resonance frequency of the nuclear spin in the external magnetic field.

Our treatment is valid only for sufficiently low concentrations of paramagnetic ions. The quantitative criterion for the validity of the approximation we have considered is that the magnetic interaction energy of nearest neighbor paramagnetic ions be small compared to the interaction energy of the paramagnetic ion with the nearest nuclear spins.

In particular, Ref. 9 gives experimental data on the dependence, on temperature and concentration of Cr atoms, of the relaxation time for protons in potassium-chrome alums highly diluted with aluminum. A simple estimate shows that the condition for applicability of our treatment is fulfilled for $N_{Cr}/N_{Al} < 10^{-3}$. In particular, samples I, II and III of Ref. 9 satisfy this condition.

The dependence of T_1 on the concentration of paramagnetic atoms, given by formula (4), is confirmed by experiment. As for the temperature dependence of T_1 (where our result is the same as the dependence obtained in Ref. 9 by a numerical method), unfortunately, it is impossible at present to make a quantitative comparison with experiment, since there are no experimental data on the temperature dependence of the paramagnetic relaxation time of highly diluted alums. However, we note that with the value of ρ for undiluted potassium-chrome alums, formula (4) gives, for samples I, II and III of Ref. 9, satisfactory agreement with the experimental data for $T = 20°$ K.

4. Summarizing, we see that our calculations are in accord with the generally accepted picture of the mechanism of nuclear magnetic relaxation in

ionic crystals. In the case of a nuclear spin equal to ½, the nuclear magnetic relaxation is always caused by the interaction of the nuclear spins with the spins of paramagnetic impurities. In the case of a nuclear spin greater than ½, nuclear magnetic relaxation at high temperatures is produced by quadrupole effects, and at low temperatures by the interaction of the nuclear spins with the spins of paramagnetic impurities. The temperature at which these two interactions are equally effective decreases with decreasing concentration of paramagnetic impurities .

[1] I. Waller, Z. Physik **79**, 370 (1932).

[2] G. R. Khutsishvili, J. Exptl. Theoret. Phys. (U.S.S.R.) **22**, 382 (1952); Trudy Inst. Phys., Acad. Sci., Georgian SSR **1**, 31 (1953).

[3] G. R. Khutsishvili, Trudy Inst. Phys., Acad. Sci., Georgian SSR **2**, 115 (1954).

[4] G. R. Khutsishvili, Trudy Inst. Phys., Acad. Sci., Georgian SSR (in press).

[5] R. V. Pound, Phys. Rev. **79**, 685 (1950).

[6] Foley, Sternheimer and Tycko, Phys. Rev. **93**, 734 (1954).

[7] J. Van Kranendonk, Physica **20**, 781 (1954).

[8] P. L. Sagalyn, Phys. Rev. **94**, 885 (1954).

[9] N. Bloembergen, Physica **15**, 386 (1949).

Translated by M. Hamermesh
85

Radiative Corrections to the Scattering of Electrons by Electrons and Positrons

R. V. POLOVIN
Physico-technical Institute, Academy of Sciences, Ukrainian SSR

(Submitted to JETP editor June 6, 1955)
J. Exptl. Theoret. Phys. (U.S.S.R.) 31, 449-458 (September, 1956)

The radiative corrections to the scattering of electrons by electrons and positrons are calculated with accuracy up to α^3. Consideration is given to the general case and the limiting case of large energies.

1. ELASTIC SCATTERING OF ELECTRONS BY ELECTRONS

THE scattering of electrons by electrons and positrons, including the radiative corrections of lowest order, can be represented by means of the diagrams shown in Fig. 1, where p_1, p_2, p_1', and p_2' represent the four-dimensional momenta of the first and second electrons before and after scattering, k the four-dimensional momentum of a photon, p the momentum of a virtual electron, μ and ν the polarizations of virtual photons, and $q = p_1' - p_1$. (We do not consider diagrams containing proper energy parts for a real electron, since on regularization they reduce to zero). The matrix element corresponding to the ith graph will

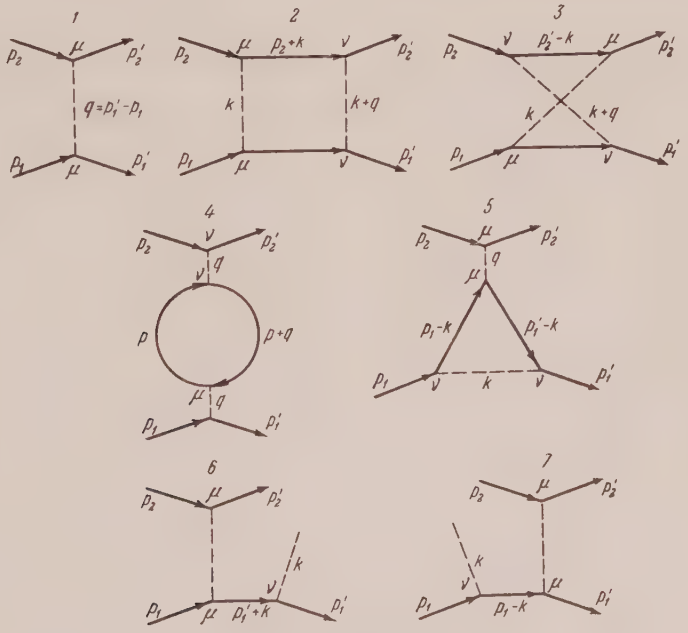

FIG. 1.

be denoted by U_i. Along with the diagrams shown, one must also consider diagrams obtained from them by means of the interchanges

1) $p_1 \rightleftarrows p_2$; $p_1' \rightleftarrows p_2'$; 2) $p_1' \rightleftarrows p_2'$; 3) $p_1 \rightleftarrows p_2$.

The matrix elements of such diagrams will be denoted by U_i', $\tilde{U}_i$, and $\tilde{U}_i'$, respectively.

On integration the matrix elements corresponding to diagrams 4 and 5 of Fig. 1 diverge in the region of large momenta of the virtual particles. These divergences are regularized in the usual way,[1] and we carry out the integration over a finite relativistically invariant four-dimensional region.[2] The matrix elements corresponding to diagrams 2, 3, and 5 also diverge on integration over the region of small momenta of the virtual particles ("infrared catastrophe"). To avoid this difficulty one proceeds, as is well known, to ascribe to the photon a "mass" λ, which then appears in the cross section for elastic scattering. On combining the cross sections of purely elastic scattering and inelastic scattering (with emission of a long-wavelength photon, with energy not exceeding ΔE), the

quantity λ cancels out and does not appear in the final result. The inelastic scattering is represented in diagrams 6 and 7 of Fig. 1.

The matrix elements corresponding to the diagrams of Fig. 1 are formed according to Feynman's rules.[3,2] For example, diagram 3 gives the following matrix element

$$U_3 = -\frac{\alpha^2}{\pi}\delta(p_1+p_2-p_1'-p_2') \quad (1)$$
$$\times \int (\bar{u}_1' \gamma_\nu (i\hat{p}_1 - i\hat{k} + 1)^{-1} \gamma_\mu u_1)$$
$$\times (\bar{u}_2' \gamma_\mu (i\hat{p}_2' - i\hat{k} + 1)^{-1} \gamma_\nu u_2)$$
$$\times d^4k/(k^2+\lambda^2)[(k+q)^2+\lambda^2],$$

where $\hat{p} = p_\mu \gamma_\mu$, $\bar{u} = u^* \gamma_4$, $\alpha = 1/137$, and the u are the spinor amplitudes of the electrons. (We use a system of units with $\hbar = c = m = 1$.)

The four-vectors p_1, p_2, p_1', and p_2' satisfy the law of conservation of energy and momentum, $p_1 + p_2 = p_1' + p_2'$, from which there result the following equations between the scalar products:

$$p_1p_1' = p_2p_2'; \quad p_1p_2 = p_1'p_2';$$
$$p_1p_2' = p_1'p_2; \quad p_1p_2 = p_1p_1' + p_1p_2' + 1;$$
$$-p_1q = p_1'q = -p_2'q = p_2q = q^2/2.$$

Making use of Dirac's equations

$$(i\hat{p}+1)u = 0; \quad \bar{u}(i\hat{p}+1) = 0,$$

we rewrite Eq. (1):

$$U_3 + U_3' = -2\pi i\alpha^2\delta(p_1+p_2-p_1'-p_2') \quad (2)$$
$$\times \{-4(p_1p_2')(\bar{u}_1'\gamma_\mu u_1)(\bar{u}_2'\gamma_\mu u_2)\,b$$
$$+2[(\bar{u}_1'\gamma_\nu\gamma_\sigma\hat{p}_2'u_1)(\bar{u}_2'\gamma_\nu u_2)$$
$$+(\bar{u}_1'\gamma_\nu u_1)(\bar{u}_2'\hat{p}_1\gamma_\sigma\gamma_\nu u_2)]\,b_\sigma$$
$$-(\bar{u}_1'\gamma_\nu\gamma_\sigma\gamma_\mu u_1)(\bar{u}_2'\gamma_\mu\gamma_\tau\gamma_\nu u_2)\,b_{\sigma\tau}\},$$

where

$$b_{(,\sigma,\sigma\tau)} = \frac{1}{\pi^2 i} \quad (3)$$
$$\times \int \frac{(1, k_\sigma, k_\sigma k_\tau)\,d^4k}{(k^2-2p_1k)(k^2-2p_2'k)(k^2+\lambda^2)[(k+q)^2+\lambda^2]}.$$

The symbol $(1, k_\sigma, k_\sigma k_\tau)$ means that in the first case it is to be replaced by 1, in the second by k_σ, and in the third by $k_\sigma k_\tau$.

First we shall show how the scalar integral is calculated.[4] From the formula

$$\frac{1}{ab}\int_0^1 [ax + b(1-x)]^{-2}\,dx$$

and the formulas obtained from it by differentiating with respect to a and b, together with the four-dimensional integral

$$\int \frac{d^4k}{(k^2-2pk+L)^4} = \frac{\pi^2 i}{6(L-p^2)},$$

we obtain

$$b = \iiint_{000}^{111} \frac{z^2(1-x)\,dy\,dx\,dz}{[xz(1-z)q^2 + \lambda^2 - z(1-x)\lambda^2 - z^2(1-x)^2p_y^2]^2}, \quad (4)$$

where $p_y = \gamma p_1 + (1-\gamma)p_2'$. The quantity λ^2 appearing in the integral (4) is small in comparison with q^2, p_y^2, and unity. But it cannot be simply neglected, since this would give a divergent integral. Therefore we break the integral (4) up into three integrals, in which the integration with respect to x is carried out over the intervals $(0, \epsilon)$, $(\epsilon, 1-\epsilon_1)$, $(1-\epsilon_1, 1)$, with $\epsilon \ll 1$, $\epsilon_1 \ll 1$.

In the second of these integrals we can drop terms containing λ^2, and in the third those in $-z(1-x)\lambda^2$.

The first integral is again broken up into two integrals, in which the integration with respect to z is carried out over the intervals $(0, z_c)$ and $(z_c, 1)$, with $\lambda^2 \ll -z_c^2 p_y^2 \ll z_c q^2 \epsilon$ and $z_c \ll 1$. In the integration over the integral $(0, z_c)$ we drop $z^2p_y^2$, and in the integral $(z_c, 1)$, the terms containing λ^2. When the expressions obtained are combined, the quantities z_c, ϵ, and ϵ_1 cancel, and we obtain

$$b = \frac{2}{q^2} \ln \frac{q^2}{\lambda^2} M(\Phi_b); \quad M(x) = \frac{x}{\operatorname{sh} 2x}, \tag{5}$$

where Φ_b is defined by the relation

$$(p_2' - p_1)^2 = q_b^2 = 4 \operatorname{sh}^2 \Phi_b.$$

We proceed to the calculation of b_σ. This integral is a four-vector, which can depend only on the vectors p_1, p_2' and q. Since b_σ remains unchanged by the interchange $p_1 \rightleftarrows p_2'$, it has the form

$$b_\sigma = X_b (p_{1\sigma} + p_{2\sigma}') + Y_b q_\sigma, \tag{6}$$

where X_b and Y_b are scalars depending on the scalar products of the vectors p_1, p_2' and q.

Taking the scalar products of Eq. (6) by $p_{1\sigma}$ and q_σ, we obtain two equations for the determination of X_b and Y_b:

$$(-1 + p_1 p_2') X_b - {}^1/_2 q^2 Y_b = {}^1/_2 (F^b - G), \tag{7}$$
$$-q^2 X_b + q^2 Y_b = {}^1/_2 (H^b - F^b - q^2 b).$$

The integrals H^b, F^b, and G appearing in the right members differ from b by the absence from the denominator of the factors $(k+q)^2 + \lambda^2$, $k^2 + \lambda^2$, and $k^2 - 2p_2' k$, respectively. They are calculated in the same way as b:

$$H^b = F^b = -N(\Phi_b) - 2M(\Phi_b) \ln \lambda, \tag{8}$$

$$G = \frac{1}{\operatorname{sh} 2\Phi} \Big[F(e^{-2\Phi} - 1) + \Phi^2 + 2\Phi \ln (1 - e^{-2\Phi}) + \frac{\pi}{2} \Big], \tag{9}$$

where

$$N(x) = \frac{1}{\operatorname{sh} 2x} \Big[x^2 - 2x \ln (2 \operatorname{ch} x) - F(e^{-2x}) + \frac{\pi^2}{12} \Big]; \tag{10}$$

$$F(x) = \int_0^x \ln (1+y) \frac{dy}{y}. \tag{11}$$

The function $F(x)$ satisfies the relations:

$$F(1) = \frac{\pi^2}{12}; \quad F(-1) = -\frac{\pi^2}{6}; \tag{12}$$
$$F(x) + F\left(\frac{1}{x}\right) = \frac{\pi^2}{6} + \frac{1}{2} \ln^2 x;$$
$$F(x-1) + F(1/x - 1) = {}^1/_2 \ln^2 x,$$

and the quantity Φ is defined by the equation

$$(p_1' - p_1)^2 = q^2 = 4 \operatorname{sh}^2 \Phi.$$

We calculate, finally, the tensor integral $b_{\sigma\tau}$. Noting that $b_{\sigma\tau}$ can depend only on the vectors p_1, p_2' and q, and that this quantity is unchanged by the interchange $p_1 \rightleftarrows p_2'$, we find that this integral has the form

$$b_{\sigma\tau} = (p_{1\sigma} + p_{2\sigma}')(p_{1\tau} + p_{2\tau}') K_b + (p_{1\sigma} - p_{2\sigma}')(p_{1\tau} - p_{2\tau}') L_b + [(p_{1\sigma} + p_{2\sigma}') q_\tau + q_\sigma (p_{1\tau} + p_{2\tau}')] W_b + q_\sigma q_\tau Z_b + \delta_{\sigma\tau} T_b, \tag{13}$$

where K_b, L_b, W_b, Z_b, and T_b are scalars depending on the scalar products of the vectors p_1, p_2', and q.

Multiplying Eq. (13) by $p_{1\tau}$, $q_{1\tau}$ and contracting on the indices σ and τ, we obtain a system of three equations, in the right members of which there appear integrals H_σ^b, F_σ^b, G_σ differing from H^b, F^b, G by the presence of the factor k_σ in the numerator. These integrals are calculated in just the same way as b_σ. Then, equating the coefficients of the vectors $p_{1\sigma}$, $p_{2\sigma}'$, q_σ, we obtain a system of six equations for the determination of the five unknowns K_b, L_b, W_b, Z_b, T_b. The extra equation serves as a check on the calculations.

$U_2 + U_2'$ and the other matrix elements are calculated analogously. In the calculation of U_2, additional poles appear in the denominator of the integrand; these are avoided according to the Feynman rule, i.e., an infinitely small negative imaginary part is added to the squares of the four-dimensional momenta: $p^2 \to p^2 - i\epsilon$. Instead of the quantity Φ_b, which occurs in the matrix element U_3, the expression for U_2 contains the quantity $\Phi_a - \pi i/2$, which is defined by the

relation $(p_1 - p_2)^2 = q_a^2 = 4\,\mathrm{sh}^2\,\Phi_a$.

The cross section for purely elastic scattering is given by the following formula:

$$d\sigma_{\text{elas.}} = \frac{1}{2v}\frac{1}{4} SS' \Big\{ |U_1 + U_1' + \tilde{U}_1 + \tilde{U}_1'|^2 + 2\,\mathrm{Re}\sum_{i=2}^{5} (U_1 + U_1' + \tilde{U}_1 + \tilde{U}_1')^* \times (U_i + U_i + \tilde{U}_i + \tilde{U}_i' \Big\} d\Omega, \quad (14)$$

where v is the velocity of the electron in the center-of-mass system (c. m. s.), S indicates summation over the orientations of the electron spins in the initial state, S' the same for the final state, and $d\Omega$ is the element of solid angle into which the electron is scattered.

Since the quantities U_i contain δ-functions, the formula (14) contains a factor $|2\pi\delta(p_1 + p_2 - p'_1 - p'_2)|^2$, which is to be replaced, as shown in Ref. 2, by $2\pi\rho_f$, where ρ_f is the number of final states in unit range of the energy of the system, given by $\rho_f = v/16\pi^3(1-v^2)$.

We shall now show how the summation over the orientations of the electron spins is carried out. Multiplying u by the operator $\beta(-i\hat{p}+1)/2E$ (with $\beta = \gamma_4$ and E the energy of the electron in the c. m. s.) and using the equation $\beta\gamma_\lambda\beta \ldots \beta\gamma_\lambda\beta = \gamma_\lambda \ldots \gamma_\lambda$, we obtain, for example,

$$SS' (\bar{u}'_1 \gamma_\lambda u_1)^* (\bar{u}'_2 \gamma_\lambda u_2)^* (\bar{u}'_1 \gamma_\nu (\hat{p}_1 + \hat{p}'_2) \gamma_\mu u_1) (\bar{u}'_2 \gamma_\mu \hat{q} \gamma_\nu u_2)$$
$$= \frac{1}{4E^4}\,\mathrm{Sp}\{\gamma_\lambda(-i\hat{p}'_1 + 1)\gamma_\nu(\hat{p}_1 + \hat{p}'_2)\gamma_\mu(-i\hat{p}'_1 + 1)\} \times \frac{1}{4}\,\mathrm{Sp}\{\gamma_\lambda(-i\hat{p}'_2 + 1)\gamma_\mu\hat{q}\gamma_\nu(-i\hat{p}_2 + 1)\}, \quad (15)$$

$$SS' (\bar{u}'_2 \gamma_\lambda u_1)^* (\bar{u}'_1 \gamma_\lambda u_2)^* (\bar{u}_1 \gamma_\nu (\hat{p}_1 + \hat{p}'_2) \gamma_\mu u_1) (\bar{u}'_2 \gamma_\mu \hat{q} \gamma_\nu u_2)$$
$$= \frac{1}{4E^4} \cdot \frac{1}{4}\,\mathrm{Sp}\{\gamma_\lambda(-i\hat{p}'_2 + 1)\gamma_\mu\hat{q}\gamma_\nu(-i\hat{p}_2 + 1)\gamma_\lambda(-i\hat{p}'_1 + 1)\gamma_\nu(\hat{p}_1 + \hat{p}'_2)\gamma_\mu(-i\hat{p}_1 + 1)\}. \quad (16)$$

In expressions of the type of (16) we carry out the summation by the formulas:[5]

$$\gamma_\mu\gamma_{j_1}\gamma_{j_2}\ldots\gamma_{j_{2n-1}}\gamma_\mu = -2\gamma_{j_{2n-1}}\ldots\gamma_{j_2}\gamma_{j_1}, \quad (17)$$

$$\gamma_\mu\gamma_{j_1}\gamma_{j_2}\ldots\gamma_{j_{2n}}\gamma_\mu = 2\gamma_{j_{2n}}\gamma_{j_1}\gamma_{j_2}\ldots\gamma_{j_{2n-1}} + 2\gamma_{j_{2n-1}}\ldots\gamma_{j_2}\gamma_{j_1}\gamma_{j_{2n}}.$$

For the calculation of the traces of the matrices the following rule can be formulated.[2,6] To calculate $1/4\,\mathrm{Sp}(\gamma_{j1}\gamma_{j2}\gamma_{j3}\ldots)$ we draw a circle, and put in correspondence with each matrix γ_i a point i on the circumference. The points are placed on the circumference in the same order as the matrices occur in the product. We join these points in pairs by straight lines. Then each straight line joining points i and k corresponds to a factor δ_{ik}; to each way of joining the points there corresponds in the expansion of the trace a term of the form $(-1)^P\delta_{ik}\delta_{lm}\delta_{np}\ldots$, where P is the number of points of intersection of the straight lines. For example, for the calculation of $1/4\,\mathrm{Sp}(\gamma_i\gamma_k\gamma_l\gamma_m\gamma_n\gamma_p)$ one must draw diagrams, some of which are shown in Fig. 2. To these diagrams there correspond the following terms in the expansion of the trace:

$$^1/_4\,\mathrm{Sp}(\gamma_i\gamma_k\gamma_l\gamma_m\gamma_n\gamma_p) = +\delta_{im}\delta_{kl}\delta_{np} - \delta_{il}\delta_{km}\delta_{np} + \delta_{in}\delta_{km}\delta_{lp} - \delta_{im}\delta_{kn}\delta_{lp} + \ldots$$

An analogous rule exists for the calculation of the product of two traces.[6] We draw two circles side by side. On each of them we place points $i, k, \ldots$ in the same order as the matrices γ_i, γ_k in one of the products. We join by dotted lines those pairs of points, over which summations are taken [we are considering the case in which these points belong to different traces; otherwise the expression can be simplified by means of the formulas (17)]. Then we join by solid straight lines pairs of points belonging to the same trace (both those with "dummy" and those with "speaking" indices.). To the line joining points with the

indices i and k there corresponds a factor δ_{ik} (these points can belong to the same trace or to different traces). To each such diagram there corresponds a term $(-1)^P \delta_{ik}\delta_{lm}\ldots$, where $i-k$, $l-m$, ... are the pairs of points joined by the system of solid and dotted lines and P is the number of intersections of solid lines. If a given assignment of the indices to pairs $i-k$, $l-m$, ... has several diagrams corresponding to it, then the coefficient of the term $\delta_{ik}\delta_{lm}\ldots$ in the expansion of the product of traces is found by combining the coefficients corresponding to the individual diagrams.

By using this method one can, for example, show that

$$\begin{aligned}&{}^1/_4 \operatorname{Sp}(\gamma_\mu\gamma_i\gamma_\nu\gamma_k\gamma_\lambda\gamma_l)\,{}^1/_4 \operatorname{Sp}(\gamma_\mu\gamma_m\gamma_\nu\gamma_n\gamma_\lambda\gamma_p) \\ &= 6\delta_{im}\delta_{kn}\delta_{lp} + 2(\delta_{im}\delta_{kl}\delta_{np} + \delta_{kn}\delta_{il}\delta_{mp} + \delta_{lp}\delta_{ik}\delta_{mn}) \\ &\quad + 2(\delta_{im}\delta_{kp}\delta_{ln} + \delta_{kn}\delta_{ip}\delta_{lm} + \delta_{lp}\delta_{in}\delta_{km}) \\ &\quad + 2(\delta_{in}\delta_{kp}\delta_{lm} + \delta_{ip}\delta_{ln}\delta_{km}) \\ &\quad - 2(\delta_{ik}\delta_{ln}\delta_{mp} + \delta_{ik}\delta_{lm}\delta_{np} + \delta_{kl}\delta_{mn}\delta_{ip} \\ &\quad + \delta_{kl}\delta_{mp}\delta_{in} + \delta_{il}\delta_{np}\delta_{km} + \delta_{il}\delta_{mn}\delta_{kp}).\end{aligned} \tag{18}$$

Since in using this procedure one has to take into account all ways of joining the given pairs of points, we state the formula[6] determining the number N of these ways:

$$N(n, m, k) = \frac{n!}{(m+k-1)!} \times \sum_{l=0}^{(n-m)/2} \frac{(m+k+l-1)!}{(l!)^2} \frac{[(n-m-2l-1)!!]^2}{(n-m-2l)!}, \tag{19}$$

where n is the number of "dummy" indices in each of the traces, m is the number of pairs of "speaking" indices, and k is the number of pairs of "speaking" indices belonging wholly to one trace ($0! = 1$; $(-1)!! = 1$).

After calculating the traces and integrals, we obtain the following expression for the cross section for elastic scattering of electrons by electrons:[6]

$$d\sigma^{e-e}_{\text{elas.}} = \frac{1}{8}\alpha^2(1-v^2) \times \operatorname{Re}\sum_{i=1}^{5}(C_i^{(1)} - C_i^{(2)} + \tilde{C}_i^{(1)} - \tilde{C}_i^{(2)})\,d\Omega, \tag{20}$$

where

$$\begin{aligned}C_1^{(1)} &= (q_a^4 + 4q_b^4 + 8q_b^2 + 8)\,q^{-4}; \\ C_1^{(2)} &= (-q_a^4 + 4)\,q^{-2}q_b^{-2}; \\ C_2^{(2)} &= \frac{4\alpha}{\pi}\frac{\Phi_a - \frac{\pi i}{2}}{\operatorname{th} 2\Phi_a}\ln\frac{q^2}{\lambda^2}C_1^{(2)} \\ &\quad - \frac{\alpha}{\pi q_b^2}\left\{\frac{1}{q^2+4}[2G(-q^2q_a^4 \right. \\ &\quad + q_b^4 - 5q_a^4 + 6q^2 - 4q_a^2 + 24) \\ &\quad + 8q_b^2\ln q] + 2\left[N\left(\Phi_a - \frac{\pi i}{2}\right)\right. \\ &\quad + 2M\left(\Phi_a - \frac{\pi i}{2}\right)\ln q\Big](q^2 + q_a^2 + 8) \\ &\quad \left. + 4M\left(\Phi_a - \frac{\pi i}{2}\right)q_b^2\right\}; \\ C_3^{(1)} &= -\frac{4\alpha}{\pi}\frac{\Phi_b}{\operatorname{th} 2\Phi_b}\ln\frac{q^2}{\lambda^2}C_1^{(1)} \\ &\quad - \frac{\alpha}{\pi q^2}\left\{\frac{1}{q^2+4}[G(-q^2q_a^4 \right. \\ &\quad - 3q^2q_b^4 - 2q^4 - 16q_a^2q_o^2 - 48q_b^2 - 32) \\ &\quad + 2\ln q\cdot(q^2q_a^2 + 6q^2 \\ &\quad - 4q_a^2 - 8)] + [N(\Phi_b) \\ &\quad + 2M(\Phi_b)\ln q](q_b^2 + 2)(q^2 - 2q_a^2) \\ &\quad \left. - M(\Phi_b)(q_a^2q_b^2 + 6q_b^2 + 8)\right\}; \\ C_3^{(2)} &= -\frac{4\alpha}{\pi}\frac{\Phi_b}{\operatorname{th} 2\Phi_b}\ln\frac{q^2}{\lambda^2}C_1^{(2)} \\ &\quad - \frac{\alpha}{\pi q_o^2}\left\{\frac{1}{q^2+4}[G(q^2q_b^4 + q^2q_a^4 \right. \\ &\quad + 8q_b^4 + 4q^2q_a^2 + 4q^2 - 8q_a^2 - 16) \\ &\quad - 2\ln q(q^2q_a^2 + 6q^2 + 8)] \\ &\quad + [N(\Phi_b) + 2M(\Phi_b)\ln q] \\ &\quad \times(q_b^4 + q_a^2q_b^2 + 2q^2 + 2q_a^2 + 8) \\ &\quad \left. + M(\Phi_b)(q_a^2q_b^2 + 2q_a^2 - 6q^2 - 8)\right\}; \\ C_4^{(1)} &= -\frac{2\alpha}{\pi}JC_1^{(1)}; \quad C_4^{(2)} = -\frac{2\alpha}{\pi}JC_1^{(2)}; \\ C_5^{(1)} &= -\frac{\alpha}{\pi}\left[lC_1^{(1)} - \frac{4(q^2-2)}{q^2}M(\Phi)\right]; \\ C_5^{(2)} &= -\frac{\alpha}{\pi}\left[lC_1^{(2)} - \frac{2(q^2-4q_a^2-6)}{q_b^2}M(\Phi)\right]; \\ l &= 4\left[(2\Phi\operatorname{cth}2\Phi - 1)\left(\ln\frac{1}{\lambda} - 1\right)\right. \\ &\quad \left. + \frac{\Phi}{2}\operatorname{th}\Phi\right] - (4 + 2q^2)M(\Phi); \\ J &= (1 - {}^1/_3\operatorname{cth}^2\Phi)(1 - \Phi\operatorname{cth}\Phi) - {}^1/_9.\end{aligned} \tag{21}$$

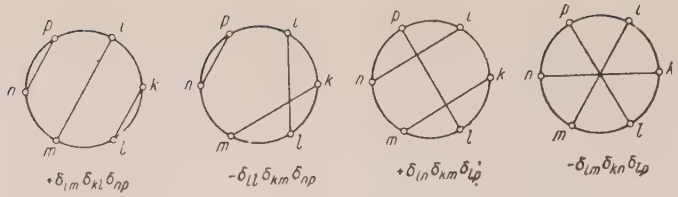

FIG. 2.

$C_2^{(1)}$ is obtained from $C_3^{(1)}$ by the interchange $q_a^2 \rightleftarrows -4-q_b^2$, $\Phi_b \rightleftarrows \Phi_a - \pi i/2$ and change of sign, and $\widetilde{C}_i^{(k)}$ is obtained from $C_i^{(k)}$ by the interchange $q \rightleftarrows q_b$, $\Phi \rightleftarrows \Phi_b$.

If in the expressions (20) we retain only the first terms $C_1^{(k)}$ and $\widetilde{C}_1^{(k)}$, then we obtain the Möller formula.[7]

2. ELASTIC SCATTERING OF ELECTRONS BY POSITRONS

The cross section for scattering of positrons by positrons, including the radiation corrections, is given by Eq. (20).

To find the cross section for scattering of electrons by positrons (or of positrons by electrons) one must put

$$p_1 = p_-; \quad p_1' = p_-'; \tag{22}$$
$$p_2 = -p_+'; \quad p_2' = -p_+;$$

where p_- is the four-vector momentum of the electron and p_+ is the four-vector momentum of the positron. Equation (20) then takes the form:

$$d\sigma_{\text{elas}}^{p-e} = \frac{1}{8}\alpha^2(1-v^2) \times \operatorname{Re}\sum_{i=1}^{5}(D_i^{(1)} - D_i^{(2)} + \widetilde{D}_i^{(1)} - \widetilde{D}_i^{(2)})\,d\Omega, \tag{23}$$

where the quantities $D_i^{(k)}$ are obtained from $C_i^{(k)}$ by the interchange $q_b^2 \rightleftarrows -4-q_a^2$, $\Phi_b \rightleftarrows \Phi_a - \pi i/2$, and the quantities $\widetilde{D}_i^{(k)}$ are obtained from $D_i^{(k)}$ by the interchange $q^2 \rightleftarrows -4-q_a^2$, $\Phi \rightleftarrows \Phi_a - \pi i/2$.

If in the expression (23) we retain only the first terms $D_1^{(k)}$ and $\widetilde{D}_1^{(k)}$, then we obtain the Bhabha formula.[8]

3. INELASTIC SCATTERING

In order to eliminate the "mass" λ of the photon, appearing in Eq. (20) in connection with the "infrared catastrophe", it is necessary, as is well known, to consider along with the elastic scattering the inelastic scattering of electrons by electrons with the emission of a photon of energy not exceeding ΔE ($\Delta E \ll 1$; $\Delta E \ll p$). This cross section is given by the following formula:

$$d\sigma_{\text{inelas}}^{e-e} = \frac{\alpha^3(1-v^2)}{32\pi^2} \times (C_1^{(1)} - C_1^{(2)} + \widetilde{C}_1^{(1)} - \widetilde{C}_1^{(2)}) \times \int_{|\mathbf{k}|\leqslant E}\left(\frac{p_{1\nu}}{p_1\cdot k} + \frac{p_{2\nu}}{p_2\cdot k} - \frac{p_{1\nu}}{p_1'\cdot k} - \frac{p_{2\nu}'}{p_2'\cdot k}\right)^2 \times \frac{d^3\mathbf{k}}{(\mathbf{k}^2+\lambda^2)^{1/2}}\,d\Omega. \tag{24}$$

We note that the cross section for inelastic scattering depends in an essential way on the reference system. In the c. m. s. Eq. (24) leads to the following result:[6]

$$d\sigma_{\text{inelas. c. m.}}^{e-e} = \frac{\alpha}{\pi}\,d\sigma_0\left\{4\ln\frac{2\Delta E}{\lambda}\left(\frac{2\Phi}{\operatorname{th}2\Phi} - \frac{2\Phi_a}{\operatorname{th}2\Phi_a} + \frac{2\Phi_b}{\operatorname{th}2\Phi_b} - 1\right) + \frac{4\Phi_a}{\operatorname{th}\Phi_a} + \frac{4}{\operatorname{sh}2\Phi_a}[H(\pi, v)\operatorname{ch}2\Phi_a - H(\vartheta, v)\operatorname{ch}2\Phi - H(\pi-\vartheta, v)\operatorname{ch}2\Phi_b] + 4[N(\Phi_a)\operatorname{ch}2\Phi_a - N(\Phi)\operatorname{ch}2\Phi - N(\Phi_b)\operatorname{ch}2\Phi_b] + 4\ln(2\operatorname{ch}\Phi_a)\left(\frac{2\Phi_a}{\operatorname{th}2\Phi_a} - \frac{2\Phi}{\operatorname{th}2\Phi} - \frac{2\Phi_b}{\operatorname{th}2\Phi_b}\right)\right\}, \tag{25}$$

where ϑ is the angle of scattering in the c. m. s., and

$$H(\vartheta, v) = \frac{1}{\sin(\vartheta/2)}\int_{\cos(\vartheta/2)}^{1}\left(\frac{\ln[(1+v\zeta)/2]}{1-v\zeta} - \frac{\ln[(1-v\zeta)/2]}{1+v\zeta}\right)\frac{d\zeta}{\sqrt{\zeta^2-\cos^2(\vartheta/2)}}.$$

In the laboratory system (l. s.) the formula is[9]

$$d\sigma^{e-e}_{\text{inelas l.s.}} = \frac{\alpha}{\pi} d\sigma_0 \Big[4 \Big(1 - \frac{2\Phi}{\text{th } 2\Phi} + \frac{2\Phi_a}{\text{th } 2\Phi_a} - \frac{2\Phi_b}{\text{th } 2\Phi_b} \Big) \ln \frac{\lambda}{2\Delta E} + 1 + \frac{2\Phi}{\text{th } 2\Phi} + \frac{2\Phi_a}{\text{th } 2\Phi_a} + \frac{2\Phi_b}{\text{th } 2\Phi_b} - \frac{2}{\text{th } 2\Phi} \int_0^{2\Phi} x \operatorname{cth} x\, dx + \frac{2}{\text{th } 2\Phi_a} \int_0^{2\Phi_a} x \operatorname{cth} x\, dx - \frac{2}{\text{th } 2\Phi_b} \int_0^{2\Phi_b} x \operatorname{cth} x\, dx - R(\Phi_a, \Phi_b; \Phi) - R(\Phi_a, \Phi; \Phi_b) + R(\Phi_b, \Phi; \Phi_a) \Big], \tag{26}$$

where

$$R(\Phi_a, \Phi_b; \Phi) = \frac{2\Phi}{\text{th } 2\Phi} \int_0^1 \mu \ln \frac{\mu + 1}{\mu - 1} dx;$$

$$\mu = A (A^2 - B^2)^{-1/2}; \quad A = \text{sh}(2\Phi x) \text{ch } 2\Phi_a + \text{sh}[2\Phi(1-x)] \text{ch } 2\Phi_b; \quad B = \text{sh } 2\Phi.$$

The cross section for inelastic scattering of electrons by positrons is obtained from Eq. (25) by the interchange $\Phi_a \rightleftarrows \Phi_b$.

4. SCATTERING IN THE EXTREME RELATIVISTIC CASE

In the limiting case

$$p \gg 1, \quad p \sin(\vartheta/2) \gg 1, \quad p \cos(\vartheta/2) \gg 1,$$

where p is the momentum of the electron in the c. m. s., the scattering cross section (elastic + inelastic) of electrons by electrons in the l. s. is given by the formula

$$d\sigma^{e-e}_{\text{l.s.}} = \frac{\alpha^2 (1 - v^2)}{4\chi^2 (1-\chi)} \Big\{ \frac{1}{2} (2 - 3\chi + 3\chi^2 - \chi^3) + \frac{\alpha}{\pi} \Big[2 (1 - 2\Phi + 2\Phi_a - 2\Phi_b) \ln \frac{1}{2\Delta E} (2 - 3\chi + 3\chi^2 - \chi^3) + \frac{\Phi}{3} (28 - 48\chi + 48\chi^2 - 17\chi^3) + \Phi_a (2 - 2\chi + \chi^2) + \Phi_b (2 - 2\chi + 3\chi^2 - \chi^3) - \Phi_a^2 (2 - \chi) - \Phi_b^2 (2 - \chi + 2\chi^2 - \chi^3) - \Phi^2 (6 - 5\chi + 5\chi^2 - 2\chi^3) + 2\Phi\Phi_a (6 - 7\chi + 6\chi^2 - 2\chi^3) - 2\Phi\Phi_b (10 - 17\chi + 16\chi^2 - 5\chi^3) + 2\Phi_a\Phi_b (2 - 3\chi + 3\chi^2 - \chi^3) - \frac{37}{18} (2 - 3\chi + 3\chi^2 - \chi^3) - \frac{\pi^2}{4} \chi (2 - \chi) \Big] \Big\} d\Omega + \text{terms obtained by the interchange } \chi \to 1 - \chi; \ \Phi \rightleftarrows \Phi_b, \tag{27}$$

where $\chi = \sin^2(\vartheta/2)$.

In the same limiting case the cross section for scattering of electrons by positrons is given by the formula:*

$$d\sigma^{e-p}_{\text{l. s.}} = \frac{\alpha^2 (1 - v^2)}{4\chi^2} \Big\{ (1 - \chi + \chi^2)^2 + \frac{\alpha}{\pi} \Big[4 (1 - 2\Phi + 2\Phi_b - 2\Phi_a) \ln \frac{1}{2\Delta E} (1 - \chi + \chi^2)^2 - \Phi_a^2 (2 - 9\chi + 19\chi^2 - 15\chi^3 + 6\chi^4) - \Phi^2 (6 - 15\chi + 19\chi^2 - 9\chi^3 + 2\chi^4) - 2\Phi_b^2 (1 - 3\chi + 4\chi^2 - 3\chi^3 + \chi^4) - 2\Phi\Phi_a (10 - 17\chi + 24\chi^2 - 17\chi^3 + 10\chi^4) + 2\Phi\Phi_b (6 - 12\chi + 13\chi^2 - 6\chi^3 + 2\chi^4) + 2\Phi_a\Phi_b (2 - 6\chi + 13\chi^2 - 12\chi^3 + 6\chi^4) + \frac{\Phi}{3} (28 - 42\chi + 51\chi^2 - 23\chi^3 + 6\chi^4) + \frac{\Phi_a}{3} (6 - 23\chi + 51\chi^2 - 42\chi^3 + 28\chi^4) + \Phi_b (2 - 5\chi + 6\chi^2 - 5\chi^3 + 2\chi^4) - \frac{37}{9} (1 - \chi + \chi^2)^2 + \frac{\pi^2}{4} \chi^2 (5 - 6\chi + 4\chi^2) \Big] \Big\} d\Omega. \tag{28}$$

In the limiting case of large energies and small

*Equations (20), (21), (27), and (28) have also been obtained in Ref. 9.

scattering angles ($p \gg 1$, $p \sin(\vartheta/2) \gtrsim 1$), the cross section for scattering of electrons in the l. s. has the form

$$d\sigma^{e-e}_{\text{l. s.}} = \frac{\alpha^2(1-v^2)}{4\sin^4(\vartheta/2)}(1-\delta_R)\,d\Omega; \tag{29}$$

$$\delta_R = \frac{\alpha}{\pi}\left[2\left(1-\frac{1}{3}\operatorname{cth}^2\Phi\right)(1-\Phi\operatorname{cth}\Phi) - \frac{2}{9}\right.$$
$$+4(2\Phi\operatorname{cth}2\Phi-1)\left(\ln\frac{1}{2\Delta E}-1\right)+4\Phi_a(2\Phi\operatorname{cth}2\Phi-1)$$
$$\left.-\left(1+\frac{4\Phi}{\operatorname{sh}4\Phi}\right)+\frac{4}{\operatorname{th}2\Phi}\int_0^{\Phi} x\operatorname{th}x\,dx+\frac{2}{\operatorname{th}2\Phi}\int_0^{2\Phi} x\operatorname{cth}x\,dx\right].$$

In the c. m. s. a simpler formula is obtained.[10]

Equation (29) also gives the cross section for scattering of electrons by positrons in the limiting case of large energies and small scattering angles.

In the limiting case

$$\ln 2p \gg 1; \quad \ln\left(2p\sin\frac{\vartheta}{2}\right)\gg 1; \quad \ln\left(2p\cos\frac{\vartheta}{2}\right)\gg 1 \tag{30}$$

the cross section for scattering of electrons by electrons and positrons is of the form

$$d\sigma_{\text{l. s.}} = d\sigma_0(1-\delta_R), \tag{31}$$

where $d\sigma_0$ is the cross section for the main effect, and $\delta_R = \delta_1+\delta_2+\delta_3+\delta_4+\delta_5+\delta_{\text{inelas.}}$ (δ_2 corresponds to diagram 2 in Fig. 1, δ_3 to diagram 3, ... , and $\delta_{\text{inelas.}}$ to diagrams 6 and 7):

$$\delta_2 = -\frac{4\alpha}{\pi}\left(2\Phi_a\ln\frac{1}{\lambda}+\Phi_a^2\right);$$

$$\delta_3 = \frac{4\alpha}{\pi}\left(2\Phi_a\ln\frac{1}{\lambda}+\Phi_a^2\right);$$

$$\delta_4 = -\frac{4\alpha}{\pi}\frac{\Phi_a}{3}; \quad \delta_5 = \frac{4\alpha}{\pi}\left(2\Phi_a\ln\frac{1}{\lambda}+\Phi_a^2\right);$$

$$\delta_{\text{inelas}} = \frac{4\alpha}{\pi}\left(2\Phi_a\ln\frac{\lambda}{2\Delta E}+\frac{5}{2}\Phi_a^2\right); \quad \Phi_a = \ln 2p,$$

so that

$$\delta_R = \frac{\alpha}{\pi}\left(8\ln 2p\ln\frac{1}{2\Delta E}+14\ln^2 2p\right). \tag{32}$$

In conclusion, the writer expresses his gratitude to Prof. A. I. Akhiezer for much aid in performing the present research.

[1] F. J. Dyson, Phys. Rev. 75, 486, 1736, (1949).

[2] A. I. Akhiezer and V. B. Berestetskii, *Quantum Electrodynamics*, Moscow, 1953.

[3] R. P. Feynman, Phys. Rev. 76, 769 (1949).

[4] L. M. Brown and R. P. Feynman, Phys. Rev. 85, 231 (1952).

[5] E. R. Caianello and S. Fubini, Nuovo Cimento 9, 1218 (1952).

[6] R. V. Polovin, Dissertation, Kharkov, 1953.

[7] C. Möller, Ann. der Phys. 14, 531 (1932).

[8] H. Bhabha, Proc. Roy. Soc. (London) 154A, 195 (1936).

[9] M. L. G. Redhead, Proc. Roy. Soc. (London) 220A, 219 (1953).

[10] A. I. Akhiezer and R. V. Polovin, Dokl. Akad. Nauk SSSR 90, 55 (1953).

Translated by W. H. Furry
88

On the Possibility of Introducing an Effective Dielectric Constant at High Frequencies

E. A. KANER AND M. I. KAGANOV
Physico-Technical Institute, Academy of Sciences, Ukrainian SSR

(Submitted to JETP editor June 6, 1955)
J. Exptl. Theoret. Phys. (U.S.S.R.) 31, 459-461 (September, 1956)

It is shown that it is possible to introduce an effective dielectric constant $\epsilon_{eff} = (4\pi/cZ)^2$ in the anomalous skin-effect range.

1. AS is well known[1,2], the introduction of an effective dielectric constant $\epsilon_{eff} = (4\pi/cZ)^2$ (where $Z = R + iX$ is the surface impedance of the metal) is based on the fact that Z is practically independent of the polarization of the incident wave and of the angle of incidence φ. According to Ginzburg, this is so if

$$|\varepsilon'| \gg 1, \quad \varepsilon' = \varepsilon(\omega) - 4\pi i\sigma/\omega \ ; \qquad (1)$$

a rigorous proof has been given for frequencies and temperatures at which the normal skin effect occurs*.

Condition (1) is equivalent to the requirement that

$$|\delta| \ll \lambda \ (\delta = c/\omega\sqrt{\varepsilon'}, \quad \lambda = c/\omega),$$

i.e., that the depth of penetration of the electromagnetic wave into the metal be much smaller than the wavelength in vacuum. The latter condition is satisfied even in the anomalous skin-effect range; this fact suggests that in this range, as well as under normal skin effect, the surface impedance may be independent of the polarization and of the angle of incidence. The present communication is devoted to a rigorous proof of this proposition* .

2. By definition,

$$Z_s = (4\pi/c)\,E_x(0)/H_y(0);$$

$$Z_p = -(4\pi/c)\,E_y(0)\,H_x(0).$$

The index s corresponds to polarization of the electric field in the plane of the metal surface, the index p to polarization in the plane of incidence. We consider oblique incidence (at angle φ) of an electromagnetic wave of frequency ω upon a half-space ($z > 0$) occupied by a metal. On the usual assumptions of the theory of the anomalous skin effect[3], we find the following expressions for the surface impedance:

1) In the case of specular reflection of electrons from the metal-vacuum boundary:

$$Z_s = i\,\frac{8\delta}{c\lambda}\int_0^\infty \frac{dt}{t^2 + iK_1\,(tl/\delta) - (\delta/\lambda)^2\cos^2\varphi}; \qquad (2)$$

$$Z_p = i\,\frac{8\delta}{c\lambda}\int_0^\infty \frac{1 - \sin^2\varphi\,\dfrac{1 - i\gamma^2\,(\lambda/\delta)^2\,t^2K_2\,(tl/\delta)}{1 - i\,(\lambda/\delta)^2\,K_2\,(tl/\delta)\,(1+\gamma^2t^2)}}{t^2 + iK_1(tl/\delta) - (\delta/\lambda)^2\cos^2\varphi + i\sin^2\varphi\,\dfrac{K_3\,(tl/\delta)}{1 - i\,(\lambda/\delta)^2\,K_2\,(tl/\delta)\,(1+\gamma^2t^2)}}\,dt.$$

Here

$$\delta = \frac{c}{\sqrt{2\pi\sigma\omega}}; \quad \lambda = \frac{c}{\omega}; \quad \sigma = \frac{\sigma_0}{1 + i\omega\tau};$$

$$l = \frac{l_0}{1 + i\omega\tau}; \quad \gamma = \frac{l}{\lambda\sqrt{6\omega\tau}},$$

σ_0 is the static conductivity of the metal, $l_0 = v_0\tau$ is the length of the free path, v_0 is the limiting Fermi velocity and τ is the relaxation time of the conduction electrons.

$$K_1(w) = 3w^{-3}\,[(1 + w^2)\,\mathrm{arctg}\,w - w], \quad K_1(0) = 3;$$
$$K_2(w) = 6w^{-3}\,[w - \mathrm{arctg}\,w], \quad K_2(0) = 2;$$
$$K_3(w) = K_2(w) - K_1(w);$$

for $w \gg 1$, $K_1(w) \approx \pi/6w$ and $K_2(w) \approx 6/w^2$.

2) With diffuse scattering of the electrons from the metal surface, we have:

* $\epsilon(\omega)$ is the dielectric constant of the metal, σ is its conductivity, and ω is the angular frequency of the electromagnetic wave.

* The Proof given in Ref. 1 (Sec. 2) seems to us not quite convincing, since it assumes in advance the existence of ϵ'.

$$Z_s = i\frac{4\pi}{c}\frac{\delta}{\lambda}\left(\alpha + 1 + \sum_{j=1}^{n} s_j - n\right)^{-1}, \quad (3) \qquad \alpha = \frac{1}{\pi} \quad (4)$$

$$Z_p = i\frac{4\pi}{c}\frac{\delta}{\lambda}\left(\beta + 1 + \sum_{j=1}^{m} p_j - m\right)^{-1}; \qquad \times \int_0^\infty \ln\left\{\frac{(t^2+1)^{n-1}\,(t^2 + iK_1(tl/\delta) - (\delta/\lambda)^2\cos^2\varphi}{(t^2+s_1^2)(t^2+s_2^2)\ldots(t^2+s_n^2)}\right\} dt;$$

$$\beta = \frac{1}{\pi}\int_0^\infty dt \times \ln\left\{\frac{(t^2+1)^{m-1}\left[t^2 + iK_1(tl/\delta) - (\delta/\lambda)^2\cos^2\varphi + i\sin^2\varphi\,\frac{K_3(tl/\delta)}{1 - i(\lambda/\delta)^2 K_2(tl/\delta)(1+\gamma^2t^2)}\right]}{(t^2+p_1^2)(t^2+p_2^2)\ldots(t^2+p_m^2)}\right\};$$

s_j ($j = 1, 2, \ldots, n$) are the roots of the characteristic equation

$$t^2 + iK_1(tl/\delta) - (\delta/\lambda)^2\cos^2\varphi = 0,$$

in the plane of the complex variable t. p_j ($j = 1, 2, \ldots, n$) are the roots of the equation

$$t^2 + iK_1(tl/\delta) - (\delta/\lambda)^2\cos^2\varphi + i\sin^2\varphi\,\frac{K_3(tl/\delta)}{1 - i(\lambda/\delta)^2 K_2(tl/\delta)(1+\gamma^2t^2)} = 0$$

in the same plane. The other symbols are as before.

In the derivation of Eqs. (2)-(4), the collision integral was written in the form

$$(\partial f/\partial t)_{\text{col}} = (f - \bar{f})/\tau.$$

The bar over f means an average over angles in momentum space. With oblique incidence, $\overline{f_1} \neq 0$ (f_1 is the nonequilibrium contribution to the Fermi distribution function), because of the presence of a z component of the electromagnetic field. Calculation of the term $\overline{f_1}/\tau$ leads to the appearance, in the right member of the kinetic equation, of a term $(v_0^2/12\pi\sigma_0)\,\text{div}\,\mathbf{E}$ (because $\overline{f_1}$ is proportional to the charge density $\rho = (1/4\pi)\,\text{div}\,\mathbf{E}$). For good metals, this term is negligible in comparison with $\mathbf{E}\cdot\mathbf{v}_0$, up to frequencies in the infrared region of the spectrum.

It is evident from Eqs. (2)-(4) that in the general case ($\varphi \neq 0$), Z_s differs from Z_p and depends on three parameters of the dimensions of a length: δ, the skin-depth of penetration of the wave into the metal; l, the length of the free path of the electrons; and λ, the length of the wave in vacuum. We will determine how important this dependence is in various cases.

At all frequencies up to $\omega \lesssim 10^{16}$ sec^{-1}, and at any temperatures, the wavelength λ is large in comparison with the skin depth δ and the path length l. In fact,

$$\left|\frac{l}{\lambda}\right| = \frac{v_0}{c}\,\frac{\omega\tau}{(1+\omega^2\tau^2)^{1/2}} \ll 1;$$

$$\left|\frac{\delta}{\lambda}\right| = \left(\frac{\omega}{2\pi\sigma_0}\right)^{1/2}(1+\omega^2\tau^2)^{1/4} \ll 1,$$

since even for $\omega\tau \gg 1$

$$|\,\delta/\lambda\,| \approx \omega/\sqrt{2\pi ne^2/m} \sim \omega\cdot 10^{-16}.$$

It is therefore permissible, in the integrands in (2) and (4), to go to the limit $\lambda \to \infty$; then we get directly $Z_p = Z_s$. Under these conditions, the surface impedance is independent of the angle of incidence φ and essentially agrees with the expression obtained in Ref. 3 [Eq. (21)]. This is correct to the first nonvanishing term in $1/\lambda$, for arbitrary ratio between l and δ.

The same argument (cf. Sec. 1) proves the possibility of introducing an effective dielectric constant in all ranges of frequency and temperature.

3. We will calculate a correction to the surface impedance, depending on the angle of incidence. In the limiting case of normal skin effect, when

$$|\,l/\delta\,| = (v_0/c)(2\pi\sigma_0/\omega)^{1/2}\omega\tau(1+\omega^2\tau^2)^{-3/4} \ll 1$$

(low frequencies, high temperatures), the largest small parameter --- in terms of which it is convenient to expand --- is δ/λ. Then l/δ may be

set equal to zero everywhere. The result, as was to be expected, is that we arrive at the known expression for the surface impedance under normal skin effect [cf., for example, Eq. (2.2) in Ref. 1].

In the opposite limiting case $|l/\delta| \gg 1$, which is realized at high frequencies ($10^6 \leq \omega \leq 10^{11}$) and low temperatures (anomalous skin effect), the expansion parameter is l/λ. We approximate $K_j(tl/\delta)$ asymptotically for large values of the argument and expand expressions (2) and (4) in powers of l/λ. After some calculations we find:

Specular reflection of electrons from the surface:

$$Z_p(\varphi) = Z_p(0)\left\{1 - \sin^2\varphi\,\frac{9\pi^{1/3}}{16}\left(1 + \frac{i}{\sqrt{3}}\right)\beta p^{-1/3}\right\}; \tag{5}$$

$$Z_p(0) = Z_s(0) = {}^8/_9\,(\sqrt{3}\,\pi\omega^2 l_0/c^4\sigma_0)^{1/3}\,(1 + i\sqrt{3});$$

Diffuse reflection:

$$Z_p(\varphi) = Z_p(0)\left\{1 - \sin^2\varphi\,\frac{\pi^{2/3}}{32}\,\frac{\beta^2 p^{-2/3}}{1 + p^2q^2}\right. \tag{6}$$

$$\times\left[5pq + \frac{11}{\sqrt{3}} + \frac{2}{\pi}\left(\frac{pq}{\sqrt{3}} + 1\right)\ln a\right.$$

$$\left.\left. + i\left(\frac{11pq}{\sqrt{3}} - 5 + \frac{2}{\pi}\left(\frac{pq}{\sqrt{3}} - 1\right)\ln a\right)\right]\right\};$$

$$Z_p(0) = Z_s(0) = (\sqrt{3}\,\pi\omega^2 l_0/c^4\sigma_0)^{1/3}(1 + i\sqrt{3}),$$

$$a = 8p/\pi\sqrt{6}\beta^3.$$

Here we have used the notation of Ref. 1:

$$\beta = v_0/c;\ p = \sqrt{{}^3/_2}\ (l_0/\delta_0)\,(\omega\tau)^{-3/2}$$

$$= (3\pi/\omega)\,(v_0/c)\,(ne^2/3\pi m)^{1/2};$$

$$q = \sqrt{{}^2/_3}\ (\delta_0/l_0)\ (\omega\tau)^{1/2}$$

$$= (2c/\sqrt{3}\,l_0)\,(m/4\pi ne^2)^{1/2};\ pq = (\omega\tau)^{-1}.$$

The coefficients of $\sin^2\varphi$ in Eqs. (5) and (6) are of order 10^{-3} to 10^{-5} for representative values of the quantities occurring in them: $\beta \sim 10^{-2}$, $\omega \sim 10^{11}$ sec^{-1}, $l_0 \sim 10^{-3}$ cm., $\delta_0 \sim 10^{-5}$ cm.

In closing, the authors express their thanks to V. L. Ginzburg, I. M. Lifshitz and M. Ia. Azbeliu for valuable discussions.

[1] V. L. Ginzburg and G. P. Motulevich, Usp. fiz. nauk 55, 469 (1955).

[2] V. L. Ginzburg, Dokl. Akad. Nauk SSSR 97, 999 (1954).

[3] G.E.H. Reuter and E. H. Sondheimer, Proc. Roy. Soc. (London) A195, 336 (1948).

Translated by W. F. Brown
89

On Polarization Effects in the Radiation of an Accelerated Electron

A. A. SOKOLOV AND I. M. TERNOV
Moscow State University

(Submitted to JETP editor June 18, 1955)
J. Exptl. Theoret. Phys. (U.S.S.R.) **31**, 473-478 (September, 1956)

The polarization effects in the radiation of an accelerated electron are investigated by quantum methods, but in classical approximation. The formulas obtained describe both the linear and circular polarization.

1. AMPLITUDES OF THE LINEAR AND CIRCULAR POLARIZATIONS OF THE PHOTON FIELD

IN considering the spontaneous emission of photons, we must choose the commutation relations for the amplitudes of the vector potential in the form

$$a'^{+}_{s'} a_s = 0, \quad a_s a'^{+}_{s'} = (\delta_{ss'} - \varkappa_s \varkappa_{s'}/\varkappa^2)\,\delta_{\varkappa,\varkappa'}. \tag{1}$$

For the determination of the polarization properties of the radiation it is necessary, moreover, to resolve the vector potential amplitude **a** into components such that each will characterize a definite state of polarization. In the study of the linear polarization one must resolve the amplitude of the vector potential **a** into two mutually perpendicular components (cf, e.g., Ref. 1):

$$\mathbf{a} = \beta_2 q_2 + \beta_3 q_3 = \mathbf{a}_2 + \mathbf{a}_3, \tag{2}$$

$$\beta_2 = [\mathbf{nj}]/\sqrt{1-(\mathbf{nj})^2}, \tag{3}$$

$$\beta_3 = (\mathbf{n}(\mathbf{nj}) - \mathbf{j})/\sqrt{1-(\mathbf{nj})^2},$$

$$q_s q^{+}_{s'} = \delta_{ss'}, \quad s, s' = 2, 3. \tag{4}$$

The vector **j** must be fixed in some specified direction, for which one can take, for example, that of the magnetic field vector **H**.

In the study of the circular polarization one must resolve the vector potential into two components in a different way:

$$\mathbf{a} = \gamma_1 q_1 + \gamma_{-1} q_{-1} = \mathbf{a}_1 + \mathbf{a}_{-1}, \tag{5}$$

where the vectors $\vec{\gamma}$ are related to the vectors $\vec{\beta}$ by

$$\gamma_\lambda = 2^{-1/2}(\beta_2 + i\lambda\beta_3), \tag{6}$$

and $\lambda, \lambda' = +1, -1$, $q_\lambda q^{+}_{\lambda'} = \delta_{\lambda\lambda'}$. For $\lambda = 1$ we find the intensity of the radiation having left-circular polarization, and for $\lambda = -1$ that with right-circular polarization.

We write the expression for the intensity of the radiation in the form:

$$W_i = \sum_\nu \int_0^\pi d\theta \sin\theta\, W_i(\nu, \theta), \tag{7}$$

with the spectral and angular distribution of radiative intensity

$$W_i(\nu, \theta) = ce^2 S_i. \tag{8}$$

The symbol i will denote the state of polarization ($i = 2, 3, 1, -1$), and θ is the angle that the wave vector $\varkappa$ makes with the z axis. The quantity

$$S = (\bar{\alpha}\mathbf{a})(\bar{\alpha}^{+}\mathbf{a}^{+}) \tag{9}$$

is related to the amplitudes of the photon field and the matrix element

$$\bar{\alpha} = \int \psi_n^{+} e^{-i\varkappa\mathbf{r}} \alpha \psi_n d^3x,$$

describing the transition of the electron from the quantum state n to the state $n' = n - \nu$. In the study of the linear polarization we shall have to determine two expressions for S:

$$S_2 = (\bar{\alpha}\mathbf{a}_2)(\bar{\alpha}^{+}\mathbf{a}_2^{+}) = \bar{\alpha}_x\bar{\alpha}_x^{+}(1 - \varkappa_x^2/(\varkappa_x^2 + \varkappa_y^2)) \tag{10}$$

$$+ \bar{\alpha}_y\bar{\alpha}_y^{+}(1 - \varkappa_y^2/(\varkappa_x^2 + \varkappa_y^2))$$

$$- (\bar{\alpha}_x\bar{\alpha}_y^{+} + \bar{\alpha}_y\bar{\alpha}_x^{+})\varkappa_x\varkappa_y/(\varkappa_x^2 + \varkappa_y^2),$$

$$S_3 = (\bar{\alpha}\mathbf{a}_3)(\bar{\alpha}^+\mathbf{a}_3^+) = \bar{\alpha}_z\bar{\alpha}_z^+\left(1-\frac{\varkappa_z^2}{\varkappa_x^2+\varkappa_y^2}\right) \quad (11)$$

$$-(\bar{\alpha}\boldsymbol{\varkappa})(\bar{\alpha}^+\boldsymbol{\varkappa})\left(\frac{1}{\varkappa^2}-\frac{1}{\varkappa_x^2+\varkappa_y^2}\right)$$

$$-(\bar{\alpha}_x\bar{\alpha}_z^+ + \bar{\alpha}_z\bar{\alpha}_x^+)\frac{\varkappa_x\varkappa_z}{\varkappa_x^2+\varkappa_y^2}$$

$$-(\bar{\alpha}_y\bar{\alpha}_z^+ + \bar{\alpha}_z\bar{\alpha}_y^+)\frac{\varkappa_z\varkappa_y}{\varkappa_x^2+\varkappa_y^2}.$$

Equation (10) describes the photons with polarization vector (i.e., the electric field vector) in the plane of the orbit (σ component), and Eq. (11) is for those with polarization vector perpendicular to the plane of the orbit (π component). Both formulas are written with the convention that the vector j is directed along the z axis, i.e., along H.

In the study of the circular polarization we have for the quantity S the two values

$$S_{\pm1} = (\bar{\alpha}\mathbf{a}_{\pm1})(\bar{\alpha}^+\mathbf{a}_{\pm1}^+) \quad (12)$$

$$= {}^1/_2(\bar{\alpha}\bar{\alpha}^+) - {}^1/_2(\bar{\alpha}\mathbf{n})(\bar{\alpha}^+\mathbf{n}) \pm (i/2)(\mathbf{n}[\bar{\alpha}\bar{\alpha}^+]),$$

with the quantities $S_{\pm1}$ not depending on the direction of the vector j. As is well known, in the classical case, the polarization is characterized by the ratio between the squares of the amplitudes of two mutually perpendicular oscillations, and also the phase difference δ between these oscillations, which for an unpolarized beam takes all possible values. In our case we shall set the squares of the amplitudes of the oscillations proportional to W_2 and W_3, and the phase will be given by

$$\sin\delta = (W_{-1} - W_1)/2\sqrt{W_2W_3}.$$

It is obvious that the total intensity of the radiation will be equal to the sum of the appropriate components

$$W = W_2 + W_3 = W_{-1} + W_1. \quad (13)$$

Thus, in order to give a complete specification of the polarization properties of the radiation, not knowing the phases, we must calculate not only the intensities of the linear polarizations (W_2 and W_3), but also those of the circular polarizations (W_{-1} and W_1).

For unpolarized radiation we have

$$W_2 = W_3 = W_{-1} = W_1 = \tfrac{1}{2}W. \quad (14)$$

In the case of linear polarization

$$W_2 = W, \quad W_3 = 0. \quad (15)$$

If the radiation has circular polarization, then

$$W_{-1} = W, \quad W_1 = 0. \quad (16)$$

The simultaneous presence of partial linear and partial circular polarization

$$W_2 \neq W_3, \quad W_{-1} \neq W_1 \quad (17)$$

corresponds to elliptically polarized radiation, since $\delta \neq 0$.

2. RADIATION OF THE ACCELERATED ELECTRON WITH INCLUSION OF POLARIZATION EFFECTS

As has been shown (cf. Refs. 2 and 3), when an electron moves in a homogeneous magnetic field the frequency of the radiation is given in extreme relativistic approximation by

$$\omega = c\varkappa = (E_n - E_{n'})/\hbar = \nu c/R, \quad (18)$$

where R is the radius of the orbit and

$$E_n = \sqrt{2eHc\hbar + m^2c^4} \quad (19)$$

is the energy of the electron. When one goes over to the classical approximation ($\hbar \to 0$), which involves the use of the asymptotic formula connecting generalized Laguerre polynomials with Bessel functions (cf. Ref. 4)

$$\lim_{n\to\infty,\ \nu,\ z\neq\infty} I_{n,\,n-\nu}(z^2/4n) = J_\nu(z), \quad (20)$$

the matrix elements take the form:

$$|\bar{\alpha}_x|^2 = \beta^2 J_\nu'^2(\nu\beta\sin\theta), \quad (21)$$

$$|\bar{\alpha}_y|^2 = \sin^{-2}\theta J_\nu^2(\nu\beta\sin\theta);$$

$$\bar{\alpha}_x\alpha_y^+ = -\bar{\alpha}_y\bar{\alpha}_x^+$$

$$= (i\beta/\sin\theta)J_\nu(\nu\beta\sin\theta)J_\nu'(\nu\beta\sin\theta);$$

$$|\bar{\alpha}_z|^2 = \bar{\alpha}_x\bar{\alpha}_z^+ = \bar{\alpha}_z\bar{\alpha}_x^+ = \bar{\alpha}_y\bar{\alpha}_z^+ = \bar{\alpha}_z\bar{\alpha}_y^+ = 0.$$

Then we get a formula for the radiation density that indicates not only the spectral and angular distribution but also the polarization:

$$W_i(\nu, \theta) = (e^2\beta^2 c / 2\pi R^2)\, \nu^2 \{\beta\lambda_2 J'_\nu(\nu\beta \sin\theta) \qquad (22)$$

$$- \lambda_3 \operatorname{ctg}\theta J_\nu(\nu\beta \sin\theta)\}^2.$$

In calculating the intensities of polarized radiation we must set the constants λ_2 and λ_3 equal to the following values: a) for the linearly polarized beam with polarization vector lying in the plane of the orbit ($i = 2$, σ component)

$$\lambda_2 = 1, \quad \lambda_3 = 0, \qquad (23)$$

b) for the linearly polarized beam with polarization vector perpendicular to the plane of the orbit ($i = 3$, π component)

$$\lambda_2 = 0, \quad \lambda_3 = \pm 1. \qquad (24)$$

As is well known, in the extreme relativistic case the direction of the vector $\varkappa$ almost coincides with the direction of motion of the electron (i.e., the vector $\varkappa$ is directed along the tangent to the circle). In this case the polarization vector for $\lambda_2 = 1$, $\lambda_3 = 0$ is directed along the radius toward the center, and for $\lambda_2 = 0$, $\lambda_3 = 1$ it is directed almost along the z axis (Fig. 1).

In calculating the intensity of circularly polarized radiation we must set

$$\lambda_2 = \pm\lambda_3 = 2^{-1/2}. \qquad (25)$$

From Eq. (22) we see that for the νth harmonic the light propagated along some arbitrary direction θ will as a rule be elliptically polarized.

The ratio of the squared amplitudes and the value of the phase that characterize this elliptical polarization are

$$\frac{W_3(\nu, \theta)}{W_2(\nu, \theta)} = \frac{\operatorname{ctg}^2\theta J_\nu^2(\nu\beta \sin\theta)}{\beta^2 J'^2_\nu(\nu\beta \sin\theta)}; \qquad (26)$$

$$\delta = \arcsin \frac{\cos\theta}{|\cos\theta|} = \pm\frac{\pi}{2}.$$

From the latter equation it is seen that for $\theta = \pi/2$ (i.e., in the plane of the motion of the electron) the radiation becomes linearly polarized, since $W_3 = 0$. For $0 < \theta < \pi/2$, i.e., in a direction making an acute angle with the magnetic field, the light emitted is elliptically polarized with right-handed rotation, and for $\pi/2 < \theta < \pi$, with left-handed rotation. With increase of $|\cos\theta|$ the elliptical polarization begins to go over into circular. In particular, for the nonrelativistic case ($\beta \ll 1$), when almost the whole intensity is in the fundamental mode ($\nu = 1$), we have

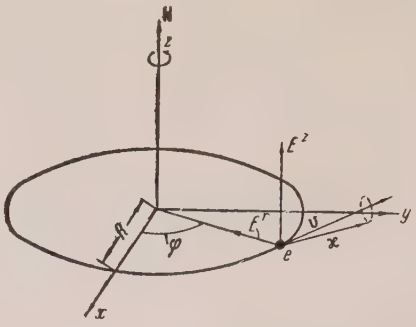

FIG. 1

$$J_1(\beta \sin\theta) \approx {}^1/_2 \beta \sin\theta, \qquad (27)$$
$$J'_1(\beta \sin\theta) \approx {}^1/_2.$$

Then the ratio in Eq. (26) becomes

$$W_3(\theta) / W_2(\theta) = \cos^2\theta. \qquad (28)$$

From this one sees that the beam in the direction of the magnetic field ($\theta = 0$) must be right-circularly polarized, and that directed against the field ($\theta = \pi$) is left-circular. This result for the nonrelativistic case is well known and is used in the analysis of the Zeeman effect.

To study the extreme relativistic case $1 - \beta^2 \ll 1$ it is necessary to approximate the Bessel functions by the formulas (cf. Ref. 2):

$$J'_\nu(\nu\beta \sin\theta) = \frac{\varepsilon}{\pi\sqrt{3}} K_{2/3}\left(\frac{\nu}{3}\varepsilon^{3/2}\right), \qquad (29)$$

$$J_\nu(\nu\beta \sin\theta) = \frac{\sqrt{\varepsilon}}{\pi\sqrt{3}} K_{1/3}\left(\frac{\nu}{3}\varepsilon^{3/2}\right),$$

where $\epsilon = 1 - \beta^2 \sin^2\theta$. Then the intensity of the polarized radiation [cf. Eq. (22)] will depend on the harmonic number ν and on the angle θ in the following way

$$W_i(\nu, \theta) = (e^2\beta c / 2\pi R^2)(\nu^2 / 3\pi^2) \tag{30}$$

$$\times \left[\lambda_2 \varepsilon K_{2/3}\left(\frac{\nu}{3}\varepsilon^{3/2}\right) - \cos\theta \lambda_3 \sqrt{\varepsilon} K_{1/3}\left(\frac{\nu}{3}\varepsilon^{3/2}\right)\right]^2.$$

To find the dependence of the degree of polarization on the angle θ alone, we sum the expression (30) over the harmonics ν. Since in the extreme relativistic case the maximum of the intensity lies in the high frequency region, we can replace the summation over ν by an integration. Then, using the integrals

$$\int_0^\infty \nu^2 K_{2/3}^2\left(\frac{\nu}{3}\varepsilon^{3/2}\right) d\nu = \frac{21}{16}\pi^2 \varepsilon^{-1/2}; \tag{31}$$

$$\int_0^\infty \nu^2 K_{1/3}^2\left(\frac{\nu}{3}\varepsilon^{3/2}\right) d\nu = \frac{15}{16}\pi^2 \varepsilon^{-1/2};$$

$$\int_0^\infty \nu^2 K_{1/3}\left(\frac{\nu}{3}\varepsilon^{3/2}\right) K_{2/3}\left(\frac{\nu}{3}\varepsilon^{3/2}\right) d\nu = \frac{6\pi}{\sqrt{3}}\varepsilon^{-1/2},$$

we find that

$$W_i(\nu, \theta)\sin\theta\, d\theta \tag{32}$$

$$= \sin\theta\, d\theta \int_0^\infty W_i(\nu, \theta)\, d\nu = W f_i(\xi)\, d\xi,$$

where $\xi = \cos\theta / \sqrt{1-\beta^2}$ and W is the total energy radiated per unit time,

$$W = {}^2/_3 (e^2 c / R^2)(E / mc^2)^4. \tag{33}$$

For the function $f_i(\xi)$ we have the following expression:

$$f_i(\xi) = \frac{3}{2}\left\{\frac{7}{16}\lambda_2^2(1+\xi^2)^{-5/2}\right. \tag{34}$$

$$\left. + \frac{5}{16}\lambda_3^2\xi^2(1+\xi^2)^{-7/2} - \frac{4}{\pi\sqrt{3}}\lambda_2\lambda_3\xi(1+\xi^2)^{-3}\right\}.$$

Curves of the dependence of f_i on ξ (i.e., on the angle θ) for the linearly polarized components are given in Fig. 2. The curves f_2 and f_3 characterize the radiated intensity of the linearly polarized light. The curves f_1 and f_{-1} of Fig. 3 characterize the intensity of the circularly polarized radiation, namely, the left-circular ($\lambda_2 = \lambda_3 = 1/\sqrt{2}$) and the right-circular ($\lambda_2 = -\lambda_3 = 1/\sqrt{2}$), respectively.

Finally, the curves f_0 (cf. Figs. 2 and 3) correspond to the total intensity of the radiation, equal to the sum of the linearly polarized intensities (Fig. 2) or of the circularly polarized intensities (Fig. 3). These curves are identical in the two diagrams.

From the curves given it is seen that in the plane of the electron's motion ($\theta = \pi/2$) the light emitted must be linearly polarized, with its polarization vector directed along the axis of r. For $\theta < \pi/2$ the radiation has predominantly right-circular polarization, and for $\theta > \pi/2$, left-circular.

Integrating Eq. (30) with respect to the angle θ, we find the polarization properties of the radiation as they depend on the harmonic order ν. Making use of the integrals

$$\int_0^\pi \varepsilon^2 K_{2/3}^2\left(\frac{\nu}{3}\varepsilon^{3/2}\right)\sin\theta\, d\theta \tag{35}$$

$$\approx \frac{\pi\varepsilon_0}{\sqrt{3}\nu}\left\{\int_{2/3\nu\varepsilon_0^{3/2}}^\infty \frac{K_{2/3}(x)}{x}dx + 3K_{2/3}\left(\frac{2}{3}\nu\varepsilon_0^{3/2}\right)\right\};$$

$$\int_0^\pi \varepsilon\cos^2\theta K_{1/3}^2\left(\frac{\nu}{3}\varepsilon^{3/2}\right)\sin\theta\, d\theta$$

$$\approx \frac{\pi\varepsilon_0}{\sqrt{3}\nu}\int_{2/3\nu\varepsilon_0^{3/2}}^\infty \frac{K_{2/3}(x)}{x}dx;$$

$$\varepsilon_0 = 1 - \beta^2 = (mc^2/E)^2$$

and introducing the variable $y = (2\nu/3)(mc^2/E)^3$, we obtain

$$W_i(\nu)\, d\nu = \int_0^\pi W_i(\nu, \theta)\sin\theta\, d\theta = W\varphi_i(y)\, dy, \tag{36}$$

where

$$\varphi_i(y) = \frac{9\sqrt{3}}{16\pi} y\left\{(\lambda_2^2 + \lambda_3^2)\right. \tag{37}$$

$$\left. \times \int_y^\infty K_{5/3}(x)\, dx + (\lambda_2^2 - \lambda_3^2) K_{2/3}(y)\right\}.$$

Summing Eq. (37) over the states of polarization, we obtain for the spectral intensity of the radiation the formula found in Ref. 5 (cf. also Ref. 6). From this it is seen that on integration over the angles the circular polarization disappears completely, since the intensities for the two cases, right-circular polarization ($\lambda_2 = \lambda_3 = 1/\sqrt{2}$) and left-circular polarization ($\lambda_2 = -\lambda_3 = 1/\sqrt{2}$), become

equal.

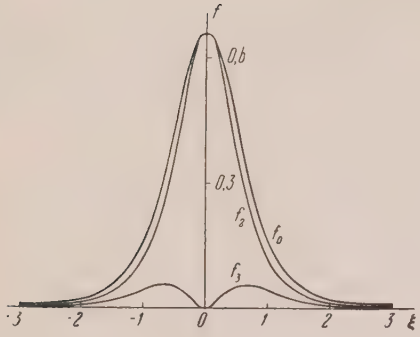

FIG. 2

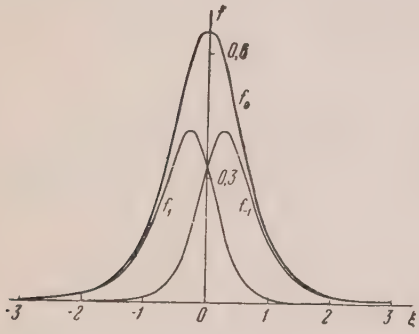

FIG. 3

The radiation intensities of the linear polarizations of the light will be different. Curves of the dependence of φ on γ (i.e., on the harmonic order ν) are shown in Fig. 4. It is seen from the curves that the bulk of the intensity is in the radiation corresponding to the σ component (cf. the curve of φ_2 for $\lambda_2 = 1$, $\lambda_3 = 0$). The total intensity of the radiation is represented by the curve φ_0.

Integrating the expression (37) over all frequencies, we find the total intensities of the polarized radiations (cf. also Ref. 4):

$$W_2 = W\int_0^\infty \varphi_2(y)\,dy = {}^7/_8 W, \qquad (38)$$

$$W_3 = W\int_0^\infty \varphi_3(y)\,dy = {}^1/_8 W. \qquad (39)$$

These same values can be obtained also from Eq. (32) by integrating over the variable ξ.

The theory of the polarization of the radiation of an accelerated electron can also find applications in the study of the radio radiation of the sun and the galaxy, in which polarization properties have already been found experimentally. But the field of radio astronomy in question requires special consideration and is beyond the scope of our present problem.

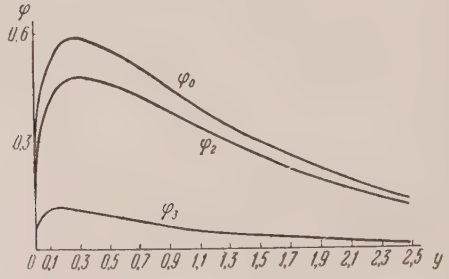

FIG. 4

Note added in proof: Recently, the polarization effects from the accelerated electron, as a function of the direction of emission, have been studied experimentally[7] for particular monochromatic parts of the spectrum ($\lambda \sim 5500$ A, etc.) by the group headed by F. A. Korolev at the 260 mev synchrotron. Theoretical curves drawn by Eq. (30) for the σ and π components (these curves had approximately the shape of the curves for the whole spectrum shown in Fig. 2) agreed fairly well with the corresponding experimental data.

[1] A. A. Sokolov, J. Phys. (U.S.S.R.) 9, 363 (1945).

[2] Sokolov, Klepikov and Ternov, J. Exptl. Theoret. Phys. (U.S.S.R.) 24, 249 (1953).

[3] A. A. Sokolov and I. M. Ternov, J. Exptl. Theoret. Phys. (U.S.S.R.) 25, 698 (1953).

[4] Sokolov, Matveev and Ternov, Dokl. Akad. Nauk SSSR 102, 65 (1955).

[5] D. D. Ivanenko and A. A. Sokolov, Dokl. Akad. Nauk SSSR 59, 1551 (1948).

[6] J. Schwinger, Phys. Rev. 75, 1912 (1949).

[7] Abstracts of reports at the All-Union Conference on High-Energy Particle Physics, Acad. of Sciences of USSR Press, 1956, p. 167; F. A. Korolev *et al.*, Dokl. Akad. Nauk SSSR 110, No. 4 (1956).

Translated by W. H. Furry
91

Isentropic Relativistic Gas Flows

F. I. FRANKL'
Kirghiz State University

(Submitted to JETP editor June 25, 1955)
J. Exptl. Theoret. Phys. (U.S.S.R.) **31**, 490-492 (September, 1956)

General baroclinic isentropic relativistic gas flows are analyzed. Equations of vorticity, and a nonlinear equation of propagation of sound waves are derived. In the case of barotropic flow, a relativistic generalization of Thompson's theorem is found.

IN classical hydrodynamics, one can prove that for a barotropic isentropic gas flow* the circulation of the velocity around any closed curve moving with the fluid remains constant in time. In such a flow, vorticity of the velocity field can neither be created nor destroyed. If the flow is at one time described by a velocity potential, it retains this property for all time.

We shall prove that analogous theorems** hold in relativistic hydrodynamics. The situation differs only in that the ordinary 3-velocity of classical hydrodynamics must now be replaced not by the relativistic 4-velocity

$$u_i = g_{ik}u^k = g_{ik}dx^k/ds$$

(s being the proper time), but by the "pseudo-velocity"

$$v_i = Ju_i, \tag{1}$$

where $J = (w/\rho)$ is the relativistic heat content per unit of rest-energy. Here w is the relativistic heat-content per unit of proper volume, and ρ is the rest-energy per unit proper volume, i.e., the rest-energy which the gas would have at absolute zero temperature. The dimensionless state-parameter J is always greater than unity.

By S we denote entropy per unit of rest-energy. In relativistic thermodynamics[1], S satisfies the equation

$$TdS = dJ - dp/\rho \tag{2}$$

where p is the pressure. We make no assumptions about the properties of the gas. We assume an equation of state $p = p(\rho, T)$, and a dependence of the internal energy-density e on ρ and T, these relations being completely arbitrary, subject only to the laws of relativistic thermodynamics and to the identity $w = e + p$. We further introduce the dimensionless relativistic sound-velocity

$$\bar{a} = a/c = \sqrt{(\partial p/de)_S} \tag{3}$$

where c is the velocity of light.

We shall prove that, when the ordinary velocity is replaced by the pseudovelocity v_i, the relativistic theory gives a system of equations for v_i and S completely analogous to the equations of classical hydrodynamics. We carry through the analysis for the case of rectilinear coordinates in special relativity, i.e., assuming g_{ik} constant. The transition to general relativity can be made in the usual way, by rewriting the equations in a form which is invariant under general coordinate transformations.

The energy-momentum equations are*

$$\partial T_i^k / dx_k = 0, \quad T_i^k = wu_iu^k - \delta_i^k p \tag{4}$$

and the equation of conservation of mass is

$$\partial(\rho u^k)/\partial x_k = 0. \tag{5}$$

Using Eq. (5) we reduce Eq. (4) to the form

$$\rho u^k \, dv_i / \partial x_k = \partial p / \partial x_i \tag{6}$$

(the relativistic Euler equations), and hence, by means of Eq. (2) to the form

$$u^k \, \partial v_i / \partial x_k = \partial J / \partial x_i - T \, \partial S / \partial x_i. \tag{7}$$

* By isentropic we mean a flow in which the entropy of each small element of the gas remains constant in time; by barotropic we mean a flow in which the entropy per unit mass is the same for all elements.

** Khalatnikov[2] was the first to investigate relativistic potential flows. We shall here discuss in greater detail flows possessing vorticity.

* The sign of the tensor g_{ik} is chosen so that the differential of proper times is $ds = (g_{ik}dx^i dx^k)^{1/2}$.

Because of the identity

$$g^{kl}u_k u_l = 1$$

the expression (1) for the pseudovelocity implies

$$g^{kl}v_k v_l = J^2. \tag{8}$$

Differentiation with respect to x_i gives

$$g^{kl}v_l\,\partial v_k / \partial x_i = J\,\partial J / \partial x_i$$

or

$$u^k\,\partial v_k / \partial x_i = \partial J / \partial x_i. \tag{9}$$

Subtracting Eq. (9) from Eq. (7), we find

$$u^k\left(\frac{\partial v_i}{\partial x_k} - \frac{\partial v_k}{\partial x_i}\right) = -T\frac{\partial S}{\partial x_i}. \tag{10}$$

These are the well-known vorticity equations of classical hydrodynamics, with the curl of the velocity replaced by the curl of the pseudovelocity. Multiplying Eq. (10) by u^i and contracting, we obtain immediately the equation of conservation of particle entropy

$$dS / ds = u^i\,\partial S / \partial x_i = 0. \tag{11}$$

We proceed to transform the equation of continuity (5). Putting $u^k = v^k/J$, we find

$$\frac{\rho}{J}\frac{\partial v^k}{\partial x_k} + J\frac{d(\rho / J)}{ds} = 0.$$

From Eq. (11) and (2) we deduce

$$\frac{d(\rho / J)}{ds} = \frac{\rho}{J^2}(\bar{a}^{-2} - 1)\frac{dJ}{ds}, \tag{12}$$

and so the continuity equation takes the form

$$(dv^k / \partial x_k) + (\bar{a}^{-2} - 1)\,dJ / ds = 0. \tag{13}$$

From Eq. (8) we have

$$J\,dJ / ds = v^i\,dv_i / ds$$

or

$$dJ / ds = u^i\,dv_i / ds = u^i u^k\,dv_i / dx_k. \tag{14}$$

Therefore, Eq. (13) becomes

$$[g^{ik} + (\bar{a}^{-2} - 1)\,u^i u^k]\,dv_i / \partial x_k = 0. \tag{15}$$

This equation, when both flow and sound velocities are small, reduces to the classical equation of propagation of sound, including the effect of wind-velocity. In terms of general coordinates, and in general relativity, the corresponding equation is

$$[g^{ik} + (\bar{a}^{-2} - 1)\,u^i u^k] \times [(\partial v_i / \partial x_k) - \Gamma^l_{ik} v_l] = 0. \tag{16}$$

The whole system of hydrodynamical equations is contained in Eqs. (10) and (15).

The theorem governing the circulation around a line moving with the fluid in a barotropic flow is obtained as follows. In a barotropic flow Eq. (7) gives

$$u^k\,\partial v_i / \partial x_k = \partial J / \partial x_i \tag{17}$$

$$\text{or} \quad \partial v_i / ds = \partial J / \partial x_i,$$

where d means differentiation along the path of a fluid-element. Let δ denote differentiation along the line around which we are considering the circulation of pseudovelocity

$$\Gamma = \oint v_i\,\delta x^i. \tag{18}$$

Then

$$d\Gamma / ds = \oint [(dv_i/ds)\,\delta x^i + v_i \delta\,dx^i / ds]$$

$$= \oint [(\partial J / \partial x_i)\,\delta x^i + v_i\,\delta u^i)$$

$$= \oint [\delta J + {}^1\!/_2\, J\delta(u_i u^i)] = \oint \delta J = 0,$$

showing that Γ remains constant in time. Strictly speaking, we must say that the circulation of pseudovelocity around a fluid line is equal in two successive positions, if each fluid element along the line has lived through the same interval of proper-time in moving from the earlier to the later position. From this theorem follows the impossibility of creating or destroying vortices of pseudovelocity in a barotropic flow.

If in a barotropic flow the pseudovelocity is derived from a potential ($v_i = d\varphi/dx_i$), then the relativistic Euler equations follow automatically. In this case

$$g^{ik}\frac{\partial \varphi}{\partial x_i}\frac{\partial \varphi}{\partial x_k} = J^2,$$

and so

$$g^{ik}\frac{\partial \varphi}{\partial x_i}\frac{\partial^2 \varphi}{\partial x_k \partial x_l} = J\frac{\partial J}{\partial x_l} = \frac{J}{\rho}\frac{\partial p}{\partial x_l}$$

which gives

$$u^k \partial v_k / \partial x_l = \rho^{-1} \partial p / \partial x_l,$$

i.e., Eq. (6). In a potential flow, the equation of sound-propagation (15) becomes

$$[g^{ik} + (\bar{a}^{-2} - 1) u^i u^k] \partial^2 \varphi / \partial x_i \partial x_k = 0. \qquad (19)$$

In a barotropic flow, $\bar{a}$ depends only on J, and hence, by Eq. (8) on the pseudovelocity; therefore, Eq. (19) contains only the potential φ and its derivatives, and the entire problem in this case reduces to the solution of the single equation (19).

[1] L. D. Landau and E. M. Lifshitz, *Mechanics of Continuous Media*, 2nd Edition, Moscow, 1954.

[2] I. M. Khalatnikov, J. Exptl. Theoret. Phys. (U.S.S.R.) 27, 529 (1954).

Translated by F. J. Dyson
93

Production of Positive π-Mesons in Hydrogen by 660 MEV Protons

A. G. Meshkovskii, Iu. S. Pligin, Ia. Ia. Shalamov and V. A. Shebanov

(Submitted to JETP editor May 25, 1956)
J. Exptl. Theoret. Phys. (U.S.S.R.) 31, 560-564 (October, 1956)

With observation angles of 29° and 46° relative to a proton beam there were obtained energy spectra for the production of charged π-mesons in the process $p + p \rightarrow \pi^+$. Differential cross sections were measured for the angles of 29°, 46° and 65° in the laboratory system.

IT is known that the production of positive mesons takes place by means of two reactions

$$p + p \rightarrow \pi^+ + d, \quad (1)$$

$$p + p \rightarrow \pi^+ + p + n. \quad (2)$$

The total cross section for meson production by the process $p + p \rightarrow \pi^+$, that is, the sum of cross sections of the reactions (1) and (2) was investigated previously for various observational angles with proton energies in the range 340-440 mev[1-4]. Reaction (1) was studied with proton energies of 460-660 mev[5,6].

The present research, carried out with the synchrocyclotron of the Institute for Nuclear Problems of the USSR Academy of Sciences, investigated the energy spectra of mesons produced by 660 mev protons in reactions (1) and (2), without separating the two reactions, with angles of 29°, 46° and 65° with respect to the beam.

1. METHOD OF MEASUREMENT AND DESCRIPTION OF THE SET-UP

The method of magnetic analysis was used to record the π-mesons and to determine their energies. The schematic layout of the apparatus is shown in Fig. 1. The beam of 660 mev protons passed through collimators K_1 and K_2 and struck target M. On leaving the collimator K_2 the beam had a rectangular cross section 1×3 cm for the 29° measurements and 2×3 cm for the 46° and 65° angles. The proton beam intensity was measured by means of the ionization chambers I_1 and I_2, which were calibrated with a Faraday cylinder. The magnetic field, perpendicular to the plane of the drawing, was produced in the gap between two pole pieces of special shape, the cross section of which is shown in the Figure (section AB).

The π-mesons produced in the target at an angle α to the beam were deflected by the magnetic field and were recorded in a telescope of four scintillation counters *I-IV*, consisting of stilbene crystals *1-4* and photomultipliers *1a-4a* of the FEU-19 type. Special precautions were taken to avoid the influence of the magnetic field on the photomultipliers of the scintillation counters. To do this the photomultipliers were placed in many-layered nonmagnetic screens of "Armco" iron and permalloy and removed from the strong magnetic field region. The photocathodes of the photomultipliers *1a* and *2a* were connected to the crystals by plexiglass light pipes *1b* and *2b* each 80 cm long. The thickness of the crystals *1* and *2* (1.5 cm each) were selected so as to ensure a sufficient magnitude of light impulses in the crystal from the recorded mesons by comparison with the impulses produced in the plexiglass light pipes by the passage of the particles.

The target M was located 20 cm from the edge of the magnetic pole pieces. At the same distance from the other edge crystal *2* was located. The aluminum filter *5* was placed between crystals *2* and *4*. The thickness of the filter was chosen so that the protons having the same impulse as the recorded mesons would not get through the filter and would not be counted by the telescope.

The counters *III* and *IV* were in the general nonmagnetic screen. The independence of the number of coincidences *1234* on the voltage of counters *I-IV* (the voltage plateau of the counters) was checked periodically. The scintillation counter impulses entered the cathode followers and after passing through coaxial cables of 200 Ω wave impedance came into wide band amplifiers and from there to a coincidence circuit with a resolving time of 2×10^{-8} sec.

The effect of π-meson production on hydrogen was determined by the difference paraffin-carbon. The paraffin target was a parallelopiped of thickness $d = 0.5$ cm (Fig. 1). The dispersion angle of the recorded π-mesons was approximately ±1°.

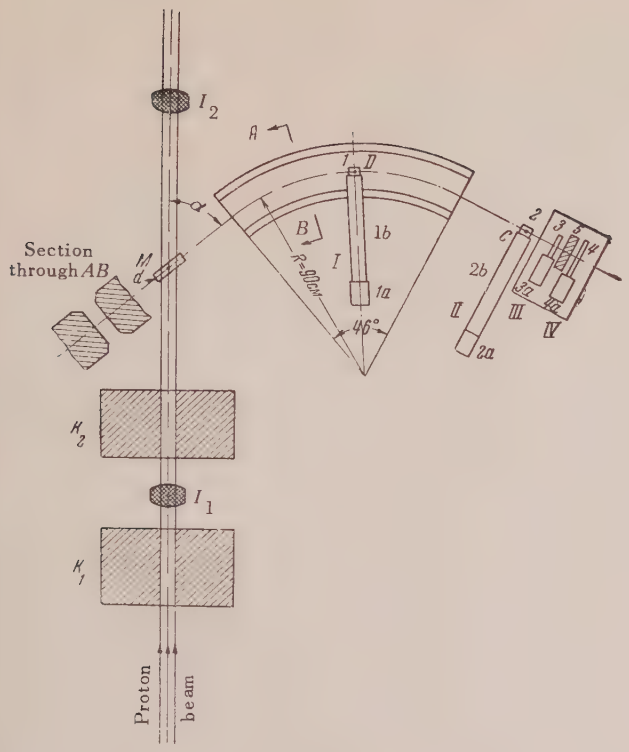

FIG. 1. Schematic layout of the apparatus

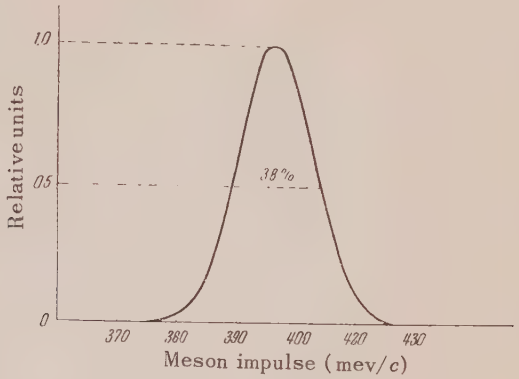

FIG. 2. The resolution curve.

The magnitude of the magnetic field in the gap varied during the experiments from 5000 to 17000 oersteds, which ensured the recording of mesons in the impulse range of 130 to 450 mev/c. The topography of the magnetic field along the curve *MDC* was measured with a fluxmeter with varying values of current in the magnet winding. The fluxmeter was calibrated in a magnetic field, the value of which was measured by the method of nuclear resonance.

The topography of the magnetic field investigated by this means and the meson trajectories determined by the orientation of the target and counters served as a basis for the computing of the impulse distribution of mesons recorded by our system (resolution curves). During the computation the multiple Coulomb scattering of π-mesons by the matter in the system as well as the ionization energy losses in the target and crystal l were taken into account. The mean square angle of dispersion was calculated by the usual formula. From the resolution curves obtained the mean values of meson impulses and effective solid angles were determined for the mesons recorded by the system. One of these resolutions curves for the case of an average impulse of 396 mev/c is shown in Fig. 2.

The curve half-width constitutes 3.8%. The resolution worsens in the region of smaller impulses, reaching 10% for an impulse of 150 mev/c.

The indicated computations were made by G. M. Adel'son according to the Monte Carlo method with the electronic computer of I. S. Brook in the Institute of Energetics of the USSR Academy of Science. The calculations comprised 10^9 operations.

2. CONTROL EXPERIMENTS AND CORRECTIONS

In making the measurements it was important to be sure that the described system did not record electrons originating from the conversion of photocurrents during decay of the π^0-mesons produced in the targets. To evaluate the possible addition of electrons, control experiments were carried out in which the number of particles were measured entering the telescope with a magnetic field of opposite direction to that for recording only negative π-mesons and electrons. In doing this the carbon and paraffin targets had the same cascade length in the direction of the motion of recorded π-mesons. Experiments showed that the number of particles recorded with the paraffin target did not differ within the limits of statistical accuracy from the number counted by the system with the carbon target. It was therefore concluded that the possible electron background produced by the $p + p \to \pi^0$ process could not exceed 2-3%. This value was not taken into account in subsequent calculations.

The number of recorded mesons was corrected for the nuclear absorption of mesons by the system's matter and decay in flight. In calculating the correction for the nuclear absorption the interaction cross section was taken to be equal to the geometrical cross section of the nucleus for all elements except hydrogen, for which the dependence of the cross section on the energy of π-mesons was taken

TABLE II

The angle of mesons ejection in the laboratory system, degrees	Production cross sections of mesons in reactions (1) and (2) in cm^2 $sterad^{-1}$, calculated for 1 nucleon	
	In the laboratory system	In the center-of-mass system
29	$(3.01 \pm 0.24) \cdot 10^{-27}$	$(1.07 \pm 0.08) \cdot 10^{-27}$
46	$(2.12 \pm 0.14) \cdot 10^{-27}$	$(1.06 \pm 0.07) \cdot 10^{-27}$
65	$(1.20 \pm 0.12) \cdot 10^{-27}$	$(0.99 \pm 0.10) \cdot 10^{-27}$

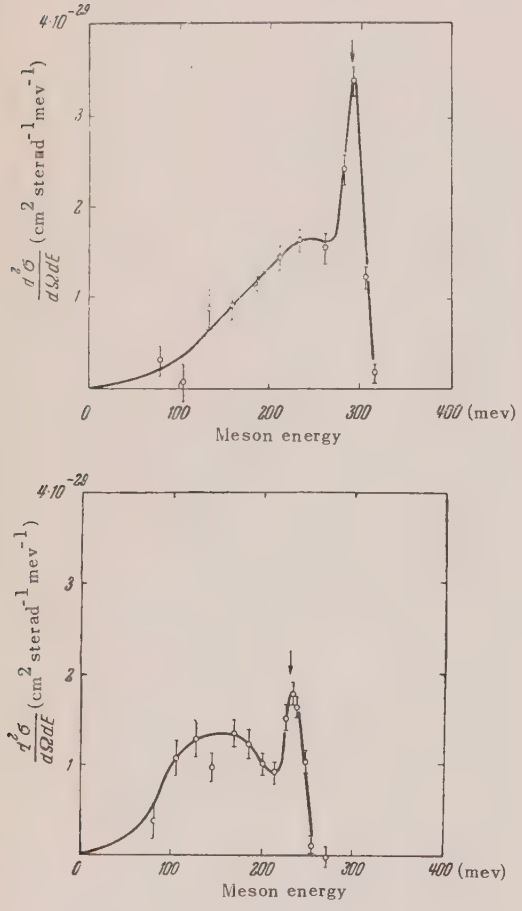

FIG. 3. Spectrum of π^+-mesons in the laboratory system from the reactions $p + p \to \pi^+ + p + n$ and $p + p \to \pi^+ + d$ with meson flight angles with respect to the proton beam: $a - 29°$, $b - 46°$.

into account[7]. In calculating the decay corrections, an evaluation of the possible effect on the telescope recording of the decay μ-mesons showed it to be negligibly small. The decay and nuclear absorption corrections are shown in Table I. The correction for multiple Coulomb scattering was automatically accounted for by the method of calculating impulse intervals and effective solid angles described in Sec. 1.

3. THE DATA

The spectra of mesons produced in hydrogen with observation angles of 29° and 46° are shown in Fig. 3. The ordinates represent differential cross section of meson production $d^2\sigma / d\Omega\, dE$ $cm^2/$ $sterad^{-1}/mev^{-1}$, calculated for one nucleon; the abscissas, meson energies in mev. We do not reproduce the meson spectrum for the 65° angle because it was obtained when measurements were made with a different version of our apparatus in which the resolution of the system was not sufficiently good to determine the shape of the differential spectrum with adequate precision.

The meson spectra recalculated in the center-of-mass system for two colliding protons are shown in Fig. 4. Above the graphs are shown the values of the angles in the center-of-mass system, as a function of the meson energy.

The solid curves, shown in Figs. 3 and 4, are the best approximations to the experimental points. The figures show only the statistical errors of measurement. The systematic errors on the order of 5% are accounted for during the integration of the spectra, i.e., in calculating the cross sections $d\sigma / d\Omega$. The results of computations are shown in Table II. Included in this table also are the results of integrating the spectrum obtained with an observational angle of 65°.

4. DISCUSSION OF RESULTS

The energy of π-mesons recorded in our system was determined by the computation method indicated in Sec. 1. In accordance with this, the abscissa axis in Fig. 3 was calibrated. For reaction (1), proceeding with the formation of a deuteron, the energy of π-mesons can also be computed from

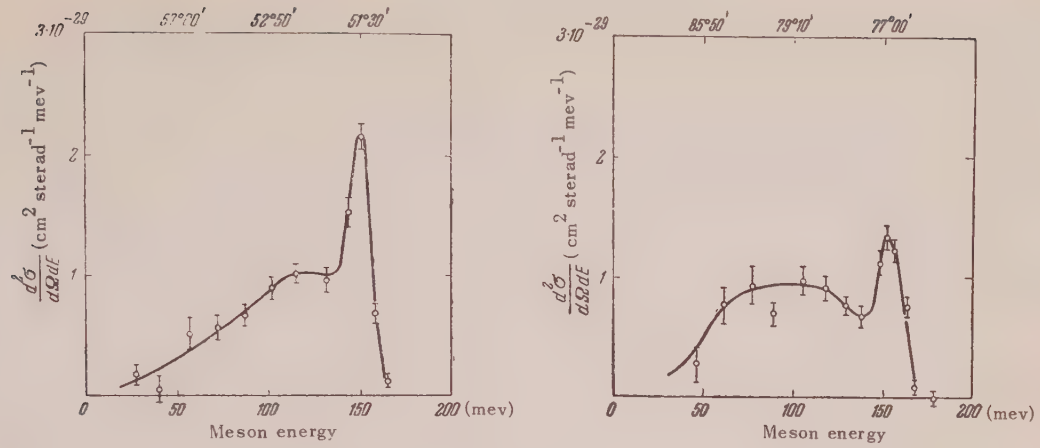

FIG. 4. The spectrum of π^+-mesons in the center-of-mass system from the reactions $p + p \to \pi^+ + p + n$ and $p + p \to \pi^+ + d$ with laboratory angles: $a - 29°$, $b - 46°$.

the conservation laws. The result of this calculation is shown by arrows in Fig. 3, the location of which agrees well (with a precision of 1-2%) with the peak position corresponding to reaction (1). Such a coincidence indicates the correctness of the calculations which serve as the basis of our methodology.

It follows from Table II that the meson production cross section $d\sigma/d\Omega$ in the reactions (1) and (2) recalculated in the center-of-mass system, remains constant (within experimental errors) for the three angles investigated by us, with the mean cross section value being $1.05 \times 10^{-27}/\text{cm}^2/\text{sterad}^{-1}$. If in accordance with this experimental fact one makes the assumption that the angular distribution of the mesons produced in the process $p + p \to \pi^+$ is nearly isotropic in the center-of-mass system, then the total cross section of charged meson production by 660 mev protons on protons turns out to be $\sigma(pp \to \pi^+) = 13.2 \times 10^{-27}$ cm^2. This quantity can also be evaluated if from the cross section for all the inelastic processes at this energy $\sigma pp = (16.7 \pm 1.2)\ 10^{-27}$ cm^2 [8] one subtracts the production cross section of neutral π-mesons. $\sigma(pp \to \pi^0) = (3.6 \pm 0.3) \times 10^{-27}$cm^2 [9]. As a result, we obtain $\sigma(pp \to \pi^+) = (13.1 \pm 1.2) \times 10^{-27}$ cm^2. The agreement of this value with our estimate and the observed independence of the differential cross section on the angle make the above-mentioned assumption quite probable, viz., the process $p + p \to \pi^+$ in the center-of-mass system is close to isotropic.

The contribution of reaction (1) to the total cross section of the process $p + p \to \pi^+$ can be evaluated by comparing out data with those of Meshcheriakov and Neganov[6] who studied reaction (1). Namely, for the observational angles of 29° and 46° the number of mesons from the reaction (1) constitutes 23.6 ± 2.6% and 10.8 ± 1.5% of all the mesons produced at the corresponding angle as a result of the $p + p \to \pi^+$ process.

The relatively small part of reaction (1) in the total process $p \to p \to \pi^+$ and the adequate energy resolution of our system allow an approximate judgment about the shape of the meson spectra produced by reaction (2). It follows from Fig. 4 that the maxima of these spectra are in the energy range 100-120 mev in the center-of-mass coordinate system.

In conclusion we express our thanks to A. I. Alikhanov for his continuous interest in the investigation and for valuable advice, to M. G. Meshcheriakov for the opportunity to carry out the current experiemnts and to G. M. Adel'son for making the computations. We also express thanks to the operating personnel of the synchrocyclotron of the Institute for Nuclear Problems of the USSR Academy of Sciences.

[1] Peterson, Iloff and Sherman, Phys. Rev. **84**, 372 (1951).

[2] Block, Passman and Havens, Phys. Rev. **88**, 1239 (1952).

[3] Passman, Block and Havens, Phys. Rev. **88**, 1247 (1952).

[4] A. H. Rosenfeld, Phys. Rev. **96**, 130 (1954).

[5] Meshcheriakov, Neganov, Bogachev and Sidorov, Dokl. Akad. Nauk SSSR **100**, 673 (1955).

[6] M. G. Meshcheriakov and B. S. Neganov, Dokl. Akad. Nauk SSSR 100, 677 (1955).

[7] Ignatenko, Mukhin, Ozerov and Pontecorvo, J. Exptl. Theoret. Phys. (U.S.S.R.) 30, 7 (1956); Soviet Phys. JETP 3, 10 (1956).

[8] Dzhelepov, Moskalev, Starov, Golovin and Medved, Report at the All Union Conference on the Physics of High Energy Particles, May 1956.

[9] A. A. Tiapkin and Iu. D. Prokoshkin, *ibid.*

Translated by H. Kruglak
119

The Role of Spin in the Radiation from a "Radiating" Electron

A. N. MATVEEV
Moscow State University

(Submitted to JETP editor June 20, 1955)
J. Exptl. Theoret. Phys. (U.S.S.R.) 31, 479-489 (September, 1956)

It is shown that in the case of energies which are not too great the magnitudes of the spin corrections are of the second order of smallness with respect to the magnitudes of the quantum corrections, while in the case of extreme relativistic energies the spin essentially changes the character of the differential spectrum and the magnitude of the total energy of radiation.

1. INTRODUCTION

THE opinion exists that the spin does not play an essential role in the radiation of a radiating electron. This opinion is based on the consideration that the spin contribution to the wave function of an electron in a magnetic field decreases with increase in the energy of the electron. However, one cannot conclude from this that the spin is nonessential, since in the calculation of the matrix elements of radiative transitions not only the wave functions, which are distinguished from each other only by small spin contributions , are different, but the various operators whose matrix elements are being calculated are also different. Hence the question of the role of spin cannot be decided on the basis of general considerations[1-3]. An actual calculation is necessary.

A remark is necessary concerning the statement of the problem. Simply raising the question of isolating the "role of spin" within the framework of relativistic theory appears artificial in itself. A statement of the question which has an exact sense is the following: to compare under the same external conditions the radiation from an electron and from a boson with zero spin and with mass and charge equal to the mass and charge of an electron.

The present work is devoted to the clarification of the question of the role of spin in the radiation of an electron moving in a constant magnetic field. The calculation is carried out without taking account of damping.

2. QUANTUM MECHANICAL FORMULAS FOR THE INTENSITY OF RADIATION, WITH AND WITHOUT TAKING ACCOUNT OF SPIN

In order to obtain by a single method formulas characterizing the radiation with and without taking account of spin, it is convenient to carry out the calculation in the scheme of Lorentz forces rather than in the Hamiltonian scheme.

From the covariant definition of the four-dimensional energy-momentum vector $p_\mu(\mathbf{p}, iW/c)$

$$p_\mu[\sigma] = \frac{1}{c}\int_\sigma T_{\mu\nu}\, d\sigma_\nu \tag{2.1}$$

and the relationship

$$\delta p_\mu[\sigma] / \delta\sigma(x) = c^{-1}\partial T_{\mu\nu}/\partial x_\nu, \tag{2.2}$$

which follows from it, one obtains for Δp_μ, the change in the energy-momentum during a transition from the hypersurface σ_1 to the hypersurface σ_2, the following expression:

$$\Delta p_\mu = c^{-2}\int_{\sigma_1}^{\sigma_2} dx\, F_{\mu\nu} j_\nu, \tag{2.3}$$

where $F_{\mu\nu}$ is the electromagnetic field tensor, j_ν is the four-dimensional current, and the fact that

$$\partial T_{\mu\nu}/\partial x_\nu = c^{-1} F_{\mu\nu} j_\nu \tag{2.3a}$$

has been taken into account.

The operators in (2.3) are taken in the Heisenberg representation. Removing the hypersurfaces $\sigma_1(t_1)$ and $\sigma_2(t_2)$ in (2.3) to infinity ($t_2 \to \infty$, $t_1 \to -\infty$, $t_2 - t_1 = T \to \infty$), averaging the change in momentum over the time interval, and changing from bound operators to free field operators, we obtain from (2.3)

$$\overline{\Delta p_\mu} = \frac{1}{c^3 T}\int_{-\infty}^{\infty} dx \sum_{n=0}^{\infty}\left(\frac{-i}{\hbar c}\right)^n \int_{-\infty}^{t} dx_1 \int_{-\infty}^{t_1} dx_2 \ldots \int_{-\infty}^{t_{n-1}} dx_n, \tag{2.4}$$

$$[j^{(0)}_{\lambda_n}(x_n) A^{(0)}_{\lambda_n}(x_n), \ldots [j^{(0)}_{\lambda_2}(x_2) A^{(0)}_{\lambda_2}(x_2),$$

$$[j^{(0)}_{\lambda_1}(x_1) A^{(0)}_{\lambda_1}(x_1), \quad F^{(0)}_{\mu\nu}(x) j^{(0)}_\nu(x)],]\ldots].$$

In this formula it is to be kept in mind that

$$\frac{1}{T}\int_{-\infty}^{\infty} dt \ldots = \lim_{T\to\infty}\frac{1}{T}\int_{-T/2}^{T/2} dt \ldots, \tag{2.4a}$$

and that the square brackets denote commutators.

Averaging (2.4) over the state of a single-electron in the absence of photons, and limiting ourselves to the first nondisappearing term, we obtain

$$\langle\overline{\Delta p_\mu}\rangle_{1,0} = -\frac{i}{hc^4T}\int_{-\infty}^{\infty} dx \tag{2.5}$$

$$\times\int_{-\infty}^{t} dx'\,\langle 1,0 \mid [j_\lambda(x')A_\lambda(x'),\ F_{\mu\nu}(x)j_\nu(x)] \mid 1,0\rangle.$$

For simplicity the indices (0) used on the free operators have been omitted.

An average over the photonic vacuum gives (in Gaussian units)

$$\langle [j_\lambda(x')A_\lambda(x'),\ F_{\mu\nu}(x)j_\nu(x)]\rangle_0 \tag{2.6}$$

$$= 2\pi ch\left\{j_\lambda(x')j_\lambda(x)\frac{\partial}{\partial x_\mu}D^{(+)}(x'-x) - j_\lambda(x)j_\lambda(x')\frac{\partial}{\partial x_\mu}D^{(+)}(x-x')\right\},$$

where $D^{(+)}$ signifies the positive-frequency D function.

The integral in (2.5) in the surface of changing (t, t') is taken over the half-surface with boundary $t = t'$. For definiteness let us take the first component of (2.6). If we make the exchange $x \leftrightarrow x'$ in the integral, then the region of integration with respect to (t, t') will be the other half-surface with the same boundary $t = t'$. This exchange also makes the first expression under the integral sign coincide with the second expression, with the exception that a derivative with respect to x'_μ occurs instead of a derivative with respect to x_μ. However,

$$(\partial/\partial x_\mu)D^{(+)}(x-x') = -(\partial/\partial x'_\mu)D^{(+)}(x-x'). \tag{2.7}$$

Hence, the integrands coincide completely and a change in sign occurs. Consequently,

$$\langle\overline{\Delta p_\mu}\rangle_{1,0} = \frac{2\pi i}{c^3T}\int_{-\infty}^{\infty} dx \tag{2.8}$$

$$\times\int_{-\infty}^{\infty} dx'\,\langle 1 \mid j_\lambda(x)j_\lambda(x') \mid 1\rangle\frac{\partial}{\partial x_\mu}D^{(+)}(x-x').$$

The radiation W is equal (with reversed sign) to the magnitude of the fourth component of the change in momentum $\overline{\Delta p_\mu}$ multiplied by c/i. Hence,

$$W = \frac{1}{c^2T}\frac{1}{4\pi^2}\int d^3\mathbf{x}\,\langle 1 \mid ([\mathbf{x}_0, \mathbf{j}(-\varkappa)], [\mathbf{x}_0, \mathbf{j}(\varkappa)]) \mid 1\rangle, \tag{2.9}$$

where the brackets [ ] indicate vector derivation and $\varkappa_0 = \varkappa/|\varkappa|$. The changing of the four-dimensional current

$$j(\varkappa) = \int_{-\infty}^{\infty} dx e^{-i\varkappa x}j(x) \tag{2.10}$$

into its Fourier components is carried out in Eq. (2.9), and the fourth component of the current is excluded with the aid of the law of conservation of charge

$$\partial_\nu j_\nu(x) = 0. \tag{2.11}$$

The current operators have the following form:

a) For the Dirac equation

$$\mathbf{j}(x) = ec\Psi^+\boldsymbol{\alpha}\Psi = iec\overline{\Psi}\boldsymbol{\gamma}\Psi, \tag{2.12a}$$

b) For the scalar equation

$$\mathbf{j}(x) = \frac{e}{2m}\left\{\Phi^*(\mathbf{p}\Phi) - (\mathbf{p}\Phi^*)\Phi - 2\frac{e}{c}\Phi^*\mathbf{A}\Phi\right\}, \tag{2.12b}$$

where $\mathbf{A}$ is the vector potential of the external field (c is a number).

The wave functions of an electron in a constant magnetic field may be found by iteration. They may be given in the following form (the components of the vector potential being $A_x = -\frac{1}{2}Hy$, $A_y = \frac{1}{2}Hx$, $A_z = 0$):

a) For the Dirac equation

$$\Psi = \Psi_{n,l,k_z,\varepsilon,s} = L_z^{-1/2}e^{-ic\varepsilon K_n t + ik_z z}\Psi_{n,l,k_z,\varepsilon,s}(x,y); \tag{2.13}$$

$$\Psi_{n,l,k_z,\varepsilon,s}(x,y) = \sqrt{\frac{\gamma}{\pi}}\begin{vmatrix} sf(\varepsilon,s)e^{i(n-1-l)\varphi}I_{n-1,l}(\gamma\rho^2), \\ if(\varepsilon,-s)e^{i(n-l)\varphi}I_{n,l}(\gamma\rho^2), \\ \varepsilon f(-\varepsilon,s)e^{i(n-1-l)\varphi}I_{n-1,l}(\gamma\rho^2), \\ is\varepsilon f(-\varepsilon,-s)e^{i(n-l)\varphi}I_{n,l}(\gamma\rho^2), \end{vmatrix} \tag{2.13a}$$

where (ρ, φ, z) are the cylindrical coordinates of the point (x, y, z);

$$I_{n,n'}(\xi) = \frac{1}{\sqrt{n!n'!}} e^{-\xi^2/2} \xi^{(n-n')/2} Q_{n'}^{(n-n')}(\xi),$$

$$Q_n^{(m)}(\xi) = \frac{\Gamma(n+m+1)}{\Gamma(m+1)} {}_1F_1(-n, m+1, \xi),$$

$$f(\varepsilon, s) = \frac{1}{2}\left(1 + \varepsilon \frac{k_0}{K_n}\right)^{1/2} \left(1 + s \frac{k_z}{\sqrt{K_n^2 - k_0^2}}\right)^{1/2},$$

$$\gamma = \frac{eH}{2ch}, \quad K_n = \sqrt{k_0^2 + 4\gamma n + k_z^2}, \quad k_0 = \frac{mc}{h},$$

n is the principal quantum number, l is the radial quantum number, $\epsilon = 1$ denotes the electronic state, $\epsilon = -1$, the positron state, s is the spin variable, and L_z is the normalized length in the direction of the z axis;

b) for the scalar equation

$$\Phi_{n,l,k_z} = (k_0/K_n^{(1)} L_z)^{1/2} \times \exp\{-icK_n^{(1)} t + ik_z z\} \varphi_{n,l}(x, y); \tag{2.14}$$

$$\varphi_{n,l}(x, y) = \sqrt{\gamma/\pi}\, e^{i(n-l)\varphi} I_{n,l}(\gamma\rho^2), \tag{2.14a}$$

where $K_n^{(1)} = \sqrt{k_0^2 + 4\gamma(n + \frac{1}{2}) + k_z^2}$, and the significance of the other quantities is the same as in case a). The factor $(k_0/K_n^{(1)})^{1/2}$ occurs because of normalization to the current of a single charge. Introducing the notation

$$\tilde{\alpha} = \int \Psi^+_{n',l',k_z',1,s'} \times \alpha e^{-ix_x x - ix_y y} \Psi_{n,l,0,1,s}\, dx\, dy, \tag{2.15a}$$

$$\tilde{\mathbf{P}} = \int \varphi^*_{n',l'} e^{-ix_x x - ix_y y} \mathbf{P} \varphi_{n,l}\, dx\, dy, \tag{2.15b}$$

where the α are the Dirac matrices and $\mathbf{P} = \mathbf{p} - (e/c)\mathbf{A}$, we obtain from Eq. (2.9) [on taking account of Eqs. (2.12a) and (2.12b)], the following formulas characterizing the radiation with and without taking account of spin

$$W = \frac{ce^2}{2\pi} \frac{1}{2} \times \sum_{n',l'} \sum_{s,s'} \int d^3\varkappa\, ([\varkappa_0, \tilde{\alpha}^+][\varkappa_0, \tilde{\alpha}])\, \delta(K - K' - \varkappa), \tag{2.16a}$$

$$K = K_n, \quad K' = K_{n'},$$

$$W^{(1)} = \frac{ce^2}{2\pi} \sum_{n',l'} \int d^3\varkappa\, \frac{1}{h^2 K^{(1)\prime} K^{(1)}} \times ([\varkappa_0, \tilde{\mathbf{P}}^*][\varkappa_0, \tilde{\mathbf{P}}])\, \delta(K^{(1)} - K^{(1)\prime} - \varkappa), \tag{2.16b}$$

$$K^{(1)} = K_n^{(1)}, \quad K^{(1)\prime} = K_{n'}^{(1)},$$

where in formula (2.16a) the initial state has been averaged over the spin states and in formula (2.16b) the fact that $[\varkappa_0, \varkappa] = 0$ has been used.

On carrying out the calculation intended in formula (2.16) and using the well-known recurrence relations between the Laguerre polynomials, we can, after a series of transformations, obtain expressions for the intensity of radiation in the following form:

a) $W = \sum_{m=0}^{n} W_m$;

$$W_m = \frac{\gamma}{\pi} ce^2 A \int \frac{\Phi_m(\xi)}{A - \xi} \delta[\varphi_m(\xi)]\, d^3\xi, \tag{2.17a}$$

$$\xi = \varkappa / 2\sqrt{\gamma}, \quad A = K / 2\sqrt{\gamma},$$

$$\varphi_m(\xi) = \xi - A + \sqrt{A^2 - m + \xi^2 \cos^2\vartheta};$$

$$\Phi_m(\xi) = \operatorname{ctg}^2\vartheta (I^2_{n,n-m} + I^2_{n-1,n-1-m}) + \frac{\xi^2 \sin^2\vartheta}{A^2} (I'^2_{n,n-m} + I'^2_{n-1,n-1-m}) + \frac{\xi^2 \sin^2\vartheta}{A^2} (I_{n,n-m} I'_{n,n-m} - I_{n-1,n-1-m} I'_{n-1,n-1-m}),$$

where the argument of the function I is equal to $\xi^2 \sin^2\vartheta$, and the primes indicate derivatives with respect to that argument;

b) $W^{(1)} = \sum_{m=0}^{n} W_m^{(1)}$;

$$W_m^{(1)} = \frac{\gamma}{\pi} ce^2 A \int \frac{\Phi_m^{(1)}(\xi)}{A^{(1)} - \xi} \delta[\varphi_m^{(1)}(\xi)]\, d^3\xi; \tag{2.17b}$$

$$\frac{1}{2}\Phi_m^{(1)}(\xi) = \operatorname{ctg}^2\vartheta I^2_{n,n-m} + \frac{\xi^2 \sin^2\vartheta}{A^{(1)2}} I'^2_{n,n-m},$$

where

$$A^{(1)} = K^{(1)} / 2\sqrt{\gamma}, \quad \varphi_m^{(1)}(\xi) = \xi - A^{(1)} + \sqrt{A^{(1)2} - m + \xi^2 \cos^2\vartheta}.$$

A comparison of formulas (2.17a) and (2.17b) allows us to draw conclusions concerning the "role of spin" without any approximation whatsoever. The difference in the magnitudes of $A^{(1)}$ and A leads to a difference in magnitudes of order $1/n$ in these formulas and is completely nonessential, since to our specified accuracy $A^{(1)}$ can be replaced by A and $\varphi^{(1)}$ by φ in formula (2.17b). Moreover, on taking into account the equalities

$$I_{n-1,\,n'-1}(x) = \frac{n+n'-x}{2\sqrt{nn'}} I_{n,\,n'}(x) - \frac{x}{\sqrt{nn'}} I'_{n,\,n'}(x), \tag{2.18}$$

$$I'_{n-1,\,n'-1}(x) = \frac{n+n'-x}{2\sqrt{nn'}} I'_{n,\,n'}(x) + \frac{1}{2x}\left[2\sqrt{nn'} - \frac{(n+n'-x)^2}{2\sqrt{nn'}}\right] I_{n,\,n'}(x),$$

we may show that in the first and second parentheses in the expression for Φ_m in Eq. (2.17a) $I_{n,n'}$ and $I_{n-1,n'-1}$ can be equated with an accuracy of magnitude $\sim\sqrt{1-\beta^2}$, so that these terms coincide with the corresponding terms for $\Phi_m^{(1)}$ in Eq. (2.17b). Thus the "role of spin" is determined by the term in the third parenthesis in the expression for $\Phi_m(\xi)$ in Eq. (2.17a). As will be shown, this role is by no means small in the extreme relativistic case.

In the entire following exposition, in order to shorten the notation in the formulas, magnitudes characterizing the radiation from a "radiating" electron will be represented as the sum of two components. The first component, designated by the index (1), gives the "spinless" part of the radiation". More exactly, this first part characterizes the corresponding physical magnitude of the radiation from a "radiating" boson (with spin 0).

In order to simplify the formulas, it is convenient to go over to a continuous spectrum. Corresponding to what was said above, further calculations can be carried out with formula (2.17a), in which the "spinless part" of the radiation is contained.

Let us transform the integral for W_m in (2.17a) into a surface integral by means of the well-known formula

$$\int \ldots \delta(\varphi)\, d\tau = \int\limits_{\varphi=0} \ldots \frac{d\sigma}{|\nabla\varphi|}, \tag{2.19}$$

where $d\sigma$ is an element of the surface $\varphi = 0$. Then, instead of (2.17a), we obtain

$$W_m = \frac{\gamma}{\pi} ce^2 A \int\limits_{S_m} \frac{\Phi_m(\xi)}{(\partial\varphi_m/\partial n)(A-\xi)}\, d\sigma, \tag{2.20}$$

where S_m is a surface in (ξ) space determined by the equation $\varphi_m(\xi) = 0$, $d\sigma$ is an element of the surface, and n is the outward normal.

In the entire frequency region in which we are interested we can direct our considerations to the continuous sepctrum. Hence, for the production of the total energy of radiation we change from a sum over m to the integral

$$W = \int\limits_0^n W_m\, dm. \tag{2.21}$$

In this transition the family of surfaces S_m fills the entire region, the boundary of which is determined by the equation $\varphi_n = 0$. Let us take into account the fact that during the transition from one surface to another the identity

$$\varphi_m \equiv 0, \tag{2.22}$$

holds, and this leads to the equations

$$dm = 2(A-\xi)(\partial\varphi_m/\partial n)\, dn, \tag{2.23}$$

$$m = 2A\xi - \xi^2 \sin^2\vartheta. \tag{2.24}$$

On putting Eq. (2.23) into Eq. (2.21), taking account of the value of W_m as given by Eq. (2.20), and noting that $d\sigma\, dn = d^3\xi$ is an element of volume in the infinite space in which we are operating, we finally obtain

$$W = \frac{2\gamma}{\pi} ce^2 A \int \Phi_{\nu'}(\xi)\, d^3\xi, \tag{2.25}$$

where

$$\nu' = 2A\xi - \xi^2 \sin^2\vartheta.$$

For what is to follow, it is convenient to go over to different units. In the units used here the wave number of the basic classical oscillation ("first harmonic" in the sense of the classical theory of the "radiating" electron) is equal to

$$\xi_0 = 1/2\,A. \tag{2.26}$$

As a new independent variable we take the ratio of ξ to ξ_0, that is, that which in the classical theory of the radiating electron is called the number of the harmonic. Setting

$$\nu = 2A\xi, \tag{2.27}$$

we finally obtain

$$W = \frac{ce^2\beta^2}{4\pi R^2}\int\limits_{Vn} \Phi_{\nu'}\left(\frac{\nu}{2A}\right) d^3\nu, \tag{2.28}$$

where $R = \sqrt{n/\gamma}$ is the classical radius of the trajectory of the electron,

$$\nu' = \nu[1 - (\nu/4n)\beta^2 \sin^2\vartheta],$$

$$\beta = \sqrt{n}/A,\ \sqrt{1-\beta^2} = mc^2/E.$$

The region V_n is the former region, but $\nu = 2A\xi$ in the new units.

3. THE DIFFERENTIAL SPECTRUM

In what follows we shall use approximations of the functions $I_{n,n'}$ which will be correct for the entire region of variation of the arguments and indices of these functions. The approximations were obtained by Klepnikov[4] and have the following form:

$$I_{n,n'}(x) = \frac{1}{\pi\sqrt{3}}\sqrt{1 - \frac{x}{(\sqrt{n}-\sqrt{n'})^2}}\, K_{1/3}\left\{\frac{2}{3}(nn')^{1/4}(\sqrt{n}-\sqrt{n'})\times\left[1 - \frac{x}{(\sqrt{n}-\sqrt{n'})^2}\right]^{3/2}\right\}, \tag{3.1}$$

$$I'_{n,n'} = \frac{1}{\pi\sqrt{3}}\frac{(nn')^{1/4}}{\sqrt{n}-\sqrt{n'}}\left[1 - \frac{x}{(\sqrt{n}-\sqrt{n'})^2}\right] \times K_{2/3}\left\{\frac{2}{3}(nn')^{1/4}(\sqrt{n}-\sqrt{n'})\left[1 - \frac{x}{(\sqrt{n}-\sqrt{n'})^2}\right]^{3/2}\right\}. \tag{3.2}$$

On putting Eqs. (3.1) and (3.2) into formula (2.28), we obtain

$$W = W^{(1)} + W^{(2)}; \tag{3.3}$$

$$W^{(1)} = \frac{ce^2}{R^2}\frac{1}{3\pi^2}\int\frac{\nu^2\, d\nu}{1-\nu/2n}\sin\vartheta\, d\vartheta\left\{\varepsilon_\vartheta\cos^2\vartheta K^2_{1/3}\left(\frac{1}{3}\frac{\nu}{1-\nu/2n}\varepsilon_\vartheta^{3/2}\right) + \varepsilon_\vartheta^2 K_{2/3}\left(\frac{1}{3}\frac{\nu}{1-\nu/2n}\varepsilon_\vartheta^{3/2}\right)\right\}; \tag{3.3a}$$

$$W^{(2)} = \frac{ce^2}{R^2}\frac{1}{3\pi^2}\int\frac{\nu^2\, d\nu}{1-\nu/2n}\sin\vartheta\, d\vartheta\,\frac{1}{2}\left(\frac{\nu}{2n}\right)^2\left(1-\frac{\nu}{2n}\right)^{-1}\varepsilon_\vartheta^2 \times\left[K^2_{1/3}\left(\frac{1}{3}\frac{\nu}{1-\nu/2n}\varepsilon_\vartheta^{3/2}\right) + K^2_{2/3}\left(\frac{1}{3}\frac{\nu}{1-\nu/2n}\varepsilon_\vartheta^{3/2}\right)\right], \tag{3.3b}$$

where

$$\varepsilon_\vartheta = 1 - \beta^2\sin^2\vartheta.$$

The fact that in spherical coordinates $d^3\nu = \nu^2 d\nu \sin\theta\, d\theta\, d\varphi$ has been taken account of in formula (3.3), and the integration has been carried out with respect to the angle φ, on which, as a consequence of axial symmetry, the expression under the integral sign does not depend. The region of integration is set by the law of conservation of energy-momentum. As stated above, the component $W^{(1)}$ corresponds to the radiation of the spinless particle.

In order to obtain the differential spectrum it is necessary to carry out the integration in expressions (3.3) with resepct to the angle θ. Because of the exponential fall-off in the expression under the integral sign as θ departs from $\pi/2$, we may carry out an exchange of the variables $\cos\theta = x$ and extend the limits of integration to infinity. We encounter here a number of integrals which may be evaluated with the aid of Mellin transformation theory. In order for this to be done, a substitution must be made for the squares of the functions K with the aid of Nicholson's integral.

$$K_\mu(z)\, K_\nu(z) = 2\int\limits_0^\infty K_{\mu-\nu}(2z\,\mathrm{ch}\, t)\,\mathrm{ch}\,(\mu+\nu)\, t\, dt, \tag{3.4}$$

and then the function K_0 must be expressed with

the aid of a relation obtained by means of Mellin's theorem from the well-known equation

$$\int_0^\infty K_\nu(x)\, x^{\mu-1}\, dx = 2^{\mu-2}\,\Gamma\left(\frac{\mu-\nu}{2}\right)\Gamma\left(\frac{\mu+\nu}{2}\right). \quad (3.5)$$

The result obtained is an absolutely convergent integral in which we may interchange the order of the integrations. Then with the aid of the multiplication formula for Γ-functions

$$\Gamma(z)\,\Gamma\left(z+\frac{1}{n}\right)\ldots\Gamma\left(z+\frac{n-1}{n}\right) = (2\pi)^{(n-1)/2}\, n^{1/2-nz}\,\Gamma(nz) \quad (3.6)$$

the expressions under the integral signs may be considerably simplified and the integrals evaluated. For example, for the integral

$$I = \int_0^\infty \varepsilon_x^2\,[K_{1/3}^2(p\varepsilon_x^{3/2}) + K_{2/3}^2(p\varepsilon_x^{3/2})]\, dx, \quad (3.7)$$

where $\varepsilon_x = 1-\beta^2+x^2$, $p>0$, there results, after the evaluations just mentioned, the expression

$$I = \frac{\varepsilon_0^{3/2}}{3\pi i}\int_{k-i\infty}^{k+i\infty} p_0^{-\mu}\, 2^{\mu-2}\,\varphi(\mu)\, d\mu; \quad (3.8)$$

$$\varphi(\mu) = \frac{4\pi}{\sqrt{3}}\, 2^{-\mu}\,\Gamma\left(\frac{\mu}{2}-\frac{1}{6}\right)\Gamma\left(\frac{\mu}{2}-\frac{5}{6}\right),$$

$$p_0 = p\varepsilon_0^{3/2}.$$

The path of integration goes parallel to the imaginary axis, to the right of the poles of the integrand. From Eq. (3.8) it follows immediately that

$$\int_0^\infty \varepsilon_x^2\,[K_{1/3}^2(p\varepsilon_x^{3/2}) + K_{2/3}^2(p\varepsilon_x^{3/2})]\, dx = \frac{\pi}{\sqrt{3}}\,\frac{\varepsilon_0}{p}\, K_{2/3}(2p\varepsilon_0^{3/2}). \quad (3.9)$$

The other integrals are evaluated analogously.

On carrying out the evaluations just mentioned, we obtain the following formulas for the differential spectrum:

$$W = \int_{\nu=1}^{2n} dW_\nu, \quad dW_\nu = dW_\nu^{(1)} + dW_\nu^{(2)}, \quad (3.10)$$

$$dW_\nu^{(1)} = \frac{1}{\pi\sqrt{3}}\,\frac{ce^2}{R^2}\,\varepsilon_0\nu\, d\nu \int_{\frac{2}{3}\frac{\nu}{1-\nu/2n}\varepsilon_0^{3/2}}^\infty K_{5/3}(x)\, dx, \quad (3.10a)$$

$$dW_\nu^{(2)} = \frac{1}{\pi\sqrt{3}}\,\frac{ce^2}{R^2}\,\varepsilon_0\nu\, d\nu \left(\frac{\nu}{2n}\right)^2\left(1-\frac{\nu}{2n}\right)^{-1} \times K_{2/3}\left(\frac{2}{3}\,\frac{\nu}{1-\nu/2n}\,\varepsilon_0^{3/2}\right). \quad (3.10b)$$

These formulas are correct for energies $E \ll E_{1/2} = mc^2\,(2Rmc/3h)^{1/2}$, as well as for energies $E \sim E_{1/2}$ and $E \gg E_{1/2}$, for the radiation of the entire spectrum. The formulas for the differential spectrum which were obtained earlier by Sokolov and Ternov[5] and Schwinger[6], and which are exact to within magnitudes of the first order in h, are special cases of formula (3.10) and may easily be obtained from it. For example, taking account of the fact that

$$\nu = \omega/\omega_0, \qquad 1/2n = (h/Rmc)\,(mc^2/E),$$

$$\varepsilon_0 = 1-\beta^2 = (mc^2/E)^2,$$

$$\omega_c = {}^3/_2\,\omega_0\,(E/mc^2)^3,$$

we immediately obtain from Eq. (3.10a)

$$dW^{(1)} \approx \frac{3\sqrt{3}}{4\pi}\,\frac{e^2}{R}\left(\frac{E}{mc^2}\right)^4 \frac{\omega_0\omega}{\omega_c^2}\, d\omega \times \int_{(\omega/\omega_c)/(1-\hbar\omega/E)}^\infty K_{5/3}(x)\, dx, \quad (3.11)$$

for $(h\omega/E) \ll 1$, and this coincides with Schwinger's formula. Similarly, we may obtain Sokolov and Ternov's formula, for which the same limiting condition holds.

In order to analyze the spectra it is convenient to transform to another variable $\xi = h\omega/E$. Then the formula for the differential spectrum of the "radiating" electron takes the following form:

$$dW = \frac{ce^2}{\pi\sqrt{3}}\left(\frac{mc}{h}\right)^2 \xi\, d\xi\left[\int_{\xi/(1-\xi)\zeta}^\infty K_{5/3}(x)\, dx + \frac{\xi^2}{1-\xi}\, K_{2/3}\left(\frac{\xi}{1-\xi}\,\frac{1}{\zeta}\right)\right], \quad (3.12a)$$

while the formula characterizing the radiation of the spinless particle is given by the equation

$$dW^{(1)} = \frac{ce^2}{\pi\sqrt{3}}\left(\frac{mc}{h}\right)^2 \xi\, d\xi \times \int_{\xi/(1-\xi)\zeta}^\infty K_{1/3}(x)\, dx, \quad \zeta = \frac{3}{2}\,\frac{h}{Rmc}\left(\frac{E}{mc^2}\right)^2. \quad (3.12b)$$

In the cases which are most interesting from the point of view of the influence of spin, namely, those of extremely relativistic energies ($\zeta \gg 1$), the following formulas, applicable to almost the entire spectrum, excluding the part in immediate proximity to the high frequency end, are obtained from Eq. (3.12):

a) for the electron

$$dW \approx \frac{ce^2}{R^2}\frac{3^{1/6}\,\Gamma(2/3)}{\pi}\left(\frac{Rmc}{h}\right)^{4/3}\left(\frac{E}{mc^2}\right)^{4/3} \times d\xi\xi^{1/3}(1-\xi)^{2/3}(1+\xi^2/2(1-\xi)), \tag{3.13a}$$

b) for the spinless particle

$$dW^{(1)} \approx \frac{ce^2}{R^2}\frac{3^{1/6}\,\Gamma(2/3)}{\pi}\left(\frac{Rmc}{h}\right)^{4/3} \times \left(\frac{E}{mc^2}\right)^{4/3} d\xi\xi^{1/3}(1-\xi)^{2/3}. \tag{3.13b}$$

The formulas obtained allow us to investigate the differential spectrum of the electron and the spinless particle for any energies. From the formulas for the differential spectrum it is immediately clear that for arbitrary energies and for the entire spectral region the spectrum of the radiating boson lies below the spectrum of the radiating electron. For increasing energies ($\zeta \to \infty$) the maximum density of the radiation of the electron comes together at the far end of the spectrum. The maximum density of the boson's radiation does not coalesce at the end of the spectrum in this case, but comes together at a point of the spectrum lying at approximately one third the distance from the beginning. A very typical case, showing the difference between the spectra of the radiating electron and boson, is shown in Fig. 1. This

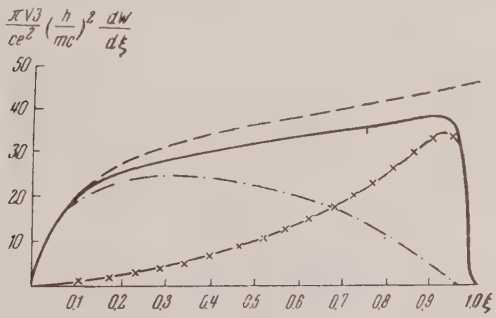

FIG. 1.

Figure shows the spectra for $\zeta = 100$. The spectrum of the electron is shown by the continuous line, while the "dash-dot" line shows the spectrum of the boson, and the "dash-cross" line shows the "difference" in density of the radiation of the electron and boson (the "role of spin"). The dashed line shows the spectrum given by classical theory. The remaining part of the spectrum given by classical theory, that on the high-frequency side, is not shown in the Figure, since, in virtue of the law of conservation of energy, these higher frequencies cannot actually be radiated.

It is clear from Fig. 1 that the difference in density of the radiation of the electron and boson is quite significant in this extreme relativistic case, and that the main contribution to the density of radiation is produced in the second half of the spectrum "at the expense of spin".

4. TOTAL ENERGY OF RADIATION

In order to obtain the total energy of radiation we must carry out an integration over ν in Eq. (3.10). Changing the variable of integration to

$$x = \frac{2}{3}\frac{\nu}{1-\nu/2n}\varepsilon_0^{3/2}, \tag{4.1}$$

we can represent the total energy of radiation in the form

$$W = W_{kl}\,\varphi(\zeta), \quad \varphi(\zeta) = \varphi^{(1)}(\zeta) + \zeta^2\varphi^{(2)}(\zeta); \tag{4.2}$$

$$\varphi^{(1)}(\zeta) = \frac{9\sqrt{3}}{16\pi}\int_0^\infty \frac{x^2K_{5/3}(x)\,dx}{(1+\zeta x)^2}; \tag{4.3}$$

$$\varphi^{(2)}(\zeta) = \frac{9\sqrt{3}}{8\pi}\int_0^\infty \frac{x^3K_{2/3}(x)\,dx}{(1+\zeta x)^4}. \tag{4.4}$$

These integrals may be evaluated with the help of Mellin transformation theory. The integral for $\varphi^{(1)}(\zeta)$ with respect to ζ is absolutely convergent ($\zeta > 0$). The integral

$$Q(\zeta) = \int_0^\infty \frac{xK_{5/3}(x)\,dx}{1+\zeta x} \tag{4.5}$$

is also absolutely convergent. Hence, Eq. (4.3) can be written in the form

$$\varphi^{(1)}(\zeta) = -(9\sqrt{3}/16\pi)\,\partial Q/\partial\zeta. \tag{4.6}$$

Using the same method used in obtaining the formulas for the differential spectrum, we can show that

$$Q = \frac{\pi}{4}\alpha^2\frac{1}{2\pi i} \times \int_{k-i\infty}^{k+i\infty} \frac{\Gamma(s/2-5/6)\,\Gamma(s/2+5/6)}{\sin\pi s}\left(\frac{\alpha}{2}\right)^{-s} ds, \tag{4.7}$$

$$\alpha = 1/\zeta, \quad 5/3 < k < 2.$$

On evaluating this integral we obtain

$$Q(\zeta) = -\frac{2}{3}\pi^2 \frac{1}{\zeta^2}\left[\Phi_{5/3}\left(\frac{i}{\zeta}\right) + \frac{\sqrt{3}}{2\pi}\zeta\right], \tag{4.8}$$

where we have introduced the notation

$$\Phi_\nu(z) = i^{-\nu}[J_\nu(z) - \mathbf{J}_\nu(z)] + i^{\nu}[J_{-\nu}(z) - \mathbf{J}_{-\nu}(z)], \tag{4.8a}$$

and J_ν and $\mathbf{J}_\nu$ are the well-studied functions of Bessel and Anger.

An evaluation of (4.4) by an analogous method leads to the integral

$$\int_0^\infty \frac{K_{2/3}(x)\,dx}{1+\zeta x} = \frac{\pi^2}{2\sin^2(2\pi/3)}\frac{1}{\zeta}\Phi_{2/3}\left(\frac{i}{\zeta}\right). \tag{4.9}$$

Hence, we finally obtain the following expressions for the total energy of radiation:

a) for the electron

$$W = W_{kl}\varphi(\zeta),\ \varphi(\zeta) = \frac{3\sqrt{3}}{8}\pi\left\{\frac{\partial}{\partial\zeta}\frac{\Phi_{5/3}(i/\zeta)}{\zeta^2} - \frac{\zeta^2}{3}\frac{\partial^3}{\partial\zeta^3}\frac{\Phi_{2/3}(i/\zeta)}{\zeta} - \frac{\sqrt{3}}{2\pi}\frac{1}{\zeta^2}\right\}, \tag{4.10a}$$

b) for the spinless particle

$$W^{(1)} = W_{kl}\varphi^{(1)}(\zeta), \tag{4.10b}$$

$$\varphi^{(1)}(\zeta) = \frac{3\sqrt{3}}{8}\pi\left\{\frac{\partial}{\partial\zeta}\frac{\Phi_{5/3}(i/\zeta)}{\zeta^2} - \frac{\sqrt{3}}{2\pi}\frac{1}{\zeta^2}\right\}.$$

In order to find the asymptotic expressions for the total energy of radiation for $\zeta \ll 1$, it is necessary to use the well-known asymptotic expansion of the Anger functions[8], with the aid of which we obtain

$$\varphi(\zeta) \approx 1 - \frac{55\sqrt{3}}{24}\zeta + \frac{64}{3}\zeta^2 - \frac{8855\sqrt{3}}{108}\zeta^3 + \frac{89600}{81}\zeta^4 - \ldots \tag{4.11a}$$

$$\varphi^{(1)}(\zeta) \approx 1 - \frac{55\sqrt{3}}{24}\zeta + \frac{56}{3}\zeta^2 - \frac{6545\sqrt{3}}{108}\zeta^3 + \frac{56000}{81}\zeta^4 - \ldots \tag{4.11b}$$

The asymptotic expansion (4.11a) of the exact formula (4.10a) coincides with the asymptotic expansion found in Ref. 4 by direct evaluation of the total energy of radiation in the asymptotic sense.

The first correction term was evaluated by Sokolov, Klepikov and Ternov[7]. This term has also recently been obtained by Schwinger[6].

For $\zeta \gg 1$ we may use series for the Bessel and Anger functions and keep the desired number of terms. As follows directly from Eq. (4.10), the main terms in the total energy of radiation have the following form:

a) for the electron

$$W^{(\infty)} \approx (32\,\Gamma(2/3)/(27\cdot 3^{4/3})) \times (ce^2/R^2)(Rmc/h)^{4/3}(E/mc^2)^{4/3}; \tag{4.12a}$$

b) for the spinless particle

$$W^{(1)(\infty)} \approx (2\Gamma(2/3)/(3\cdot 3^{4/3})) \times (ce^2/R^2)(Rmc/h)^{4/3}(E/mc^2)^{4/3}. \tag{4.12b}$$

It is clear from this that in the extreme relativistic case ($\zeta \gg 1$) the spinless particle radiates only approximately 9/16th as much as the electron. Thus the "role of spin" is very significant in the radiation in the extreme relativistic case.

In the case of $\zeta \ll 1$ the "role of spin" is determined by the ratio obtained from Eqs. (4.11a) and (4.11b).

$$\frac{W}{W^{(1)}} \approx 1 + \frac{8}{3}\zeta^2 - \frac{275\sqrt{3}}{18}\zeta^3 + \ldots \tag{4.13}$$

Thus it is clear that in this case the spin corrections are of second order of smallness as compared to the quantum corrections (second order in h). This is the reason that Schwinger[6], in calculating the first quantum correction for the radiation from the spinless particle, obtained the same result which Sokolov, Klepikov and Ternov[7] obtained earlier from the Dirac electron.

It should be remarked that for $h \to 0$ the exact formulas (2.17a) and (2.17b) go over into the exact formulas of the classical theory of the radiation from a "radiating" electron. This may be shown with the help of the relation

$$\lim_{n\to\infty;\ \nu,z\neq 0} I_{n,n-\nu}\left(\frac{z^2}{4n}\right) = J_\nu(z). \tag{4.14}$$

It follows from this that there must be no factor of type $1 + (mc^2/E)^2$ in the formulas, since this factor does not depend on h and does not disappear for a transition to the classical limit $h \to 0$.

With respect to the physical reason for the difference in the radiation of the electron and the spinless particle, Sokolov (see Ref. 3) has shown

that in the case of extreme relativistic energies this difference evidently depends on the behavior characteristics of the spin magnetic moment of the electron. It should be noted, first of all, that in the relativistic case the electron, in a manner of speaking, "loses" its magnetic moment in accordance with the formula

$$\mu \approx \mu_0 mc^2/E, \quad \mu_0 = eh/2mc. \qquad (4.15)$$

However, on the other hand, with increasing energy the interaction with the high-frequency parts of the virtual field of the photons plays an increasingly significant role in the radiation.

The matrix elements characterizing the radiation at the expense of the magnetic moment and at the expense of the charge interaction are proportional to the magnitudes $\sim \mu H \sim \mu \varkappa A$ and $\sim eA$, respectively. Consequently, the ratio of the energy of radiation W_μ at the expense of the magnetic moment to the energy of radiation W_e at the expense of the charge interaction is equal to $(W_\mu/W_e) \sim (\mu\omega_{max}/ec)^2$ in order of magnitude. In the case of $\zeta \ll 1$, the maximum frequency is given by $\omega_{max} \approx \omega_0 (E/mc^2)^3$, while for $\zeta \gg 1$ it is given by $\omega_{max} \approx E/h$. Hence, we obtain at once

$$W_\mu / W_e \sim \begin{cases} \zeta^2 & \text{for } \zeta \ll 1, \\ 1 & \text{for } \zeta \gg 1. \end{cases}$$

Thus the statement of Sokolov corresponds completely with the results of the present work.

I wish to express my gratitude to Professors A. A. Sokolov, N. P. Klepikov and I. M. Ternov for many discussions of the questions considered in the present work.

[1] M. Neuman, Phys. Rev. 90, 682 (1953).

[2] N. F. Nelipa, J. Exptl. Theoret. Phys. (U.S.S.R.) 27, 421 (1954).

[3] Sokolov, Matveev and Ternov, Dokl. Akad. Nauk SSSR 102, 65 (1955).

[4] N. P. Klepikov, J. Exptl. Theoret. Phys. (U.S.S.R.) 26, 19 (1954).

[5] A. A. Sokolov, and I. M. Ternov, J. Exptl. Theoret. Phys. (U.S.S.R.) 25, 698 (1953).

[6] J. Schwinger, Proc. Natl. Acad. Sci. U.S. 40, 132 (1954).

[7] Sokolov, Klepikov and Ternov, J. Exptl. Theoret. Phys. (U.S.S.R.) 24, 249 (1953).

[8] G. N. Watson, *A Treatise on the Theory of Bessel Functions* (Macmillan, New York, 1945), Chapter X.

Translated by M. G. Gibbons
92

SOVIET PHYSICS JETP VOLUME 4, NUMBER 3 APRIL, 1957

Two-Nucleon Potential of Intermolecular Type and Nuclear Saturation

D. D. IVANENKO AND B. K. KERIMOV
Moscow State University

(Submitted to JETP editor, April 18, 1955)
J. Exptl. Theoret. Phys. (U.S.S.R.) 31, 105-112 (July, 1956)

A study is made of the statistical model of the nucleus with uniform density distribution of the nucleons, on the basis of a two-nucleon interaction potential of the type of the Lennard-Jones intermolecular potential with a hard barrier. It is shown that saturation can be obtained with a certain choice of the parameters in the potential.

1. THE explanation of the stability of atomic nuclei is one of the main problems of the theory of nuclear structure, directly related to the explanation of saturation, which consists of the fact that in medium-weight and heavy nuclei the density of nucleons and the binding energy per nucleon are roughly constant. The existence of saturation has always placed restrictions on the choice of one or another kind of theory of the nuclear forces, which it is still impossible to determine uniquely. At first it seemed possible to achieve saturation by means of exchange forces of various kinds.[1] But the data on the scattering of nucleons (n–p and p–p) at moderately high energies ($\gtrsim$ 100 mev)

evidently show that the exchange forces play a considerably smaller part than is needed for the explanation of saturation. It is also impossible to explain saturation if the nuclear forces are only nonexchange forces of attraction, for example in the form of a rectangular well or a Yukawa potential. In such a case the collapsed state would have to be the most stable one. In recent papers[2-4] it has been shown that a two-nucleon central potential, consisting of a spin-exchange force of large magnitude and a repulsive Wigner force of relatively small magnitude (with radial dependences of the form $e^{-k_0 r}/r$), leads to the observed saturation of the nuclear density and binding energy. On the other hand, it has recently been suggested[5] that there is a possibility of explaining saturation by taking into account many-particle forces acting between three and more nucleons. In this case it turned out that the introduction of (non-exchange) many-particle repulsive forces (mainly involving three particles) obtained from the pseudoscalar meson theory leads to a qualitative explanation of the observed saturation. It is still of interest to examine in more detail the influence of two-particle repulsive forces on the saturation.

In the present paper we show the possibility of explaining saturation on the basis of a semi-phenomenological two-nucleon interaction potential of the type of the intermolecular potential of Lennard-Jones, involving a hard wall, containing an ordinary nonexchange repulsive force acting at small distances along with the attractive Yukawa force. For simplicity, we shall not include spin terms; their role in saturation has been elucidated previously.[2-4] Without trying at present to fix the precise form of the two terms of the potential, which is obviously not yet essential, we must emphasize that the explanation of a fairly considerable number of experimental facts about the scattering of nucleons in all probability demands that, along with the attractive forces at distances $r > r_c$, there also be present a strong repulsion at small distances $r < r_c$.[6,7] We shall show that a special law of this type, of a form that can be generalized without difficulty (for example by adding our repulsive term to the "best" known potential from pseudoscalar mesodynamics) can explain the absence of a collapsed state in nuclei, just as is found for liquids and solids. Despite the fact that the presence of some repulsive part in nuclear forces at the smallest distances can evidently be inferred also on the basis of theoretical considerations[6,7] (though not completely conclusive ones) and also from certain hypothetical models of the structure of nucleons, one still must not forget the preliminary nature of both the empirical and the theoretical arguments in favor of such forces: precise choice of the shape of the potential remains out of the question.

Accordingly we assume that repulsive forces act between two nucleons at distances $r > r_c$ along with fuses of attraction, and at distances $r < r_c$ there exists only a stronger repulsion ("hard core"):

$$U_{12}(r) = +\infty, \quad \text{if} \quad r < r_c; \qquad U_{12}(r) = B\frac{e^{-r/a}}{(r/a)^2} - C\frac{e^{-r/a}}{r/a}, \quad \text{if} \quad r > r_c. \tag{1}$$

B and C are parameters to be determined later; $r \equiv r_{12} = |\mathbf{r}_1 - \mathbf{r}_2|$ is the distance between nucleons 1 and 2. The choice of the nucleon potential in the form (1) means that the nucleons behave like hard spheres of diameter r_c interacting through the nuclear potential.

In the case of an interaction potential with a repulsive core r_c the wave function Ψ of the ground state of a nucleus containing A particles can be written as a product of a Slater determinant and a symmetric function $\Theta(r_1, r_2, \ldots, r_A)$ of the space coordinates of the A nucleons:[5]

$$\Psi = \left(\frac{1}{\sqrt{A!}}\sum_{P}^{A!}(-1)^P \prod_{i=1}^{A}\psi_i(q_i)\right) \times \Theta(\mathbf{r}_1, \mathbf{r}_2, \ldots \mathbf{r}_A), \tag{2}$$

where $\psi_i(q_i)$ is the wave function of the ith nucleon

$$\psi_i(q_i) = \psi_i(\mathbf{r}_i)\, a_i(s_i) = \Omega^{-1/2}\exp\{i\mathbf{k}_i\mathbf{r}_i\}\, a_i(s_i), \tag{3}$$

$a_i(s_i)$ is the spin function of the ith particle, and $\Omega = (4\pi/3)R^3$ is the volume of the nucleus.

The introduction of the spatial correlation between the A particles by means of the factor Θ assures the fulfillment of the boundary conditions requiring that the wave function (2) vanish when any two nucleons approach each other to a distance $r \leq r_c$. For simplicity we take the function Θ in a form that takes into account only the correlation between pairs of nucleons:

$$\Theta(\mathbf{r}_1, \mathbf{r}_2, \ldots \mathbf{r}_A) = \sum_{i<j=1}^{A} g(r_{ij}) \tag{4}$$

(where $r_{ij} \equiv |\mathbf{r}_i - \mathbf{r}_j|$), omitting for the present the

obvious generalizations to take into account various configurations inside the nucleus (deuteron, α -particle, etc.) which could be stimulated by many-particle forces. For simplicity we assume $g(r_{ij})$ to be a simple step function

$$g(r_{ij}) = \begin{cases} 1, & r_{ij} > r_c \\ 0, & r_{ij} < r_c . \end{cases} \tag{5}$$

By means of Eqs. (1) to (4) we obtain from the equation defining the mean value of the potential energy operator

$$V = \int \Psi^* U \Psi_{12} d\mathbf{r}_1 \ldots d\mathbf{r}_A, \tag{6}$$

the following expression for the total average potential energy of a nucleus composed of A nucleons

$$V = V^0 + V^a, \tag{7}$$

where

$$V^0 = \frac{1}{2} B \iint (d\mathbf{r}_1)(d\mathbf{r}_2) \frac{e^{-r/a}}{(r/a)^2} \rho^2 g^2(r_{12}) \tag{8}$$

$$- \frac{1}{2} C \iint (d\mathbf{r}_1)(d\mathbf{r}_2) \frac{e^{-r/a}}{r/a} \rho^2 g^2(r_{12}); \tag{9}$$

$$V^a = \frac{1}{4} C \iint (d\mathbf{r}_1)(d\mathbf{r}_2) \frac{e^{-r/a}}{r/a} |\rho(\mathbf{r}_1, \mathbf{r}_2)|^2 g^2(r_{12})$$

$$- \frac{1}{4} B \iint (d\mathbf{r}_1)(d\mathbf{r}_2) \frac{e^{-r/a}}{(r/a)^2} |\rho(\mathbf{r}_1, \mathbf{r}_2)|^2 g^2(r_{12}).$$

For the ordinary and matrix densities of the nucleons $\rho(r)$ and $\rho(\mathbf{r}_1, \mathbf{r}_2)$, we have by Eq. (3)

$$\rho(\mathbf{r}_1, \mathbf{r}_2) = \sum_{i=1}^{A} \psi_i^*(\mathbf{r}_i) \psi_i(\mathbf{r}_2) \tag{10}$$

$$= 3\rho(\mathbf{r}) \frac{\sin Kr - Kr \cos Kr}{(Kr)^3},$$

$$\rho(\mathbf{r}) = \rho(\mathbf{r}_1, \mathbf{r}_1) \tag{11}$$

$$= \sum_{i=1}^{A} \psi_i^*(\mathbf{r}) \psi_i(\mathbf{r}) = \frac{2}{3\pi^2} K^3,$$

where K is the maximum magnitude of the wave number k of a nucleon in the Fermi distribution. The density $\rho(r)$ must satisfy the condition

$$\int \rho \, d\tau = A. \tag{12}$$

Using Eqs. (5) and (10) and the relation

$$\int (d\mathbf{r}_1)(d\mathbf{r}_2) F(r_{12}) g^2(r_{12}) \tag{13}$$

$$= \Omega \int_{r > r_c} (d\mathbf{r}) F(r),$$

we obtain from Eq. (9), after integration, the exchange potential energy of the nucleus as a function of the density of the nucleon distribution in the form

$$V^a = Q_1 \Omega F_1(b_0, \varkappa_0, \rho) \tag{14}$$

$$+ \frac{Q_0}{5} \Omega F_1(b_0, \varkappa_0, \rho) - \frac{Q_0}{10} \Omega \left[F_0(b_0, \varkappa_0, \rho) \right.$$

$$\left. - \frac{1}{12\varkappa_0^2} \rho^{2/3} (Z - Z_2) + \left(\frac{1}{8\varkappa_0^3} \rho + \frac{1}{24\varkappa_0^5} \rho^{5/3} \right) Z_1 \right].$$

Here

$$F_0(b_0, \varkappa_0, \rho) = e^{-b_0} \left[\frac{1}{b_0^5} - \frac{\varphi_3(b_0)}{\varkappa_0^2} \rho^{2/3} \right. \tag{15}$$

$$- \left(\frac{1}{b_0^5} - \frac{\varphi_2(b_0)}{\varkappa_0^2} \rho^{2/3} \right.$$

$$\left. + \frac{1}{24 b_0 \varkappa_0^4} \rho^{4/3} \right) \cos \frac{b_0}{\varkappa_0} \rho^{1/3}$$

$$\left. - \left(\frac{1}{\varkappa_0 b_0^4} \rho^{1/3} + \frac{1}{24} \frac{b_0 + 1}{b_0^2 \varkappa_0^3} \rho \right) \sin \frac{b_0}{\varkappa_0} \rho^{1/3} \right];$$

$$F_1(b_0, \varkappa_0, \rho) = \frac{1}{8} e^{-b_0} \left[\varphi(b_0) + \frac{1}{2b_0} \left(\frac{1}{b_0} - 1 \right) \frac{1}{\varkappa_0^2} \rho^{2/3} \right.$$

$$+ \left(- \varphi(b_0) + \frac{1}{3 b_0 \varkappa_0^2} \rho^{2/3} \right) \cos \frac{b_0}{\varkappa_0} \rho^{1/3}$$

$$\left. + \left(- b_0 \varphi(b_0) - \frac{1}{6} \right) \frac{\rho^{1/3}}{\varkappa_0} \sin \frac{b_0}{\varkappa_0} \rho^{1/3} \right]$$

$$+ \left(\frac{1}{48} + \frac{1}{16\varkappa_0^2} \rho^{2/3} \right) (Z - Z_2) - \frac{1}{24\varkappa_0^3} \rho Z_1;$$

$$Q_0 = 576 \pi B a^3 \varkappa_0^6; \quad Q_1 = 576 \pi C a^3 \varkappa_0^6;$$

$$b_0 = r_c / a; \quad \varkappa_0 = b_0 / \alpha.$$

$$\varphi(b_0) = \frac{1}{b_0^4} - \frac{1}{3b_0^3} + \frac{1}{6b_0^2} - \frac{1}{6b_0}; \quad Z = \int_{\varkappa_0}^{\infty} \frac{e^{-\alpha u}}{u} du;$$

$$\varphi_2(b_0) = \frac{1}{12}\left(\frac{1}{b_0^3} + \frac{1}{b_0^2} - \frac{1}{b_0}\right); \tag{16}$$

$$Z_1 = \int_{x_0}^{\infty} e^{-\alpha u} \sin u \frac{du}{u};$$

$$\varphi_3(b_0) = \frac{1}{12}\left(-\frac{5}{b_0^3} + \frac{1}{b_0^2} - \frac{1}{b_0}\right);$$

$$Z_2 = \int_{x_0}^{\infty} e^{-\alpha u} \cos u \frac{du}{u};$$

$$\alpha = \varkappa_0 \rho^{-1/3}; \quad \varkappa_0 = (1/2a)(2/3\pi^2)^{1/3}.$$

After integration we obtain from Eq. (8) the expression for the ordinary potential energy,

$$V^0 = {}^1/_2 B\rho^2 4\pi a^3 e^{-b_0}\Omega \tag{17}$$
$$- {}^1/_2 C\rho^2 4\pi a^3 e^{-b_0}(1 + b_0)\Omega.$$

The expressions (14) and (17) give the potential energy of a nucleus of nucleons distributed with constant density ρ in the volume Ω. For $\rho = \rho_0 = \text{const}$ for $r \leq R$ and $\rho = 0$ for $r > R$, we have from (12)

$$\rho = A/\Omega = 3A/4\pi R^3. \tag{18}$$

From this we get the potential energy of the nucleus as a function of its radius R and the parameters of the interaction potential

$$V = V^0 + V^a = \frac{3}{2} Be^{-b_0} a^3 \frac{A^2}{R^3} \tag{19}$$
$$- \frac{3}{2} e^{-b_0}(1 + b_0) Ca^3 \frac{A^2}{R^3}$$
$$- \frac{8}{15\pi^2} B\Phi_1(b_0, a, R)$$
$$+ \frac{16}{15\pi^2}(B + 5C)\Phi_2(b_0, a, R);$$

$$\Phi_1(b_0, a, R) = \frac{R^3}{a^3} F_0(b_0, \varkappa_0, \rho); \tag{20}$$

$$\Phi_2 = \frac{R^3}{a^3} F_1(b_0, \varkappa_0, \rho)$$

with $\rho = 3A/4\pi R^3$.

In the case of nucleons regarded as impenetrable spheres of radius r_c, the kinetic energy of a gas consisting of A nucleons contains, in addition to the Fermi term, a supplementary term $\sim r_c$.[5]

$$T = T_F\left(1 + \frac{2{,}16\, r_c A^{1/3}}{R}\right) \tag{21}$$
$$= \left(\frac{3}{\pi}\right)^{4/3} \frac{3}{160} \frac{\hbar^2}{MR^2} A^{5/3}\left[1 + \frac{2{,}16\, r_c A^{1/3}}{R}\right].$$

The total energy is

$$E = V + T = V^0 + V^a + T. \tag{22}$$

From the requirement that the energy E be a minimum it follows that the value of the parameter R corresponding to the equilibrium state of the nucleus must be proportional to $A^{1/3}$. To determine the values of the potential parameters that give the equilibrium state we make use of an empirical value of the radius R_s of the nucleus. For this purpose we set

$$R = R_s x = r_0 A^{1/3} x. \tag{23}$$

The dimensionless quantity x determines the variation of the radius of the nucleus around its equilibrium value $R_s = r_0 A^{1/3}$. For $x = 1$ we have the stable radius $R = R_s = r_0 A^{1/3}$, which corresponds to a state of the nucleus with normal density. For the empirical constant r_0 we can take from the experimental data one of the two values (cf. Refs. 5, 8, 9, 10)

$$r_0 \approx 1.4 \times 10^{-13} \text{ cm}, \tag{24}$$

$$r_0 \approx 1{,}2 \times 10^{-13} \text{ cm}. \tag{25}$$

Using Eq. (23), we get from Eqs. (19), (21) and (22) the expression for the total energy of the nucleus

$$E = T + V^0 + V^a \tag{26}$$
$$= \left\{\left(\frac{a_2}{x^2} + \frac{b_2}{x^3}\right) + \frac{(a_0 - a_1)}{x^3}\right.$$
$$\left. - (a_3 \Psi_1(b_0, \beta x) - a_4 \Psi_2(b_0, \beta x))\right\} A.$$

Here

$$a_0 = \frac{3e^{-b_0}}{2\beta^3} B, \quad a_1 = \frac{3e^{-b_0}(1+b_0)}{2\beta^3} C;$$

$$a_3 = \frac{8}{15\pi^2} B, \quad a_4 = \frac{16}{15\pi^2}(B + 5C);$$

$$a_2 = \left(\frac{3}{\pi}\right)^{1/3} \frac{3h^2}{160\, M r_0^2}, \quad b_2 = 2{,}16\, a_2 b,$$

$$\beta = \frac{r_0}{a}, \quad b = \frac{r_c}{r_0}, \quad b_0 = \frac{r_c}{a};$$

$$\Psi_1(b_0, \beta x) = \Phi_1(b_0, a, R),$$

$$\Psi_2(b_0, \beta x) = \Phi_2(b_0, a, R)$$

with $R = r_0 A^{1/3} x$.

From the stability conditions

$$(\partial E / \partial x)_{x=1} = 0, \quad (\partial^2 E / \partial x^2)_{x=1} > 0 \qquad (27)$$

and the empirical value of the binding energy, found without taking into account the Coulomb and surface energies,

$$(E(x))_{x=1} = -\alpha_0 A, \quad \alpha_0 \approx 14 \text{ mev} \qquad (28)$$

we find the parameters B and C as functions of the constants b_0, β and r_0 in the form

$$B = \frac{1}{P(b_0, \beta)} \left\{ 3\alpha_0 + a_2 + 10\, n_0 (2a_2 + 3b_2) \times \frac{3\Psi_2(b_0, \beta) + \Psi_2'(b_0, \beta)}{n_2 + 10\, n_0 \Psi_2'(b_0, \beta)} \right\} = \chi_1(b_0, \beta, r_0); \qquad (29)$$

$$C = \frac{2a_2 + 3b_2 + [n_1 + n_0 \Psi_1'(b_0, \beta) - 2n_0 \Psi_2'(b_0, \beta)] B}{n_2 + 10 n_0 \Psi_2'(b_0, \beta)} = \chi_2(b_0, \beta, r_0);$$

$$P(b_0, \beta) = [3\Psi_1(b_0, \beta) + \Psi_1''(b_0, \beta)] n_0 - [3\Psi_2(b_0, \beta) + \Psi_2''(b_0, \beta)] 2n_0 - 10\, n_0 \frac{3\Psi_2(b_0, \beta) + \Psi_2'(b_0, \beta)}{n_2 + 10\, n_0 \Psi_2'(b_0, \beta)} \times [n_1 + n_0 \Psi_1'(b_0, \beta) - 2n_0 \Psi_2'(b_0, \beta)],$$

$$n_0 = 8/15\pi^2; \quad n_1 = 9e^{-b_0}/2\beta^3; \quad n_2 = 9e^{-b_0}(1 + b_0)/2\beta^3,$$

$\Psi_1(b_0, \beta)$, $\Psi_2'(b_0, \beta)$, etc. are the values of the functions $\Psi_1(b_0, \beta x)$ $\Psi_2(b_0, \beta x)$ and their derivatives at $x = 1$.

Substituting Eqs. (29) into the inequality of (27), we have

$$6a_2 + 12b_2 + 4(n_1\chi_1(b_0, \beta, r_0) - n_2\chi_2(b_0, \beta, r_0)) - n_0\Psi_1''(b_0, \beta) + 2n_0(\chi_1(b_0, \beta, r_0) + 5\chi_2(b_0, \beta, r_0))\Psi_2''(b_0, \beta) > 0. \qquad (30)$$

Moreover, the expressions for $\Psi_1(b_0, \beta)$, $\Psi_2(b_0, \beta)$, and their derivatives involve the values of the integrals (16) and their derivatives for $x = 1$, the function

$$Z = -\operatorname{Ei}(-b_0) = \int_{b_0}^{\infty} \frac{e^{-w}\, dw}{w}$$

and so on.

2. For given values of the constants r_0 and a consistent with the experimental data the inequality (30) makes it possible to set a lower limit to the values of the parameter $b_0 = r_c / a$ for which the nucleus can be in equilibrium. We assume that the effective radius of action of the two-nucleon force (1) is equal to the Compton wavelength of the π-meson:

$$a = h / 2\pi m_\pi c = 1.4 \times 10^{-13} \text{ cm}. \qquad (31)$$

For the values (24) and (31) of the quantities r_0, a, the inequality (30), which corresponds to the possibility of nuclear equilibrium, can be satisfied if $b_0 = r_c / a > 0.357$, or $r_c > 0.357\, a = 0.5 \times 10^{-13}$ cm. Thus the existence of an equilibrium state of the system of nucleons imposes a lower limit on the value of the radius r_c of the repulsive core of the assumed interaction potential (1). With the values $b_0 = 0.38$ and $b_0 = 0.43$, corresponding to the values of r_c used also in Refs. 5,6 and 7, we finally obtain from Eqs. (29), (31), and (24) the following systems of values for the parameters of our chosen two-nucleon potential (1):

$$B = 395.56 \text{ mev}; \quad C = 278.64 \text{ mev}; \qquad (32)$$

$$a = 1.4 \times 10^{-13} \text{ cm};$$

$$r_0 = 1.4 \times 10^{-13} \text{ cm}; \quad b_0 = r_c / a = 0.38;$$

$$r_c = 0.532 \times 10^{-13} \text{ cm};$$

and

$$B = 935.167 \text{ mev}; \quad C = 610.029 \text{ mev}; \qquad (33)$$

$$a = 1{,}4\times10^{-13} \text{ cm};$$

$$r_0 = 1.4\times10^{-13} \text{ cm}; \quad b_0 = r_c/a = 0.43;$$

$$r_c = 0.6\times10^{-13} \text{ cm}.$$

The ordinary repulsive potential energy $V^0/A = (a_0 - a_1)/x^3$, the exchange attractive potential energy $V^a/A = -a_3\Psi_1 + a_4\Psi_2$, and the total energy per nucleon, $E/A = V^0/A + V^a/A + T/A$ are shown as functions of the nuclear radius $x = R/r_0A^{1/3}$ in Figs. 1 and 2, for the values of

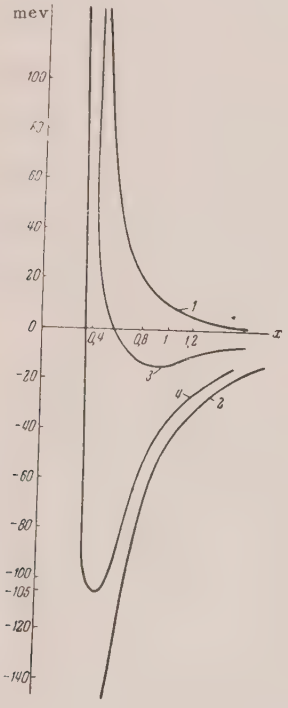

FIG. 1. Dependence on nuclear radius R of 1) the ordinary repulsive potential energy V^0/A, 2) the exchange attractive potential energy V^a/A, 3) the total energy per nucleon E/A, and 4) the sum $(V^0/A)+(V^a/A)$, for the parameter values (32).

the parameters given in Eqs. (32) and (33). From these diagrams it is seen that the total potential energy $(V^0/A)+(V^a/A)$ of the nucleons in the case of forces given by Eq. (1) has a minimum value

$$W/A = V^0/A + V^a/A \approx -105 \text{ mev}$$

for the case corresponding to Eq. (32), at a nuclear radius $R = R_0 \approx 0.5\, r_0 A^{1/3} = 0.7\times10^{-13}A^{1/3}$, and a minimum value $W/A \approx -51$ mev for the case corresponding to Eq. (33), at a nuclear radius $R = R_0 \approx 0.8\, r_0 A^{1/3} = 1.12\times10^{-13}A^{1/3}$. Finally, for values of the constants r_0 and a from Eqs. (25) and (31) and $b_0 = 0.38$, we have from (29)

$$B = 321{,}580 \text{ mev}, \; C = 228{,}970 \text{ mev},$$
$$a = 1.4\times10^{-13} \text{ cm}, \qquad (34)$$
$$r_0 = 1.2\times10^{-13} \text{ cm}, \; b_0 = r_c/a = 0.38,$$
$$r_c = 0.532\times10^{-13} \text{ cm}.$$

For the parameter values (34) the total potential energy $W/A = V^0/A + V^a/A$ has a minimum value of ~ -128.2 mev at nuclear radius $R = R_0 = 0.5r_0A^{1/3} = 0.6\times10^{-13}$ cm. Because of the presence of the short-range repulsive force ($\sim Be^{-x}/x^2$) in

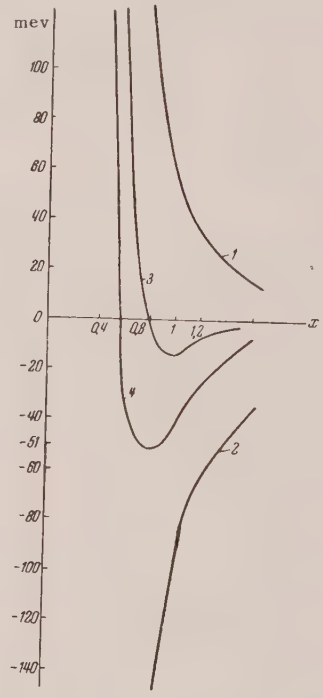

FIG. 2. Dependence on the nuclear radius R of 1) V^0/A, 2) V^a/A, 3) E/A, and 4) $(V^0/A)+(V^a/A)$ for the parameter values (33).

the expression for the two-nucleon potential energy, Eq. (1), the potential energy W of the nucleus is positive (repulsion) for small radii, and thus the collapsed state of the nucleus is not stable. Owing to the presence of kinetic energy the total energy E/A takes a minimum value equal to the empirical value ~ -14 mev at a nuclear radius $R = R_s = r_0A^{1/3}$ which corresponds to a state of the nucleus with normal density. In all the cases we are considering the behavior of E/A as a function of the nuclear radius shows that the state with normal density ($x = 1$) is stable with respect to both

increase and decrease of the radius of the nucleus and that the binding energy is proportional to the mass number A, and not to A^2. In the case $B = 0$ the two-nucleon potential (1) goes over into the ordinary attractive potential of Yukawa supplemented by a repulsion of the Jastrow type at small distances:

$$U_{12} = \begin{cases} \infty & \text{for } r < r_c, \\ -C\dfrac{e^{-r/a}}{(r/a)} & \text{for } r > r_c. \end{cases} \qquad (35)$$

According to Eq. (26) the binding energy of the nucleus for the interaction law (35) is

$$E = T + V^0 + V^a \qquad (36)$$
$$= \left\{\frac{a_2}{x^2} + \frac{b_2}{x^3} - \frac{b_3}{x^3} + b_4 \Psi_2(b_0, \beta x)\right\} A.$$

Here

$$b_3 = 3e^{-b_0}(1 + b_0)\, C / 2\beta^3; \quad b_4 = 16C / 3\pi^2.$$

It can easily be shown that for the energy expression (36) the requirements (27) and (28) are not compatible, i.e., equilibrium of the nucleus at the normal nuclear density cannot be secured. Thus when the statistical model is used the two-nucleon attractive Yukawa potential with a repulsive core r_c at small distances in the strict sense of the Jastrow model does not permit the establishment of nuclear stability. On the other hand we have shown that our proposed two-nucleon potential of the Lennard-Jones intermolecular type, which in our opinion represents in a semiphenomenological way the results of mesodynamics with suitable parameters, actually leads to saturation of the binding energy at a normal density of nucleons corresponding to the equilibrium nuclear radius. For the two systems of parameter values given in Eqs. (32) and (33) we present a graphical representation of the attractive and repulsive potential energies, and also of the total interaction potential energy between two nucleons, as functions of the distance between the two nucleons (Fig. 3). It is seen from the diagram that the total interaction force between two nucleons at large distances ($r \geq r_m$) is attractive, and at small distances ($r < r_m$) it is a repulsive force. The distance $r = r_m$ between the nucleons corresponds to the deepest point in the potential well U_m.

It must be remarked that the introduction of a correlation function of exponential form, as is used, for example, in the theory of liquids, must lead to a further weakening of the connection between the nucleons, in general agreement with the requirements of the shell model.

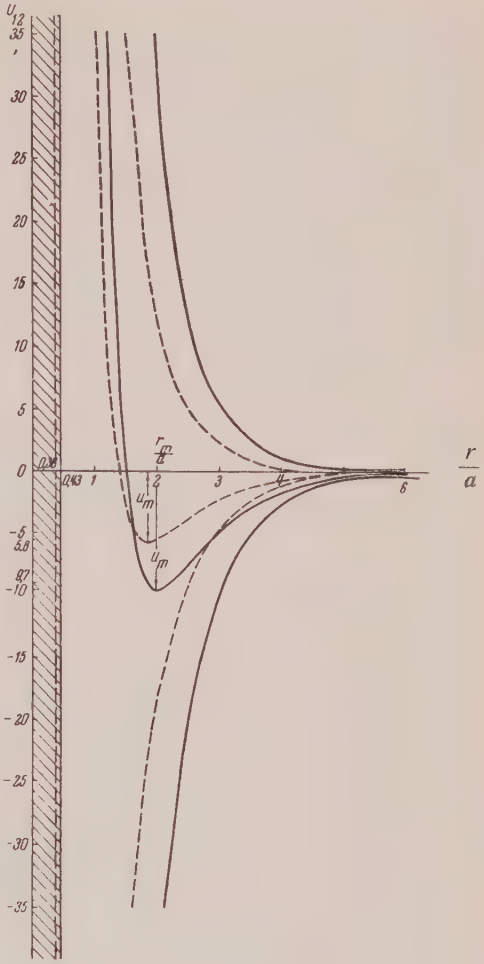

FIG. 3. Graph of the dependences of $-C\dfrac{e^{-r/a}}{(r/a)}$, $B\dfrac{e^{-r/a}}{(r/a)^2}$, and the total interaction potential energy $U_{12}(r)$ between two nuclei on the distance r between them; dashed curves are for the parameter values (32), solid curves for the values (33).

In conclusion we express our gratitude to L. I. Morozovskaia for carrying out our numerous calculations.

Note added in proof. Brueckner and others[11] have come to the conclusion that the two-nucleon potential of pseudoscalar mesodynamics without the "pair term" gives the required saturation of the energy at the radius $R_s = 1.15 \times 10^{-13} A^{1/3}$, if in addition to a repulsive core (r_c), taken different for the singlet and triplet states, one includes repulsion in the odd P-state.

[1]J. Blatt and V. Weisskopf, *Theoretical Nuclear Physics*.

[2]B. Kermov, J. Exptl. Theoret. Phys. (U.S.S.R.) 24, 299 (1953).

[3]A. Sokolov and B. Kerimov, J. Exptl. Theoret. Phys. (U.S.S.R.) 26, 430 (1954).

[4]B. Kerimov and A. Dzhavadov, J. Exptl. Theoret. Phys. (U.S.S.R.) 30, 900 (1956); Soviet Phys. JETP 3, 713 (1956).

[5]S. D. Drell and K. Huang, Phys. Rev. 91, 1527(1953).

[6]R. Jastrow, Phys. Rev. 81, 165 (1951).

[7]M. M. Levy, Phys. Rev. 86, 806 (1953); 88, 725 (1952).

[8]Pidd, Hammer, and Raka, Phys. Rev. 92, 436 (1953).

[9]V. L. Fitch and J. Rainwater, Phys. Rev. 92, 789 (1953).

[10]L. N. Cooper and E. M. Henley, Phys. Rev. 92, 801 (1953).

[11]Brueckner, Levinson, and Mahmoud, Phys. Rev. 95, 217 (1954).

Translated by W. H. Furry
13

SOVIET PHYSICS JETP VOLUME 4, NUMBER 3 APRIL, 1957

Theory of Localized Electron States in an Isotropic Homopolar Crystal

M. F. DEIGEN
Institute of Physics, Academy of Sciences, Ukrainian SSR

(Submitted to JETP editor July 1, 1955)
J. Exptl. Theoret. Phys. (U.S.S.R.) 31, 504-511 (September, 1956)

The behavior of an electron localized near a defect in a nonmetallic homopolar crystal is examined, taking into account the "condenson" interaction of the electron with the crystal. We have calculated the energy levels of the system and the energy of thermal dissociation of the electron, considering the motion of the electron quantum mechanically, and the motion of the atoms in the lattice either classically or quantum mechanically. It is shown that the condenson interaction leads to a difference between the energies of thermal and of photodissociation of an electron. We have determined the shape of the absorption band due to a localized electron (the position of the maximum, the halfwidth and its temperature dependence). As an illustration we give numerical calculations in the case of a Coulomb potential of the defect (for instance, an impurity atom with a valence electron).

1. INTRODUCTION

JUST as the presence of defects accompanied by localized electron states leads to the occurrence of a number of peculiarities in the optical, magnetic, photoelectric and other properties in ionic crystals, the presence of defects in homopolar crystals can also essentially change their properties.

It is well known that any attempt at a quantitative consideration of the energy level scheme of the electrons of an impurity atom leads to the calculation of the motion of a valence electron in the field of the ionized impurity in a medium characterized by a dielectric constant ϵ. We must at once remark that such a calculation which does not consider the interaction of the electron with the vibrations of the lattice is unable to consider quantitatively the width of the absorption band of impurity atoms, its temperature dependence, the difference between the energies of thermal and photodissociation, the difference between the energies of thermal and photo dissociation of impurity atoms, and so on.

In one of the papers[1] by the author and Pekar we investigated the question of the states of conduction electrons in a perfect homopolar crystal. It turned out that in a homopolar crystal also the interaction of the "extra" electron with the dielectric can partially be of an internal character. If as a result of an elastic deformation there occurs a region of increased density and thus a higher dielectric constant in some parts of the crystal, the electron must, according to macroscopic electrostatic theory, drift to those regions. Therefore, a region of higher density presents a potential trap to a conduction electron, and because of the inertia of the displacement of the atoms, it will not follow

the motion of the electron.

If an electron localized in one of the discrete levels of such a trap is able to maintain such a region of higher density, this can lead to a self-adjustment of the electron state (as in the case of the polarons) and such a state we shall call a "condenson" in this paper. As a calculation showed, a condenson with a larger radius does not exist, and the macroscopic approximation for this solution therefore becomes illegitimate.

In Ref. 1 we gave only qualitative criteria for the existence of condensons. In the present paper we evaluate the energy levels and other parameters of the states of an electron localized near a defect in a homopolar crystal, taking into account the condenson interaction of the electron with the vibrations of the lattice. The calculation is given both semi-classically and by consistent quantum-mechanical methods.

It turns out that in the case considered the presence of a potential trap of a defect ensures the existence of localized states with a larger radius. Therefore, it is possible to make numerical calculations, using the macroscopic approximation and in particular to calculate the energies of thermal and photodissociation of an electron.

2. THE HAMILTONIAN OF THE SYSTEM

We calculate the behavior of an extra electron in a homopolar crystal with a defect. We denote the potential energy of the electron in the field of the defect by $Q(r)$.

As was shown in Ref. 1, the energy of interaction of an electron with an elastically deformed dielectirc (in the isotropic case and in the case of a cubic crystal) can be written in the macroscopic approximation in the form

$$V(r) = a(u_{11} + u_{22} + u_{33}). \tag{1}$$

Here the expression in brackets is the trace of the deformation tensor, and a is the coupling constant.

The energy of the lattice vibrations can be written in the form

$$H_{ac} = H_{\parallel} + H_{\perp}. \tag{2}$$

where $H_{||}$ and $H_{\perp}$ are, respectively, the energies of the longitudinal and transverse vibrations. In the approximation we use here the electron interacts only with the longitudinal acoustic vibrations as follows from the considerations in Ref. 1.

The energy of these can be put in the form

$$H_{\parallel} = \frac{\rho}{2}\sum_{\varkappa}\dot{u}_{\varkappa}^2 + \frac{1}{2}\left(K + \frac{4}{3}\mu\right)\sum_{\varkappa} u_{\varkappa}^2\varkappa^2 \tag{3}$$

where ρ is the density of the crystal, K and μ are the compressibility and shear moduli, $\varkappa$ is the wave vector, and $u_{\varkappa}$ the Fourier component of the displacement vector u in the expansion

$$\mathbf{u} = \sum_{\varkappa}\mathbf{u}_{\varkappa}\chi_{\varkappa}(r), \tag{4}$$

$$\chi_{\varkappa}(r) = \sqrt{2/L^3}\begin{cases}\cos \varkappa r, & \varkappa_x \leqslant 0,\\ \sin \varkappa r, & \varkappa_x > 0,\end{cases} \tag{5}$$

where L is the periodicity length of the crystal.

If we introduce normal coordinates by the equations

$$p_{\varkappa} = \dot{u}_{\varkappa}\sqrt{\rho/\hbar\omega_{\varkappa}}\ ; \quad q_{\varkappa} = u_{\varkappa}\sqrt{\rho\omega_{\varkappa}/\hbar}, \tag{6}$$

where $\omega_{\varkappa} = v_e\varkappa$, while $v_e = [K+4/3\mu]^{1/2}\,1/2\rho$ is the velocity of the longitudinal waves, (3) can be written in the form

$$H_{\parallel} = {}^1/_2\sum_{\varkappa}\hbar\omega_{\varkappa}(q_{\varkappa}^2 + p_{\varkappa}^2). \tag{7}$$

The transition to a quantum mechanical description of the motion of the atoms is accomplished by the substitution $p_{\varkappa} \to -i\partial/\partial q_{\varkappa}$.

The Hamiltonian of the system electron + defect + crystal can be written as follows:

$$\hat{H} = -(\hbar^2/2\mu_0)\Delta + V(r) + Q(r) + \hat{H}_{\parallel}. \tag{8}$$

Here we have already used the effective mass method[2], and μ_0 is the effective mass of the electron.

Considering Eq. (4), expression (1) for the interaction energy of the electron with the dielectric can be written in the form

$$V(r) = a\sum_{\varkappa} u_{\varkappa}\,|\,\varkappa\,|\,\chi_{-\varkappa}(r). \tag{9}$$

We have finally for the Hamiltonian of the system

$$\hat{H} = -(\hbar^2/2\mu_0)\Delta + Q(r) + a\sum_{\varkappa} u_{\varkappa}\,|\,\varkappa\,|\,\chi_{-\varkappa}(r) + {}^1/_2\sum_{\varkappa}\hbar\omega_{\varkappa}(q_{\varkappa}^2 - \partial^2/\partial q_{\varkappa}^2). \tag{10}$$

The Hamiltonian of a free "condenson" can be obtained from (10) if we put $Q(r) = 0$.

The solution of the Schrödinger equation

$$\hat{H}\Psi = E\Psi \tag{11}$$

which corresponds to (10) determines the energy levels E and the wave functions of the system Ψ.

3. ENERGY LEVELS AND QUANTUM STATES OF THE SYSTEM IN THE SEMI-CLASSICAL APPROXIMATION. THE ENERGIES OF THERMAL AND PHOTODISSOCIATION OF AN IMPURITY CENTER.

By the semi-classical approximation we mean here that way of evaluating the behavior of the system in which the electron motion is calculated quantum mechanically, but the motion of the atoms in the lattice classically.

If we use the adiabatic approximation, the state of the system can be evaluated in two stages: first of all, the configuration of the medium (dedermined by the coordinates $u_\varkappa$) is supposed to be fixed, and the corresponding state of the electron is determined from the wave equation

$$\cdot\left[-\frac{\hbar^2}{2\mu_0}\Delta + Q(r) + a\sum_\varkappa u_\varkappa |\varkappa| \chi_{-\varkappa}(r)\right]\psi(r) = E\left[u_\varkappa\right]\psi(r). \tag{12}$$

After that we calculate the motion of the atoms (medium), the potential of which is supposed to be equal to

$$E[u_\varkappa] + U[u_\varkappa]. \tag{13}$$

For the adiabatic discussion mentioned a moment ago it is convenient to introduce the functional

$$F[\psi, u_\varkappa] = (\hbar^2/2\mu_0)\int |\nabla\psi|^2 d\tau + \int Q(r)\,|\psi|^2 d\tau + a\sum_\varkappa u_\varkappa |\varkappa| \int |\psi|^2 \chi_{-\varkappa}(r)\, d\tau + (\rho/2)\sum \omega_\varkappa^2 u_\varkappa^2. \tag{14}$$

If in this functional all $u_\varkappa$ are kept fixed while its extremum is found with respect to ψ under the auxiliary condition

$$\int |\psi|^2 d\tau = 1, \tag{15}$$

then we get, in accordance with the quantum mechanical variational principle, the extremal function $\psi(r)$ as an eigenfunction of Eq. (12), but with the sum of the first three terms of (14) equal to $E[u_\varkappa]$. In that way, after the extremum with respect to ψ is found, $E[\psi, u_\varkappa]$ transforms into the potential energy of the atoms in the presence of a localized electron. The equilibrium configuration of the medium is in turn determined by the minimum of (13), and therefore the ground state of the system is determined by the absolute minimum of the functional (14) with respect to ψ and $u_\varkappa$.

The absolute minimum F can be found by first taking the variation with respect to $u_\varkappa$ and then with respect to ψ. In the result of the variation with respect to $u_\varkappa$ we have

$$u = -\frac{a}{|\varkappa|} K_{-\varkappa} \frac{1}{K + {}^4/_3\mu}, \tag{16}$$

$$K_{-\varkappa} = -\int |\psi|^2 \chi_{-\varkappa}(r)\, d\tau.$$

Substitution of (16) into (14) transforms F into a functional depending on ψ only,

$$J[\psi] = \frac{\hbar^2}{2\mu_0}\int |\nabla\psi|^2 d\tau + \int Q(r)\,|\psi|^2 d\tau - \frac{a^2}{2(K + {}^4/_3\mu)}\sum_\varkappa K_{-\varkappa}^2. \tag{17}$$

It is easily shown that

$$\sum_\varkappa K_{-\varkappa}^2 = \int \psi^4 d\tau. \tag{18}$$

Hence,

$$J[\psi] = \frac{\hbar^2}{2\mu_0}\int |\nabla\psi|^2 d\tau + \int Q(r)\,|\psi|^2 d\tau - \frac{a^2}{2(K + {}^4/_3\mu)}\int \psi^4 d\tau. \tag{19}$$

Now we must find the minimum of J, taking the variation with respect to ψ. We obtain the minimum value of $J[\psi] - J[\psi_{1s}]$ and this will give us the energy of the thermal dissociation of a localized electron (if we neglect the small energy of a "free" condenson).

The Schrödinger level of the ground state (the energy of photodissociation) is determined from the relation

$$E_0 = \frac{\hbar^2}{2\mu_0}\int |\nabla\psi_{1s}|^2 d\tau + \int Q(r)\,|\psi_{1s}|^2 d\tau - \frac{a^2}{K + {}^4/_3\mu}\int \psi_{1s}^4 d\tau. \tag{20}$$

Hence, the difference between the energies of photo- and thermal-dissociation of a localized electron is found to be equal to

$$| E_0 - J | = \frac{a^2}{2(K + 4/3\,\mu)} \int \psi_{1s}^4 \, d\tau. \qquad (21)$$

In that way also, in the case of homopolar crystals (as for ionic crystals), the energies of photo- and thermal dissociation are different, the energy of photo-dissociation being larger in absolute magnitude than the energy of thermal-dissociation.

It is possible to investigate the extremal properties of $J[\psi]$, if the actual shape of $Q(r)$ is given. We shall assume that $Q(r)$ is a Coulomb potential. This will, for instance, be the case, if we calculate the energy states of an impurity atom with a valence electron. In the macroscopic approximation the potential energy of a valence electron can is the effective charge of the ionized impurity. In that case (19) can be rewritten as follows,

$$J[\psi] = \frac{\hbar^2}{2\mu_0} \int | \nabla\psi |^2 \, d\tau - \frac{Ze^2}{\varepsilon} \qquad (22)$$

$$\times \int \frac{1}{r} | \psi |^2 \, d\tau - \frac{a^2}{2(K + 4/3\,\mu)} \int \psi^4 \, d\tau.$$

To investigate the extremal properties of (22), we treat it in the same way as was done in Ref. 1. We assume that there is a function leading to the minimum J. We introduce a function

$$\chi_0(r) = k^{3/2} \psi_0(kr). \qquad (23)$$

This function is normalized for $k > 0$, if $\psi_0(r)$ is normalized, and goes over into $\psi_0(r)$ for $k = 1$. Substituting (23) into (22), we get the following result:

$$J(k) = -a_1 k + a_2 k^2 - a_3 k^3, \qquad (24)$$

$$a_1 = \frac{2Ze^2}{\varepsilon} \int \frac{1}{r} | \psi_0(r) |^2 \, d\tau;$$

$$a_2 = \frac{\hbar^2}{2\mu_0} \int | \nabla\psi_0(r) |^2 \, d\tau; \qquad (25)$$

$$a_3 = \frac{a^2}{2(K + 4/3\mu)} \int | \psi_0(r) |^4 \, d\tau.$$

It follows from (24) that $J(k)$ is equal to zero for $k = 0$, then becomes negative, and reaches a minimum for $k = 1$ (provided $2a_2 = a_1 + 3a_3$), after that increases, passes through a maximum, and for still larger values of k decreases again. The full drawn curve in Fig. 1 shows J as a function of k. As $k \to \infty$, $J(k) \to -\infty$. As was noted in Ref. 1, this limiting behavior cannot be correct, as for $k \to \infty$ the effective radius of the electron r_e goes to zero so that the basis for the macroscopic approximation, for the method of effective masses, and so on, breaks down.

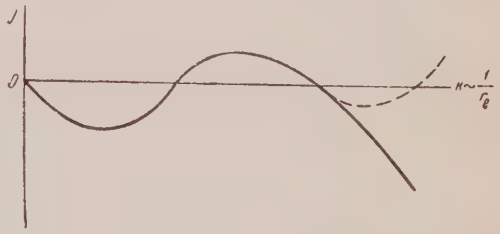

FIG. 1

However, in contradistinction to the case considered in Ref. 1, the functional of the system discussed here possesses a minimum, and this minimum occurs, generally speaking, for such a value of the effective radius r_e that the macroscopic and the other approximations used are still valid. Therefore, we can here discuss the problem quantitatively.

At the same time the qualitative discussion given in Ref. 1 shows that, if we generalize the functionals F and J to be applicable also for small values of the radius of the electron state, and taking, illegitimately, the limit $k \to \infty$ we are led to the conclusion that there may exist a minimum of condenson origin for those values of the radius.

Therefore, the most general functional of the system, valid for both small and large radii of the electron state, can, generally speaking, have two maxima (dotted curve in Fig. 1). In the framework of the variational method we can only attach any importance to the lowest of the two states.

Further, we shall only consider those crystals in which the first minimum lies more deeply than the second. The opposite case is apparently not very probable.

The minimum of the functional (22) can be found by straightforward variational methods. As a first qualitative approximation we choose a monotonically decreasing function without nodes,

$$\psi(r) = (\alpha^3 / 7\pi)^{1/2} (1 + \alpha r) e^{-\alpha r}. \qquad (26)$$

Substituting (26) into (22) we find a minimum

$J = J(\alpha)$, and using expression (21) we are able to determine the difference between the energies of thermal and photo-dissociation,

$$| E_0 - J | = 5{,}55 \times 10^{-3} a^2 \alpha_m^3 / (K + {}^4/_3 \mu), \qquad (27)$$

where α_m is the value of the parameter α corresponding to the minimum of J.

For an estimate of the size of the condenson effect we chose the values of the parameters nearly equal to the corresponding magnitudes for diamond and sulphur, namely, $\epsilon = 6$, $\mu_0 = m$, $K + 4/3\mu \approx 10^{11}$, $a = 2.5$, $Z = 1$. We then get $| E_0 - J | \approx 0.2$ ev. As can be seen from this estimate, the difference between the energies of thermal and photo-dissociation can be shown to be considerable. In crystals with large ϵ, for instance, germanium or silicon, the values of J and E_0 are so small (hundredths of ev) that we can only hope to discover the difference in their magnitudes at very low temperatures.

4. OPTICAL PROPERTIES OF LOCALIZED CENTERS. QUANTUM MECHANICAL CALCULATION OF THE MOTION OF THE ATOMS

For a determination of the parameters of the absorption band of localized centers both the electron motion and the motion of the atoms in the lattice must be calculated quantum mechanically.

For an evaluation of the parameters of the ground state we take instead of (11) the equivalent variational functional[3],

$$\overline{H} = \int \Psi^* \hat{H} \Psi d\tau dq \qquad (28)$$

$$= \frac{\hbar^2}{2\mu_0} \int | \nabla \Psi |^2 d\tau dq + \int Q(r) | \Psi |^2 d\tau dq + a \int \sum_{\varkappa} u_{\varkappa} | \varkappa | \chi_{-\varkappa}(r) | \Psi |^2 d\tau dq + \frac{1}{2} \sum_{\varkappa} \hbar\omega_{\varkappa} \int \Psi^* \left(q_{\varkappa}^2 - \frac{\partial^2}{\partial q_{\varkappa}^2} \right) \Psi d\tau dq$$

with the normalization condition

$$\int | \Psi |^2 d\tau dq = 1, \quad d\tau = dxdydz, \qquad (29)$$

$$dq = dq_1 dq_2 \ldots dq_{\varkappa} \ldots$$

As in Ref. 3 we choose for the first approximation our function in the form

$$\Psi(r \ldots q_{\varkappa} \ldots) = \psi(r)\, \Phi(\ldots q_{\varkappa} \ldots). \qquad (30)$$

Substituting (30) into (28), using condition (29), and taking the variation with respect to Φ^* we get for Φ the equation

$$\left(\sum_{\varkappa} H_{\varkappa} \right) \Phi = \lambda \Phi, \qquad (31)$$

$$H_{\varkappa} = \frac{\hbar\omega_{\varkappa}}{2} \left[q_{\varkappa}^2 - \frac{\partial^2}{\partial q_{\varkappa}^2} \right] - \frac{a q_{\varkappa}}{\sqrt{(K + {}^4/_3 \mu)}} K_{-\varkappa} \sqrt{\hbar\omega_{\varkappa}}. \qquad (32)$$

Expression (32) can be rewritten in the following form:

$$H_{\varkappa} = \frac{\hbar\omega_{\varkappa}}{2} \left[(q_{\varkappa} - q_{\varkappa 0})^2 - \frac{\partial^2}{\partial q_{\varkappa}^2} \right] - \frac{a^2}{2(K + {}^4/_3 \mu)} K_{-\varkappa}^2, \qquad (33)$$

$$q_{\varkappa 0} = a K_{-\varkappa} / \sqrt{\hbar\omega_{\varkappa} (K + {}^4/_3 \mu)}. \qquad (34)$$

Hence it follows immediately that Eq. (31) reduces to a set of oscillator equations,

$$H_{\varkappa} \Phi_{\varkappa} = \lambda_{\varkappa} \Phi_{\varkappa}, \qquad (35)$$

where $\Phi_{\varkappa}$ is an eigenfunction of the harmonic oscillator problem. The solution of (31) can be written in the form

$$\Phi = \prod_{\varkappa} \Phi_{\varkappa}, \quad \lambda = \sum_{\varkappa} \hbar\omega_{\varkappa} \left(n_{\varkappa} + \frac{1}{2} \right) - \frac{a^2}{2(K + {}^4/_3 \mu)} \sum_{\varkappa} K_{-\varkappa}^2. \qquad (36)$$

Substituting (36) into (28), using condition (18) changes $\overline{H}$ into a functional depending on ψ only,

$$H_0[\psi] = \frac{\hbar^2}{2\mu_0} \int | \nabla \psi |^2 d\tau + \int Q(r) | \psi |^2 d\tau - \frac{a^2}{2(K + {}^4/_3 \mu)} \int \psi^4 d\tau + \sum_{\varkappa} \hbar\omega_{\varkappa} (n_{\varkappa} + {}^1/_2) \qquad (37)$$

or, taking (19) into account,

$$\overline{H}_0 = J_0[\psi] + \sum_{\varkappa} \hbar\omega_{\varkappa} (n_{\varkappa} + {}^1/_2). \qquad (38)$$

This functional must be minimized with respect to ψ. Its extremal properties are determined by those of $J_0[\psi]$ which were examined in detail in the previous section. Thus we have, for instance,

in the case of a defect potential of the form $Q(r) = Ze^2/\epsilon r$,

$$\overline{H}_0 = J_0(\alpha_m) + \sum_\varkappa \hbar\omega_\varkappa (n_\varkappa + 1/2). \quad (39)$$

The calculation of the parameters of an excited state is analogous to the calculation of the parameters of the ground state.

Replacing Eq. (11) by the equivalent variational principle (28) and choosing as a first approximation the function in the form

$$\Psi_i = \varphi(r)\,\Phi(\ldots q'_\varkappa \ldots), \quad (40)$$

we can obtain for the functional of an excited state after minimizing (with respect to Φ) the expression

$$\overline{H}_i = J_i(\varphi) + \sum_\varkappa \hbar\omega_\varkappa (n'_\varkappa + 1/2). \quad (41)$$

One can also find the minimum with respect to φ by straightforward variational methods once the form of $Q(r)$ is explicitly given. In particular, for $Q(r) = -Ze^2/\epsilon r$ it is plausible to choose φ in the form

$$\varphi = \pi^{-1/2}\beta^{5/2} e^{-\beta r} r\cos\vartheta. \quad (42)$$

Substitution of (42) into (41) and finding the minimum determines β_m and J_{im}.

As Pekar and Krivoglaz[4] have shown, for localized centers of any structure in crystals with arbitrary dispersion laws for the eigenfrequencies of the lattice vibrations the position of the maximum of the absorption band is defined by the relation

$$\hbar\Omega_{max} = |J_0 - J_i| = \hbar\sigma_1, \quad (43)$$

$$\sigma_1 = \frac{1}{2}\sum_\varkappa (q_{\varkappa 0} - q_{\varkappa i})^2 \omega_\varkappa,$$

where $q_{\varkappa 0}$ and $q_{\varkappa i}$ are the coordinates of the equilibrium position of the system when the electron is respectively in the ground or in an excited state.

In the case of large energy release the halfwidth of the absorption curve is determined as follows:

1) high temperatures ($\hbar\omega_\varkappa / kT \ll 1$)

$$\vartheta = 4\sqrt{\ln 2}\,\sqrt{kT\hbar\sigma_1}; \quad (44)$$

2) low temperatures ($\hbar\omega_\varkappa / kT \gg 1$)

$$\vartheta = 2\sqrt{2\ln 2}\,\hbar\sqrt{\sigma_2}\,; \quad (45)$$

$$\sigma_2 = \frac{1}{2}\sum_\varkappa (q_{\varkappa 0} - q_{\varkappa i})^2 \omega_\varkappa^2.$$

Substituting expression (34) for $q_{\varkappa 0}$ and $q_{\varkappa i}$ we have

$$\sigma_1 = \frac{1}{2}\,\frac{a^2}{(K + 4/3\,\mu)\,\hbar}\sum_\varkappa (K_{-\varkappa 0} - K_{-\varkappa i})^2, \quad (46)$$

$$\sigma_2 = \frac{1}{2}\,\frac{a^2}{(K + 4/3\,\mu)\,\hbar}\sum_\varkappa (K_{-\varkappa 0} - K_{-\varkappa i})^2\,\omega_\varkappa.$$

The calculations lead to the following values of σ_1 and σ_2:

$$\sigma_1 = \frac{1}{2\pi}\,\frac{a^2}{\hbar\,(K + 4/3\,\mu)}\,\alpha_m^3\Big\{0.0348 - \frac{2}{7}\,\frac{[1 + 5v/(v+1) + v^3/2(v+1)^2}{(v+1)^5} + \frac{9}{256}\,\frac{1}{v^3}\Big\}, \quad (47)$$

$$\sigma_2 = \frac{a^2}{2\hbar\sqrt{(K + 4/3\,\mu)\,\rho}}\,\frac{\alpha_m^4}{\pi^2}\Big\{0.107 + \frac{0.139}{v^4} - \frac{8}{7}\Big[\frac{-7v^8 - 480\,v^6 - 930\,v^4 - 32\,v^2 + 9}{6\,(v^2-1)^6} + \frac{2\,v^2 \ln v}{(v^2-1)^7}\,(27\,v^6 + 141\,v^4 + 77\,v^2 - 5)\Big]\Big\},$$

where $V = \alpha_m/\beta_m$.

If we take $\epsilon = 6$, $\mu_0 = m$, $K + 4/3\mu = 10^{11}$, $a = 2.5$, the half-width of the absorption curve is equal to 0.1 ev at $T = 0$. Thus we are able to find, by determining the condenson interaction, a value for the halfwidth of the absorption curve even at the absolute zero.

The discussion of the condenson interaction of an electron of an impurity center with the lattice vibrations given here for a homopolar crystal must also be given for the cases of molecular or ionic crystals. In the latter case this interaction must lead to a deepening of the polaron level and a widening of the absorption band of the localized centers.

[1] M. F. Deigen and S. I. Pekar, J. Exptl. Theoret. Phys. (U.S.S.R.) 21, 803 (1951).

[2] S. I. Pekar, J. Exptl. Theoret Phys. (U.S.S.R.) 16, 933 (1946).

[3] S. I. Pekar, *Investigations on the electron theory of crystals*, Moscow-Leningrad, 1951; German translation: *Untersuchungen über die Elektronentheorie der Kristalle*, Akademie Verlag, Berlin, 1954.

[4] S. I. Pekar and M. A. Krivoglaz, Trudy. Inst. Phys., Acad. Sci., Ukrainian SSR **4**, 37.(1953).

Translated by D. ter Haar
95

Letters to the Editor

On the Absorption of K^--Mesons by Helium Nuclei

S. G. MATINIAN
Institute of Physics, Academy of Sciences, Georgian SSR
(Submitted to JETP editor May 27, 1956)
J. Exptl. Theoret. Phys.(U.S.S.R.) **31**, 528-529 (September, 1956)

THE hypothesis of isobaric invariance in strong interactions plays an important role in the well-known scheme of Gell-Mann,[1] which satisfactorily describes a whole set of facts about heavy mesons and hyperons. As is known, experiments confirm irobaric invariance in strong pion-nucleon and nucleon-nucleon inetractions.[2]

Great interest exists concerning the experimental verification of this hypothesis in situations involving the creation, scattering and absorption of heavy mesons and hyperons. One of the means to this end consists in the experimental verification of relations between cross sections for different processes, when the difference is only in the charge states of the participating particles.

A whole series of such relations was derived by Okun'.[3] Recently, Lee proposed some experiments to verify charge independence in the strong interactions of K^--mesons with the nuclei of deuterium and helium, and established various relations between the cross sections of different processes occurring upon the absorption of K^--mesons.

The purpose of this note is to derive further relations between the cross sections of different reactions occurring when helium absorbs K^--mesons. Upon the absorption of K^--mesons by helium, the following reactions take place, with the emission of Σ-hyperons and π-mesons:

$$\begin{aligned} &K^- + He^4 \to \Sigma^0 + He^3 + \pi^-; \\ &K^- + He^4 \to \Sigma^- + He^3 + \pi^0; \\ &K^- + He^4 \to \Sigma^- + H^3 + \pi^+; \\ &K^- + He^4 \to \Sigma^0 + H^3 + \pi^0; \\ &K^- + He^4 \to \Sigma^+ + H^3 + \pi^-. \end{aligned} \tag{1}$$

The intitial particles appear in a state of isotopic spin $T = 1/2$.

Decomposing the appropriate wave functions into the final state wave functions, and taking account of the conservation of total isobaric spin, we obtain the following differential cross-sections:

$$\begin{aligned} \sigma_1(\Sigma^+ + H^3 + \pi^-) &= {}^1/_3 \,|\, A_0^{1/2} + 2^{-1/2} A_1^{1/2} \,|^2; \\ \sigma_2(\Sigma^0 + H^3 + \pi^0) &= {}^1/_3 \,|\, A_0^{1/2} \,|^2; \\ \sigma_3(\Sigma^0 + He^3 + \pi^-) &= {}^1/_3 \,|\, A_1^{1/2} \,|^2; \\ \sigma_4(\Sigma^- + He^3 + \pi^0) &= {}^1/_3 \,|\, A_1^{1/2} \,|^2; \\ \sigma_5(\Sigma^- + H^3 + \pi^+) &= {}^1/_3 \,|\, A_0^{1/2} - 2^{-1/2} A_1^{1/2} \,|^2, \end{aligned} \tag{2}$$

where $A_t^{1/2}$ is the transition amplitude from a state of total isobaric spin 1/2 to a state of isobaric spin t of the system: π-meson $-\Sigma$-hyperon.

Thus in particular there follows the result of Lee:[4]

$$\sigma_3(\Sigma^0 + He^3 + \pi^-) = \sigma_4(\Sigma^- + He^3 + \pi^0). \tag{3}$$

In addition, we obtain the following relations among cross sections:

$$\begin{aligned} &\sigma_1(\Sigma^+ + H^3 + \pi^-) + \sigma_5(\Sigma^- + H^3 + \pi^+) \\ &= 2\sigma_2(\Sigma^0 + H^3 + \pi^0) + \sigma_4(\Sigma^- + He^3 + \pi^0) \end{aligned} \tag{4}$$

and the inequality

$$\begin{aligned} &\sigma_2(\Sigma^0 + H^3 + \pi^0) + \sigma_4(\Sigma^- + He^3 + \pi^0) \\ &\geqslant {}^2/_3\, \sigma_5(\Sigma^- + H^3 + \pi^+). \end{aligned} \tag{5}$$

Additional inequalities appear as consequences of (4) and (5):

$$\begin{aligned} &\sigma_1(\Sigma^+ + H^3 + \pi^-) + \sigma_3(\Sigma^0 + He^3 + \pi^-) \\ &\geqslant {}^1/_3\, \sigma_5(\Sigma^- + H^3 + \pi^+), \end{aligned} \tag{5'}$$

$$\begin{aligned} &\sigma_1(\Sigma^+ + H^3 + \pi^-) + {}^1/_3\, \sigma_5(\Sigma^- + H^3 + \pi^+) \\ &\geqslant \sigma_2(\Sigma^0 + H^3 + \pi^0). \end{aligned} \tag{5''}$$

The author expresses his gratitude to G. R. Khutsishvili for his valuable advice and guidance.

[1] M. Gell-Mann, *Report of Pisa Conference on Elementary Particles*, NYO 7138, 1955 (unpublished).

[2] E. Fermi, Nuovo Cimento Suppl. **1**, 17 (1955).

[3] L. B. Okun', J. Exptl. Theoret. Phys. (U.S.S.R.) 30, 1172 (1956); Soviet Phys. JETP 3, 944 (1956).

[4] T. D. Lee, Phys. Rev. 99, 337 (1955).

Translated by C. R. Lubitz
106

Photoprotons from A^{40}

A. P. Komar and I. P. Iavor
Leningrad Physico-Technical Institute
Academy of Sciences, USSR
(Submitted to JETP editor June 7, 1956)
J. Exptl. Theoret. Phys. (U.S.S.R.) 31, 531
(September, 1956)

THE angular distribution of photoprotons from A^{40} has been examined. They were obtained by irradiating the A^{40} with the γ-beam from a synchrotron of maximum energy 90 mev.

Photoprotons with energy of 2-10 mev were registered in a Wilson cloud chamber filled with argon at a pressure of 1.4 atmos and mixed with the vapor of ethyl alcohol and water. The Wilson chamber, 30 cm in diameter and 7 cm deep, worked on a compression cycle of period 10-15 sec. The argon in the chamber was irradiated with a collimated γ-beam of diameter 1.6 cm, admitted to the chamber through an aluminum window (100μ) in the side wall. Proton tracks resulting from the (γ, p)-reaction were photographed stereoscopically

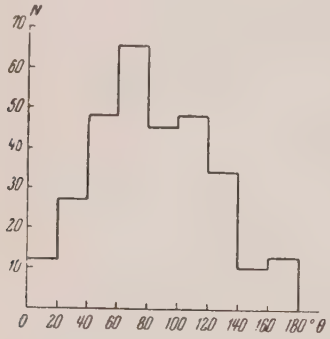

Angular distribution of photoprotons from A^{40}. N – number of proton tracks; θ – angle between the γ-beam and direction of ejected proton.

We examined 302 proton tracks. The angles were measured to an accuracy of 1-2% by a reprojection system. The histogram in the Figure was constructed by combining the tracks in 20° intervals. One clearly sees the forward directionality with a maximum at approximately 70°. The shape of the photoproton angular distribution obtained in this work is in satisfactory agreement with that obtained by Spicer[1], using nuclear emulsions and a maximum γ-beam energy of 22.5 mev.

From the character of the angular distribution of the photoprotons it follows that electric dipole absorption is occurring in the argon nuclei. The asymmetry is probably due to a direct photoeffect or quadrupole absorption of γ-rays.

[1] B. M. Spicer, Phys. Rev. **100**, 791 (1955).

Translated by C. R. Lubitz
108

The Effect of Uniform Compression upon the Magnetic Properties of Bismuth at Low Temperatures

B. I. Verkin, I. M. Dimitrenko
and B. G. Lazarev
Physico-Technical Institute
Academy of Sciences, Ukrainian SSR
(Submitted to JETP editor June 21, 1956)
J. Exptl. Theoret. Phys. (U.S.S.R.) 31, 538-540
(September, 1956)

SEVERAL papers have recently been published dealing with investigations of the influence of uniform compression upon the various properties of metals at low temperatures. Thus, Alekseevskii and his co-workers[1] have studied the effect of uniform compression upon the galvanomagnetic properties of bismuth and its alloys, and Overton and Berlincourt[2] have instituted an investigation into the effect of uniform pressure upon the oscillations of the Hall coefficient and the variation of the magnetoresistance of bismuth in a magnetic field.

In view of the fact that uniform compression of a crystal in all probability alters the structure, the degree of filling, and the possible overlapping of the electronic energy zones which govern the de Haas-van Alphen effect, an experimental study of the effect of uniform compression upon the oscillations of the magnetic susceptibility seems to be called for.

Bismuth was selected as the first subject of such investigation. The required pressures were produced by means of the method previously developed by one of the present authors in conjunction with Kan[3].

A bismuth monocrystal was fixed with a predetermined orientation into a special holder, and was placed within a cylindrical high-pressure bomb of beryllium copper, the latter being prepared in the laboratory from pure copper and beryllium. The bomb was filled with water and

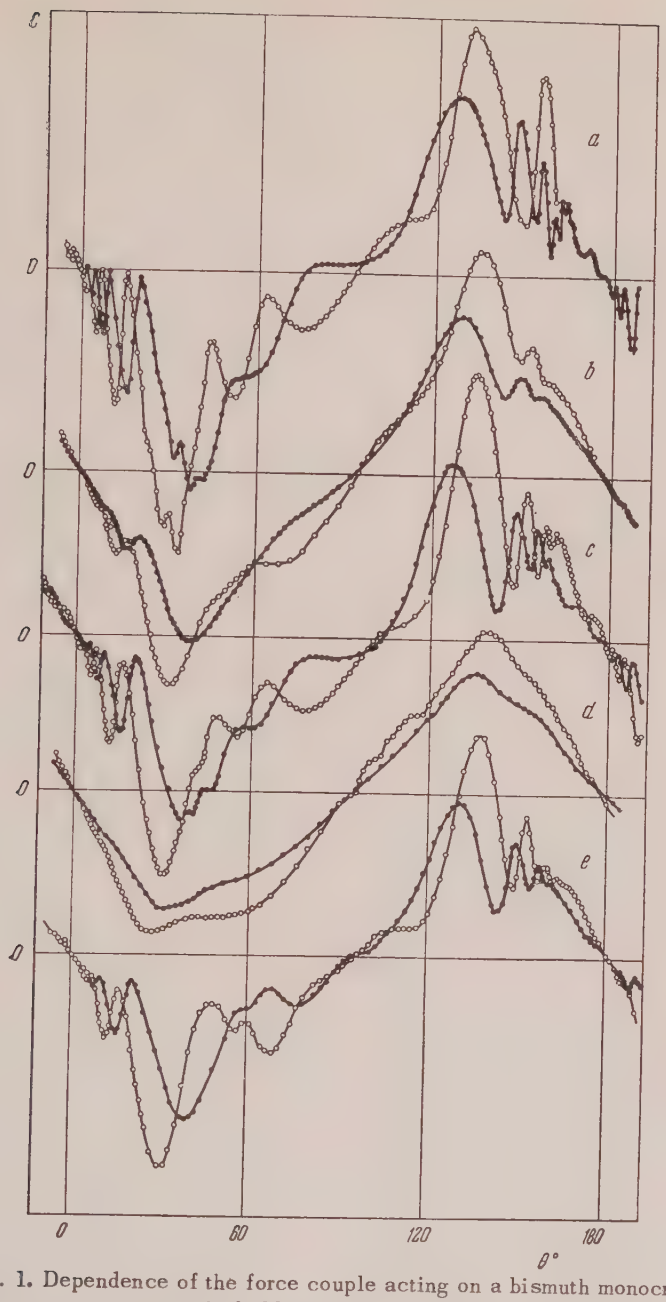

FIG. 1. Dependence of the force couple acting on a bismuth monocrystal in a homogeneous magnetic field upon the angle between the field vector and the trigonal axis of the crystal; $T = 4.2^\circ$ K, ●—H = 15,560 oersteds, O—H = 17,960 oersteds. Curve a — uncompressed specimen; b — under pressure $\sim$ 1500 kg/cm^2; c — pressure removed; d — pressure $\sim$ 1500 kg/cm^2 reapplied; e — second pressure removed.

attached to the quartz rod of the suspension system used for studying the de Haas-van Alphen effect[4]. Measurements were then made of the force couple acting upon the small bismuth monocrystal in a homogeneous magnetic field, within the massive, but magnetically isotropic, high-pressure bomb.

The bismuth monocrystal was so oriented that its binary axis lay parallel to the axis of the bomb, and hence, to the axis of the suspension; the trigonal axis and the field vector lay in the horizontal plane, making various angles θ with each

other. The angular dependence of the force couple (the rotation diagram) acting upon the bismuth monocrystal was investigated at $T = 4.2°$ K for two constant values of the field.

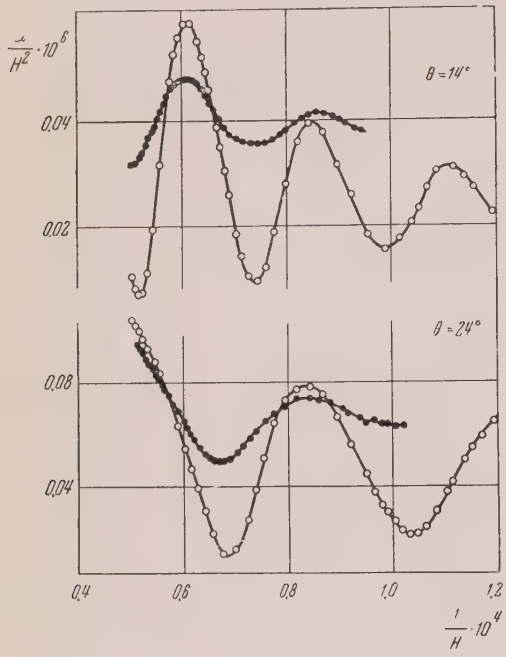

FIG. 2. Dependence of the difference between the components of the susceptibility of a bismuth monocrystal upon the intensity of the applied magnetic field at $T = 4.2°$ K; ●—under pressure ~ 1500 kg/cm^2; O—pressure removed.

Curves *a*, *c* and *e* of Fig. 1 represent the rotation diagrams for the bismuth monocrystal determined in the absence of pressure; curve *b* is the rotation diagram for the same plane, but with a pressure ~ 1500 kg/cm^2, while *d* is the rotation diagram for the same plane obtained upon removal and reapplication of a pressure on the order of 1500 kg/cm^2. It is evident that uniform compression of the bismuth monocrystal leads to a substantial reduction (by several times) in the amplitude of the oscillations. Removal of the pressure (curves *c* and *e* of Fig. 1) leads to almost complete restoration of the original form of the rotation diagram. The slight incompleteness of this restoration (actually a small pressure effect) is in all probability associated with deformation of the sample. It should be mentioned that a similar type of hysteresis is observed when the effect of pressure upon the galvanomagnetic properties of metals is investigated[1,2].

The dependence of the difference between the two components of the susceptibility of the bismuth monocrystal upon the field intensity was investigated for various values of θ. Two curves of this sort are presented in Fig. 2. It is evident that uniform compression of the bismuth monocrystal leads to a substantial reduction in the amplitude of the oscillations with field strength, to an increase in the constant component of the susceptibility difference (the median line about which the oscillations take place), and also to a change in the period of the oscillations. Analysis of the curves showing the dependence of the difference in the components of the susceptibility upon the field strength for θ = const shows that for θ in the vicinity of 0 and 180° the period of the oscillations increases under pressure, while for θ near 90° it decreases. The change in the period of the oscillations of the susceptibility of bismuth monocrystals under pressure on the order of 1500 kg/cm^2 is inconsiderable (it does not exceed a few percent).

[1] N. E. Alekseevskii and N. B. Brandt, J. Exptl. Theoret. Phys. (U.S.S.R.) **28**, 379 (1955); Soviet Phys. JETP **1**, 382 (1955).

[2] W. Overton and T. Berlincourt, Phys. Rev. **99**, 1165 (1955).

[3] B. G. Lazarev and L. C. Kan, J. Exptl. Theoret. Phys. (U.S.S.R.) **14**, 470 (1944).

[4] B. I. Verkin and I. F. Mikhailov, J. Exptl. Theoret. Phys. (U.S.S.R.) **25**, 471 (1953).

Translated by S. D. Elliott
114

On $K_{\mu 3}$-Decay

S. G. MATINIAN
Academy of Science, Georgian SSR

(Submitted to JETP editor May 27, 1956)
J. Exptl. Theoret. Phys. (U.S.S.R.) 31, 529-530
(September, 1956)

AT the present time there have been definitely established five different decay schemes for *K*-mesons with masses ~ 965 m_e. The decay products are known for three of these ($K_{\pi 2}$, $K_{\mu 2}$, $K_{\pi 3}$).

It has recently been established[1,2] that one of

the neutral particles emerging from the $K_{\mu 3}$ decay should be a π^0-meson, and that the mass of the other particle is zero. On the other hand, a half-integral spin for the K-meson leads to difficulties when one examines the process of K-meson formation in nuclear collisions[1,3].

The most probable decay scheme appears to be:

$$K_{\mu 3} \to \mu + \pi^0 + \nu. \tag{1}$$

The purpose of this note is to calculate the energy spectrum of the μ-mesons and π^0-mesons in the $K_{\mu 3}$-decay and to estimate the decay constant.

Regarding the $K_{\mu 3}$ as a scalar (or pseudoscalar) particle and limiting consideration to the direct coupling of fields, one obtains for the interaction Hamiltonian density:

$$H' = g\,(\bar{\Psi}_\mu \gamma \psi_\nu)(\varphi_\pi^+ \varphi_K), \tag{2}$$

where $\gamma = \gamma_5$ or 1, respectively, for scalar or pseudoscalar particles, and g is a constant with the dimensions of a length.

For finding the energy spectrum of the μ- and π^0-mesons, the method of Ref. 4 is convenient. The results are the same for both scalar and pseudoscalar $K_{\mu 3}$-mesons, due to the vanishing rest mass of the neutrino.

The energy spectrum of the μ-mesons:

$$w dE_\mu = \frac{g^2}{32\pi^3} \frac{(A - 2ME_\nu)\sqrt{E_\mu^2 - m_\mu^2}}{M(B - 2ME_\mu)^2} \times \{C + DE_\mu - 2M^2 E_\mu^2\}\, dE_\mu \tag{3}$$

The energy spectrum of the π^0-mesons:

$$w dE_\pi = \frac{g^2}{32\pi^3} \frac{(G - 2ME_\pi)^2}{M(F - 2ME_\pi)} \sqrt{E_\pi^2 - m_\pi^2}\, dE_\pi; \tag{4}$$

E and E_π are the total energies of the μ- and π^0-mesons in the rest system of the $K_{\mu 3}$-meson ($\hbar = c = 1$);

$$A = M^2 + m_\mu^2 - m_\pi^2; \quad B = M^2 + m_\mu^2; \tag{5}$$
$$C = m_\mu^2 (m_\pi^2 - m_\mu^2 - M^2);$$
$$D = M(M^2 + 3m_\mu^2 - m_\pi^2);$$
$$F = M^2 + m_\pi^2; \quad G = M^2 + m_\pi^2 - m_\mu$$

Integrating (4) from m_π to $(M^2 + m_\pi^2 - m_\mu^2)/2M$ we obtain for the total probability of decay

$$w_{\mu 3} = (g m_\pi)^2 (32\pi^3)^{-1}\, 0.95 \cdot 10^{23}\ \text{sec}^{-1}, \tag{6}$$

From this, using $\tau \approx 10^{-8}$ sec, we find

$$(g^2/4\pi)\, m_\pi^2 \approx 10^{-13}. \tag{7}$$

The correctness of the scheme corresponding to Eq. (1) for K_{e3}-decay is not yet established with sufficient certainty[1]. A similar calculation for the scheme

$$K_{e3} \to e + \nu + \pi^0 \tag{8}$$

gives

$$w_{e3} = (g' m_\pi)^2 (32\pi^3)^{-1} \cdot 6{,}42 \cdot 10^{23}\ \text{sec}^{-1} \tag{9}$$

where g' is the corresponding coupling constant for the four fields. Comparing (6) and (9) we obtain

$$w_{\mu 3}/w_{e3} \approx 0{,}16\,(g/g')^2. \tag{10}$$

From the results of Ref. 5, it follows that $w_{\mu 3}/w_{e3} \approx 0.5$. Then we have $g' = 0.6\,g$. However, it is necessary to note that the present statistics are inadequate for an unambiguous answer to the question of the ratio of $w_{\mu 3}$ and w_{e3}, and consequently of the equality of the constants g and g'.

In conclusion, we remark that the $K_{\mu 3}$-decay scheme can be connected with the $K_{\mu 2}$-decay in the following way*:

$$K_{\mu 3} \xrightarrow{\eta} (K_{\mu 2}) + \pi^0 \xrightarrow{f} \mu + \nu + \pi^0, \tag{11}$$

where η is the strong interaction constant (those interactions which do not violate "strangeness"), and f is the weak interaction constant (e.g., the universal weak Boson-Fermion interaction[7]).

Finally, the author considers it his pleasant duty to express his gratitude to G. R. Khutsishvili for constant help during the course of this work.

* In Ref. 6, the $K_{\mu 3}$-scheme was connected with the scheme $K_{\pi 2}(K_{\mu 3} \to K_{\pi 2} \to \pi + \pi^0 \to \mu + \nu + \pi^0)$, but led to the result $w_{K_{\mu 3}}/w_{K_{\pi 2}} \approx 10^{-14}$, in contradiction to experiment.

[1] Kaplon, Klarmann and Yekutieli, Phys. Rev. 99, 1528 (1955).

[2] Huang, Kaplon and Yekutieli, Bull. Am. Phys. Soc. 1, 64 (1956).

[3] A. Pais and R. Serber, Phys. Rev. 99, 1551 (1955).

[4] O. Kofoed-Hansen, Phil. Mag. 42, 1411 (1951).

[5] J. Grussard, *et al.*, Nuovo Cimento 3, 731 (1956).

[6] G. Gosta and N. Dellaporta, Nuovo Cimento 2, 519 (1955).

[7] K. Iwata, *et al.*, Progr. Theor. Phys. 13, 19 (1955).

Translated by C. R. Lubitz
107

Measurement of the Lifetimes of *K*-Mesons

M.IA. BALATS, P.I. LEBEDEV AND IU.V. OBUKHOV

(Submitted to JETP editor June 7, 1956)
J. Exptl. Theoret. Phys. (U.S.S.R.) 31, 531-533
(September, 1956)

THE measurement of the mean life of charged *K*-mesons from cosmic radiation has been carried out at sea level, using scintillation counters and a high-speed oscillograph[1]. A charged unstable particle formed in a slab of lead A (Fig. 1) passed through counters C_1 and C_2, and reached counter C_1 inside which was a brass absorber (10 gm/cm^2) Counters C_3 and C_3' then registered the decay products of the particles which came to rest in C. The data on the liquid scintialltion counters are collected below in a Table.

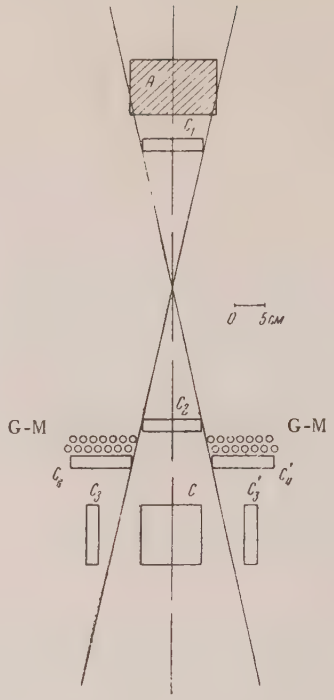

FIG. 1. Schematic diagram of set-up.

TABLE

Counter	Area cm^2	Thickness, cm	Solvent	Conc. of Terphenyl, g/l	Amount of FEU-19
C_1, C_2, C_3, C_3'	10×20	2	Toulene	3.5	1
C_4, C_4'	10×26	2	Benzene	1.4	2
C	10×20	10	Benzene	0.9	1

Pulses from the photomultipliers of the counters C_1, C_2, C_3 and C_3' were amplified, time-formed and fed to a coincidence counter[2]. The amplifier band width was 210 *mc*, the amplification factor ~6. In channels C_1 and C_2 pulses of length 4 × 10^{-8} sec were formed, in channels C_3 and C_3', of length 6 × 10^{-9} sec. The resolution curve of the coincidence circuit is given in Fig. 2. Triple coincidences $C_1 + C_2 + C_3$ or $C_1 + C_2 + C_3'$ triggered the oscilloscope and pulses coming from counter C were fed to the input of the vertical deflection amplifier. They were then photographed

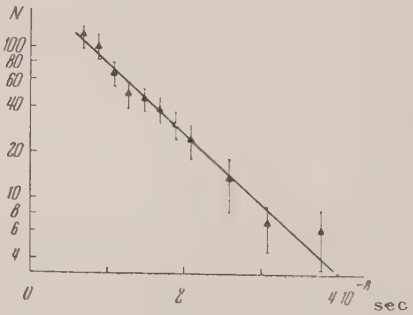

FIG. 2. Resolution curve for triple coincidences $C_1 + C_2 + C_3$.

on the oscilloscope screen. The duration of the sweep was 1.3×10^{-7} sec, and the minimum rise in the amplifier 2.5×10^{-9} sec. The precision of measuring the time between impulses was determined basically by the time dispersion of the photomultiplier belonging to counter C. To reduce this dispersion, we used a specially selected multiplier, type FEU-19. The exposed central part of the photocathode measured 5×12 mm, and the overall voltage was 4500 v.

The experimental error, connected with the time dispersion of a given FEU-19 tube, did not exceed 1.6×10^{-9} sec. In the photomultiplier there sometimes occurred a secondary spurious impulse following the basic impulse, but not connected with the passage of a particle through C. Such cases could imitate the decay of a K-meson when the set-up was triggered by shower particles. In view of this, it was necessary to reduce to a minimum the number of times the apparatus was triggered by showers.

In the first phase of this work, this was accomplished by including C_4 and C_4' in anticoincidence with $C_1 + C_2 + C_3$ or $C_1 + C_2 + C_3'$. The efficiency of this method was 96%. The presence of a group of Geiger-Muller counters covering C_4 and C_4' further reduced the number of times the system was triggered by showers. It is necessary to note that such a system excludes K-mesons accompanied by wide showers. Later on, the anticoincidence counters were replaced by a system of delayed coincidences, by introducing into channels C_1 and C_2 additional delay cables (1.4×10^{-8} sec).

From the resolution curve of Fig. 2 it can be seen that the probability of triggering the system by the simultaneous passage of particles through C_1, C_2, C_3 (C_3') did not exceed 0.02.

In order to take account of the secondary photomultiplier impulses, and the time displacement between pulses which resulted from the different flight times of two related particles, we measured the distribution of time intervals between pulses in counter C. In phase I of the work, this was done by including C_4 and C_4' in anticoincidence, while in phase II, we disconnected the additional delay cables. In such control investigations the number of delays in counter C was negligibly small. The results of these control experiments were included in the interpretation of the results.

The smallest energy of μ-meson decay which could also trigger the set-up was 25 mev. Therefore, we excluded cases of $\pi \to \mu + \nu$. The $\mu \to e + 2\nu$ decay could trigger the set-up, but in view of the fact that the resolution of the coincidence circuit was 4×10^{-8} sec, the probability of such an event was sufficiently small.

From among a total of 1600 cases, 64 were observed with a decay in an interval $10^{-8} - 4 \times 10^{-8}$ sec. The integral distribution of decay times is

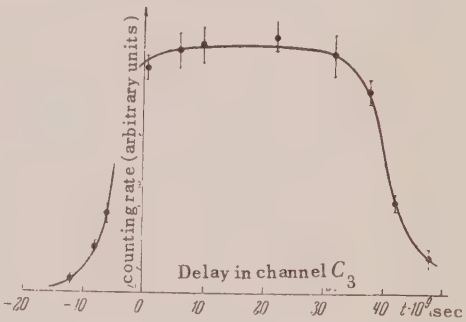

FIG. 3. Integral spectrum of K-meson decay time.

drawn in Fig. 3. It yields a mean lifetime of K-mesons of $(9.5 \pm 2.0) \times 10^{-9}$ sec, assuming a single-exponent decay. This result is in accord with Refs. 3-5.

[1] Balats, Lebedev and Obukhov, P.T.E. (in press).

[2] R. L. Garwin, Rev. Sci. Instr. **24**, 618 (1953).

[3] L. Mezzetti and J. W. Keuffel, Phys. Rev. **95**, 858 (1954).

[4] K. W. Robinson, Phys. Rev. **99**, 1606 (1955).

[5] V. Fitch and R. Motley, Phys. Rev. **101**, 496 (1956).

Translated by C. R. Lubitz
109

A Method of Investigation of Radial-Phase Oscillations of Electrons in a Synchrotron

IU. M. ADO
P. N. Lebedev Physical Institute
Academy of Sciences, USSR

(Submitted to JETP editor June 8, 1956)
J. Exptl. Theoret. Phys. (U.S.S.R.) 31, 533-534
(September, 1956)

IT is well known that in electron accelerators of synchrotron type, the accelerating electrons fill

part of the orbit in sort of bunch, whose azimuthal dimensions are determined by the radial-phase (synchrotron) oscillations.

At the start of the synchrotron acceleration cycle, the amplitude of radial-phase oscillation is appreciable and reaches 180°. As the electron energy E increases, the amplitude damps out as $E^{-1/4}$. (Generally speaking, this is true only for small oscillations. The larger ones decay somewhat faster[1].) However, after the electrons acquire sufficient energy there occurs intense electromagnetic radiation[2] which should, according to theory, cause noticeable synchrotron oscillations due to the quantum nature of the rediation[3]. Therefore, in the electron accelerators of high energy (~1000 mev) one should expect a diminution of the azimuthal dimensions of the electron bunch at the beginning of the acceleration cycle, and an increase later.

In this communication we propose an experimental method for investigating these radial-phase oscillations of electrons in the process of being accelerated to high energies. The method is based on the use of optical radiation from the electrons. Inasmuch as the radiation is sharply directed along the tangents to the orbit, it will be found in the form of short light pulses (thin radiation beams) whose length and shape are determined by the electron distribution, according to the amplitude of radial phase oscillation. Thus the problem of investigating the synchrotron oscillations is reduced to one of examining the light pulses. In the actual work we used a fast-acting optical shutter based on the Kerr effect in nitrobenzene (Kerr cell). Let us note that while the relaxation time in nitrobenzene is $10^{-9} - 10^{-12}$ sec (see, e.g., Refs. 4 and 5), we do not have to take it into account for the frequency of operation of the shutter, which is at best 100 *mc*.

The Kerr cell used in this work is represented schematically in the Figure. It consists of two

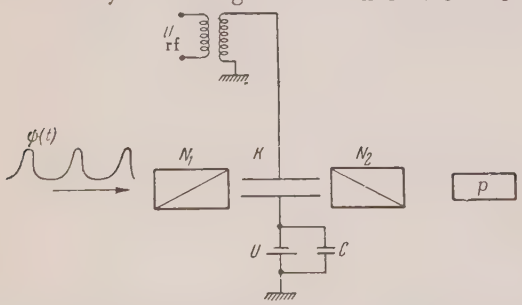

Schematic diagram of Kerr cell. p – radiant energy detector.

crossed Nicols, N_1 and N_2, between which is located a condenser K immersed in nitrobenzene. A steady voltage U is applied to the condenser, and at the same time, an alternating voltage U_{rf} from the generator which excites the synchrotron resonator. This makes the shutter operation frequency coincide with the frequency of appearance of the light pulses. When light rays from an electron bunch are transmitted through such a Kerr cell, the radiation detector p, with a sufficiently long time constant, will register a light beam J averaged in time. The magnitude of J depends on the time displacement θ between the shutter operation and the appearance of the light pulse. Designating by $\psi(t)$ and $f(t)$ the functions which describe the form of light pulse and the light transmission curve of the Kerr cell, $J(\theta)$ can be written as follows:

$$J(\theta) = \frac{1}{T}\int_0^T f(t-\theta)\,\psi(t)\,dt, \qquad (1)$$

where T is the period of circulation of electrons in synchrotron orbit.

The function $J(\theta)$ is found experimentally by measuring J at different values of θ between the limits 0 and T. A change in θ at high frequencies (~60 *mc*) can be accomplished by inserting delay lines between the generator of the voltage U_{rf}, and the condenser K. The function $f(t)$ is also experimentally determined. In form it coincides with the light intensity distribution, after modulation by the Kerr cell of the uninterrupted light beam. It is easy to find, using low-frequency modulation (the time t must be measured within a period T of the alternating voltage). It is necessary to make the low-frequency alternating voltage amplitude equal to the amplitude of U_{rf}. The unknown function $\psi(t)$ is found by solving integral equation (1).

Since the frequency of electron circulation in the synchrotron is known, the time in the function $\psi(t)$ can be replaced by the azimuthal angle α. Then $\psi(\alpha)$ will determine the distribution of electrons along the orbit. The alternating voltage U_{rf} should be impressed on the condenser K in the form of pulses, short with respect to the acceleration time and synchronized with the accelerating cycle. A shift of these pulses with respect to zero magnetic field of the accelerator allows a measurement of the azimuthal spread of the electron bunch at different stages of acceleration.

This method was applied to the synchrotron of the P. N. Lebedev Physical Institute, Academy of Sciences, USSR, having a maximum energy of 260 mev, an orbit radius of 81 cm, a circulation fre-

quency of 58 *mc* and acceleration time of 10,000 μ-sec. Preliminary investigation shows the azimuthal spread of the electron bunch at the end of the cycle is $100 \pm 10°$.

A detailed description of the method and results of this experiment will be published at a later date.

The author expresses his sincere gratitude to Prof. P. A. Cerenkov for valuable discussions.

[1] N. H. Frank, Phys. Rev. **70**, 177 (1946).

[2] D. D. Ivanenko and A. A. Sokolov, *Classical Theory of Fields*, Moscow, 1949.

[3] M. Sands, Phys. Rev. **97**, 470 (1955).

[4] I. R. Fabelinskii, Izv. Akad. Nauk SSSR, Fiz. Ser. **9**, 186 (1945).

[5] W. Hanle and O. Maercks, Z. Physik **114**, 407 (1939).

Translated by C. R. Lubitz
110

On the Derivation of a Formula for the Energy Spectrum of Liquid He^4

L. P. PITAEVSKII
Institute for Physical Problems
Academy of Sciences, USSR

(Submitted to JETP editor June 10, 1956)
J. Exptl. Theoret. Phys. (U.S.S.R.) **31**, 536-537
(September, 1956)

As is well known, Feynman [1], using a wave function of a special form, has obtained an expression for the spectrum of the elementary excitations in liquid He^4. A hydrodynamical derivation of this formula is presented below.

We shall begin with the Hamiltonian for a quantum liquid in the form[2]

$$\hat{H} = \frac{1}{2}\int m\hat{\mathbf{v}}n\hat{\mathbf{v}}d\tau + \hat{H}^1[n], \qquad (1)$$

where n is the number of atoms per unit volume and $\hat{H}^1[n]$ is the velocity-independent part of the Hamiltonian. We shall assume it to be a function of n. We set $n = \bar{n} + \delta n$ and expand $\hat{H}$ in terms of the second order in δn. The first-order term drops out and we obtain

$$\hat{H} = \hat{H}^1[\bar{n}] + \frac{m\bar{n}}{2}\int \hat{\mathbf{v}}^2 d\tau + \int \varphi(\mathbf{r}, \mathbf{r}')\,\delta n \delta n' d\tau d\tau', \qquad (2)$$

where φ is the second functional derivative of $\hat{H}^1$ with respect to n. Transforming now to Fourier components

$$\delta n = \sum_{\mathbf{k}} n_{\mathbf{k}} e^{i\mathbf{kr}}$$

and taking into account the equation of continuity in the form

$$\dot{\delta n} + \bar{n}\,\mathrm{div}\,\hat{\mathbf{v}} = 0, \qquad (3)$$

as well as the fact that φ depends only upon $|r - r'|$, we obtain

$$\hat{H} = \hat{H}^1[\bar{n}] + \sum_{\mathbf{k}}\left(\frac{m|\dot{n}_{\mathbf{k}}|^2}{2\bar{n}k^2} + \frac{1}{2}\varphi_{\mathbf{k}}|n_{\mathbf{k}}|^2 V\right). \qquad (4)$$

This expression has the form of a sum of the Hamiltonians of oscillators having frequencies:

$$\omega^2(\mathbf{k}) = (k^2\varphi_{\mathbf{k}}\bar{n}/m)\,V. \qquad (5)$$

For the determination of φ_k we note that the average value of the potential energy of an oscillator in the ground state is equal to $\hbar\omega/4$, whence

$$^1/_2\varphi_{\mathbf{k}}\overline{|n_{\mathbf{k}}|^2}V = {}^1/_4\hbar\omega(\mathbf{k}). \qquad (6)$$

As is well known, however, $S(k) = |\bar{n}_k|^2/\bar{n}$ is the Fourier component of the correlation function for the atoms of a liquid, which can be determined from diffraction experiments. Substituting φ_k from (6) into (5), we find for the energy of excitation

$$E(\mathbf{k}) = \hbar\omega(\mathbf{k}) = \hbar^2k^2/2mS(\mathbf{k}),$$

which agrees with Feynman's result.

In conclusion, I would like to express my thanks to L. D. Landau for his advice.

[1] R. P. Feynman, Phys. Rev. **94**, 262 (1954).

[2] L. D. Landau, J. Exptl. Theoret. Phys. (U.S.S.R.) **11**, 592 (1941).

Translated by S. D. Elliott
112

The Effect of a Transverse Magnetic Field on the Thermal Conductivity of Metals

Z. Ia. Evseev
Donetz Industrial Institute, Stalino
(Submitted to JETP editor February 26, 1956)
J. Exptl. Theoret. Phys. (U. S.S.R) 31, 331
(August, 1956)

LET us consider a metal, in which there is a heat flow $Q = Q_x$ and a magnetic field $H = H_z$. For the calculation of the coefficient of thermal conductivity we use the model of Sommerfeld,[1] according to which the flow depending on the motion of electrons under the action of the temperature gradient is set equal to zero. Accordingly,[2]

$$I_x = -\frac{3ne}{mv^3}\int \xi f v d\varepsilon, \qquad Q_y = \frac{3n}{2v^3}\int \eta f v^3 d\varepsilon \quad (1)$$

and analogously for I_y and Q_x. Here $(-e)$ is the charge on the electron, m is the mass of the electron, v is the velocity, ξ and η are the components of the velocity along the x and y axes, ϵ is the kinetic energy of the electron. The distribution function is taken to have the form

$$f = f_0 + \xi\chi_x + \eta\chi_y, \quad (2)$$

where f_0 is the Fermi distribution function, and the functions χ_x and χ_y (found with the aid of the kinetic equation, in which the term taking into account collisions, was derived by Lorentz[3]) equal:

$$\chi_x = -l(f_1 - qf_2)/v(1+q^2), \qquad \chi_y = -l(f_1 q + f_2)/v(1+q^2). \quad (3)$$

Here l is the length of the mean free path of the electron, and the rest of the variables are defined as follows:

$$q = \omega t/v = (eH/mc)\,l/v; \qquad f_1 = \partial f_0/\partial x - eE_x \partial f_0/\partial\varepsilon; \qquad f_2 = \partial f_0/\partial y - eE_y \partial f_0/\partial\varepsilon; \quad (4)$$

E_x and E_y are the components of the electric field resulting from the motion of the electrons under the action of the temperature gradient.

Calculation shows that the dependence of l on v for the present problem is immaterial, because the terms containing the derivative of l with respect to v, are small and do not enter into the expression for the coefficient for thermal conductivity $\varkappa$.

Making the usual calculation for the coefficient of thermal conductivity $\varkappa = -Q_x/\partial T/\partial x$ (in the present problem $I_x = I_y = 0$, $Q_y = 0$) with accuracy to the terms $\sim (kT/\bar{\varepsilon})^3$ ($\bar{\varepsilon}$ is the Fermi level), we obtain

$$\varkappa = \varkappa_0\left[1 - \frac{4\pi^2}{15}\left(\frac{kT}{mv^2}\right)^2 \frac{q^2(4+2q^2+3q^4)}{(1+q^2)^3}\right], \quad (5)$$

where $\varkappa_0 = \pi^2 nlk^2 T/3mv$ is the coefficient of thermal conductivity in the absence of a magnetic field.

Approximate calculation shows that formula (5) gives a decrease in the thermal conductivity of less than 0.01% of $\varkappa_0$ in a field of 10,000 Oersteds.

It can be shown that consideration of the effect is necessary for metals of the type of Bi which have a small number of conduction electrons.

In conclusion I must thank K. B. Tolpygo for a number of suggestions and E. I. Rashba for certain advice in the course of carrying out the work.

---

[1] A. Sommerfeld, Z. Physik 48, 51 (1928).
[2] H. Bethe and A. Sommerfeld, Electron Theory of Metals.
[3] G. Lorents, Theory of the Electron.

Translated by F. P. Dickey
56

Application of the Theory of Random Processes to Radiation Transfer Phenomena

L. M. Biberman and B. A. Veklenko
Moscow Power Institute
(Submitted to JETP editor April 17, 1956)
J. Exptl. Theoret. Phys. (U.S.S.R.) 31, 341-342
(August, 1956)

IN this note the motion of the photon is treated as a random process under the following very general assumptions: the medium is isotropic; its properties may be functions of time and space; the photon may be scattered, absorbed by an atom and reemitted, or absorbed in a collision of the second kind; the polarization of the radiation and the motion of the atom excited by a photon are not taken into account.

We begin with the function

$$f_{v_1}^{v_2}(r_1, \eta_1, \nu_1, t_1; r_2, \eta_2, \nu_2, t_2)\, dV_2\, d\eta_2\, d\nu_2,$$

It represents the probability that a photon, which at time t_1 and position $\mathbf{r}_1$ possesses a frequency ν_1 and a velocity ν_1 whose direction is specified by a set of direction cosines denoted by η_1, will at time t_2 be found in the element of volume dV_2 surrounding the point $\mathbf{r}_2$, with a frequency in the interval ν_2 to $\nu_2 + d\nu_2$, and with a velocity ν_2 whose direction lies in the interval η_2 to $\eta_2 + d\eta_2$.

In introducing different values for the speed of the photon, we have in mind free photons ($v=c$, where c is the speed of light) and photons absorbed by atoms ($v = 0$). In the case of photons absorbed by atoms, η and v' stand for the direction of their motion and the frequency before absorption. It is necessary to take these parameters into account inasmuch as in a given case the indicatrix of radiation may depend on the previous history of the photon. Such a choice of the function $f_{v_1}^{v_2}$ permits the motion of the photon to be regarded as a random process of mixed type without aftereffects. Therefore the same function $f_{v_1}^{v_2}$ must satisfy the generalized Markoff equation

$$f_{v_1}^{v_2}(1;2) = \sum_{v_3}\int f_{v_1}^{v_3}(1;3)\, f_{v_3}^{v_2}(3;2)\, dV_3 d\eta_3 d\nu_3, \quad (1)$$

where $f_{v_1}^{v_2}(1;2)$ is an abbreviation for the function introduced above.

Setting $t_3 = t_2 - \Delta t$ in (1) and letting Δt approach zero, we obtain the first integro-differential equation of Kolmogoroff-Feller for processes of mixed type

$$\begin{aligned}&\partial f_{v_1}^{v_2}(1;2)/\partial t_2 \qquad (2)\\ &= \sum_{v_3}\int f_{v_1}^{v_3}(1;\mathbf{r}_2,\eta_3,\nu_3,t_2) k_{v_3}^{v_2}(\mathbf{r}_2, t_2;\eta_3,\nu_3;\eta_2,\nu_2)\, d\eta_3 d\nu_3\\ &- f_{v_1}^{v_2}(1;2)\sum_{v'}\int k_{v_2}^{v'}(\mathbf{r}_2, t_2;\eta_2,\nu_2;\eta',\nu')\, d\eta' d\nu'\\ &- \sigma_{v_2}(\mathbf{r}_2, t_2, \nu_2)\, f_{v_1}^{v_2}(1;2) - \mathbf{v}(2)\,\mathrm{grad}\, f_{v_1}^{v_2}(1;2).\end{aligned}$$

The last term is the scalar product of the photon velocity at the point 2 with the gradient of the function $f_{v_1}^{v_2}$ at this same point.

Similarly, setting $t_3 = t_1 + \Delta t$ and letting Δt approach zero, we obtain a second equation

$$\begin{aligned}&-\partial f_{v_1}^{v_2}(1;2)/\partial t_1 \qquad (3)\\ &= \sum_{v_3}\int k_{v_1}^{v_3}(\mathbf{r}_1, t_1;\eta_1,\nu_1;\eta_3,\nu_3)\, f_{v_3}^{v_2}(\mathbf{r}_1, t_1;\eta_3,\nu_3;2)\, d\eta_3 d\nu_3\\ &- f_{v_1}^{v_2}(1;2)\sum_{v'}\int k_{v_1}^{v'}(\mathbf{r}_1, t_1;\eta_1,\nu_1;\eta',\nu')\, d\eta' d\nu'.\\ &- \sigma_{v_1}(\mathbf{r}, t_1, \nu_1)\, f_{v_1}^{v_2}(1;2) + \mathbf{v}(1)\,\mathrm{grad}\, f_{v_1}^{v_2}(1;2).\end{aligned}$$

The quantity $k_{v_1}^{v_2}(\mathbf{r}, t; \eta_1, \nu_1; \eta_2, \nu_2)$ in Eqs.(2) and (3) is the probability of change of state of the photon normalized per unit time. It takes into account scattering of the photon and its re-radiation by an atom; $\sigma_{v_1}(\mathbf{r}, t, \nu)$ takes into account processes of photon destruction, and its form is determined only by the initial velocity of the photon.

Explicit expressions for $k_{v_1}^{v_2}$ and σ_{v_1} are given below: $k_0^0 = 0$; $k_0^c = Ap_k(\eta_1, \nu_1; \eta_2, \nu_2)$, where A is the probability of spontaneous emission and $p_k(\eta_1, \nu_1; \eta_2, \nu_2)$ is the indicatrix of emission; $k_c^0 = k(\mathbf{r}, t, \nu_1)\, c\, \delta(\eta_1 - \eta_2)$, in which $k(\mathbf{r}, t, \nu_1)$ is the photon absorption coefficient of the atoms; $k_c^c = \varkappa(\mathbf{r}, t, \nu_1)\, cp_\varkappa(\eta_1, \nu_1; \eta_2, \nu_2)$, where $\varkappa(\mathbf{r}, t, \nu_1)$ is the coefficient and $p_\varkappa(\eta_1, \nu_1; \eta_2, \nu_2)$ the indicatrix of scattering; $\sigma_0(\mathbf{r}, t)$ is the probability of collisions of the second kind, calculated for a single excited atom; $\sigma_c(\mathbf{r}, t, \nu)$ is the coefficient of true absorption.

If we substitute the values of $k_{v_1}^{v_2}$ and σ_{v_1} into (2) and (3), then instead of each of these expressions we obtain a system of four integro-differential equations in the functions f_0^0, f_0^c, f_c^0 and f_c^c, which can be transformed into a system of integral equations. We note that simple transformations permit producing integro-differential or integral equations that contain only one of the functions $f_{v_1}^{v_2}$.

If the distribution of the sources of radiation and of collisions of the first kind in the volume V under consideration is known, then with the aid of the function $f_{v_1}^{v_2}$ it is easy to obtain the concentration of excited atoms and the radiation intensity as functions of space and time. Thus, by applying the theory of random processes it is possible under very general assumptions about the interaction of radiation with matter to derive the complete system of equations that describe the nonstationary process of radiation transfer in an isotropic medium whose properties are functions of space and time. Naturally the equations of radiation transfer (that are well known in the literature) the equations for the volume density of radiation and for the concentration of excited atoms,

can all be derived as special cases of the relations given above. It is to be noted that the first equation of Kolmogoroff-Feller permits the derivation of the complete system of equations for the desired probability densities. Comparison of the two equations permits determining the symmetry properties of the function $f_{v_1}^{v_2}(1;2)$ with respect to an interchange of indices, from which follows the general formulation of the principle of optical reversibility.

The probability density $f_{v_1}^{v_2}(1;2)$ considered here is closely connected, of course, with the transmission and reflection functions of V. A. Ambartsumian and with the probability of emergence of a photon employed by V. V. Sobolev. The authors hope to take up these problems in detail.

Translated by J. Heberle
63

The Lagrangian Function for a System of Identically Charged Particles

V. N. Golubenkov, Ia. A. Smorodinskii
(Submitted to JETP editor Dec. 2, 1955)
J. Exptl. Theoret. Phys. (U.S.S.R.) 31, 330
(August, 1956)

Darwin[1] has shown that it is possible to write the Lagrangian function for a system of charged particles, correct to the second order terms in the ratio of the velocity of the particle to the velocity of light. This is possible because the radiation of light is a third order effect in v/c and does not enter in the second order approximation.

It is of interest to point out the possibility of obtaining the Lagrangian function for a system of identically charged particles to a higher order of approximation. It is well known that in a system of identical particles (with precisely the same ratio of charge to mass) the radiation is proportional to the fifth power of v/c and not to the third power. Therefore the Lagrangian function for such a system can be written to the term v^4/c^4. It is easiest to use the method given in the book of Landau and Lifshitz[2] for its calculation.

It is not difficult to show that the third order terms in the Lagrangian function go to zero. A calculation of the fourth order terms leads to the following expression, which must be added to the second order Lagrangian function.

$$L^{(4)} = -\sum_a \frac{m_a v_a^6}{16c^4} + \frac{e^2}{8c^4}\sum_{b>a}\frac{1}{R_{ab}}\{2(\mathbf{v}_a\mathbf{v}_b)^2 \quad (1)$$

$$- v_a^2 v_b^2 + (\mathbf{nv}_a)^2 v_b^2 + (\mathbf{nv}_b)^2 v_a^2 - 3(\mathbf{nv}_a)^2(\mathbf{nv}_b)^2\}$$

$$+ \frac{e^2}{8c^4}\sum_{b>a}\{2(\mathbf{nv}_a)(\mathbf{v}_a\dot{\mathbf{v}}_a) - 2(\mathbf{nv}_b)(\mathbf{v}_b\dot{\mathbf{v}}_a) - v_a^2(\mathbf{n}\dot{\mathbf{v}}_b)$$

$$+ v_b^2(\mathbf{n}\dot{\mathbf{v}}_a) + (\mathbf{nv}_a)^2(\mathbf{n}\dot{\mathbf{v}}_b) - (\mathbf{nv}_b)^2(\mathbf{n}\dot{\mathbf{v}}_a)$$

$$- 3R_{ab}(\dot{\mathbf{v}}_a\dot{\mathbf{v}}_b) + R_{ab}(\mathbf{n}\dot{\mathbf{v}}_b)(\mathbf{n}\dot{\mathbf{v}}_a)\},$$

where $\mathbf{n}$ is a unit vector in the Direction $\mathbf{R}_{ab}$. Of course in making calculations the terms that contain the total derivative with respect to time are dropped.

The accelerations can be expressed here through the coordinates and velocities of the charges, consistent with the equations of motion, obtained by completely neglecting the retarded potentials, that is, from the Lagrangian function of zero approximation. Thus in the simplest case of two charges we have

$$\dot{\mathbf{v}}_1 = (e^2/m)\,\mathbf{n}/R^2; \qquad \dot{\mathbf{v}}_2 = -(e^2/m)\,\mathbf{n}/R^2,$$

where $\mathbf{R}_{21} = -\mathbf{R}_{12} = \mathbf{R}$ and $\mathbf{R}/R = \mathbf{n}$; after substituting in (1) we obtain

$$L^{(4)} = -\frac{mv_1^6}{16c^4} - \frac{mv_2^6}{16c^4} \quad (2)$$

$$+ \frac{e^2}{8c^4}\left\{\frac{1}{R}[2(\mathbf{v}_1\mathbf{v}_2)^2 - v_1^2v_2^2 + (\mathbf{nv}_1)^2v_2^2 + (\mathbf{nv}_2)^2v_1^2\right.$$

$$- 3(\mathbf{nv}_1)^2(\mathbf{nv}_2)^2] + \frac{3e^2}{m}[(\mathbf{nv}_1)^3 + (\mathbf{nv}_2)^2]$$

$$\left. - \frac{e^2}{m}(v_1^2 + v_2^2) + \frac{2e^4}{m^2R^3}\right\}.$$

The Lagrangian function of two identical charges with accuracy to the fourth order can be used for investigating the relativistic corrections in the scattering of high speed protons, and also for generalizing the well-known formula of Breit for the interaction of electrons (see Refs. 3,4). The calculation of the formula of Breit to fourth order was carried out by Maksimov; the results however are very lengthy, and we will not include them here.

The authors thank L. A. Maksimov for consideration of the work.

[1] C. Darwin, Phil. Mag. 39, 537 (1920).
[2] L. D. Landau and E. M. Lifshitz, *Classical Theory of Fields*.
[3] G. Breit, Phys. Rev. 34, 553 (1939).
[4] L. Landau, Z. Phys. Sowjetunion 8, 487 (1932).

Translated by F. P. Dickey
55

Charge Renormalization for an Arbitrary, Not Necessarily Small, Value of e_0

K. A. TER-MARTIROSIAN

(Submitted to JETP editor April 6, 1956)
J. Exptl. Theoret. Phys. (U.S.S.R.) 31, 157-159
(July, 1956)

RECENTLY Taylor[1], combining the results of Landau, Abrikosov and Khalatnikov[2] with the general theory of Gell-Mann and Low[3], attempted to prove in general that the only case in which the present electrodynamics does not lead to a contradiction is that with the renormalized charge e_c equal to zero (since otherwise the "seed" charge e_0 turns out to be imaginary and the interaction operator is non-Hermitian). In accordance with Ref. 3, Taylor writes the quantity $e_c^2 d_c(e_c^2, \xi)$ [d_c is the renormalized propagation function of the photon, and $\xi = \ln(-k^2/m^2)$] in the form of some function of only one variable*:

$$e_c^2 d_c = \Phi(\lambda_c),\ \lambda_c(\xi) \cdot\cdot e_c^2 \Big/ \left[1 - \frac{e_c^2}{3\pi}\xi - e_c^2 f_c(e_c^2)\right], \quad (1)$$

where $f_c(e_c^2)$ is some unknown function. Comparing Eq. (1) with the results of Ref. 2, Taylor shows that $\lim_{y\to 0} y f_c(y) = 0$, and

$$\Phi(\lambda_c) \approx \lambda_c, \quad \text{if} \quad \lambda_c \to +0. \quad (2)$$

With $\xi = L$, $L = \ln(\Lambda^2/m^2)$, where Λ is the cut-off limit for momentum, Eq. (1) determines the charge renormalization

$$e_0^2 = e_0^2 d(L) = e_c^2 d_c(L) = \Phi[\lambda_c(L)]. \quad (1')$$

If in Eq. (1) e_c^2 is regarded as an arbitrary fixed quantity, then for $L \to \infty$, $\lambda_c \to -3\pi/L$. Taylor obtains the result stated above by assuming that (2) holds also for $\lambda_c \to -0$:

$$\Phi(\lambda_c) \approx \lambda_c, \ \lambda_c \to -0, \quad (2')$$

i.e., that $\lambda_c \Phi(\lambda_c)$ is a function of λ_c continuous at zero. Indeed, for $L \to \infty$, $\lambda_c \approx -3\pi/L \to -0$, it follows from (1′) and (2′) that

$$e_0^2 \approx -3\pi L, \quad (3)$$

i.e., e_0 turns out to be an imaginary quantity.

Unfortunately, it is so far quite impossible to find any basis for the assumption on the continuity of the function $\lambda_c \Phi(\lambda_c)$ at the point $\lambda_c = 0$, so that Taylor's whole proof remains without foundation. Even the reverse appears more probable: that the function $\Phi(\lambda)$ has an essential singularity at $\lambda = 0$, for example, of the type $\exp(1/\lambda)$; this would correspond to the fact that all expansions in powers of e_c^2 are apparently asymptotic series. In any case one can display many functions $\Phi(\lambda)$ for which the condition (2) is fulfilled (i.e., the relation (1) of Gell-Mann and Low goes over for $e_c^2 \to 0$ into the formula $d_c = [1 - (e_c^2 \xi/3\pi)]^{-1}$ of Landau, Abrikosov and Khalatnikov), but (2′) and consequently also (3), are invalid**.

If, however, we consider all quantities before renormalization and confine ourselves to a simpler problem than the one attacked by Taylor, the whole discussion can be carried through quite rigorously. In fact, we assume that the "seed" coupling constant e_0^2 is an arbitrary fixed quantity. Moreover, $e_c^2 = e_c^2(e_0^2, L)$. We shall show that under these conditions $e_c^2 \to 0$ for $L \to \infty$ not only for $e_0^2 \ll 1$, but for arbitrary $e_0 \gtrsim 1$.

Indeed, according to Gell-Mann and Low[3], we have***

$$e_0^2 d(e_0^2, L - \xi) = \Phi(\lambda_0),\ \lambda_0(\xi) = e_0^2 \Big/ \left[1 + \frac{e_0^2}{3\pi}(L - \xi) - e_0^2 f_0(e_0^2)\right], \quad (4)$$

where $\Phi(\lambda)$ is the same function as in (1), and $f_0(e_0^2)$ is some unknown function. For $e_0 \to 0$ this equation goes over into the relation

$$d = \left[1 + \frac{e_0^2}{3\pi}(L - \xi)\right]^{-1} \quad (5)$$

of Ref. 2 only if

$$\lim_{y \to 0} [y f_0(y)] = 0 \quad (6)$$

and, moreover, the relation (2) must be satisfied. [The condition (6) must be fulfilled in any case: otherwise, for $e_0^2 \to 0$, Φ would depend on a quantity different from $e_0^2[1 + (e_0^2/3\pi)(L - \xi)]^{-1}$, and (5) would be in contradiction with (4)]. It must be noted that Eqs. (2) and (6) are not independent conditions; one follows from the other. In

fact, the functions $f_0(y)$ and $\Phi(y)$ can be expressed in terms of each other, since they are connected by the condition

$$d(e_0^2, 0) = 1, \quad (\xi = L),$$

which, by Eq. (4) gives

$$e_0^2 = \Phi\left[\frac{e_0^2}{1 - e_0^2 f_0(e_0^2)}\right] = \Phi\left[\frac{1}{e_0^{-2} - f_0(e_0^2)}\right]$$

or

$$f_0(y) = 1/y - [\Phi^{-1}(y)]^{-1}, \qquad (7)$$

where $\Phi^{-1}(y)$ is the function inverse to $\Phi(y)$. If (6) is satisfied, it follows that $\Phi^{-1}(y) \to y$ for $y \to 0$. But the function inverse to $\Phi^{-1}(y) \approx y$ will be $\Phi(y) \approx y$; i.e., we get Eq. (2). In an analogous way, Eq. (6) follows at once from (2) and (7).

From Eqs. (4) and (2) it follows at once that $e_c^2 \to 0$ for $L \to \infty$. Indeed, let us suppose that e_0^2 has a fixed (and arbitrary) value, and $L - \xi \to \infty$. Then, by Eq. (4), $\lambda_0(\xi) \to 3\pi/(L - \xi)$, i.e., according to Eq. (2),

$$e_0^2 d(e_0^2, L - \xi) \approx 3\pi/(L - \xi)$$

with increasing accuracy as $L - \xi$ is made larger. Since $e_c^2 d_c \equiv e_0^2 d$,

$$e_c^2 d_c(e_c^2, \xi) \approx 3\pi/(L - \xi), \quad L - \xi \to \infty.$$

For $\xi \to 0$, when $d_c \approx 1$, this equation gives

$$e_c^2 \approx 3\pi/L \to 0, \quad L \to \infty,$$

which was to be proved.

We note that if in Eq. (4) we regard e_0^2 as dependent on L, (as Taylor indeed assumed), the proof does not go through, since as L increases the quantity $e_0^2(L) f_0[e_0^2(L)]$ in Eq. (4) can change in such a way that λ_0 will not decrease, and will in general not be small for $L \to \infty$.

The writer expresses his gratitude to B. L. Ioffe and A. D. Galanin for discussion of the manuscript and valuable remarks.

* Cf. Ref. 3, Eq. (5.6). Account is taken of the relation $(-k^2/m^2)\Phi(e_c^2) = \exp(-3\pi/\lambda_c)$ if the function f_c of Eq. (1) is related to the function φ of Ref. 3 in the following way: $f_c = (1/e_c^2) + \ln\varphi(e_c^2)$ (the quantities k^2 and e^2 of Gell-Mann and Low are here denoted by $-k^2$ and e_c^2).

** For example, as Landau has remarked, for the function $[\ln(1 + e^{1/\lambda})]^{-1}$ the relation (2) holds, but the condition (2′) does not: for $\lambda \to -0$

$$[\ln(1 + e^{1/\lambda})]^{-1} \approx e^{1/|\lambda|}.$$

*** Cf. Eq. (B.11) of Ref. 3; note that

$$\frac{-k^2}{\lambda^2} G(e_0^2) = \exp(-3\pi/\lambda_0),$$

if in Eq. (4) $f_0(e_0^2) = e_0^{-2} + \ln G(e_0^2)$. Therefore,

$$F\left[\frac{-k^2}{\lambda^2} G(e_0^2)\right] \equiv \Phi(\lambda_0),$$

if $\Phi(y)$ is determined by the function F of Ref. 3 by the equation $\Phi(y) = F(e^{-3\pi/y})$.

[1] J. C. Taylor, Proc. Roy. Soc. (London) **A234**, 296 (1956).

[2] Landau, Abrikosov and Khalatnikov, Dokl. Akad. Nauk SSSR **95**, 497, 773, 1177 (1954).

[3] M. Gell-Mann and F. E. Low, Phys. Rev. **95**, 1300 (1954).

Translated by W. H. Furry
29

A Polarization Method for Measuring the Velocities of Particles with Intrinsic Magnetic Moment

S. G. KORNILOV
Saratov State University

(Submitted to JETP editor March 13, 1955)
J. Exptl. Theoret. Phys. (U.S.S.R.) **31**, 512-513 (September, 1956)

MEASUREMENT of the velocities of particles in a beam (spectrometry) is a typical problem of physical experiment. A polarization method can be used for particles which possess an intrinsic magnetic moment. The spectrometer resembles the type which is used to determine the magnetic moments of individual particles. In the path of the beam there is placed a polarizer, a device for rotating the plane of polarization, an analyzer and, finally, a particle detector. The device for spin rotation can be constructed in such a way as to change the orientation only for particles which possess a given energy. The analyzer removes the remaining particles. The detector readings correspond to the number of particles of the given energy in the beam spectrum.

For neutral atoms with spin it is technically

possible to construct the spectrometer in the following manner (for definiteness we shall discuss particles with spin ½). The particles enter a nonuniform Stern-Gerlach magnetic field which splits the beam into two components. Then the reorienting intrument (which will be described in detail below) flips the spins of atoms possessing a given velocity. Then the particles traverse a Stern-Gerlach field which is similar to the first field. This field further separates the two components of the beam, with the exception of the atoms which were reoriented. Instead, the latter are focused at a slit behind which the detector is placed. When necessary, on the straight line connecting the source with the slit the analyzer may contain a screen (filament) which prevents direct entry by spinless atoms in the detector. The detector can be a vacuum pressure gauge or a thermocouple.

A neutron spectrometer can contain Bloch ferromagnetic polarizers, such as are used for the measurement of the neutron magnetic moment. The sensitivity of the detectors should be determined from sources with a known spectrum. A detector of very simple geometry which permits an exact calculation of the sensitivity can also be used as a standard.

The most important part of the spectrometer is the reorienting device. This consists of a series of conductors, the current in which excites a periodic magnetic field along the particle trajectory. The field reverses its sign along the trajectory. Alternating current is used. It is evident that some particles possess such velocity that during their entire transit they will be in a field which does not change sign. The magnetic moment of such a particle precesses in the field and the field strength can be chosen to provide a spin rotation of 180° at the exit point, that is, reversal. Particles of other velocities enter a field which changes its sign. When the sign of the field changes, the direction of precession changes. As a result, during their passage the spins of such particles cannot be rotated through any appreciable angle. It is easily seen, however, that there is more than one resonance velocity, namely:

$$v_{res} = a\omega/(\pi + 2n\pi).$$

Here a is the half period of the field, ω is the current frequency, $n = 0, 1, 2 \ldots$ is the order of the maximum. The reversing system can be designed in such a way as to completely eliminate all maxima above the zeroth order. Moreover, they can be cut off by screens placed properly in the analyzer. During the measurements the resonance velocity changes with variation of ω. It is clear from elementary considerations that the resolving power of the spectrometer is approximately given by the total number N of field periods in the reorienting system and is independent of other properties of the system.

The author has calculated a few variants of the reorienting system. The quantum equation for the spin functions was solved. The particles were assumed to have a classical trajectory. For a field with a single component (in the region of the beam) when a sinusoidal current is used the probability of reversal close to resonance is

$$W(v) = {}^1/_2 - {}^1/_2 J_0 (A \sin \mu/\mu).$$

Here v is the particle velocity, J_0 is the zeroth order Bessel function, $\mu = N\omega a(1/v - 1/v_{res})$, A is a coefficient which is determined by the specific type of system. The maximum probability for reversal is 0.7. This is less than unity as a result of averaging over the current phases.

We shall take as an example the following technical realization of a reorienting system. Two parallel wires are extended in zigzag fashion along the particle trajectory so that the particle moves between them. Current from the generator is sent through these wires.

A second type of reorienting device uses constant fields. The system of conductors which produces the periodic field is supplied with direct current. In addition, an electromagnet excites a strong uniform field parallel to the magnetic moment of the particle. The reorienting mechanism is the same as in apparatus for the measurement of the magnetic moments of individual particles. The resonance velocity changes with the uniform field strength.

It is also possible to use combinations which unite characteristics of both types of reorientation devices.

With this atomic spectrometer it is possible to investigate various collision processes between atoms and molecules, chemical kinetics, the behavior of statistical systems and recoil atoms in nuclear physics. (Radicals possessing a magnetic moment can, of course, also be analyzed by the spectrometer.) The atomic spectrometer enables us to investigate processes which take place at temperatures of hundreds of thousands of degrees (and, in particular, to measure such temperatures) by analyzing the velocities of a beam of neutral atoms leaving the heated region. It

is thus possible that the spectrometer can be used in work on thermonuclear reactions, since hydrogen, deuterium and tritium atoms possess magnetic moments. With a neutron spectrometer it is possible to measure the cross sections of neutron interactions with nuclei and polarization effects, and to obtain the spectra of neutron sources. The measurable energy range goes from thermal ranges to the order of 10 mev. For large energies the size of the apparatus and the power of the generator are increased, but pulsed operation is possible.

Translated by I. Emin
96

Transformation Properties of the Electron-Positron Field Amplitudes

Iu. A. Gol'fand
P. N. Lebedev Physical Institute, Academy of Sciences, USSR
(Submitted to JETP editor, June 8, 1956)
J. Exptl. Theoret. Phys. (U.S.S.R.) 31, 535-536 (September, 1956)

ONE of the conditions for the relativistic invariance of a theory is that the state vectors Φ of the field transform according to some representation of the Lorentz group. Since any vector Φ can be obtained by operating on the vacuum state Φ_0 with creation and annihilation operators, the transformation of Φ reduces to the transformations of Φ_0 and of the creation operators, that is, of the field amplitudes. It will be shown that the field amplitudes do not transform according to the spinor representations of the Lorentz group, and that the amplitudes corresponding to electron and positron states transform independently of each other according to the same representations. We shall consider the inhomogeneous Lorentz group $\mathfrak{L}$, including space reflections but not time reflections. The question of time reflections is more complicated and requires special consideration. It is clear that the vacuum state Φ_0 is invariant under the group $\mathfrak{L}$. In order to derive the transformation properties of the field amplitudes we shall write the field operator $\psi(x)$ in the interaction representation in the following relativistically invariant form (in the following we make use of Feynman's [1] notation and set $\hbar = c = 1$)

$$\psi(x) = (2\pi)^{-3/2} \times \int \{u(p)\, a(p)\, e^{-ipx} + v(p)\, b^{+}(p)\, e^{ipx}\}\, d\Gamma. \qquad (1)$$

The integration in (1) is taken over the hypersurface given by $p^2 = m^2$, $p_4 \equiv \epsilon > 0$; $d\Gamma = (m/\epsilon)\, d^3 p$ is the invariant element of the hypersurface; $u(p) \equiv \| u_\mu^\alpha(p) \|$ is a matrix of four rows and two columns given by the two solutions of the Dirac equation for positive energy, normalized according to the condition $\bar{u}^\alpha u^\beta = \delta_{\alpha\beta}$; $v(p)$ is the charge conjugate matrix; $a(p) \equiv \begin{pmatrix} a_1(p) \\ a_2(p) \end{pmatrix}$ is the column operator consisting of electron annihilation operators, and $b^+(p)$ is the analogous column operator of positron creation operators. The operators a, b are normalized by the invariant δ-function on Γ, that is, they satisfy the anticommutation relations

$$[a(p), a^+(q)]_+ = \Delta(p-q), \text{ и т. д. } (\Delta(p) = (\varepsilon/m)\,\delta(\mathbf{p})).$$

Let us first consider the homogeneous Lorentz transformation. (Similar, though somewhat simpler, considerations hold for translations.) Under a transformation L the spinor field $\psi(x)$ transforms according to

$$\psi(x) \to \psi'(x) = S_L \psi(L^{-1}x), \qquad (2)$$

where S_L is the spinor representation of the Lorentz group, which satisfies the condition $S_{L_1} S_{L_2} = S_{L_1 L_2}$. It is easy to see that the transformation (2) is equivalent to the following system of transformations in p-space:

$$u(p) \to S_L u(L^{-1}p); \qquad a(p) \to a(L^{-1}p) \qquad (3)$$

with similar systems of transformations for v and b^+. From the relativistic invariance of the Dirac equation, however, it follows that

$$S_L u(L^{-1}p) = u(p)\, Z_L(p), \qquad (4)$$

where the second degree matrix $Z_L(p)$ is determined by the relation $Z_L(p) = u(p)\, S_L\, u(L^{-1}p)$.

The following properties of the matrix $Z_L(p)$ are easily established:

1) $Z_L(p)$ generates a representation of the Lorentz group, that is,

$$Z_{L_1}(p)\, Z_{L_2}(L_1^{-1}p) = Z_{L_1 L_2}(p). \qquad (5)$$

2) The representation (5) is unitary

$$Z_L^+(p) = Z_L^{-1}(p) = Z_{L^{-1}}(L^{-1}p).$$

Shirokov[2] has found a similar representation of the Lorentz group.

In view of (4), the transformation (3) can be written in the form

$$u(p) \to u(p); \qquad a(p) \to Z_L(p)\, a(L^{-1}p).$$

Carrying through similar considerations for the amplitudes b (making use of the charge conjugation of the u and v), we arrive at the following result: the transformation (2) reduces to the following system of transformations for the field amplitudes:

$$a(p) \to Z_L(p)\, a(L^{-1}p); \qquad b(p) \to Z_L(p)\, d(L^{-1}p). \quad (6)$$

Under this transformation the quantities $u(p)$ and $v(p)$ are not transformed at all. The transformation for the conjugate amplitudes a^+ and b^+ follow uniquely from (6).

The transformaion (6) can be represented in operator form. Let A be an operator in the space of the amplitudes $a_\alpha(p)$, $b_\alpha(p)$. The symbol $\langle A \rangle$ shall denote the expression

$$\langle A \rangle = \sum_{\alpha,\beta=1}^{4} \int a_\alpha^+(p)\, (p\alpha \mid A \mid q\beta)\, a_\beta(q)\, d\Gamma_p d\Gamma_q$$

(in order to condense the notation we have put $a_3 = b_4$, $a_4 = b_3$).

We arrive at the following relations:

$$e^{-\langle A \rangle} a_\alpha(p)\, e^{\langle A \rangle} = \sum_{\beta=1}^{4} \int (p\alpha \mid e^{A} \mid q\beta)\, a_\beta(q)\, d\Gamma_q; \quad (7)$$

$$e^{-\langle A \rangle} a_\alpha^+(p)\, e^{\langle A \rangle} = \sum_{\beta=1}^{4} \int a_\beta^+(q)\, (q\beta \mid e^{-A} \mid p\alpha)\, d\Gamma_q.$$

If, for A we take the operator $(1/2)\ i\epsilon_{\mu\nu} M_{\mu\nu}$, where $M_{\mu\nu}$ is the four-dimensional angular momentum for the representation (5), then (7) will describe the proper Lorentz transformations (6). Space reflections can be handled in a similar way.

The transformation corresponding to a translation can be put in the form of Eq. (7), setting

$$\langle A \rangle = i\alpha_\mu P_\mu = i\alpha_\mu \int p_\mu \{a^+(p)\, a(p) + b^+(p)\, b(p)\}\, d\Gamma.$$

In addition to the Lorentz transformation many other transformations can be represented in the form of Eq. (7); examples are charge conjugation, gauge transformations, etc. For instance, for a gauge transformation (with a constant phase α) we must take

$$\langle A \rangle = i\alpha Q = i\alpha \int \{a^+(p)\, a(p) - b^+(p)\, b(p)\}\, d\Gamma.$$

[1] R. P. Feynman, Phys. Rev., **76**, 749 (1949).

[2] Iu. M. Shirokov, Dokl. Akad. Nauk SSSR **94**, 857 (1954); **99**, 137 (1954).

Translated by E. J. Saletan
111

Determination of the Spins of K-Particles and Hyperons

L. I. Lapidus
Institute for Nuclear Problems
Academy of Sciences, USSR

(Submitted to JETP editor April 30, 1956)
J. Exptl. Theoret. Phys. (U.S.S.R.) **31**, 342-343
(August, 1956)

At present very little is known about the spin values of heavy mesons and hyperons. Some information can be obtained from a detailed study of the decay products[1-3]. But even for the τ-particles, which occupy the most privileged position among all the "strange" particles, there are inconsistent data[4,5].

As "strange" particles cannot be transformed into "common" particles as the result of a strong interaction, they are not produced with large probability in reactions analogous to the reaction $p + p \rightleftarrows d + \pi$, by means of which it would be possible to determine the spin of one unknown particle. The reaction

$$K^- + d \rightleftarrows \Sigma^- + p, \quad (1)$$

which is analogous to the reaction $\pi^- + d \leftrightarrows n + n$, is not forbidden for slow scalar K-particles, as is was for π-mesons, inasmuch as Σ^- and p do not appear to be identical particles. Lee[6] has shown that the reaction (1) can be used for determining the spins of the new particles.

It is not difficult to see that for the same purposes the analogous reactions with various other nuclei can be used together with (1), for example,

$$K^- + H^3 \rightleftarrows \Sigma^- + d, \quad K^- + He_2^4 \rightleftarrows \Sigma^- + He_2^3, \quad (2)$$

$$K^- + He_2^4 \rightleftarrows \Lambda^0 + H^3 \text{ , etc.} \quad (3)$$

The experimental data on the interaction of slow K-particles with nuclei seem to indicate that the first of the two capture processes

$$K^- + N \rightarrow \Lambda^0 + \pi, \quad K^- + N \rightarrow \Sigma + \pi \qquad (4)$$

is more probable than the second[4] by an order of magnitude. In connection with these, on the one hand, a study of the reaction of type (3) may be fruitful; but, on the other hand, it is of interest to examine other possibilities for obtaining information about the spins of the new particles. Some information can be obtained from a comparison of the probabilities of exchange collisions of K-particles with hydrogen and deuterons[8].

Another possibility of obtaining information about the spins of hyperons and K-particles is connected with the fact that beams of particles produced in nuclear interactions are partly polarized. As is well known, the scattering cross section of a polarized beam depends on the angle θ as well as on the azimuth φ. But if the θ dependence is connected with which transitions play a role, then the nature of the φ dependence is determined by the spin of the particle. Thus for particles with spin ½ the characteristic dependence is proportional to $\cos\varphi$, for spin 1, to $\cos\varphi + A\cos 2\varphi$, and for spin 3/2, to $\cos\varphi + a\cos 2\varphi + b\cos 3\varphi$. For particles with arbitrary spin the φ dependence is characterized by the expression

$$\sum_{n=1}^{2s} A_n \cos n\varphi,$$

where s is the spin of the particle. The origin of such a dependence is connected with the fact that the orbital angular momentum does not have a z-component ($m = 0$), so that the values of the z-component of the total angular momentum agree with the allowed values of the z-components of the spin of the particles.

Knowing, e.g., the mode of decay, it is possible to ascertain whether the particles are bosons (integral spin) or fermions (half-integral spin). Consequently, knowing, e.g., that the K-particle appears to be a boson, it is necessary to have the possibility to separate experimentally the absence of a dependence on φ for $s = 0$ from the existence of the dependence of the form $\cos\varphi + A\cos 2\varphi$ for $s = 1$.

[1] R. H. Dalitz, Phil. Mag. 44, 1068 (1953); Phys. Rev. 94, 1046 (1954); Phys. Rev. 99, 915 (1955).

[2] E. Fabri, Nuovo Cimento 11, 479 (1954).

[3] L. D. Puzikov and Ia. A. Smorodinskii, Dokl. Akad. Nauk SSSR 104, 843 (1955).

[4] Bhowmik, Evans, van Heerden and Prowse, Nuovo Cimento 3, 574 (1956).

[5] G. Costa and L. Taffara, Nuovo Cimento 3, 169 (1956).

[6] T. D. Lee, Phys. Rev. 99, 337 (1955).

[7] George, Herz, Noon and Solntseff, Nuovo Cimento 3, 94 (1956).

[8] L. B. Okun', J. Exptl. Theoret. Phys. (U.S.S.R.) 30, 218 (1956); Soviet Phys. JETP 3, 142 (1956).

Translated by J. Heberle
64

Spin-Orbit Interaction in Nuclear Magnetic Multipole Radiation

D. P. GRECHUKHIN

(Submitted to JETP editor February 12, 1956)
J. Exptl. Theoret. Phys. (U.S.S.R.) 31, 513-515
(September, 1956)

IN Moszkowski's review[1] of nuclear multipole radiation, esitmates are given for the probabilities of radiative transitions in the single-particle nuclear model. For ML-radiation with a nucleonic transition from the state (n_1, l_1, j_1, μ_1) to the state (n_2, l_2, j_2, μ_2) with the following changes of the nucleonic moments: $\Delta j = L$; $\Delta l = L + 1$ (for example, $M1$-radiation from the $d_{3/2} - s_{1/2}$ transition), the formulas which are given are unsuitable. As has been noted in Ref. 2, in proton transitions of this type, the proton spin-orbit interaction makes an essential contribution, so that the perturbation operator contains the additional term $-(e/c)\Phi \times (v)\,(\sigma \cdot \mathrm{r} \times \mathbf{A})$. In a neutron transition this term does not appear because the neutron bears no charge. However, even in this case an ML-transition is not absolutely forbidden, as is assumed in Refs. 1 and 2. Its intensity is lower [by the factor $\sim(4E^2/1840 \cdot (2L+3)]$ than the intensity of the corresponding proton transition (E is the photon energy in mev), but it is comparable with the probability of the electric multipole transition $E(L+1)$ for energies of the order of 5 mev with $A = 100$, and for energies < 1 mev in the case of transition with $L > 1$.

References 1 and 2 do not contain estimates of the probabilities for ML transitions of the type $\Delta j = L$, $\Delta l = L + 1$ when the spin-orbit coupling of the nucleon is taken into consideration. The results of such a calculation are given below. (All quantities are given in terms of the relativistic units $\hbar = m_e = c = 1$.) The transition probability is determined by the matrix element of the perturbation operator:

$$\hat{H} = -\mu_0 (e/2M)(\sigma \mathbf{H}) - e\Phi(\mathbf{r})(\sigma \cdot \mathbf{r} \times \mathbf{A}_L^0)\delta,$$

where μ_0 is the algebraic value of the magnetic moment of the nucleon in nuclear Bohr magnetons; $\Phi(r)$ is the spin-orbit interaction potential. The symbol δ is equal to 1 for a proton and 0 for a neutron. $\mathbf{A}_L^0$ is the potential of a ML-multipole photon with the wave vector k and polarization ϵ:

$$\mathbf{A}_L^0 = 4\pi \sqrt{2\pi/k}\, i^L \sum_M (\varepsilon Y^{0*}_{LM}(\theta_k, \Phi_k))\, \mathbf{Y}^0_{LM}(\theta,\varphi)\, f_L(kr)\, e^{ikt}$$

Using the relations between spherical harmonics[3] and expanding the Bessel spherical functions $f_L(kr)$ in series for $kr \ll 1$ we obtain for the perturbation operator of an ML-transition with $\Delta j = L$, $\Delta l = L + 1$:

$$\hat{H} = i^{L+1} e 4\pi \sqrt{2\pi/k} \left[\frac{(kR)^L R}{(2L+1)!!}\right] \times \left\{\frac{\mu_0}{2M}\frac{k^2}{2L+3} x^{L+1} - \Phi(x) x^{L+1}\delta\right\} \times \sqrt{\frac{L}{2L+1}} \sum_M (\varepsilon \mathbf{Y}^{0*}_{LM}(\theta_k, \Phi_k))\, (\sigma \mathbf{Y}^{+1}_{LM}(\theta, \varphi)),$$

where $x = r/R$, R is the nuclear radius and $0 \leq x \leq 1$. From perturbation theory the transition probability is

$$W_{ML} = \frac{2\pi}{2j_1+1} \sum_{\mu_1, \mu_2, \varepsilon} |\langle \Psi^+_{n_2 j_2 \mu_2} | \hat{H} | \Psi_{n_1 j_1 \mu_1} \rangle|^2 \rho_k; \quad \rho_k = \frac{k^2}{2\pi^2},$$

where the wave function of the nucleon is taken in the form

$$\Psi_{nlj\mu} = R_{jln}(x)\, \Omega_{j\mu}(\theta,\varphi) = R_{jln}(x) \sum_{m\alpha} C^{j\mu}_{lm\sigma\alpha} Y_{lm\varphi\sigma\alpha}.$$

The matrix element is separated into radial and angular parts, and we obtain for the transition probability

$$W_{ML} = 2e^2 \frac{(kR)^{2L+1}R}{[(2L+1)!!]^2} \left| \langle R^*_{j_2 l_2 n_2}(x) \left| \frac{\mu_0}{2M}\frac{k^2}{2L+3} x^{L+1} - \Phi(x) x^{L+1}\delta \right| R_{j_1 l_1 n_1} \rangle \right|^2 S,$$

where

$$S = \frac{L}{(2L+1)} \frac{(4\pi)^2}{(2j_1+1)} \sum_{\mu_1 \mu_2 \varepsilon} |\langle \Omega^+_{j_2\mu_2} | \sum_M (\varepsilon \mathbf{Y}^{0*}_{LM}(\theta_k, \Phi_k))(\sigma \mathbf{Y}^{+1}_{LM}(\theta,\varphi) | \Omega_{j_1\mu_1}\rangle|^2$$

$$= {}^3/_4\, L\, (2l_1+1)(2L+3)(2j_2+1)(C^{l_2 0}_{l_1 0 L+10})^2 \times \left[\sum_j (2j+1)\, W(j_2\, j_1 L+11;\, Lj)\, W(l_1\, j_1 \sigma 1;\, j)\, W(\sigma j_2 l_1 L+1;\, l_2 j)\right]^2.$$

In the practically important cases $l_1 = 0$ and $l_2 = 0$, the formula for S is considerably simplified:

for $l_1 = 0$ $\quad S = {}^3/_4 L\, (2j_2+1)\, W^2(j_1 \sigma L l_2;\, 1 j_2)$;

for $l_2 = 0$ $\quad S = {}^3/_4 L\, (2j_2+1)\, W^2(j_2 \sigma L l_1;\, 1 j_1)$.

For the purpose of evaluating the radial part of the transition matrix element we set:

$$\langle R^*_{j_2 l_2 n_2}(x) | \Phi(x)\, x^{L+1} | R_{j_1 l_1 n_1}(x) \rangle \approx \langle \Phi(x) \rangle_{av} \langle R^*_{j_2 l_2 n_2} | x^{L+1} | R_{j_1 l_1 n_1} \rangle \approx \frac{3}{L+4} \langle \Phi \rangle_{av},$$

where $\langle \Phi \rangle_{av}$ is the diagonal element of the spin-orbit coupling potential. According to Ref. 3, $\langle \Phi(x) \rangle_{av} \simeq -9.6 A^{1/3}$ (in our units), where A is the mass number of the nucleus. Using this value we obtain for the probability of an ML-transition with $\Delta j = L$, $\Delta l = L + 1$:

$$W_{ML} = 1.8 e^2 \frac{(kR)^{2L+1}R}{[(2L+1)!!]^2} \frac{9}{(L+4)^2} \times \left[\frac{\mu_0}{2}\frac{1}{1840}\frac{k^2}{2L+3} + 9{,}6 A^{-2/3}\delta\right]^2 S \cdot 10^{21}\, \mathrm{sec}^{-1},$$

where k is the photon energy in the units $m_e c^2 = 0.511$ mev, $e^2 = 1/137$, and R is the nuclear radius: $R = 0.85\, A^{1/3}\, 274$ ($R = 1.25 \times 10^{-13} A^{1/3}$ cm).

As can easily be ssen, the spin-orbit term for $k < 16$ (< 8 mev) is considerably larger than the first term. Indeed, for $k = 16$ we obtain $1/2\, (\mu_0/1840) k^2/(2L+3) \leq 1/5\, (256/1840) = 0.028$, which is smaller than $9.6\, A^{-2/3}$ even

when $A = 200$; therefore, the first term can be neglected in proton transitions. For neutron transitions the second term disappears and the transition probability is determined entirely by the first term in the square brackets. It is interesting to compare the probability of and $E(L+1)$ transitions of neutrons:

$$W_{ML}/W_{E(L+1)} = S_{ML}/S_{E(L+1)}$$

$$(\mu_0 k A^L/2z)^2 \leqslant (S_{ML}/S_{E(L+1)}) \quad (2kA^{L-1}/1840)^2.$$

When $k \approx 10$ and $A = 100$ the probabilities W_{M1} and W_{E2} are of the same order of magnitude, and the radiation probabilities of the higher multipoles $M2$ and $M3$ are comparable even at low energies with the probabilities for $E3$ and $E4$ transitions.

[1] S. A. Moszkowski, Phys. Rev. 89, 474 (1953).

[2] J.H.D. Jensen and M. Goeppert-Mayer, Phys. Rev. 85, 1040 (1952).

[3] Berestetskii, Dolginov and Ter-Martirosian, J. Exptl. Theoret. Phys. (U.S.S.R.) 20, 527 (1950).

Translated by I. Emin
97

A Dispersion Relation for All Scattering Angles

E. S. FRADKIN
P. N. Lebedev Physical Institute
Academy of Sciences, USSR

(Submitted to JETP editor March 17, 1956)
J. Exptl. Theoret. Phys. (U.S.S.R.) 31, 515-517
(September, 1956)

A DISPERSION relation for forward scattering has been obtained by Goldberger *et al.* [1,2]. In the present note a relation is obtained between the imaginary and real parts of the scattering amplitude for all angles.

To obtain this relation one can use Goldberger's method[1], in which it is simplest to employ the coordinate system in which the combined momentum of the nucleons (incident and scattered) is zero. However, we shall derive our dispersion relation here by using some results obtained by Nambu[3].

According to Nambu[3], the Feynman matrix element for the scattering of bosons (with momentum k and charge index α) by fermions (with momentum p and additional quantum numbers λ) can be represented independently of the type of interaction in the form

$$F_{\alpha\beta}(k, \alpha; p, \lambda; k', \beta; p', \lambda') \tag{1}$$

$$= \bar{u}^{\lambda'}(p') \sum_{n=0,1} \{(\hat{k})^{n_1} (\tau_{\alpha\beta})^{n_2} \rho_{n_1 n_2}((p-p')^2, (p+k)^2)$$

$$+ (-\hat{k})^{n_1} (\tau_{\beta\alpha})^{n_2} \rho_{n_1 n_2}((p'-p)^2,$$

$$(p-k')^2)\} u^{\lambda}(p)\, \delta(p+k-p'-k'),$$

where

$$\rho(p^2, k^2) = \int \nu_{n_1 n_2}(p^2, u)\, \delta_+(k^2+u)\, du, \tag{2}$$

$$k'^2 = k^2 = -\mu^2, \quad \tau_{\alpha\beta} = \frac{1}{2}[\tau_\alpha, \tau_\beta],$$

in which the values of u are given by $u = m^2$ and $u \geq (m+\mu)^2$.

The type of interaction affects only the dependence of ν on the arguments. By dividing $\delta_+(k^2)$ into $i\pi\delta(k^2)$ and Pk^{-2} we obtain the imaginary and real parts, respectively, of the scattering amplitude $F_{\alpha\beta}$. It is convenient to continue our investigation in the coordinate system where the combined momentum of the nucleons is zero (i.e., $p' + p = 0$). Taking the z axis in the direction of the vector p we have

$$p(E = \sqrt{m^2+p^2},\ 0, 0, p);\ p'(E, 0, 0, -p);$$

$$k(k_0 = \omega$$

$$= \sqrt{p^2 + k_x^2 + k_y^2 + \mu^2};\ k_x, k_y, -p);\ k'(\omega, k_x, k_y, p).$$

From (1) and (2) we obtain (hereafter $\delta(p+k-p'-k')$ will be omitted]:

$$F_{\alpha\beta} = D_{\alpha\beta} + i\tilde{A}_{\alpha\beta};\ \tilde{A}_{\alpha\beta} = a_{\alpha\beta} + b_{\alpha\beta}; \tag{3}$$

$$D_{\alpha\beta}(k, p, \lambda'\lambda) = \bar{u}(p')^{\lambda} \tag{4}$$

$$\sum_{n=0,1} \left\{ (\hat{k})^{n_1} (\tau_{\alpha\beta})^{n_2} \int \frac{\nu_{n_1 n_2}((p-p')^2, u)\, du}{(p+k)^2+u} \right.$$

$$\left. + (-\hat{k})^{n_1} (\tau_{\beta\alpha})^{n_2} \int \frac{\nu_{n_1 n_2}((p-p')^2, u)}{(p'-k)^2+u}\, du \right\} u^{\lambda}(p')^{\lambda};$$

$$a_{\alpha\beta} = \pi \bar{u}^{\lambda'}(p') \tag{5}$$

$$\times \sum_{n=1,0} \{(\hat{k})^{n_1} (\tau_{\alpha\beta})^{n_2} \nu_{n_1 n_2}((p'-p)^2, -(p+k)^2)\} u^{\lambda}(p);$$

when $-(p+k)^2 \geqslant (m+\mu)^2$;

and $$b_{\alpha\beta} = \pi \bar{u}^{\lambda'}(p') \times \sum \{(-\hat{k})^{n_1} (\tau_{\beta\alpha})^{n_2} v_{n_1 n_2}((p'-p)^2, -(p'-k)^2)\} u^{\lambda}(p), \tag{6}$$

when $-(p'-k)^2 \geq (m+\mu)^2$ or m^2. It is easily seen from Eqs. (1), (2) and (2a) that when the polarization of the nucleon does not change, the following dispersion relations hold *:

$$D^{(1)}_{\alpha\beta}(\mathbf{p}, \omega, \lambda', \lambda) - D^{(1)}_{\alpha\beta}(\mathbf{p}, 0, \lambda', \lambda) = \frac{\omega^2 - \omega_0^2}{\pi} \int_0^\infty \frac{2\omega' A^{(1)}_{\alpha\beta}(\mathbf{p}, \omega', \lambda', \lambda) d\omega'}{(\omega'^2 - \omega^2)(\omega'^2 - \omega_0^2)}; \tag{7}$$

$$D^{(2)}_{\alpha\beta}(\mathbf{p}, \omega, \lambda', \lambda) - \frac{\omega}{\omega_0} D^{(2)}_{\alpha\beta}(\mathbf{p}, \omega_0, \lambda', \lambda) = \frac{2\omega(\omega^2 - \omega_0^2)}{\pi} \int_0^\infty \frac{A^{(2)}(\mathbf{p}, \omega', \lambda', \lambda', \lambda) d\omega'}{(\omega'^2 - \omega^2)(\omega'^2 - \omega_0^2)}, \tag{8}$$

where

$$2D^{(1),(2)}_{\alpha\beta} = D_{\alpha\beta} \pm D_{\beta\alpha}, \quad 2A^{(1),(2)}_{\alpha\beta} = A_{\alpha\beta} \pm A_{\beta\alpha}, \quad A_{\alpha\beta} = a_{\alpha\beta} - b_{\alpha\beta}. \tag{9}$$

Repeating the calculations in Ref. 2 we obtain

$$D_+(\omega, \mathbf{p}) - \frac{1}{2}\left(1 + \frac{\omega}{\omega_0}\right) D_+(\omega_0 \quad) - \frac{1}{2}\left(1 - \frac{\omega}{\omega_0}\right) D_-(\omega_0, \mathbf{p}) = \frac{2(\omega^2 - \omega_0^2)}{\pi} \int_0^\infty \frac{\omega' d\omega'}{\omega'^2 - \omega_0^2} \times \left[\frac{A_+(\omega', \mathbf{p})}{\omega' - \omega} + \frac{A_-(\omega', \mathbf{p})}{\omega' + \omega}\right] = B; \tag{10}$$

$$D_-(\omega, \mathbf{p}) - \frac{1}{2}\left(1 + \frac{\omega}{\omega_0}\right) D_-(\omega_0) - \frac{1}{2}\left(1 - \frac{\omega}{\omega_0}\right) D_+(\omega_0, \mathbf{p}) = \frac{2(\omega^2 - \omega_0^2)}{\pi} \int_0^\infty \frac{d\omega'}{\omega'^2 - \omega_0^2} \times \left[\frac{A_-(\omega', \mathbf{p})}{\omega' - \omega} + \frac{A_+(\omega', \mathbf{p})}{\omega' + \omega}\right] = B_1, \tag{11}$$

where $D_\pm (A_\pm)$ is the real (imaginary) part of the scattering amplitude of a positive (or negative) meson by a proton. Since the imaginary part of the amplitude in the integrands is taken for a fixed nucleonic energy and variable meson energy ω, there is a direct relation to experiment only for those $A(\omega')$ for which ω' is higher than the threshold energy $\omega' \geq \omega_0 = \sqrt{\mu^2 + p^2}$.

In the energy range from 0 to ω_0, $A(\omega)$ contains contributions not only from the "neutron" state ($u = m^2$) but from the entire spectrum of states with energies from $|m\mu - p^2|/|m^2 + p^2|^{1/2}$ to ω_0.

The contribution of the "neutron" state can be calculated exactly since it is equal to

$$-\pi(\bar{u}(p')\Gamma(p', k')u(p'-k')) \times (\bar{u}(p'-k')\Gamma(p'-k', p-k'-p)u(p)) \times \delta\left(\omega' - \frac{\mu^2 + 2p^2}{2(m^2 + p^2)^{1/2}}\right); \tag{12}$$

here $\Gamma(p, s)$ is $g\gamma_5\tau$ when $p^2 = -m^2$, $s^2 = -\mu^2$ (where g is the exact renormalized coupling constant in the pseudoscalar theory).

It is easily seen that $A(\omega')$ in the continous energy spectrum from $|m\mu - p^2|/(m^2 + p^2)^{1/2}$ to ω_0 can be obtained by analytic continuation in the region of imaginary momenta k.

We have finally

$$B(k) = \frac{2k^2}{\pi} \int_0^\infty \frac{dk'}{k'} \times \left[\frac{A_+(k', p)}{(\mu^2 + p^2 + k'^2)^{1/2} - (\mu^2 + p^2 + k^2)^{1/2}} + \frac{A_-(k', p)}{(\mu^2 + p^2 + k'^2)^{1/2} + (\mu^2 + p^2 + k^2)^{1/2}}\right] + \frac{2k^2}{\pi} \int_0^\infty \frac{dk'}{k'} \times \left[\frac{A_+(ik', p)}{(\mu^2 + p^2 + k^2)^{1/2} - (\mu^2 + p^2 - k'^2)^{1/2}} - \frac{A_-(k', p)}{(\mu^2 + p^2 - k'^2)^{1/2} + (\mu^2 + p^2 + k^2)^{1/2}}\right] + \frac{g^2(\mu^2 + 2p^2)(m^2 + p^2)^{1/2} k^2}{2(\mu^2 + p^2) m^3 \{\sqrt{\mu^2 + p^2 + k^2} + (\mu^2 + 2p^2)/2(m + p^2)^{1/2}\}}, \tag{13}$$

where

$$\alpha = p\left(\frac{2m\mu+\mu^2}{m^2+p^2}\right)^{1/2};$$

$$B_1(k) = \frac{2k^2}{\pi}\int_0^\infty \frac{dk'}{k'(\mu^2+p^2+k'^2)^{1/2}}\left[\frac{A_-(k',p)}{(\mu^2+p^2+k'^2)^{1/2}-(\mu^2+p^2+k^2)^{1/2}} + \frac{A_+(k',p)}{(\mu^2+p^2+k'^2)^{1/2}+(\mu^2+k^2+p^2)^{1/2}}\right]$$

$$+\frac{2k^2}{\pi}\int_0^\alpha \frac{dk'}{k'(\mu^2+p^2-k'^2)^{1/2}}\left[\frac{A_-(ik',p)}{(\mu^2+p^2+k^2)^{1/2}-(\mu^2+p^2-k'^2)^{1/2}} - \frac{A_+(ik',p)}{(\mu^2+p^2-k'^2)^{1/2}+(\mu^2+p^2+k^2)^{1/2}}\right]$$

$$-\frac{g^2(\mu^2+2p^2)(m^2+p^2)^{1/2}k^2}{2m^3(\mu^2+p^2)\{(\mu^2+p^2+k^2)^{1/2}-(\mu^2+2p^2)/2(m^2+p^2)^{1/2}\}}. \qquad (14)$$

* After the present work was completed (January 1956) the author learned that B. L. Ioffe and A. Salam had also obtained the relation (8).

[1] M. L. Goldberger, Phys. Rev. 99, 979 (1955).

[2] Goldberger, Miyazawa, and Oehme, Phys. Rev. 99, 986 (1955).

[3] Y. Nambu, Phys. Rev. 100, 394 (1955).

[4] A. Salam, Nuovo Cimento 3, 424 (1956).

Translated by I. Emin
98

A New Impulse Technique for Ion Mass Measurements

S. G. ALIKHANOV

(Submitted to JETP editor May 8, 1956)
J. Exptl. Theoret. Phys. (U.S.S.R.) 31, 517-518
(September, 1956)

PRECISE measurement of the mass of isotopes makes it possible to determine the binding energy of nucleons in a nucleus. The existing method of measuring masses through the use of a mass spectrograph involving magnetic deflection is not of sufficient accuracy for medium and heavy nuclei. Consequently, there is justification for proposing a new method of measuring masses.

We are familiar with the existing technique[1-3] for mass analysis which is based on measurement of the time of flight of ions with given energy over a specified distance. However, the energy spread of the ions formed in the source sets a limit of the order of 100 to 200 on the resolving power of this type of instrument. In the following a new method of energy focusing is proposed which is applicable to this type of spectrometer and which can considerably increase its resolving power.

This mass spectrometer has the form of a drift tube which is bounded at both ends by retarding fields with a linear potential distribution. The entire instrument is placed in a weak longitudinal magnetic field. A bunch of ions from the pulsed source is injected into the tube with simultaneous switching-off of the retarding field. Having entered a "potential well' the bunched ions begin to move from one repeller to the other, but the gain in the time of flight by the faster ions over the slower ions with given e/M will be balanced by loss of velocity in the retarding field. Ions with identical e/M and different energies will be focused at a certain point in the drift tube*. After a sufficient number of cycles, when ions with close values of e/M have been separated out, that is, their shift in time of arrival at the focal point is greater than the duration of the pulses, the latter are deflected and recorded. In view of the fact that bunches of ions of different masses will be oscillating in the tube the voltage which must be applied to the deflecting plates will be switched off only at the instant when ions of the masses to be measured are passing. The transit time of ions with mass M, charge Ze and energy U (in volts) in a drift of length l is

$$t_0 = l\sqrt{M/2UZe}. \qquad (1)$$

The time of motion of the ions in a retarding electric field of constant strength E until they are stopped is

$$t = E^{-1}\sqrt{2UM/Ze}. \quad (2)$$

Thus the time of a complete cycle with retarding fields E_1 and E_2 is

$$T = l\sqrt{2M/UZe} + 2(1/E_1+1/E_2)\sqrt{2UM/Ze}. \quad (3)$$

The condition $\partial T/\partial U = 0$ gives

$$1/E_1 + 1/E_2 = l/2U_0. \quad (4)$$

If the magnitudes of U_0, l, E_1 and E_2 are chosen to satisfy the relation (4) we shall achieve first-order space-time grouping (focusing) of ions of different energies. In that event, the time of a complete cycle will be

$$T_0 = 2l\sqrt{2M/U_0Ze}. \quad (5)$$

However, this will not satisfy the condition for second-order focusing

$$\partial^2 T/\partial U^2 = l\sqrt{M/2ZeU_0^5}$$

and the spread in time of a cycle for ions of identical mass but energy spread ΔU is

$$\Delta T_U \approx (l/2)\sqrt{M/2ZeU_0^5}\,(\Delta U)^2.$$

The difference in the period of a cycle for ions of mass difference ΔM but identical energy is

$$\Delta T_M \approx l\sqrt{2/ZeMU_0}\,\Delta M.$$

By equating these quantities we obtain a formula for the limit of resolution which is determined by the energy spread of the ions:

$$\Delta M/M = {}^1/_4(\Delta U/U_0)^2. \quad (6)$$

The precision of the measurements is determined by the duration of a pulse or its linear size. Thus the ratio of the duration of an ion pulse to its transit time must be smaller than the resolution limit. Since in the error formula $\Delta M/M = 2\Delta T/T$, the magnitude of $\Delta M/M$ is given, whereas ΔT is limited by the experimental possibilities, for the purpose of improving accuracy, it is necessary either to lengthen the tube (which is impracticable) or to cause the ions to complete the number of cycles which is required by the formula

$$N = (2M/\Delta M)\,\Delta T/T. \quad (7)$$

On the assumption that the retarding fields and the accelerating potential are supplied by the same source of power the stability of the latter is given by $\Delta V/V = \Delta M/M$. The strength of the longitudinal magnetic field is set at a value such that increase in the sensitivity of the instrument will not diminish its resolving power, that is, it will focus ions whose transverse energy component is below the limit given by

$$H \sim R^{-1}\sqrt{(2M/Ze)\,\Delta U}, \quad (8)$$

where R is the radius of the tube.

Thus ions which are scattered by the residual gas will be lost in the walls at scattering angles which are greater than the permissible values. If, for example, the parameters are as follows: $U_0 = 100$ v, $\Delta U = 0.2$ v, $l = 50$ cm, $M = 100$, $\Delta T = 0.05\,\mu$sec, we obtain $T_0 = 145\,\mu$sec, $\Delta M/M = 10^{-6}$ and $N = 690$. At a pressure of $1 - 5 \times 10^{-6}$ mm Hg, the number of ions which reach the detector is a few percent of the initial number.

* Of course it would be possible to employ a field with a quadratic potential distribution so that the oscillation period of the ions would be absolutely independent of their energies, but there are great experimental difficulties involved in the generation of such a field.

[1] A. E. Cameron and D. F. Eggers, Rev. Sci. Instr. 19, 605 (1948).

[2] I. I. Ionov and B. A. Mamyrin, J. Tech. Phys. (U.S.S.R.) 23, 2101 (1953).

[3] H. S. Katzenstein and S. S. Friedland, Rev. Sci. Instr. 26, 324 (1955).

Translated by I. Emin
99

Electron Broadening of Spectral Lines

I. I. SOBEL'MAN

(Submitted to JETP editor May 12, 1956)
J. Exptl. Theoret. Phys. (U.S.S.R.) 31, 519-520
(September, 1956)

THERE is considerable experimental evidence of the fact that collisions with electrons play an important part in the broadening of atomic spectral lines in a plasma[1-5]. Moreover, there is every

reason to believe that a number of lines of metals in stellar atmospheres are broadened due to collisions with electrons[6]. At the same time the existing theory of the broadening of spectral lines does not apply to electrons, because its basic assumption that the relative motion of the atom and of the perturbing particle is quasiclassical is correct only for heavy particles[7].

The shape of a line that is broadened due to the interaction of an atom with the particles surrounding it (in this case with electrons) is obtained from the integral

$$A = \int \prod_i \psi^*_{n''i} \psi_{n'i} d\mathbf{r}_i, \qquad \text{where}$$

$\psi_{n'i}$ and $\psi_{n''i}$ are the wave functions of the relative motion of the atom and electrons for the initial and final states of the atom, respectively.

The calculation of A is greatly simplified if broadening by electrons is regarded as being of impact character[7] (in the terminology of classical theory). In this case the instants of time during which an electron is close to the atom are disregarded, since it is possible to neglect radiation during the actual collision. For integration in the intervals between collisions, when the distance to the nearest electron is large, simple asymptotic expressions can be used for the functions ψ_{ni}. The entire calculation can be carried through to the end in this general form. This is extremely important. A number of articles[8-10] on electron broadening have recently appeared. Their authors attempt to solve the problem without making any assumptions in advance regarding the mechanism of the broadening. Because of the difficulties of the calculation they confine themselves to the Born approximation, which is of doubtful validity in this case, as collisions with relatively slow electrons, whose energy is 0.5 to 1 ev, is of the greatest practical interest.

As will be shown below, the general equations which we derive give the results obtained in Refs. 8-10 for the Born approximation.

Our calculations showed that electron impact broadening is of dispersive character; for the line width γ and shift Δ we obtain:

$$\gamma = 2Nv\sigma_r, \tag{1}$$

$$\sigma_r = \frac{\pi}{k^2} \sum_{l=0}^{\infty} (2l+1) \{1 - \cos 2 (\eta'_l - \eta''_l)\};$$

$$\Delta = Nv\sigma_i, \quad \sigma_i = \frac{\pi}{k^2} \sum_{l=0}^{\infty} (2l+1) \sin 2 (\eta'_l - \eta''_l), \tag{2}$$

where $k = \mu v/\hbar$, $\hbar \sqrt{l(l+1)}$ is the angular momentum; η'_l and η''_l are the quantum-mechanical scattering phases for the initial and final states of the atom.

In the quasi-classical approximation Eqs. (1) and (2) go over into the corresponding formulas of classical theory. Indeed (see Ref. 11), in scattering by the field $\hbar D_n/R^n$

$$\eta_l = -\frac{\mu D_n k^{n-2}}{2\hbar l^{n-1}} \frac{\Gamma(1/2)\,\Gamma((n-1)/2)}{\Gamma(n/2)}.$$

After substituting $\hbar k = \mu v$ and $k\rho \approx l$ we obtain

$$2(\eta'_l - \eta''_l) = -\frac{D'_n - D''_n}{v\rho^{n-1}} \sqrt{\pi} \frac{\Gamma((n-1)/2)}{\Gamma(n/2)} = \eta(\rho), \tag{3}$$

where $\eta(\rho)$ is the phase shift of the atomic oscillator in Weisskopf's theory[7]. Using (3) and replacing the summation over l by integration over ρ we easily obtain

$$\sigma_r = 2\pi \int_0^{\infty} \{1 - \cos \eta(\rho)\}\, \rho d\rho; \qquad \sigma_i = 2\pi \int_0^{\infty} \sin \eta(\rho)\, \rho d\rho. \tag{4}$$

Estimates show that in some cases (3) and (4) are a quite good approximation. In the transition to the Born approximation we express the cross section σ_r in terms of the scattering amplitudes:

$$\sigma_r = \pi \int_0^{\pi} |f'(\theta) - f''(\theta)|^2 \sin\theta\, d\theta,$$

$$f(\theta) = \frac{1}{2ik} \sum (2l+1) \{e^{2i\eta_l} - 1\} P_l(\cos\theta).$$

Considering that in the Born approximation

$$f(\theta) = \frac{\mu e^2}{2\hbar^2} \frac{(Z - F(\theta))}{\sin^2 \theta/2}$$

and introducing the notation $x = 4a_0^2 k^2 \sin^2(\theta/2)$ and $a_0 = \hbar^2/\mu e^2$, we obtain for the broadening cross section

$$\sigma_r = \frac{2\pi}{k^2} \int_0^{4a_0^2 k^2} x^{-2} (F'' - F')^2\, dx. \tag{5}$$

Here F' and F'' are form factors for the initial and final atomic states. Equation (5) agrees with

Eqs. (22) and (23) of Ref. 8, thus establishing the relationship with the results obtained in Refs. 8-10. We note in conclusion that when inelastic collisions are taken into consideration, Eqs. (1) and (2) are replaced by

$$\sigma_r = \frac{\pi}{k^2} \sum (2l+1) \{1 - e^{2(\beta_l' + \beta_l'')} \cos 2(\eta_l' - \eta_l'')\}, \quad (6)$$

$$\sigma_i = \frac{\pi}{k^2} \sum (2l+1) e^{2(\beta_l' + \beta_l'')} \sin 2(\eta_l' - \eta_l''). \quad (7)$$

Here $\eta_l + i\beta_l$ are complex scattering phases.

[1] A. Kantrowitz, Phys. Rev. **90**, 368 (1953).

[2] Petschek, Rose, Glick, Kaul and Kantrowitz, J. Appl. Phys. **26**, 83 (1955).

[3] H. Baranger, Phys. Rev. **91**, 436 (1953).

[4] H. Olsen and W. Huxford, Phys. Rev. **87**, 922 (1952).

[5] C. Jurgens, Z. Physik **184**, 21 (1952).

[6] A. Unsold, Symposium, *Modern Problems of Astrophysics and Solar Physics*, IIL, 1954, p. 7 (Russian translation).

[7] I. I. Sobel'man, Usp. Fiz. Nauk SSSR **54**, 551 (1954).

[8] Kivel, Bloom and Margenau, Phys. Rev. **98**, 495 (1955).

[9] B. Kivel, Phys. Rev. **98**, 1055 (1955).

[10] H. Margenau and B. Kivel, Phys. Rev. **98**, 1822 (1955).

[11] L. Landau and E. Lifshitz, *Quantum Mechanics*, Moscow, 1948.

Translated by I. Emin
100

Obtaining Polarized Electron Beams

L. N. ROSENTSVEIG
Physico-Technical Institute, Academy of Sciences, USSR

(Submitted to JETP editor April 13, 1956)
J. Exptl. Theoret. Phys. (U.S.S.R.) 31, 520-521
(September, 1956)

IF one can arrange for a sufficiently intense beam of polarized electrons it is possible to carry out a series of experiments with electrons as well as with circularly polarized bremsstrahlung[1]. Some methods of obtaining polarized electrons are well known (scattering of electrons by heavy nuclei[2], the photoelectric effect on aligned atoms[3], etc.). However, the values of the polarization and intensity obtained therewith are small; these methods are particularly ineffective in the high-energy region. Below is shown the principle of operation of a source of polarized electrons, which apparently has not previously been described in the literature.

We consider field emission from a cathode, to whose surface (along the normal) is applied a strong electric field E and a magnetic field H. The behavior of the potential near the surface of the metal (see Figure), owing to the presence of the

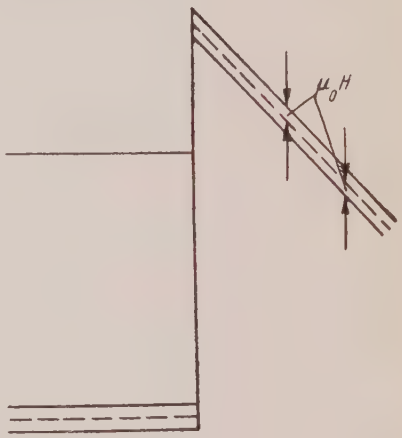

The dotted line shows the behavior of the potential with the magnetic field absent.

magnetic field, is shifted by the value $\pm\mu_0 H$ for each of the two electron groups with opposite spin orientations. But in the equilibrium state, the Fermi energies of both groups are equal, and consequently, the penetrability of the barrier differs for conduction electrons with different spin orientations. An elementary value for the ratio n_-/n_+ for the emitted electrons is given by (see, for example Ref. 4)

$$n_-/n_+ \sim \exp(2\sqrt{2\varphi/mc^2}H/E),$$

where φ is the work function. For $\varphi \sim 1$ ev (coated cathode) one needs an electric field strength of the order of $E \sim 10^6$ v/cm, and an observable polarization $\zeta = (n_+ - n_-)/(n_+ + n_-)$ is obtained, if the magnetic field is hundreds of kilogauss. Obviously, our derivation refers to the case $kT \lesssim \mu_0 H$, i.e., the cathode must be at the temperature of liquid hydrogen.

In this manner we are able to create a source of polarized electrons depending essentially on the

presence of the cathode, which gives an appreciable current in cold emission for an electric field strength $\sim 10^6$ v/cm and a temperature of $\sim 20°$ K. As for the strength of the magnetic field, we refer to what recently has been published in Ref. 5, whose authors write of producing an intensity $H = 6.5 \times 10^5$ G with a pulse lasting from 1 to 10 milliseconds, still far from the value of the threshold needed with existing technology. In spite of the fact that the time interval between such pulses far exceeds the normal interval between operating pulses of contemporary accelerators, the gain in the average current of polarized electrons of high-energy and the value of the polarization may prove to be much greater in comparison with other methods.

Depolarization of the electrons in the acceleration process may be examined for each concrete case with the aid of the formula, derived in Ref. 6.

The difference in the penetrability of the potential barrier, represented in the Figure, for electrons with different spin orientations may also be used for measuring the polarization of the electron beam* incident on the surface of the metal. In this case, the small work function and low temperature are not necessary; the potential of the measuring electrode must be chosen so that the usual classical "turning point" for electrons is somewhat lower than the peak of the barrier.

To summarize, it is possible to say that a practical realization of the source proposed here is not easy to carry out. The practicality is determined mainly by the magnitude of the circular polarization of bremsstrahlung from polarized electrons. This question is being studied in detail at the present time.

The author sincerely thanks K. D. Sinel'nikov and I. M. Lifshitz for valuable discussions.

* This possibility has been shown by K. D. Sinel'nikov.

[1] Ia. B. Zel'dovich, Dokl. Akad. Nauk SSSR 83, 63 (1952).

[2] N. F. Mott, Proc. Roy. Soc. (London) 124A, 425 (1929)

[3] A. Castler, Proc. Phys. Soc. (London) 67A, 853 (1954).

[4] R. Peierls, *Electron Theory of Metals*, 1947.

[5] H. P. Furth and R. W. Waniek, Nuovo Cimento 2, 1350 (1955).

[6] H. A. Tolhoek and S. R. de Groot, Physica 17, 17 (1951).

Translated by B. Hamermesh
101

Spectral Representation of Green's Function in the Nonrelativistic Many-Body Problem

V. L. Bonch-Bruevich
Moscow State University

(Submitted to JETP editor May 22, 1956)
J. Exptl. Theoret. Phys. (U.S.S.R.) 31, 522-523
(September, 1956)

It was previously shown[1,2] that the quantum Green's function gives very extensive information about the properties of systems of interacting particles. In this connection there is interest in investigating the general properties of Green's functions which are independent of any method of approximation. In work in the quantum theory of fields[3,4] the fruitfulness of the spectral approach to this problem was shown. In nonrelativistic theory there are certain complications, connected with the absence of Lorentz invariance; however, as will be shown below, there also exist analogous spectral theorems. For concreteness we will speak about a system of many electrons; the transition to a system of Bose particles will not present any difficulties.

We denote by $\Psi^*(x)$ and $\Psi(x)$ creation and destruction operators for electrons (in the Heisenberg representation); the symbol $\langle .. \rangle_0$ will mean the average over the ground state of the system of interacting particles, Φ_0 is the wave function of the ground state, $\Phi_{\nu,E}$ are the wave functions for the excited states, with characteristic energy E and (possibly) some other quantum number ν (the energy of the ground state is assumed to be zero). By definition

$$G_+(x, y) = i\langle \Psi(x)\, \Psi^*(y)\rangle_0;\ x = \{\mathbf{x}, x_0\},\ x_0 = t, \quad (1)$$

$$G_c(x, y) = i\langle T\{\Psi(x)\, \Psi^*(y)\}\rangle_0 = \theta(x_0 - y_0)\, G_+(x, y) + \theta(-x_0 + y_0)\, G_+(y, x). \quad (2)$$

If we assume

$$G_+(x, y) = i(\Phi_0, \Psi(x)\, \Phi_0)(\Phi_0, \Psi^*(y)\, \Phi_0) + i\sum_\nu \int dE\, (\Phi_0, \Psi(x)\, \Phi_{\nu,E})(\Phi_{\nu,E}\, \Psi^*(y)\, \Phi_0) \quad (3)$$

and use the equation of motion

$$dL/dx_0 = i(HL - LH) \tag{4}$$

(L is any operator not explicitly time-dependent, H is the total Hamiltonian of the system, $\hbar = 1$), we arrive at

$$(\Phi_0, \Psi(x)\Phi_{\nu,E}) = e^{-iEx_0}\varphi_{\nu,E}(\mathbf{x}),$$

from which

$$G_+(x, y) = i\sum_\nu \int dE e^{-iEx_0} F_{\nu,E}(\mathbf{x}, \mathbf{y}), \tag{5}$$

where $F_{\nu,E}(\mathbf{x}, \mathbf{y}) = \varphi(\mathbf{x})\varphi^*(\mathbf{y})$ [obviously, $\Phi_0, \Psi(x)\Phi_0 = 0$]. We note that, generally speaking, $F_{\nu,E}(\mathbf{x}, \mathbf{y})$ is some generalized function. In particular, it may include a δ-function singularity, so that actually the integral over E also contains a sum over possible discrete states. The spectral representation is obtained from (5) by multiplying by $(1/2\pi)\exp\{ip_0(x_0 - y_0)\}$ and integrating over $x_0 - y_0$ (to make a Fourier transformation over the spatial variables is not always convenient; because of the presence of external fields we may not have spatial uniformity). Setting

$$G_c(p_0; \mathbf{x}, \mathbf{y}) = \frac{1}{2\pi}\int_{-\infty}^{+\infty} e^{ip_0(x_0 - y_0)} G_c(x, y)\, d(x_0 - y_0), \tag{6}$$

we derive by virtue of (2) and (5)

$$G_c(p_0; \mathbf{x}, \mathbf{y}) = i\sum_\nu \int dE\, \{\delta_+(p_0 - E) F_{\nu,E}(\mathbf{x}, \mathbf{y}) - \delta_-(p_0 - E) F^*_{\nu,E}(\mathbf{y}, \mathbf{x})\}. \tag{7}$$

We emphasize that the limits of integration are not fixed beforehand, but are determined by the nature of the system (the structure of the function $F_{\nu,E}$). In particular, for an ideal Fermi gas in a completely degenerate state an elementary calculation gives

$$G_c(p_0, \mathbf{x}, \mathbf{y}) = \frac{i}{2\pi^2}\frac{m}{|\mathbf{x} - \mathbf{y}|} \times \left\{\int_0^\infty dE \sin|\mathbf{x} - \mathbf{y}|\sqrt{2m(E + W_F)}\,\delta_+(p_0 - E) - \int_{-W_F}^0 dE \sin|\mathbf{x} - \mathbf{y}|\sqrt{2m(E + W_F)}\,\delta_-(p_0 - E)\right\} \tag{8}$$

(W_F is the limiting Fermi energy). In this example there is clearly seen the well-known technical disadvantage of using the single particle Green's function for studying energy spectra: it gives the spectrum of "covered" electrons" without including the conservation of the number of particles in the intermediate states. In principle, of course, the excitation spectrum is easy to get by finding the appropriate energy differences; however, certain essential peculiarities of the spectra may thereby easily be lost if we calculate G_c by use of any approximate method. (This remark pertains to the method of mass operators developed in Ref. 1.) In this connection it is expedient to introduce another Green's function, in which the "pair" character of the phenomenon of excitation would be shown explicitly; such as, for example, the function

$$K(x, y) = \theta(x_0 - y_0)\langle\rho(x)\rho(y)\rangle_0; \quad \rho(x) = \Psi^*(x)\Psi(x). \tag{9}$$

If we assume, in agreement with Eq. (4),

$$(\Phi_0, \rho(x)\Phi_{\nu,E}) = e^{-iEx_0} r_{\nu,E}(\mathbf{x}); \quad r(\mathbf{x})r(\mathbf{y}) = R(\mathbf{x}, \mathbf{y}), \tag{10}$$

we obtain

$$K(x, y) = R_0(\mathbf{x}, \mathbf{y}) + \sum_\nu \int dE e^{-iE(x_0 - y_0)} R_{\nu,E}(\mathbf{x}, \mathbf{y})\,\theta(x_0 - y_0), \tag{11}$$

and, in spectral form,

$$K(p_0; \mathbf{x}, \mathbf{y}) = \delta_+(p_0) R_0(\mathbf{x}, \mathbf{y}) + \sum_\nu \int dE \delta_+(p_0 - E) R_{\nu,E}(\mathbf{x}, \mathbf{y}). \tag{12}$$

The frequencies that appear in (11) and (12) give the spectrum of the elementary excitations; in particular, by definition, $E \geq 0$ (at the lower limit we have the equal sign or the inequality, depending on whether there is an energy gap in the system). It is possible to show that in calculating $K_4(x, y)$ certain difficulties arise, connected with the necessity of defining the value of the Green's function, $G_c(x, y)$, for equal arguments. In a problem of the present type, however, this difficulty is illusory, and in fact the quantity $G_c(x, x)$ is easy to relate to the number density of particles n. So, for example, for a degenerate Fermi gas, we derive (for $x_0 > y_0$):

$$K(x, y) = n^2 + G_c(y, x)\, G_c(x, y) \qquad (13)$$
$$= n^2 + \frac{1}{(2\pi)^6}\int dk dk' \exp\left\{i(\mathbf{k}-\mathbf{k}', \mathbf{x}-\mathbf{y}) - i\left(\frac{k^2}{2m} - \frac{k'^2}{2m}\right)(x_0 - y_0)\right\} \times \theta\left(\frac{k^2}{2m} - W_F\right)\theta\left(-\frac{k'^2}{2m} + W_F\right).$$

A spectral representation analogous to (7) and (12) is easily derived for all other Green's functions.

We wish to express our great thanks to N. N. Bogoliubov for discussion of this work and for valuable advice.

[1] V. L. Bonch-Bruevich, Dokl. Akad. Nauk SSSR 105, 689 (1955).

[2] V. L. Bonch-Bruevich, J. Exptl. Theoret. Phys. (U.S.S.R.) 30, 342 (1956); Soviet Phys. JETP 3, 278 (1956).

[3] H. Lehmann, Nuovo Cimento 11, 324 (1954).

[4] Bogoliubov, Medvedev and Polivanov, Proc. of the All-Union Conf. on the Physics of High-Energy Particles, Moscow, 1956.

Translated by B. Hamermesh
102

Concerning the Existence of a Transition Layer on a Liquid Surface

V. A. Kizel' and A. F. Stepanov
Central Asia State University, Tashkent
(Submitted to JETP editor, May 25, 1956)
J. Exptl. Theoret. Phys. (U.S.S.R.) 31, 527-528, (September, 1956)

In connection with the recent appearance of some work of Sivukhin,[1] we present several results of our investigations.

The black dots in Figs. 1 and 2 show our values for the ellipticity ρ of reflected light for four wavelengths and for a few homogeneous nonabsorbing liquids, for light incident at Brewster's angle. Figure 3 shows the dependence of the phase difference between the components of the reflected light on the angle of incidence φ for o-xylol at $\lambda = 5460$ A.

The general method is described in an earlier work,[2] and the experimental details, elsewhere.[3] Various methods of calculation, based on the assumption that there exists a transition layer on the surface, with no other hypotheses and without making any special assumptions as to the molecular structure of the layer, lead to the expressions[1,2]

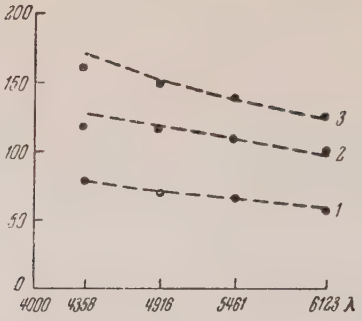

FIG. 1. The dependence of ellipticity on wavelength: *1*—ethylene glycol, *2*—*m*—xylol, *3*—CCl_4.

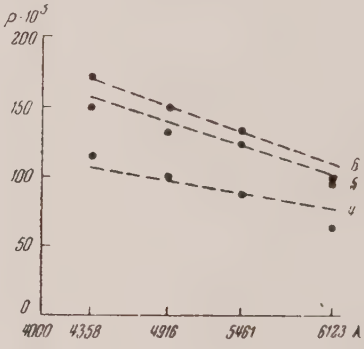

FIG. 2. The dependence of the ellipticity on wavelength for nitro benzene: *5*—cyclohexanol, *6*—chlorobenzene.

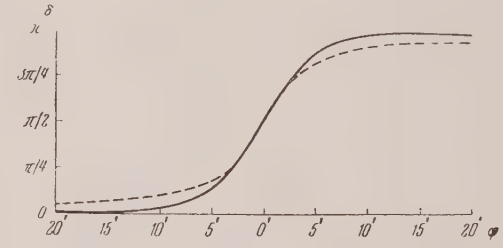

FIG. 3. The dependence of the phase difference between the components of the reflected light on the angle of incidence (Brewster's angle is taken as zero).

$$\rho = (\pi/\lambda)\sqrt{n^2+1}\,(\gamma_z - \gamma_x), \qquad (1)$$

$$\operatorname{tg}\delta = 4(\pi/\lambda)(\gamma_z - \gamma_x) \cos\varphi \sin^2\varphi/(\sin^2\varphi - \cos^2\psi), \qquad (2)$$

where n is the index of refraction in the region, ψ is the angle of refraction, and $(\gamma_z - \gamma_x)$ is a parameter, effectively independent of λ, which characterizes the properties of the layer. The values of n were determined for the given compounds.

The parameter $(\gamma_z - \gamma_x)$ was determined according to Eq. (1) from the results of very many and very accurate measurements at $\lambda = 5460$ A, and this value was used in calculations for other values of λ. The results of the calculations according to Eqs. (1) and (2) are shown by dotted lines. The measurements of δ for other wavelengths are somewhat less accurate as a result of great experimental difficulties. As can be seen, the experiment agrees sufficiently well with theory. It should be noted that measurements in the neighborhood of 0 and π are somewhat less accurate.

The existence of a transition layer on the surface seems unquestionable; this idea has been accepted in physics and physical chemistry for a relatively long time, and as far as we know has met up with no particular objections. The core of the problem, it seems to us, is in establishing a molecular mechanism for the creation of such a layer.

Measurements have been performed in which the liquid being investigated has been carefully purified by chemical methods, multiple distillation and recrystallization, and further distillation in evacuated ampoules by Martin's method. This guaranteed the absence of impurities in the liquid and on its surface or of chemical reactions on the latter. The ellipticities obtained in this way differ from those measured with the proper precautions for an uncovered surface by a negligible amount — from 5 to 10 per cent. This shows that the existence of a surface layer is not caused by impurities, but by the surface structure.

We have obtained several data establishing the connection of the ellipticity and its temperature dependence with parameters that characterize the liquid and its structure, the course of the crystallization process, etc.; all this also supports the above assumption. Details of these measurements will be published separately.

Translated by E. J. Saletan
105

A Theorem on the Equality of the Cross Sections for Photoproduction of Charged π-Mesons on Nuclei with Isotopic Spin Zero

V. L. POKROVSKII
West Siberian Branch of the Academy of Sciences, USSR

(Submitted to JETP editor June 12, 1956)
J. Exptl. Theoret. Phys. (U.S.S.R.) **31**, 537-538 (September, 1956)

THE interaction Hamiltonian H_{int} of nucleons and π-mesons with the electromagnetic field can be represented as the sum of a scalar S and the third component of a vector V_3 with respect to the group of rotations in isotopic spin space:[1]

$$H_{int} = S + V_3; \quad S = -\frac{ie}{2}\sum_\nu \mathbf{v}^\nu \mathbf{A}(x_\nu); \qquad (1)$$

$$V_3 = ie\left[\sum_\nu T_3^\nu \mathbf{v}^\nu \mathbf{A}(x_\nu) + \sum_\mu T_3^\mu \mathbf{v}^\mu \mathbf{A}(x_\mu)\right].$$

Here $\mathbf{v}^\nu$ is the velocity operator, $T_3{}^\nu$ is the projection operator for the isotopic spin of the νth nucleon; ν^μ, $T_3{}^\mu$ are the same quantities for the μth meson.

From (1) we obtain[1] the conservation law for the projection of the isotopic spin of the system of nucleons and π-mesons on the 3-axis (charge conservation law) and the following selection rules for the total isotopic spin T of the system

$$\Delta T = 0, \pm 1. \qquad (2)$$

We note that the matrix elements of the operators which correspond to transitions in which the number of nucleons is conserved are invariant under the group P_n of permutations only of the isotopic spin variables of the nucleons. Therefore the matrix element of an operator differs from zero when its direct (Kronecker) product with the representation of the group P_n (according to which the wave functions of the initial and final states transform) contains the unit representation.

We shall show that for photoproduction of charged mesons on nuclei with isotopic spin

[1] D. V. Sivukhin, J. Exptl. Theoret. Phys. (U.S.S.R.) 30, 374 (1956); Soviet Phys. JETP 3, 269 (1956).

[2] V. A. Kizel', J. Exptl. Theoret. Phys. (U.S.S.R.) 29, 658 (1955); Soviet Phys. JETP 2, 520 (1956).

[3] V. A. Kizel' and A. F. Stepanov, Proc. Lenin Centr. Asia State U., Phys., Vol. 2, Tashkent, (1956).

[4] D. V. Sivukhin, J. Exptl. Theoret. Phys. (U.S.S.R.) 18, 976 (1948); Dokl. Akad. Nauk SSSR 36, 247 (1942); Vestn. (Herald) Mosc. State Univ. 7, 63 (1952).

zero the matrix element $(\psi_f | S | \psi_i)$ vanishes. In fact, by assumption, the wave function ψ_i of the initial state transforms according to the representation of the group P_n to which corresponds Young's diagram in the form of two horizontal lines of equal length. Since a charged π-meson appears in the final state, the isotopic spin changes and with it the charge symmetry of the nucleus. The operator S is symmetric under arbitrary permutation of the charge variables. In agreement with the above, the matrix element $(\psi_f | S | \psi_i)$ vanishes.*

From the selection rule (2) and the usual rules for combining angular momenta, it follows that the isotopic spin of the nucleus in the final state may be either 1 or 2. Making use of the well-known expressions for the matrix elements of a vector (see for instance Landau and Lifshitz[2]), it can be shown that the photoproduction cross section for charged mesons of opposite signs for both possible values of the isotropic spin of the nucleus in the final state are given by

$$d\sigma_1(\pi^+) = d\sigma_1(\pi^-), \qquad d\sigma_2(\pi^+) = d\sigma_2(\pi^-). \quad (3)$$

Summing these cross sections over the possible final states, we obtain

$$d\sigma(\pi^+) = d\sigma(\pi^-).$$

The experimental values of $r = d\sigma(\pi^-)/d\sigma(\pi^+)$ for light nuclei (D, C^{12}, N^{14}, O^{16}) are, within the limits of experimental error, equal to unity.[3]

The decrease of r as the charge increases is evidently explained by the capture of negative π-mesons by nuclei.

*The matrix element $(\psi_f|S|\psi_i)$ vanishes identically if we limit ourselves to dipole interactions. Here, however, no such limitation is made.

[1] L. A. Radicati, Phys. Rev. 87, 521, 1952.

[2] L. D. Landau and E. M. Lifshitz, *Quantum Mechanics*, Part I, GTTI (1948) p. 111.

[3] R. M. Littauer add D. Walker, Phys. Rev. 82. 746 (1951); 86, 838 (1952).

Translated by E. J. Saletan
113

The Magnetic Field in the Two-dimensional Motion of a Conducting Turbulent Liquid

IA. B. ZIL 'DOVICH
Institute of Chemical Physics

(Submitted to JETP editor March 30, 1956)
J. Exptl. Theoret. Phys. (U.S.S.R.) 31, 154-155
(July, 1956)

THE problem of magnetic fields arising spontaneously in the motion of a liquid has been considered by Batchelor.[1] He came to the conclusion that the magnetic field increases without limit for sufficient conductivity in the given field. His conclusion was based on nonrigorous considerations of the analogy between the magnetic field and a velocity vortex.

In the present work, the particular case of two-dimensional motion is considered: $v_z = 0$, v_x and v_y depend only on x and y; the liquid is incompressible, div $\mathbf{v} = 0$. In this case, we have succeeded in treating the problem rigorously. The results differ essentially from the conclusions of Batchelor: In two-dimensional motion in the absence of external fields, the initial magnetic field can increase no more than a definite number of times, and thereafter certainly dies out. In the presence of external fields on the boundaries of the region of motion, the fields in the moving liquid in the stationary state are proportional to the external fields. In the absence of mean regular flow the turbulently moving, conducting liquid behaves as a diamagnet with permeability μ inversely proportional to the intensity of the turbulent mixing.

Following Batchelor, we set up the equation in the quasi-stationary approximation, neglecting the displacement current and the density of free charges. We employ $c = 1$ and the Heaviside system (without 4π), φ = scalar potential, A = vector potential, div A = 0, J = current, div J = 0, the specific resistance of the liquid is r.

The equations have the form:

$$r\mathbf{j} = \mathbf{E} + \mathbf{v}\times\mathbf{H};\ \mathbf{H} = \operatorname{curl}\mathbf{A};\ \mathbf{E} = (\partial\mathbf{A}/\partial t) - \nabla\varphi; \quad (1)$$

$$\mathbf{J} = \operatorname{curl}\nabla^2\mathbf{A}.$$

It follows from this equation that

$$(\partial\mathbf{A}/\partial t) + \mathbf{v}\times\operatorname{curl}\mathbf{A} = r\nabla^2\mathbf{A} + \nabla\varphi. \quad (2)$$

Taking the curl of (2), we obtain an equation which reduces to Batchelor's:

$$(\partial \mathbf{H}/\partial t) + \operatorname{curl}(\mathbf{v} \times \mathbf{H}) = r \nabla^2 \mathbf{H}. \qquad (3)$$

We now go to the case of two-dimensional motion of an incompressible fluid. The equation for H_z can be separated; employing div $\mathbf{v} = 0$, we get

$$\frac{\partial H_z}{\partial t} + v_x \frac{\partial H_z}{\partial x} + v_y \frac{\partial H}{\partial y} = \frac{dH_z}{dt} = r \nabla^2 H_z. \qquad (4)$$

Equation (4) is entirely analogous to the heat conduction equation in a moving liquid.

It is easy to convince oneself that in the absence of external fields, H_z only diminishes. If at any point H_z is maximal, then in the neighborhood, $\nabla^2 H_z < 0$, so that $dHz/dt < 0$, i.e., the maximum is eliminated. In order to be convinced of this cancellation, we set $H_z = 0$ at infinity or on the boundaries of the region and find, integrating by parts,

$$\frac{d}{dt} \int H_z^2 \, dV = \int H_z \frac{\partial H_z}{\partial t} \, dV \qquad (5)$$

$$= -r \int (\nabla H_z)^2 \, dV.$$

We consider the field which is obtained after the damping out of H_z. In this field, $j = j_z$, $\varphi = 0$, $E = E_z$. A has only one component, A_z, which we denote as a in what follows. The two-dimensional vector of the magnetic field with components H_x and H_y we denote by h. Expanding Eq. (3), we get the equation for h:

$$(\partial \mathbf{h}/\partial t) + (\mathbf{v} \cdot \nabla)\mathbf{h} = (d\mathbf{h}/dt) = (\mathbf{h} \cdot \nabla)\mathbf{v} + r \nabla^2 \mathbf{h}. \qquad (6)$$

Along with the dissipation term $r \nabla^2 \mathbf{h}$ this equation contains the terms $(\mathbf{h} \cdot \nabla)\mathbf{v}$ which describe the growth of the magnetic field for increase in length of the magnetic force lines, noted by Batchelor. Thus it is impossible to confirm that h or $\mathbf{h}^2$ is canceled and that $\int h^2 \, dV$ decreases monotonically.

It appears basic for us that the equation for a has the form of the heat conduction equation and a cannot increase (see above, the behavior of H_z).

In the two-dimensional case, for $H_z = 0$, we easily obtain from (2):

$$(\partial a/\partial t) + (\mathbf{v} \cdot \nabla) a = da/dt = r \nabla^2 a. \qquad (7)$$

Hence, in the absence of external fields,

$$\frac{d}{dt} \int a^2 dV = -r \int (\nabla a)^2 \, dV = -r \int h^2 dV. \qquad (8)$$

We represent the distribution of a, which is characterized by amplitude a_0 and length dimension L, which exceeds the maximum scale of the turbulent pulsation l. We denote the pulsating velocity by u; the turbulent coefficient of diffusion, the coefficient of thermal conductivity and the effective turbulent kinematic viscosity are expressed by the formula $\varkappa = ul$. For initial uniform distribution of a, evidently,

$$(\sqrt{\overline{h^2}})_0 \approx a_0 / L. \qquad (9)$$

The macroscopic leveling of a in the process of turbulent exchange is characterized by a time of the order $\tau = L^2 / n = L^2 / ul$, so that, with account of Eq. (8),

$$r\overline{h^2} = d\overline{a^2}/dt = -\overline{a^2}/\tau = -(ul/L^2)\,\overline{a^2}. \qquad (10)$$

Thus, in a time of the order τ, the mean field increases to the amoont

$$\sqrt{\overline{h^2}} = (a_0/L)\sqrt{ul/r} = \sqrt{ul/r}\,(\sqrt{\overline{h^2}})_0, \qquad (11)$$

but then both $\overline{a^2}$ and $\overline{h^2}$ fall exponentially with a period of the order of τ. The quantity ul/r is similar to the Reynolds number ul/ν (ν = molecular kinematic viscosity). We denote it by $\mathrm{Rem} = ul/r^2$. As is evident from (11), the increase in the field is limited to $\sqrt{\mathrm{Rem}}\, h_0$; in the two-dimensional case the possibility is excluded of the increase of the field from the arbitrarily small (for example, depending on fluctuations) to a finite value for a finite r (even for small ν).

Let us consider the turbulent motion in a closed region of size L, on the boundaries of which $v_n = 0$ (the index n = normal to the surface S bounding the region) in the presence of external fields. It follows from Eq. (7) that the quantity $h_t = (\operatorname{grad} a)_n$ should be continuous at the boundary. From the analogy between (7) and turbulent heat conduction, noting that r plays the role of molecular thermal conductivity and considering the flow a as a heat flow, we find:

$$r\,(\operatorname{grad} a)_n|_S \approx a_0 \varkappa / L, \qquad (12)$$

where a_0 is of the order of magnitude of the difference in a on the different boundaries of the medium. Consequently, the mean (not the mean square!) value of the field in the volume $\bar{h} \approx a_0 / L$ and the value of the tangential field at the boundary of the region, where the liquid is at rest, are related by the following:

$$\bar{h} = (r/\varkappa)\, h_t|_s. \qquad (13)$$

By analogy with macroscopic electrodynamics, we shall consider the flow in the turbulent liquid as molecular flow, the neutralized true field $\bar{h}$ we denote by $\mathfrak{B}$ and introduce $\vec{\mathfrak{H}}$; here curl $\vec{\mathfrak{H}} = 0$ in the region where there are no irregularities of flow dependent on the turbulence. From Eq. (13) we get $\mathfrak{B} = (r/\varkappa)\, \vec{\mathfrak{H}} = \vec{\mathfrak{H}}/\mathrm{Rem}$. Thus, macroscopically, the turbulent conducting liquid behaves as a diamagnet * with very small permeability $\mu \sim /\mathrm{Rem}$.

Apropos of the analogy noted by Batchelor between the vortex velocity and the magnetic field, it should be noted that for the realization of an actually stationary turbulence, a supply of mechanical energy is necessary. The supply of energy comes about either at the expense of nonpotential volume forces or at the expense of the motion of the surfaces bounding the liquid. With consideration of these factors, the set of equations and boundary conditions for the vortex are not identical to the equation and boundary conditions for a magnetic field in the absence of external magnetic fields and attendant electromotive forces.

Once again, we note that direct step-by-step consideration of the three-dimensional case has, up to the present time, not been possible, and the question of the growth of field in the three-dimensional case remains unknown.

*Czada[3] has come to the conclusion that a conducting turbulent liquid is a paramagnet with large permeability. His analysis, based on a consideration of the damping of the field (p. 140) and of the energy of the field (p. 143) is not convincing, since the energy of the pulsating components of the field can be regarded macroscopically as a part of the turbulent energy, but the damping of the field can be connected not only with the conductivity, but also with a transition of the energy into mechanical form.

[1] G. K. Batchelor, Proc. Roy Soc. (London) 201A, 405 (1950); Problems in Contemporary Physics 2, 134 (1954). (Russian translation).

[2] W. M. Elsasser, Rev. Mod. Phys. 22, 1 (1950).

[3] I. K. Czada, Problems in Contemporary Physics 2, 136 (1956); I. K. Czada, Acta Phys. Hung. 1, 235 (1952).

Translated by R. T. Beyer
27

On the Composition of Primary Cosmic Rays

V. L. Ginzburg and M. I. Fradkin
P. N. Lebedev Physical Institute

(Submitted to JETP editor May 23, 1956)
J. Exptl. Theoret. Phys. (U.S.S.R.) 31, 523-525
(September, 1956)

We consider the question of the chemical constitution of primary cosmic rays in the framework of the theory of the origin of cosmic rays developed in Refs. 1-3 and in many previous works discussed there. The concentration of cosmic particles of type i, which are designated by $N_i(\mathbf{r}, t)$, can be found from the system of equations

$$\partial N_i/\partial t = \nabla(D_i \nabla N_i) - N_i/T_i + \sum_{j>i} p_{ij} N_j/T_j + q_i, \qquad (1)$$

where $q_i(\mathbf{r}, t)$ is the number of particles of type i per unit volume per unit of time, injected into interstellar space by the source of cosmic rays (the envelopes of supernovae and novae), $D_i(\mathbf{r})$ is the diffusion coefficient of cosmic rays in interstellar space, $T_i(\mathbf{r})$ is the lifetime of particles of type i, until their break-up in collisions with atomic nuclei of the interstellar medium (i.e., principally protons) and p_{ij} is the number of particles of type i, formed by the splitting of particles of type j. In case of nuclei, one can almost always assume that the collisions lead to the formation of nuclei of another sort, while the energy per nucleon of the primary and secondary nucleons are the same. Similarly, it is possible to understand N_i in (1) to be the concentration of particles in any energy interval, lying above the energy $E_0 \sim 10^9$ ev/nucleon observed in cosmic rays on the earth. For protons, the collisions are no longer catastrophic, but by observing the well-known precautions it is possible in this case to use Eqs. (1) for the concentration of protons N_p with energy $E > E_0$. On the other hand, for electrons which experience continuous magnetic retardation losses, use of Eq.

(1) is already impossible, but we shall not consider this case (see Ref. 4 where all the questions raised in the present note are considered in great detail).

We denote the concentration of protons, α-particles, nuclei Li, Be and B, nuclei C, N, O and F, and nuclei with $Z \geq 10$ by N_p, N_α, N_L, N_M and N_H, respectively. From experiment, $N_M / N_H \approx 3.2$; $N_\alpha / N_p \approx 0.1$; $N_H / N_p \approx 1.6 \times 10^{-3}$. With respect to the concentration of nuclei of group L, we have contradictory data, but we use the lowest value[5,6] for $N_L / N_M \leq 0.1$ (i.e., $N_L / N_H \leq 0.32$) since such a value for N_L is most difficult to explain theoretically. For the lifetime of the nuclei we take the value $T_p = 4 \times 10^8$ years, $T_H : T_M : T_L : T_\alpha : T_p = 1:2:3:5:20$, which differ but little from the values in Ref. 1. It is possible to suppose that in a time $T_i \leq 4 \times 10^8$ years the structure of the galaxy and the intensity of cosmic rays has changed but little, and by virtue of this, we set $\partial N_i / \partial T = 0$ in Eqs. (1). Further, if we consider the sources of cosmic rays to be distributed uniformly, then the diffusion is unimportant and we obtain

$$N_i = \sum p_{ij} N_j T_i / T_j + T_i q_i, \qquad (2)$$

$$N_M / N_H = (T_M / T_H)(q_M / q_H + p_{MH}) = 3.2; \quad q_M / q_H = 1.33;$$

$$N_L / N_H = (T_L / T_H)[p_{LH} + p_{LM}(q_M / q_H + p_{MH})] = 1{,}8; \quad N_L / N_M = 0.56,$$

where the values $p_{LM} = p_{LH} = 0.23$, $p_{MH} = 0.27$ are assumed, and where all are minimum values; furthermore, we assume that $q_L = 0$, so that on the average in nature the elements of group L are 105 times less abundant than elements of group M.

In the equilibrium condition, even if we completely neglect the role of secondary protons (i.e., set $p_{ij} = 0$), from Eqs. (2) we get $q_p / q_H = N_p T_H / N_H T_p \approx 30$; if we consider that $p_{ij} \neq 0$, then it is possible to to show that all the protons are secondaries. At the same time, in nature, the elements of group H are, on the average, 3000 times less abundant than the protons, Thus, if we proceed from Eqs. (2), it is necessary to suppose that the sources either are nearly completely without hydrogen, or the acceleration of protons is extremely ineffective in comparison with the acceleration of nuclei. Both of these assumptions seem to be inadmissible. Further, if $N_L / N_M \leq 0.1$, then the result (2) directly contradicts the experimental data (in this case a lowering of the value $N_L / N_M \approx 0.56$ via the choice of other permissible values of the constants is not possible)*.

Furthermore, the assumption of a uniform distribution of sources, in fact contradicts the picture adopted in Refs. 1-3, according to which cosmic rays are generated in the envelopes of supernovae and novae, located in the galactic plane and, possibly, concentrated at the galactic center. Upon emergence from the layer of thickness $2h \sim 2 \times 10^{21}$ cm which is occupied by sources, cosmic rays diffuse through the rare interstellar gas, occupying a volume of radius $R_0 \sim 5 \times 10^{22}$ cm. The corresponding diffusion coefficient $D \sim lv/3 \lesssim 3 \times 10^{37}$ cm^2/year, which yields an effective mean free path (regions with quasi-uniform magnetic fields), equal to 100 parsecs (this number corresponds to a maximum as shown in Ref. 7).

For a point source, located at a distance r from the observation point (Earth), a solution of the system (1) for N_H, N_M and N_L is [assuming $q_i = Q_i \delta(r)$; $q_L = 0$; $D_i = D = \text{const}$; $T_i(\mathbf{r}) = \text{const}$; $p_{Hj} = 0$]:

$$N_H = (Q_H / 4\pi D r) \exp(-r / \sqrt{DT_H}); \qquad (3)$$

$$N_M = \frac{Q_H}{4\pi D r}\left\{\frac{Q_M}{Q_H}\exp\left(-\frac{r}{\sqrt{DT_M}}\right) + \frac{p_{MH}T_M}{T_M - T_H}\left[\exp\left(-\frac{r}{\sqrt{DT_M}}\right) - \exp\left(-\frac{r}{\sqrt{DT_H}}\right)\right]\right\}$$

$$\times\ N_L = \frac{Q_H}{4\pi D r}\left\{\frac{T_L}{T_L - T_H}\left[p_{LH} - \frac{p_{LM}p_{MH}T_H}{T_M - T_H}\right]\times\left[\exp\left(-\frac{r}{\sqrt{DT_L}}\right) - \exp\left(-\frac{r}{\sqrt{DT_H}}\right)\right] + \frac{p_{LM}T_L}{T_L - T_M}\left[\frac{Q_M}{Q_H} + \frac{p_{MH}T_M}{T_M - T_H}\right]\times\left[\exp\left(-\frac{r}{\sqrt{DT_L}}\right) - \exp\left(-\frac{r}{\sqrt{DT_M}}\right)\right]\right\}.$$

The values of $N_M/N_H = 3.2$ and $N_L/N_M \leq = 0.1$ are derived from this, if $r \leq 0.7\sqrt{DT_H} \approx 1.8 \times 10^{22}$. Simultaneously, we obtain $3.2 \geq Q_M/Q_H \geq 2.5$, and an analogous estimate for protons leads to the conclusion that $Q_p/Q_H \sim N_p/N_H \sim 10^3$. The value $r = 1.8 \times 10^{22}$ is only 1.4 times less than the distance of the sun from the galactic center (R_0

$= 2.5 \times 10^{22}$). If we consider the possibility of certain changes in the parameters, and also assume that the sources are distributed in a certain region, it is possible to get even better agreement between the calculated and observed values of N_i/N_j (for details, see Ref. 4). Thus, by including diffusion and also the nature of the source distribution for the cosmic ray and a rare interstellar medium, the question of the composition of cosmic rays is satisfactorily resolved within the framework of a theory of the origin of cosmic rays**. Because of insufficient reliable knowledge, the set of parameters used here must be investigated further and be made more precise. In particular, it is necessary to obtain a reliable value of N_L/N_M at the limits of the atmosphere, since on the basis of the theory it would be impossible to obtain the value of $N_L/N_M \ll 0.1$ without any essential changes.

* This statement was not made clear in the development in Refs. 1 and 2, since it was assumed that from experiment $N_L/N_M = 0.4 - 0.5$ (see Ref. 6); furthermore, only in Ref. 3 is this difficulty examined, with certain connections to the assumptions about preferential acceleration of nuclei in comparison with protons.

** For example, there is contained in Ref. 8 the conclusion that the smallness of the ratio N_L/N_M indicates that the lifetime of all nuclei $T_i \leq 4 \times 10^6$ years; therefore, this is entirely without basis. This conclusion was due first of all to the use of a radically different picture of the distribution of gas and magnetic fields in the galaxy (for criticism of the picture, see Ref. 8 and certain other works, see Refs. 2, 4 and 9).

[1] V. L. Ginzburg, Usp. Phys. Nauk **51**, 343 (1953); Fortschr. d. Phys. **1**, 659 (1954).

[2] V. L. Ginzburg, Izv. Akad. Nauk SSSR, Fiz. Ser. **20**, 5 (1956); Rep. of Fifth Conf. on the Problem of Cosmology, Acad. Sci. Press, 1956, p. 438.

[3] Ginzburg, Pikel'ner and Shklovskii, Astrono. Zh. **32**, 503 (1955); **33**, 447 (1956).

[4] V. L. Ginzburg and M. I. Fradkin, Astron. Zh. **33**, 577 (1956).

[5] B. Peters, *Progress in Cosmic Ray Physics*, pp. 193-242, Ch. IV, 1952.

[6] Kaplon, Noon and Racette, Phys. Rev. **96**, 1408 (1954).

[7] S. B. Pikel'ner, Rep. Third Conf. on the Problems of Cosmology, Acad. Sci. Press, 1954, p. 123.

[8] B. Rossi, Nuovo Cimento, Suppl. **2**, 275 (1955).

[9] V. L. Ginzburg, Dokl. Akad. Nauk SSSR **99**, 703 (1954).

Translated by B. Hamermesh
103

CONTENTS

(*Contents continued on inside back cover*)